The genetic heterogeneity of brachydactyly type A1: Identifying the molecular pathways

Lemuel Jean Racacho

Thesis submitted to the
Faculty of Graduate Studies and Postdoctoral Studies
in partial fulfillment of the requirements
for the Doctorate in Philosophy degree in Biochemistry
Specialization in Human and Molecular Genetics

Department of Biochemistry, Microbiology and Immunology

Faculty of Medicine

University of Ottawa

Abstract

Brachydactyly type A1 (BDA1) is a rare autosomal dominant trait characterized by the shortening of the middle phalanges of digits 2-5 and of the proximal phalange of digit 1 in both hands and feet. Many of the brachymesophalangies including BDA1 have been associated with genetic perturbations along the BMP-SMAD signaling pathway. The goal of this thesis is to identify the molecular pathways that are associated with the BDA1 phenotype through the genetic assessment of BDA1-affected families. We identified four missense mutations that are clustered with other reported BDA1 mutations in the central region of the N-terminal signaling peptide of IHH. We also identified a missense mutation in *GDF5* cosegregating with a semi-dominant form of BDA1. In two families we reported two novel BDA1-associated sequence variants in *BMPR1B*, the gene which codes for the receptor of GDF5. In 2002, we reported a BDA1 trait linked to chromosome 5p13.3 in a Canadian kindred (BDA1B; MIM %607004) but we did not discover a BDA1-causal variant in any of the protein coding genes within the 2.8 Mb critical region. To provide a higher sensitivity of detection, we performed a targeted enrichment of the *BDA1B* locus followed by high-throughput sequencing. We report the identification of a novel 9.5 Kb intergenic tandem duplication in two unrelated BDA1-affected families. *In-vitro* and *in-vivo* reporter assays demonstrated the enhancer activity of noncoding conserved sequence elements found within the duplicated interval. We also show an upregulation of the neighboring genes, *NPR3* and *PDZD2*, in the patients' fibroblasts that suggests a gain-of-function through the duplication of cis-regulatory elements on dose sensitive genes. By expanding the repertoire of BDA1-causing

mutations in *IHH*, *GDF5*, *BMPR1B* and at the *BDA1B* locus, we have begun to elucidate a common genetic pathway underlying phalangeal formation and elongation.

Acknowledgements

I am blessed to have had good people guide and direct me through a remarkable journey of learning, sacrifice and perseverance. I am grateful to Dr. Dennis Bulman for taking me under his wings as a graduate student. As a friend, mentor and supervisor he has always found a way to support me with patience and understanding. Furthermore, he has helped shape my research aptitude by teaching me the value of simplicity and clarity. From very humble beginnings in London, Ontario to the new setup in Ottawa, my passion for human genetics has followed in his footsteps. I would also like to thank my esteemed thesis advisory committee, Drs. Jeff Dilworth, Rashmi Kothary and David Picketts, for insightful conversations and very sound advice. I am extremely thankful for Dr. David Picketts and his laboratory for adopting me during the "endless" move. The BDA1 project would have not produced fruitful results if it were not for the comradery and the work of the Bulman lab personnel, past and present, notably Tara Read. To sum up the work atmosphere, one former Bulmanite so boldly and ridiculously stated "It was the bestest of times and the worstest of times, but mostly the bestest". I would like to thank long-time colleague Ruobing Zou for helping me with many aspects of lab life. Thank you Michael Huh and Matt Todd for countless and endless conversations on "abstract science" with a healthy dose of craftbeer. Most importantly, I would like to thank my family who always remind me that "in your ways always acknowledge Him". Thank you Mom and Dad for your endless support and love. To my wife Aliesha who has given me tremendous love and support during the ups and downs, I am eternally thankful to have you stand by my side. And to my son Noah for giving me a great reason to finish.

Table of Contents

List of Abbreviations

°C	degrees in Celsius
ΔΔCt	delta-delta cycle threshold
θ	theta
2q	long arm of chromosome 2
3D	three-dimensional
3C	chromosome conformation capture
5p	short arm of chromosome 5
20q	long arm of chromosome 20
A	adenine (nucleic acid); alanine (protein)
Ab	antibody
ACFD	acrocapitofemoral dysplasia
aCGH	array comparative genomic hybridization
ACTB	actin, beta
ACVRL1	activin A receptor like 1
AD	autosomal dominant
AER	apical epidermal ridge
ALP	alkaline phosphatase
AMDM	acromesomelic dysplasia Maroteaux type
AR	autosomal recessive
Arg	arginine
Asn	asparagine
ASOH	allele specific oligo-hybridization
Asp	aspartic acid
ASPED	angel-shaped phalangeal dysplasia
ATP	adenosine triphosphate
Atrx	alpha-thalassemia/mental retardation syndrome X-linked
B-gal	beta-galactose
BAC	bacterial artificial chromosome
BDA-E	brachydactyly A, B, C, D, or E
BDA1B	brachydactyly type A1, chromosome 5p13.3 locus
BLAST	basic local alignment search tool
BLAT	BLAST-like alignment tool
BMP	bone morphogenetic protein
BMPR1A	bone morphogenetic protein receptor, type 1A
BMPR1B	bone morphogenetic protein receptor, type 1B
BMPR2	bone morphogenetic protein receptor, type 2
Boc	brother of CDON
bp	basepair
bp	brachypodism
BWA	Burrows-Wheeler aligner

C	cytosine (nucleic acid); cysteine (protein)
c.	complementary DNA prefix
C-	carboxyl end
C1QTNF3	complement factor 1q, tumor necrosis factor 3
c5orf23	cDNA 5 open reading frame 23
Ca^{2+}	calcium divalent cation
CDLS	Cornelia de Lange syndrome
cDNA	complementary deoxyribonucleic acid
Cdon	cell-adhesion molecule-regulated/down-regulated by oncogenes
CDS	coding sequence
ChIP	chromatin immunoprecipitation
ChIP-seq	chromatin immunoprecipitation sequencing
chr	chromosome
cm	centimeter
cM	centimorgan
CNV	copy number variation
CO_2	carbon dioxide
Col2a1	collagen type 2 alpha 1
COSMIC	Catalogue of Somatic Mutations in Cancer
CTCF	CCCTC-binding factor (zinc finger protein)
CVT	congenital vertical talus
Cy-3 or -5	cyanine 3 or 5
Cys	cysteine
d1-4	digits 1-4
D	aspartic acid
dbSNP	database of Single Nucleotide Polymorphisms
del	deletion
DGV	Database of Genomic Variants
dH_2O	distilled water
DHH	desert hedgehog
DLR™	Dual-Luciferase® Reporter
DMEM	Dulbecco's modified Eagle medium
DNA	deoxyribonucleic acid
dNTP	deoxynucleotide triphosphate
DP	distal phalanges
Dsh	short digits mouse
dup	duplication
E	glutamic acid
E13.5	embryonic day 13.5
ECR	evolutionary conserved region
En	engrailed
ENCODE	Encyclopedia of DNA Elements
ENU	*N*-ethyl-*N*-nitrosourea
EST	expressed sequence tag

EtBr	ethidium bromide
ETS	E26 transformation-specific
Etv4	ETS translocation variant 4
EVS	Exome Variant Server
F	phenylalanine
FGF	fibroblast growth factor
FGFR2	fibroblast growth factor receptor 2
FISH	fluorescent *in-situ* hybridization
fl	forelimb
fp	forepaw
FoSTeS	fork stalling and template switching
g	gram
g.	genomic DNA prefix
G	guanine (nucleic acid); glycine (protein)
Gas1	growth arrest specific 1
GDF5	growth differentiation factor 5
gDNA	genomic deoxyribonucleic acid
Gg	*Gallus gallus*
Gli	glioma-associated oncogene
Gli3	GLI-Kruppel family 3
Gli3-A	GLI-Kruppel family 3, activated peptide
Gli3-R	GLI-Kruppel family 3, repressor peptide
Gln	glutamine
Glu	glutamic acid
Grk2	G protein-coupled protein kinase 2
GREM1	gremlin 1, DAN family BMP antagonist
H2A.Z	histone variant 2A, variant Z
H3K4me1	histone 3, lysine 4, monomethylated
H3K4me3	histone 3, lysine 4, trimethylated
H3K9me3	histone 3, lysine 9, trimethylated
H3K27ac	histone 3, lysine 27, acetylated
H3K27m3	histone 3, lysine 27, trimethylated
H4K20m1	histone 4, lysine 20, monomethylated
HapMap	international haplotype map
HDAC	histone deacetylases
HGMD	Human Gene Mutation Database
Hh	hedgehog
Hhip1	hedgehog interacting protein 1
hl	hindleg
HOXC	homeobox C cluster
HOXD	homeobox D cluster
Hs	*Homo sapiens*
HSP68	heat shock protein 68

HTS	high-throughput sequencing
Hygro	hygromycin B
id1-4	interdigit 1-4
IFT	intraflagellar transport
IHH	Indian hedgehog
IHH-N/C	Indian hedgehog protein amino end/carboxyl end
Ile	isoleucine
indel	insertion and/or deletion
ins	insertion
IPAH	idiopathic pulmonary arterial hypertension
IRD-700	infrared dye 700 nm phosphoramidite
JGI	Joint Genome Institute
kb, kD	kilobase, kilodalton
K	lysine
KCl	potassium chloride
Kif3a	kinesin family member 3A
Kif7	kinesin family member 7
LacZ	beta-D-galactosidase
lb	limbbud
LB	Luria broth
Leu	leucine
LOD	logarithm of the odds ratio
LOVD	Leiden Open Variation Database
Luc	luciferase, firefly
Luc2	luciferase 2 engineered reporter gene
Lys	lysine
M13	M13 bacteriophage
MADS	Mothers against decapentaplegic homolog 1
MAPK	mitogen-activated protein kinase
Mb	megabase
MC	metacarpal
MCPP	metacarpophalangeal pattern profile
MCS	multiple cloning site
Mef2c	myocyte enhancer factor 2C
mg, µg	milligram, microgram
$MgCl_2$	magnesium chloride
MIM	Mendelian inheritance in man
min	minute
minP	minimal promoter
miRNA	microRNA
ml, µl	milliliter, microliter

mm	millimeter
mM, μM	millimolar, micromolar
Mm	*Mus musculus*
MP	middle phalanges
mRNA	messenger RNA
N	asparagine
N-	amino end
N. Zealand	New Zealand
N/A	not available
nb	nasal bone
NCBI	National Centre for Biotechnology Information
ncRNA	noncodingRNA
ng	nanogram
NGS	next-generation sequencing
NHDF-Ad	normal human dermal fibroblast, adult
NHEJ	nonhomlogous end-joining
NHEJ1	nonhomologous end-joining factor 1
nm	nanometer
NOG	noggin
np	nasal process
NPPA	natriuretic peptide A
NPPB	natriuretic peptide B
NPPC	natriuretic peptide C
NPR2	natriuretic peptide receptor 2
NPR3	natriuretic peptide receptor 3
Ns	unknown nucleotides
NS	no significant difference
nt	nucleotide
LOVD	Leiden Open Variation Database
Oa	*Ovis aries*
OA	osteoarthritis
OD	optical density
OMIM	online Mendelian inheritance in man
Osteo	osteoblasts
p	calculated probability or p-value
P-	patient identifier prefix
p38	alias for mitogen-activated protein kinase 14 (MAPK14)
Pax	paired box
PBS	phosphate-buffered saline
pCMV	plasmid with cytomegalovirus promoter
PCR	polymerase chain reaction
PDB	Protein Data Bank

PDZ	post synaptic density protein, Drosophila disc large tumor suppressor, and zona occludens-1 protein
PDZD2	PDZ domain containing 2
sPDZD2	secreted PDZD2
PFC	preformed complex
PFR	phalanx forming region
Plzf	promyelocytic zinc finger
PP	proximal phalanges
PRC1 or-2	polycomb repressive complex 1 or 2
Pro	proline
PSSM	position-specific scoring matrix
PTCH1	patched receptor 1
PTHLH	parathyroid-like hormone
PZ	progress zone
Q	glutamine
QTL	quantitative trait loci
QV	quality value
R	arginine
RAI14	retinoic acid induced 14
rc	ribcage
RE	regulatory element
RIN	RNA integrity number
RLU	relative luciferase unit
RLuc	renilla luciferase
RNA	ribonucleic acid
RNA-seq	ribonucleic acid high-throughput sequencing
ROI	region of interest
ROR2	receptor tyrosine kinase-like orphan receptor 2
R-SMADS	receptor-regulated SMADS
RT-qPCR	reverse transcriptase quantitative PCR
rTaq	recombinant *Thermus aquaticus* DNA polymerase
Runx	runt related transcription factor family
s	seconds
SD	standard deviation
SE	standard error
S.E.M.	standard error of the mean
Ser	serine
sh	shoulder
SHH	sonic hedgehog
SHH-ZRS	sonic hedgehog zone of polarizing activity regulatory sequence
SMAD	mothers against decapentaplegic homolog
SMO	smoothened
SNP	single nucleotide polymorphism

SNV	simple nucleotide variant
SOX	SRY (sex-determining region Y)-box
SPRI	solid phase reversible immobilization
SRO	shared region of overlap
SRY	sex-determining region Y
STR	simple tandem repeat
Sufu	suppressor of fused homolog
SWI/SNF	SWItch/Sucrose NonFermentable
SYM1	symphalangism, proximal, 1A
SYM2	symphalangism, distal
SYN1	multiple synostosis
SYNS2	multiple synostosis syndrome 2
T	thymine (nucleic acid); threonine (protein)
Ta	temperature annealing
TAK1	alias for mitogen-activated protein kinase kinase kinase 7 (MAP3K7)
TARS	threonyl-tRNA synthetase
TBP	TATA-binding protein
TBX	T-box
TCAG	the Centre for Applied Genomics
Ter	termination stop codon
TF	transcription factor
TFBS	transcription factor binding site
TGF-β	transforming growth factor beta
TGF-β-GS	transforming growth factor beta glycine-serine
Thr	threonine
TK	thymidine kinase
TKV	thick veins
TM	transmembrane
Tris-HCl	2-Amino-2-hydroxymethyl-propane-1,3-diol hydrochloride
Trp	trytophan
TSS	transcription start site
U	Units
UCSC	University of California, Santa Cruz
U.S.	United States
UTR	untranslated region
UV	ultraviolet
V	valine; Volts
VAST	vector alignment search tool
W	tryptophan
Wnt	wingless-type MMTV integration site family member
WT	wildtype

X-gal	5-bromo-4-chloro-3-indolyl-beta-D-galacto-pyranoside
Z	standardized score or Z statistic
Za	zygomatic arch
ZPA	zone of polarizing activity
Zmax	LOD score, maximum
ZRS	ZPA regulatory sequence

List of Figures

List of Tables

Chapter 1. Introduction

1.1 The brachydactylies

Congenital malformations of the hand and feet that result in the gross morphological display of small, short or absent fingers and toes are collectively known as the brachydactylies, a term rooted in the Greek words "brachy" meaning short and "dactylos" meaning digits. The brachydactylies represent a subclass of limb malformations specifically affecting the long bones with growth plates exhibiting pathologic signatures of hypoplasia, aplasia and dysplasia. The 2010 edition of the Nosology and Classification of Genetic Skeletal Disorders (Warman et al., 2011) categorizes the brachydactylies under the heading "dysotoses", a collection of disorders which affect a group of bones or individual bones. This category includes the non-isolated forms of brachydactylies with or without extraskeletal anomalies which contribute towards clinical manifestations within a syndrome. Some separately classified skeletal disorders such as acrocapitofemoral dysplasia (ACFD; MIM #60778) include brachydactly as an observed feature. An earlier classification scheme presented by Bell (1951) divided the brachydactylies into five classes types A-E (BDA-E), each representing a distinctive pattern of hypoplasia targeting the middle phalanges (BDA), the distal phalanges (BDB), a mix of proximal phalanges and metacarpals (BDC), the distal phalange of the thumb (BDD), or the metacarpals (BDE) (Figure 1.1). In this classification scheme, BDA was further subdivided into subtypes 1 (BDA1; MIM #112500), 2 (BDA2; MIM #112600), and 3 (BDA3; MIM %112700). Later, Fitch (1979) re-organized the classification and instead based it on the osteological

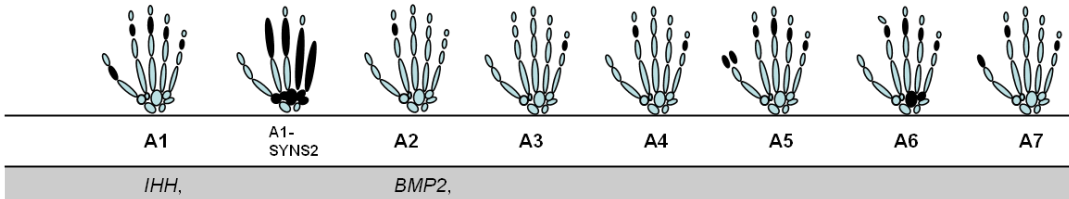

	A1	A1-SYNS2	A2	A3	A4	A5	A6	A7
Gene	*IHH, GDF5, BMPR1B*	*GDF5*	*BMP2, GDF5, BMPR1B*	n.d.	n.d	n.d	n.d	n.d
Mode of transmission	AD	AD	AD	AD	AD	AD	AD	AD

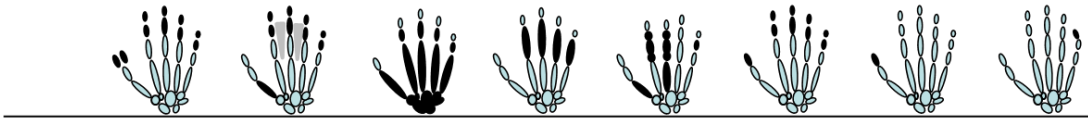

	BDB1	BDB2/ SYNS1	SYNS2	SYM1A/B	BDC	Cooks	BDD	Kirner deformity
Gene	*ROR2*	*NOG*	*GDF5*	*NOG, GDF5*	*GDF5*	*SOX9*	*HOXD13*	n.d.
Mode of transmission	AD	AD	AD	AD	AD	AD	AD	AD

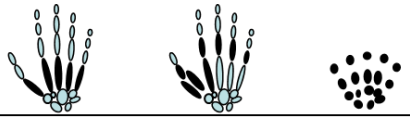

	BDE	Sugermann	Grebe, Hunter-Thompson, DuPan
Gene	*HOXD13, PTHLH*	n.d.	*GDF5, BMPR1B*
Mode of transmission	AD	AR? AD?	AR, AD

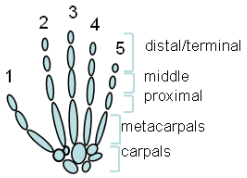

Figure 1.1. The isolated brachydactylies. Adapted from Figure 1 of Stricker and Mundlos (2011). The typical hand bone patterns that are associated with each isolated brachydactyly are displayed above its associated molecular cause and mode of inheritance. A hand bone template is shown at the bottom right for reference. Digits 1 through 5 are commonly referred to as the thumb, index, middle, ring and pinky respectively. Hypoplastic, aplastic, fused, duplicated, or deviated bones are shaded in black. Modes of transmission are either autosomal recessive (AR), autosomal dominant (AD) or both. Indeterminate molecular causes are identified as not determined (n.d.). Syndactyly is denoted by gray shaded areas within the interdigital space.

patterns at each digit. Under the new classification, BDA4 and BDA5 (MIM %112800), which were initially documented as isolated brachymesophalangies by Temtamy and McKusick (1978), were included into a broader group of BDA1-like conditions. Since then, the clinical reports of BDA6 (MIM 112910) (Osebold et al., 1985) and BDA7 (Meiselman et al., 1989) have further expanded the phenotypic spectrum of brachydactyly type A.

The rare orphan disease network database, Orphanet (www.orpha.net) has currently catalogued a total of 70 isolated and complex brachydactylies, of which only 25 have a known molecular cause. As of November 2014, the Online Mendelian Inheritance in Man (OMIM; http://www.ncbi.nlm.nih.gov/omim) has listed 306 entries of the query term "brachydactyly", and the majority of them are associated with syndromes. Of the 306 entries, 189 have a known or suspected molecular cause. The molecular causes for all of the isolated brachydactylies are presented in Figure 1.1 (reviewed in Temtamy and Algan, 2008; Stricker and Mundlos, 2011).

With the exception of BDD (MIM #113200) and BDA3, the prevalence of the various forms of brachydactyly is unknown and since few families have been reported in the literature it is assumed to be very rare in the general population. BDD has a reported prevalence of 0.4% to 4% (Temtamy and Algan, 2008). The prevalence of BDA3 is 3% to 21% (Temtamy and McKusick, 1978), showing high prevalence in different ethnic groups; 10.5 % in the Jirel population of Nepal (Williams et al., 2007) and 21% in Japanese children (Sugiura Y, 1962). The majority of the isolated brachydactylies are inherited in an autosomal dominant fashion with complete penetrance (Figure 1.1).

1.2 Brachydactyly type A1

1.2.1 Clinical description

BDA1 is primarily characterized by disproportionately short or "absent" middle phalanges of digits 2-5 of the hands (Figure 1.2) and/or digits 2-5 of the feet. Unlike Cushing's proximal symphalangism (SYM1; MIM #185800) (1916), severe BDA1 cases such as those reported by Farabee (1903) and Drinkwater (1908) display distal symphalangism where the distal and middle phalanges are fused together resembling chess pawns on hand radiographs. As a result of the fusion event, the fingers and toes appear to have only one interphalangeal joint instead of two. Henry Drinkwater (1908) noticed that in some individuals the bones existed prior to the fusion event as evident by his prospective radiographic assessment of BDA1 affected children. He further described the hands of many severely affected individuals as having one volar or palmar crease. He also reported sweaty palms and thick and bulbous fingers, alluding to the possible involvement of ectodermal dysplasia. A four generation family diagnosed with aplasia cutis congenital and brachydactyly displayed ectodermal tissue abnormalities as seen in the nails, teeth and sweat glands (Rodrigues, 2007). Although there are no reported nail dysplasias associated with BDA1, Byrnes et al. (2010, see Chapter 5) reported two BDA1 affected individuals with teeth anomalies. Prior to this report, the involvement of teeth had only been described in patients diagnosed with BDC (MIM #113100) (Holder-Espinasse et al., 2004).

Abnormalities of the epiphyses, the ball-like structures found at the ends of the diaphysis or shaft of long bones, have been described in the hand bones of some BDA1

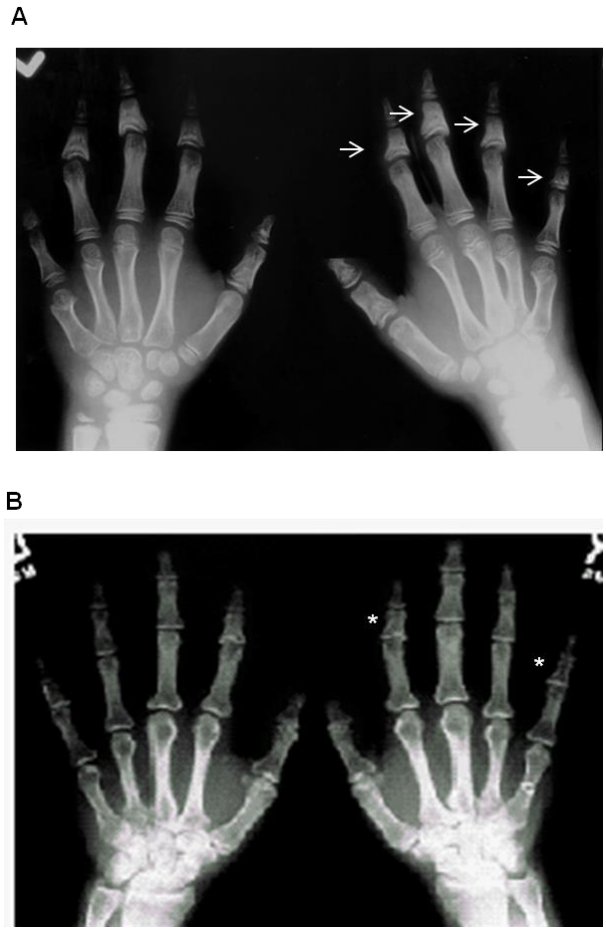

Figure 1.2. Hallmark features of brachydactyly type A1. Hand radiographs of two related individuals displaying BDA1 features of bilateral short middle phalanges of digits 2-5 and a short proximal phalange of digit 1. **(A)** The patient's hand radiograph also displays cone-shaped epiphyses (white arrows) of the middle phalanges in all digits. **(B)** The patient's hand radiograph displays remarkable shortening of the middle phalanges of digits 2 and 5 (*). Note. From "Clinical and radiological assessment of a family with mild brachydactyly type A1: the usefulness of metacarpophalangeal profiles" by Armour et al., J. Med. Genet. 2000, 37(4):292-6, Figures 2 and 4. Reprinted with permission.

families. These individuals lack the proximal epiphysis of the middle phalanx which contributes to the overall shortness of the digit, such as those described in the Farabee and Drinkwater families. In one family with a mild form of BDA1, the hand radiographs of two affected individuals displayed cone-shaped epiphyses in all of the middle phalanges (Armour et al., 2000). The malformed proximal end of the middle phalange creates a shallow concave structure for occupancy of the proximal phalange. The presence of cone-shaped epiphyses is not exclusive to BDA1 as it appears in other limb malformations with digit abnormalities as classified by the Human Phenotype Ontology project (www.human-phenotype-ontology.org).

There is considerable intra- and interfamilial clinical heterogeneity for BDA1. Although the middle phalanges and first proximal phalanges are primarily affected in BDA1 cases, hypoplasia of the first (Yang et al., 2000; Giordano et al., 2003; Byrnes et al., 2010, see Chapter 4), third (Yang et al., 2000; Giordano et al., 2003), and fifth metacarpals (Armour et al., 2000) have also been observed in some affected individuals. In these cases, the hands are broad as a result of an increase in the inter-metacarpal space. Other accompanying features include radial/ulnar clinodactyly (Drinkwater, 1908; Hoefnagel and Gerald, 1966; Sillence, 1978; Grange et al., 1998; Armour et al., 2000; Yang et al., 2000) and shortened distal phalanges (Armour et al., 2000; Yang et al., 2000). The severity of the shortening is variable such that in some mild BDA1 cases the use of metacarpophalangeal pattern profiling (MCPP), an age-standardized measurement of hand bone length (Poznanski et al., 1972; Dijkstra and Venema 1991, 1992), were instrumental at defining intermediate BDA1 cases (Armour et al., 2000). In some cases, the middle phalanges of digits 2 and 5 are severely affected, resembling the affected bone

pattern of BDA4 as described by Temtamy and McKusick (1978). In addition to the variability observed in the hands, the hand phenotype is sometimes not mirrored in the feet (Lodder et al., 2008). Thus, the intra- and interfamilial phenotype variability of BDA1 cases suggests other genetic and/or environmental factors are involved. The shortening of appendicular skeletal structures other than the hands or feet, such as the humerus, has also been identified in some individuals (Lacombe et al., 2010). Short stature has been reported in many of the published BDA1 families (Drinkwater, 1912 and 1915; Slavotinek and Donnai, 1998; Tsukahara et al., 1989; Armour et al., 2000). BDA1 has also been shown to be in association with non-skeletal clinical manifestations such as nystagmus (Tsukahara et al., 1989; Slavotinek and Donnai, 1998), mental retardation (Tsukahara et al., 1989; Grange et al., 1998; Slavotinek and Donnai, 1998), and scoliosis (Sillence, 1978; Raff et al., 1998; Slavotinek and Donnai, 1998). The involvement of various tissues suggests a much broader effect which might be caused by mutations in the genes belonging to a common signaling pathway or developmental program.

1.2.2 Epidemiology

The prevalence of BDA1 has not been determined but it has been described throughout the literature as a rare autosomal dominant malformation with complete penetrance. To date BDA1 has been reported in families of diverse populations; namely families and individuals of European, Chinese, Japanese, Middle Eastern, Mexican, and Indian ethnicity (Temtamy and McKusick 1978; Laporte et al., 1979; Piussan et al., 1983; Tsuakahara et al., 1989; Fukushima et al., 1995; Mastrobattista et al., 1995; Slavotinek et al., 1998; Raff et al., 1998; Armour et al., 2000; Yang et al., 2000; Gao et al., 2001; den Hollander et al., 2001; Giardono et al., 2003; Byrnes et al., 2009, see Chapter 3).

1.2.3 Historical perspective

BDA1 was the first reported autosomal dominant trait in humans (Farabee, 1903). The use of hand morphology, specifically digit lengths, to look at human variation was first reported in the late 1800s (Ecker, 1875; Baker, 1888). Reports describing familial transmission of physical traits were not documented until the early 1900s, coinciding with a revival in Mendel's laws of inheritance. In 1903 William Farabee, then a student of William Castle at Harvard University, reported in his PhD dissertation entitled "Heredity and Sexual Influences In Meristic Variation: A Study of Digital Malformations in Man" a three generation family from Pennsylvania displaying short stature with a striking hand and foot morphology of small and shortened digits. He reported the bilateral shortness of both the middle phalanges of digits 2-5 and the proximal phalanges of the thumbs. The shortening effect seen in the hand bones was also extended to the bones of the feet where he observed a short proximal phalanx of the big toes and short middle phalanges in all of the little toes. He noticed that the vertical transmission of this peculiar phenotype was consistent with an inheritance pattern of an autosomal dominant trait. His report was later regarded to be an important landmark in the field of human genetics as the timing of his findings came at approximately 35 years after Mendel's seminal work on heritable traits through plant hybridization experiments in peas. Farabee later described additional American families presenting with a similar phenotype (Farabee, 1905), which Henry Drinkwater, then working at the University of Edinburgh, termed Farabee-type brachydactyly (Drinkwater, 1908). A comprehensive evaluation of Farabee-type brachydactyly in three separate English families by Henry Drinkwater included a detailed quantitative assessment of various anthropometric measurements

including overall height, arm span and finger lengths (Drinkwater 1908, 1912, 1914). Although these families were phenotypically similar, Drinkwater's assessment of these families revealed no obvious relatedness to each other or to Farabee's original family. Subsequently, Haws and McKusick (1963) assessed three surviving members of Farabee's family and found additional limb bone anomalies which were not initially reported, such as distal end sloping of the radius, shallow glenoid fossa and acetabulum, elliptical humerus head and the absence of the ulnar styloid process. The suspected link between Farabee and Drinkwater's families was confirmed nearly 95 years later when McCready et al., (2002 and 2005) identified a common 5 cM haplotype on chromosome 2q35 in their descendants which suggested a common founder. This haplotype covered a genomic region which included the Indian hedgehog gene (*IHH*), reported but one year earlier by Gao et al., (2001) to harbor BDA1-causing mutations. The subsequent sequencing of *IHH* in the affected individuals revealed a G to A transition at cDNA position 347 (c.347G>A) which is predicted to cause an aspartate to asparagine substitution at peptide position 100 (p.Asp100Asn) (McCready et al., 2002).

1.2.4 Genetic heterogeneity

Given the rare incidence of its distinct morphological features in the human population and its defined autosomal dominant inheritance pattern, BDA1 families are ideal candidates for positional cloning studies to identify genes involved in bone development. In this regard, several groups have identified some of the molecular pathways underlying the BDA1 phenotype by performing linkage analyses and candidate gene sequencing on these families. In addition to the discovery of mutations in *IHH* as a cause of BDA1, Byrnes et al. (2010, see Chapter 4) reported a second BDA1 locus at

chromosome 20q11.22. The subsequent sequencing of the coding region for growth differentiation factor 5 gene (*GDF5*) revealed a missense mutation p.Arg399Cys in three affected patients. A third BDA1 locus designated *BDA1B* (MIM %6007340) was found to be linked to an 11 cM region at chromosome 5p13.3 in a single Canadian multigenerational family (Armour et al., 2002). A fourth and unknown BDA1 locus has been suggested by Kirkpatrick et al., (2003).

1.2.4.1 Mutation spectrum of *IHH* and *GDF5*

The *IHH* gene, which is located at chromosome 2q35, is encoded by three exons, transcribed into a 2074 bp transcript and translated into a 411 amino acid precursor peptide. Like all Hh proteins, the 45 kD peptide undergoes auto-catalytic cleavage producing two fragments, one a 20 kD lipid modified N-terminal signaling peptide and the other a 25 kD C-terminal peptide. The Hh signaling peptide has a cholesterol molecule that is covalently attached to its carboxyl end (Porter et al., 1996) and a palmitate is covalently attached to the cysteine residue at the amide end of the signaling peptide (Pepinsky et al., 1998).

Yang et al. (2000) reported linkage of the BDA1 trait to an 8.1 cM region at chromosome 2q35 in two unrelated Chinese families. They subsequently identified another Chinese family, sequenced *IHH* within this interval in three unrelated BDA1 individuals, and found three separate heterozygous missense variants positioned at the N-terminal signaling peptide (Gao et al., 2001). The inheritance pattern of the BDA1 trait in all three families was consistent with autosomal dominant transmission. The affected individuals of Family 1, carrying a c.332G>A (p.Glu95Lys), displayed shortened distal phalanges in addition to the classical BDA1 features as described by Fitch (1979) and by

Temtamy and McKusick (1979). The affected individuals of Family 2 displayed a more severe phenotype, reminiscent of Farabee-type BDA1, as well as a C to A transversion at cDNA position 349 (p.Asp100Glu). The affected individuals of Family 3 displayed similar missing middle phalanges as seen in Family 2 but the height of their affected members were noticeably shorter. The affected members of this family harbored a C to A transversion at cDNA position 440 (p.Glu131Lys). Interestingly, a kindred of Ashkenazi Jewish ethnicity was reported to harbor the same amino acid substitution in all of the BDA1 affected members (Byrnes et al., 2009; see Chapter 3). The similar chess-pawn shaped middle phalanges associated with the same mutation in the Chinese and Israeli families suggests the glutamine residue at amino acid position 131 maintains an important biological function of IHH signaling in the development of distal interphalangeal joints.

In 2002, McCready et al. identified a heterozygous G to A transition at *IHH* cDNA position 347 (p.Asp100Asn) in the descendants of the Farabee and Drinkwater families after establishing a common haplotype defined by microsatellite markers D2S2250 and D2S1323 at chr2q35. Byrnes et al., (2009, see Chapter 3) also identified a common and shared Farabee-Drinkwater haplotype cosegregating with a BDA1 trait in a New Zealand family. Giordano et al. (2003) identified the same mutation in a three generation family of Italian descent with moderate BDA1 features of broad hands, short middle phalanges and short stature. The report also took note of the absence of the middle phalanges in digits 2 and 5 in some individuals. A large Chinese family carried the same p.Asp100Asn mutation in all of the affected individuals but on a different haplotype (Zhu et al., 2007). This would suggest the mutation at Asp100 arose more than

once in the population. Furthermore, cDNA position 347 appears to be a mutation hotspot as it has occurred in 7 independent families (Zhu et al., 2007).

A heterozygous c.510C>T (p.Thre154Ile) was identified in all of the affected members of a five generation Chinese kindred (Liu et al., 2006). The general phenotype of the affected members included cube-shaped middle phalanges, normal proximal phalanges of the thumb, and unaffected feet. The proband also exhibited distal symphalangism of digit 5.

A BDA1 affected individual from a Mexican family, originally described by Mastrobattista et al. (1995), was assessed for mutations in *IHH* by Kirkpatrick et al. (2005). They identified a heterozygous A to G transition at cDNA position 333, which resulted in a predicted p.Glu95Gly substitution. Later, Lodder et al., (2008) identified a 3-bp deletion (c.332delGAG) in the affected members of a Dutch family. The 3-bp deletion was predicted to cause an in-frame deletion of glutamine at codon 95 yet unlike the missense mutations the authors commented that the deletion was predicted to remove a loop at the outer edge where Patched-1 (PTCH1) was predicted to interact.

In 2009, Byrnes et al. (2009, see Chapter 3) reported a heterozygous c.432G>A (p.Arg128Gln) in the affected members of an American family of European descent. The proband also displayed tarsal coalition, short arms and normal height in addition to BDA1 features. The same study also identified a heterozygous c.438C>A (p.Thr130Asn) in the affected members of a family of East Indian descent. In this family the authors also reported distal symphalangism, scoliosis and clubfoot.

A total of 9 BDA1 mutations, affecting only 5 amino acid positions, reside within a 60 amino acid region of the N-terminal signaling peptide of IHH. Of the 9,

p.Asp100Asn is the most common reported mutation associated with BDA1. The identification of families with different ethnic backgrounds carrying missense mutations at highly conserved codon positions Glu95 and Asp100 suggests that these two amino acid positions are mutation hotspots. Based on the 3D crystal structure of its paralog sonic hedgehog (SHH), several authors noted the clustering of BDA1 mutations in the central region of the N-terminal fragment which corresponds to a groove thought to be the binding site for its receptor PTCH1 (Gao et al., 2001; Lodder et al., 2008; Byrnes et al., 2009, see Chapter 3). The clustering of BDA1-causing mutations in the groove highlights the functional necessity of this domain in maintaining the integrity of proper IHH signaling during bone development. Liu et al. (2006) also noted that unlike other BDA1 mutations, the p.Thr154Ile substitution resided in a predicted beta-sheet instead of an alpha-helix. Whether this mutation acts differently than the others remains to be seen.

Unlike the tendency of the BDA1 mutations to cluster in the central region of the IHH signal peptide, homozygous mutations at its distal ends have been linked to ACFD which is an autosomal recessive skeletal dysplasia first described in 2 consanguineous European families displaying short limbs and brachydactyly (Mortier et al., 2003). Striking radiographic findings were mostly observed in the tubular bones of the hands and at the proximal part of the femur. These include cone-shaped epiphyses, premature epiphyseal closure, and an egg-shaped femoral head with a shallow femoral neck. Subsequently Hellemans et al. (2008) sequenced *IHH* in the affected members and identified two independent homozygous mutations, c.186C>T (p.Pro46Leu) and a c.618C>T (p.Val190Ala). It is possible that these mutations impede the post-translational lipid modifications or the autocatalytic cleavage of IHH. Hellemans et al.

(2008) proposed that the ACFD mutations would lead to increased chondrocyte differentiation as a result of decreased IHH signaling.

Copy number changes spanning and proximal to the *IHH* locus have been identified in 4 families. Microduplications were identified in one family diagnosed with syndactyly type 1 (SYN1) and two diagnosed with craniosynostosis and syndactyly. By performing a high density array comparative hybridization (aCGH), Klopocki et al. (2011) identified a heterozygous 59 kb duplication involving a region which includes the entire coding sequence of *IHH* and the last three exons of nonhomologous end-joining 1 gene (*NHEJ1*) in family members diagnosed with cutaneous syndactyly with no craniofacial abnormalities. They also identified a 48 kb and a 52 kb duplication downstream of the coding sequence of *IHH* in two separate families diagnosed with variable degrees of Philadelphia type craniosynostosis and cutaneous syndactyly. All three duplications shared a 9.1 kb smallest region of overlap (SRO) within the fifth intron of *NHEJ1* which happened to overlap a breakpoint resulting from a balanced translocation (2;7) (q26;p22) in a patient presenting with polymicogyria and syndactyly (Cantagrel et al., 2007). Using a transgenic *LacZ* reporter assay, the authors demonstrated specific enhancer activity for the 9.1 kb region in mouse tissues with overlapping *IHH* and *PTCH1* expression. Importantly, the X-gal stained compartments displayed a similar tissue pattern to the malformed tissues observed in the two aforementioned human conditions. The authors proposed that *cis*-regulatory sequences act distally on *IHH* to drive its tissue specific expression. The duplications would then act as a gain-of-function by augmenting *IHH* expression and activity. Similarly, a potential limb specific regulatory element was identified at the distal end of a 900 kb

tandem duplication found in the affected members of a Turkish family presenting with acrocallosal syndrome (Yuksel-Apak et al., 2012).

Currently the COSMIC database (Bamford et al., 2004) lists 32 somatic mutations in *IHH* which have been identified in lung adenocarcinomas, colon adenocarcinomas, lung squamous cell carcinomas, and uterine corpus endometrioid carcinomas. Neither BDA1 nor ACFD missense mutations overlap with somatic mutations.

Although the majority of BDA1-causal variants have been linked to *IHH*, a missense mutation in *GDF5* was identified in a French-Canadian consanguineous family cosegregating a semi-autosomal dominant form of BDA1 (Byrnes et al., 2010; see Chapter 4). In three severely affected siblings, the sequencing of the *GDF5* gene revealed a homozygous c.1195C>T (p.Arg399Cys). These individuals displayed very short middle phalanges in digits 2-5 with no distal symphalangism. They also lacked the shortening of the proximal phalange of digit 1 that is often seen in most families with *IHH* mutations. Instead, they displayed a short metacarpal of digit 1, a feature usually seen in individuals diagnosed with BDC. This would imply that GDF5 has an important role in the growth of the first metacarpals. A mildly affected family member harbored the same mutation but in a heterozygous state. Functional analysis of the mutation revealed an active but less effective stimulant of chondrogenesis in chicken micromass cultures. The authors suggested that the exchange of an arginine for a cysteine residue would disrupt the neighboring conserved 7-cysteine motif which is normally required for proper GDF5 dimerization.

Mutations within *GDF5* are also associated with BDA2, BDC, fibular hypoplasia and complex brachydactyly (MIM #228900), multiple synostoses syndrome 2 (SYNS2;

MIM #610017), proximal symphalangism 2 (SYM2; MIM #615298), acromesomelic dysplasia (Hunter-Thomson type; MIM #201250) and chondrodysplasia (Grebe type; MIM #200700). The allelic variants associated with these skeletal malformations are described in Table 1.1.

1.2.4.2 *BDA1B* locus at chromosome 5p13.3

The *BDA1B* locus at chromosome 5p13.3-p13.2 was identified by performing linkage analysis in a large Canadian kindred (Armour et al., 2002). The BDA1 trait followed an autosomal dominant inheritance with a maximum two-point LOD score, a statistical measure of the likelihood of genetic linkage between two alleles, of 6.91 at $\theta = 0.00$ for the microsatellite marker D5S477. The flanking recombinant microsatellite markers D5S819 and D5S1986 defined an 11 cM haplotype which co-segregated with all the affected members. The work published in the theses of Elizabeth McCready (2004) and Allison Grimsey (2006) described the refinement of the critical region to a 2.8 Mb region which contained 17 known and predicted protein coding genes and 10 small noncoding RNAs (ncRNA) according to NCBI build 36. A traditional position cloning strategy which involves the PCR-based sequencing of the exons for all of the protein coding genes in the critical region did not yield a candidate BDA1-causal variant. Since the mutation detection strategy has been largely focused on identifying a mutation in a protein coding gene, only 6% of the critical region has been sequenced using the dye-terminator Sanger method, leaving a vast territory of uncharacterized sequence.

The analyses of MCPPs taken from hand radiographs identified consistent features of shortened middle and distal phalanges of digits 2-5, proximal phalanges of digit 1, and metacarpals of digits 1-5, but especially of digit 5 (Armour et al., 2000). The

Table 1.1. Mutation spectrum of *GDF5*. Causal variants found in *GDF5* for each human condition are listed in sequential order along the transcript NM_000557.4. Causal variants that result in a predicted amino acid substitution or deletion are provided in parentheses with its residue position based on NP_000548.2. All three brown highlighted sequence variants were identified on the same allele (Szczaluba et al., 2005). Inheritance pattern is either autosomal dominant (AD) or autosomal recessive (AR).

Condtion	Causal variant	Inheritance	Functional consequence
BDA1	c.1195C>T (p.R399C)	AD	Partial loss
BDA1-SYNS2	c.1240C>T (p.W414R)	AD	Gain and loss
SYNS2	c.1313G>T (p.R438L) c.1424G>A (p.S475N)	AD	Gain
BDA2	c.1139G>A (p.R380Q) c.1322T>C (p.L441P)	AD	Loss
BDC	c.121delG c.158insC c.158delT c.206insG c.493delC c.517A>G (p.M173V) c.612C>A (p.S204R) c.759delG c.811ins23 c.901C>T (p.R301*) c.1199G>A (p.C400Y) c.1312C>T (p.R438C) c.1461T>G (p.Y487*) c.1493G>C (p.C498S)	AD	Haploinsufficiency Loss
SYM1B	c.1632G>T (p.R438L) c.1471G>A (p.E491K) c.1118C>G (p.L373R)	AD	Gain
Grebe	c.206insG c.297insC c.1114insGAGT c.1144delG c.1199G>A (p.C400Y) c.1285T>C (p.C429R)	AR	Loss
Hunter-Thompson	c.1330ins22	AR	Loss
DuPan	c.1133G>A (p.R378Q) c.1306C>A (p.P436T) c.1309delTTG (p.L437del) c.1315T>A (p.S439T) c.1319A>T (p.H440L) c.1322T>C (p.L441P)	AR Cis AD Cis AD Cis AD	Loss
Osteoarthritis susceptibility 5	c.-275C<T c.-48C>A		Decreased *GDF5* expression

appearance of cone-shaped epiphyses was described in two affected children. Unlike the severe form of BDA1, the affected individuals of this family did not display terminal symphalangism and mildly affected individuals were only identified through the use of MCPPs. There were no reports of learning disabilities, hypertension or nystagmus but some individuals reported asthma and/or arthritis upon examination.

1.2.5 Genetic models of BDA1

Abnormalities of the digital bones can result from perturbations which affect mesenchymal condensation, specification, patterning, segmentation, elongation and/or growth. Genetic and functional studies in mice have established the biological role of Ihh in skeletal development prior to the identification of human mutations in its gene. Karp et al. (2000) and Kobayashi et al. (2002) have demonstrated its important role in organizing the growth plate by disrupting the negative feedback loop of Ihh-Pthlh in mice, particularly affecting the proliferation rate of resting chondrocytes and the differentiation of prehypertrophic chondrocytes. IHH, a morphogen which acts locally at the perichondrium and distally at the articular cartilage, essentially regulates the widening and lengthening of the bone. *IHH* mutations which are associated with BDA1 have been postulated to decrease its signaling capacity by disrupting the Ca^{2+} binding site essential for its binding to its receptor Ptch1 and antagonist hedgehog interacting protein 1, Hhip1 (Gao et al., 2001, 2009; McLellan et al., 2008). Gao et al. (2009) created a knockin mouse model of the *IHH* mutation p.Glu95Lys and demonstrated the reduced commitment of distal chondroprogenitors entering the growth phase in the early cartilage template or anlagen, resulting in a reduction in size of the mesenchymal condensations. They further proposed the combined effects of reduced short range and increased long

range signaling capacities of the mutant protein would interfere with early chondrogenesis at distal condensations. This early effect in phalangeal development would most likely affect the middle and distal phalanges.

Another important molecule involved with phalangeal development is GDF5, which is an extracellular signaling protein belonging to the bone morphogenetic protein (BMP) family and the TGF-β superfamily of growth factors. Proteins belonging to this class of ligands require binding to its cognate receptor in order to target gene activation by nuclear translocation of canonical SMADs. Recently, Degenkolbe et al. (2013) identified a missense mutation in a single family presenting with a combined manifestation of BDA1 and SYNS2. The group proposed the reduced interaction of GDF5 with BMP type 1A receptor (BMPR1A) was selectively driven by the position of BDA1-causing mutations p.Trp414Arg and p.Arg399Cys in the protein relative to other GDF5 mutations. Taken together, the identification of *GDF5* as a novel player in defining BDA1 reinforces the involvement of the BMP-SMAD signaling pathway in regulating the development and growth of the middle phalanges, as most of the brachydactylies with mutations in the ligands and receptors of this pathway exhibit a phenotypic overlap of shortened middle phalanges. At the molecular level, the BMP signaling axis converges at the SMADs (Figure 1.3). The induction of Ihh appears to involve upstream Bmp signaling as shown by its direct activation of the *Ihh* promoter (Seki and Hata, 2004) and through the loss of Bmpr1a, which leads to decreased *Ihh* expression (Yoon et al., 2006). Minina et al. (2002) reported the modulation of *Ihh* expression through BMP signaling independent of the Ihh-Pthlh signaling axis, in

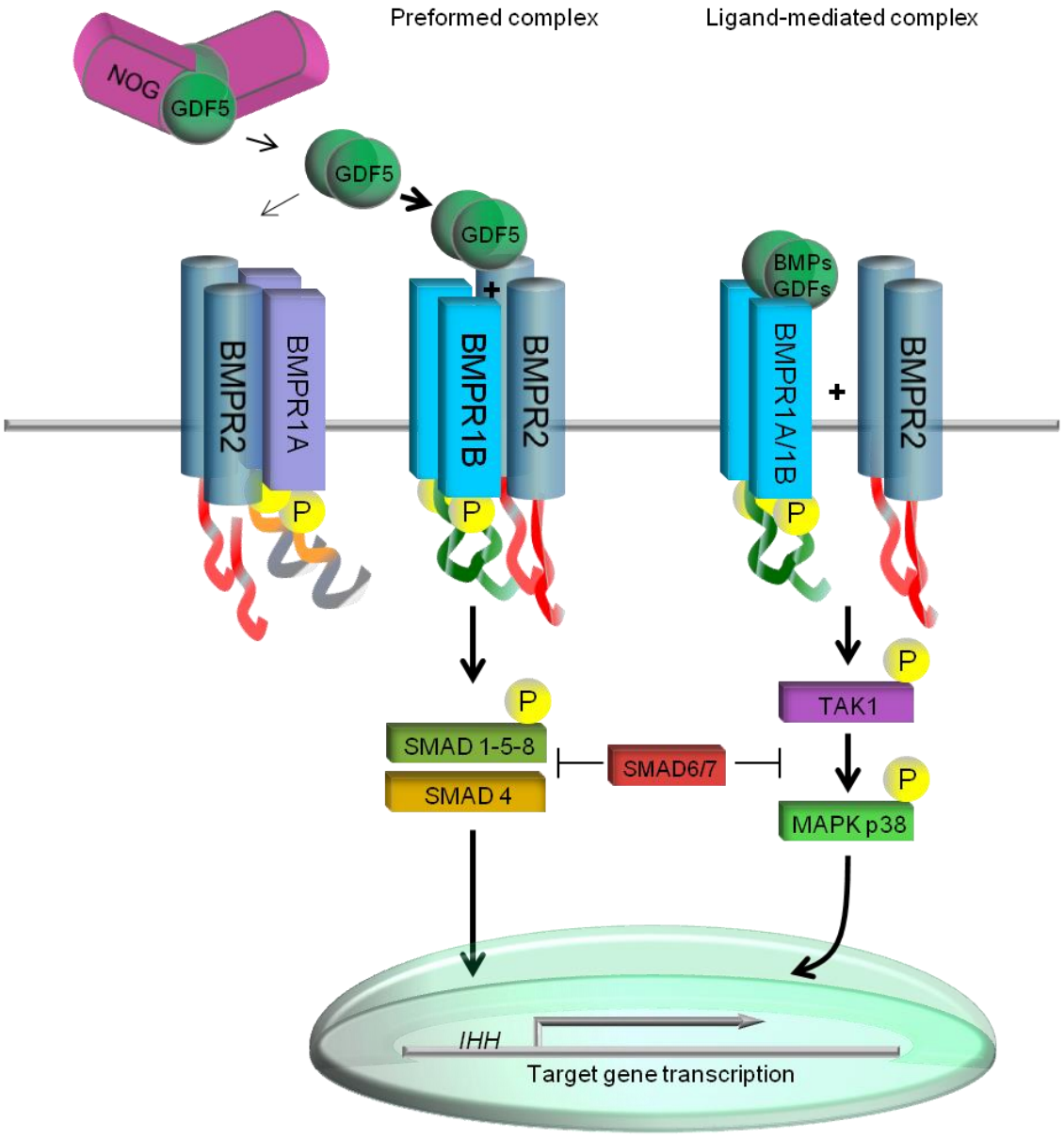

Figure 1.3. BMP-SMAD signaling pathway. BMP signaling occurs through the SMAD-dependent and SMAD-independent signaling pathways. BMP type-1 receptors can form preformed complexes (PFC) with BMP type-2 receptors without ligand. This formation primarily phosphorylates (denoted by P) the R-SMADs (SMAD1-5-8) and forms a complex with SMAD4 which together enters the nucleus to regulate gene expression (e.g. *IHH*). Ligand-mediated heterotetrameric complex formation primarily signals through TAK1 and MAPK (e.g. p38) to regulate target gene expression. SMADs 6 and 7 are inhibitors of both signaling cascades, where SMAD7 primarily represses TAK1/p38. BMPs such as GDF5 are inhibited by noggin (NOG). The binding of GDF5 to the heterotetrameric complex results in the transphosphorylation of BMPR1B at the GS motif by the constitutively active receptor kinase BMPR2, which then triggers the phosphorylation of R-SMADs.

chondrocyte proliferation and in chondrocyte hypertrophic differentiation. These results are consistent with parallel and distinct SMAD signaling pathways where receptor-regulated SMADS 1-5-8 (R-SMADS) are the major contributors of chondrogenesis (Retting et al., 2009). Thus far only two genes, *IHH* and *GDF5*, have been implicated in causing BDA1 of which the majority of the cases have been attributed to mutations in *IHH*.

1.3 The hedgehog signaling pathway

The hedgehog proteins (Hh) are evolutionary conserved morphogens that mediate many developmental programs including skeletal patterning, identity and growth. Three hedgehog genes, *Shh*, *Ihh* and *Dhh* are found in vertebrates, whereas only one homolog, *Shh*, exists in Drosophila. The hedgehogs undergo cleavage and lipid modification before they are secreted from the cell (reviewed in Gallet, 2011). The hedgehog signaling pathway is conserved from flies to mice. The current model of hedgehog signaling has been derived from its molecular interactions within the primary cilium, a highly specialized cell surface extension which senses external stimuli (reviewed in Huber and Cormier-Daire, 2012; Ryan and Chiang, 2012; Briscoe and Thérond, 2013). Genetic perturbations within this cellular compartment have associations with skeletal deficiencies and malformations, collectively known as the ciliopathies (Anderson et al., 2012).

The hedgehogs mediate intracellular signaling through its binding to Ptch1 (Figure 1.4). Without ligand, Ptch1 represses another transmembrane protein Smoothened (Smo) which promotes the cleaving of the transactivator glioma-associated

Figure 1.4. Vertebrate hedgehog signaling in the primary cilium. Adapted from Figure 2 of Anderson et al. (2012). The primary cilium is comprised of an intraflagellar transport (IFT) system that relies upon the central axoneme, a structure composed of doublet microtubules, the centrosome and basal bodies (gray), for the movement of cargo to and from the base of the cilium in a retrograde and anterograde fashion, respectively. The hedgehog (Hh) signaling pathway utilizes the IFT and its associated protein complexes to shuttle the main effector molecule glioma-associated oncogene family zinc finger 3 (Gli3) from the tip of the cilium to the base. **1.** In the absence of Hh, its receptor Patched-1 (Ptch1) keeps Smoothened (Smo) in a repressive state within cytoplasmic vesicles. The repressive state can also be achieved through the competitive binding of Hh to the antagonist hedgehog interacting protein, Hhip. Full-length Gli3 is found in association with suppressor of Fused (Sufu) and kinesin family member 7 (Kif7) at the tip of the cilium. The repression of Smo allows the Gli3-complex to migrate in a retrograde manner to the base of the cilium where the ubiquitination of Gli3 directs it to the proteosome for partial degradation into the repressive form Gli3-R. Gli3-R translocates to the nucleus to repress target gene transcription. **2.** In the presence of Hh binding to Ptch1 and to its co-modulators brother of Cdo/cell adhesion associated, oncogene regulated (Boc-Cdon) and growth arrest-specific 1 (Gas1), Ptch1 is internalized and **(3)** Smo which upon its release from the cytoplasmic vesicles is phosphorylated by G protein-coupled receptor kinase 2 (Grk2). This event recruits β-arrestin and kinesin family member 3A (Kif3a) to form an anterograde complex to transport Smo to the cilium tip. **4.** Smo relieves the repressive effects of Sufu on Gli3. Full-length and activated form Gli3 (Gli3-A) translocates to the nucleus where it activates target gene transcription. Anterograde movement is represented by a green dashed arrow. Retrograde movement is represented by a blue dashed arrow. Internalization is represented by a black dashed arrow.

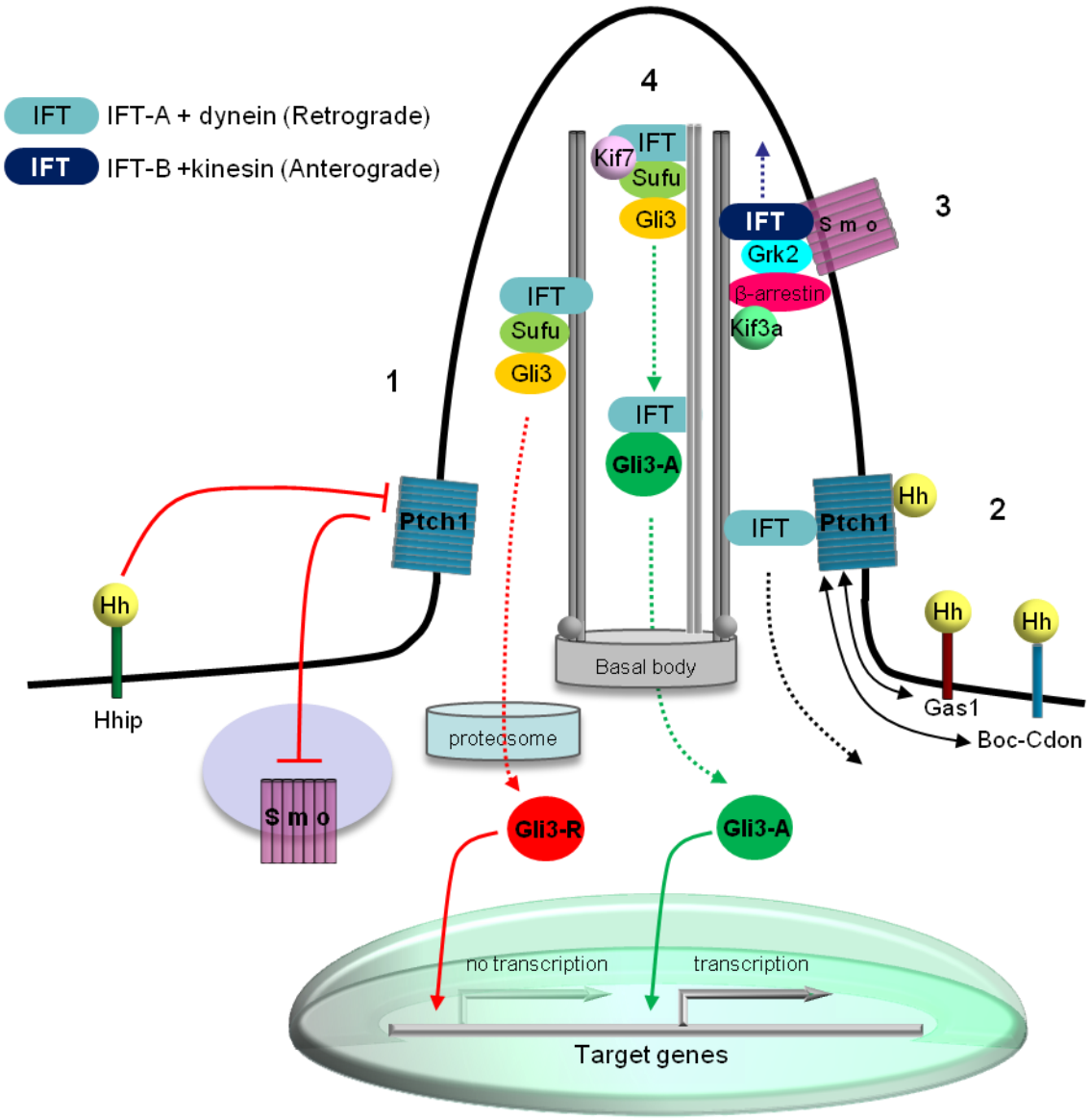
IFT
IFT-A + dynein (Retrograde)
IFT
IFT-B +kinesin (Anterograde)
4
IFT
Kif7
Sufu
Gli3
3
IFT
S m o
Grk2
β-arrestin
Kif3a
IFT
Sufu
Gli3
1
IFT
Gli3-A
Ptch1
IFT
Ptch1
Hh
2
Hh
Hh
Hh
Basal body
Gas1
Boc-Cdon
Hhip
proteasome
S m o
Gli3-R
Gli3-A
no transcription
transcription
Target genes

oncogene family zinc finger 3 (Gli3) into a repressive DNA binding factor. Upon hedgehog binding, Ptch1 triggers the release of Smo which results in the retention of full length Gli3 which then activates downstream transcriptional targets. The modifiers of hedgehog signaling include cell surface receptors Hhip, Boc, Cdon and Gas.

1.4 Embryonic limb development

Limb development in tetrapods involves highly coordinated and tightly regulated processes of limb mesenchymal initiation, specification, patterning, proliferation, cell death, and differentiation. These cellular processes will eventually form the proximal single skeletal element (stylopod), the middle two skeletal elements (zeugopod), and the distal skeletal elements (autopod) (Figure 1.5). The governing regulatory and signaling networks for each process are dynamically intertwined both spatially and temporally. These include the complex wiring of key transcriptional regulators Hox, Wnt, Bmp, Hh, and fibroblast growth factor (Fgf) proteins in facilitating the proper development of the limb (reviewed in Rabinowitz and Volkes, 2012). Mutations within the genes coding for and in regulating these proteins lead to congenital human limb malformations (Warman et al., 2011). Epigenetics also plays an important role in proper limb development and the proteins involved including chromatin remodelers, such as HDACs. Missense mutations in the histone deacetylase 8 gene (*HDAC8*) were found in a subset of patients diagnosed with Cornelia de Lange syndrome 5 (CDLS5; MIM #300882) which includes distal limb abnormalities (Deardorff et al., 2012). Moreover, the targeted deletion of *Atrx*, an ATP-dependent DNA helicase belonging to the SWI/SNF family of chromatin

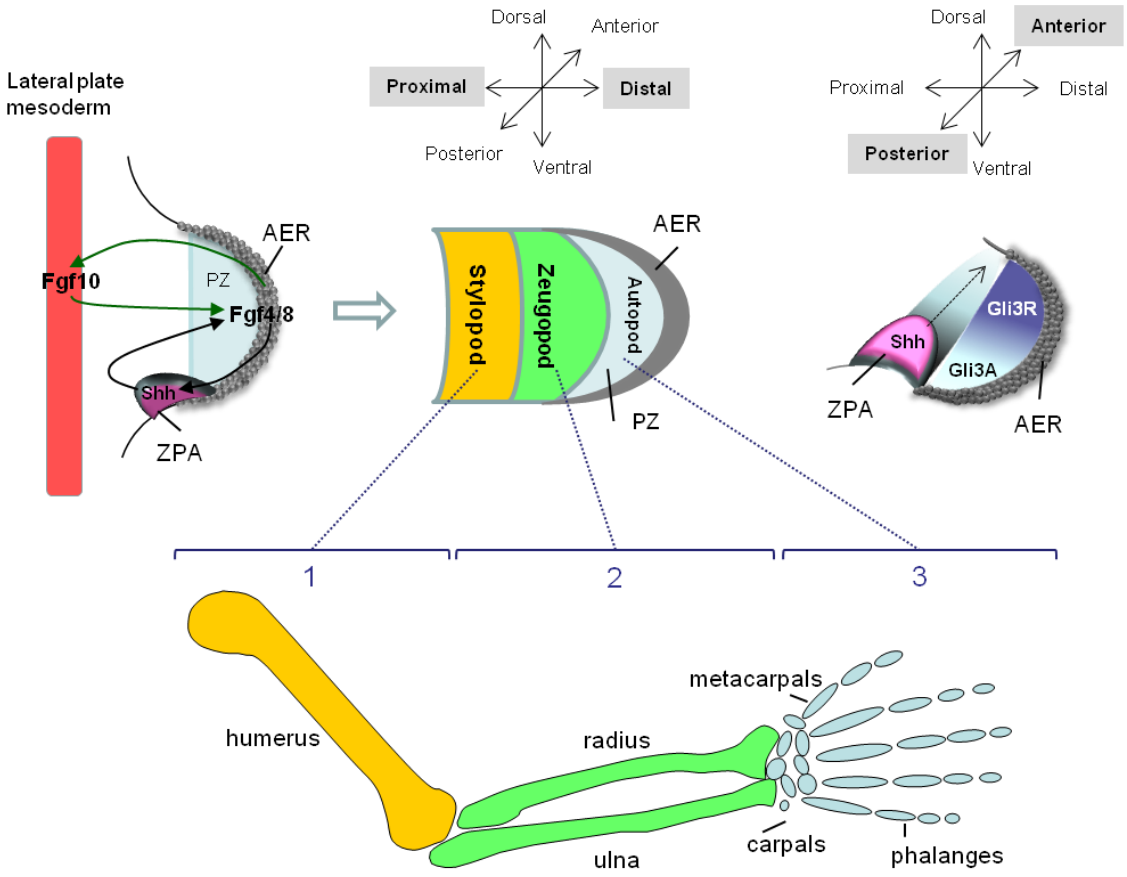

Figure 1.5. Limb development. The apical ectodermal ridge (AER) and the zone of polarizing activity (ZPA) are two major signaling structures in the limb bud (left schematic). The AER consists of specialized cells which secrete fibroblast growth factors Fgf4 and Fgf8. Signals from the lateral plate mesoderm, primarily Fgf10, maintains the production of Fgf4 and Fgf8 in a positive feedback loop (green arrows). The AER and ZPA are also regulated by a positive feedback loop (black arrows), created primarily of Fgf8 and sonic hedgehog (Shh). Both signaling structures drive the growth of mesenchymal cells in the progress zone (PZ). As the limb bud grows in the proximal-distal axis (middle schematic), the formation of future bone elements (bottom schematic) have been established in a linear order starting with the stylopod, followed by the zeugopod, then autopod through the movement of the progress zone in the distal direction (progress zone model). Digit growth and identity are driven by the Shh morphogen gradient in a posterior to anterior direction (right schematic). Shh and the activated form of Gli3 (Gli3A) are concentrated in the posterior region of the limb bud. The repressive form of Gli3 (Gli3R) is concentrated in the anterior portion of the limb bud.

remodelers, in mouse limb mesenchymal cells display shortened phalanges at later embryonic timepoints (Solomon et al., 2013). The extent and type of genetic perturbations which affect the chromatin landscape during human limb development is not fully understood.

The primary growth structure in limb development is the limb bud by which all future appendicular skeletal elements are formed (Figure 1.5). Molecular signals create spatial and temporal cues to direct its outgrowth in three spatial axis; namely, dorsal-ventral, proximal-distal, and posterior-anterior. Mapping the molecular pathways and inputs involved in limb bud outgrowth have largely been determined from "gain and loss of function" and embryological studies in chicken and mouse, specifically targeting and manipulating the limb bud at various developmental stages (reviewed in Tickle, 2006; Bénazet and Zeller, 2009; Dubok and Logan, 2011). Cell-fate mapping has identified the early specification signals within the somites responsible for positioning the limb buds of the embryo at the Hoxc5/Hoxc6 (future forelimb) and Hoxc9/Hoxc10 (future hindlimb) boundaries. The induction of the limb bud is driven by a combination of canonical Wnt/β-catenin signaling and T-box transcription factors such as Wnt2b and Tbx5 for the forelimb and Wnt2c and Tbx4 for the hindlimb. Extracellular signals such as Fgf10 and retinoic acid are also required for the initiation process (Sekine et al., 1999, Mic et al., 2004) thus proving that early molecular signals both establish and prime the cells destined to form the limb bud.

The limb bud consists of spatially and functionally distinct cellular compartments, an inner mesenchymal cell mass originating from the lateral plate mesoderm, and an outer ectodermal layer. The growth and patterning of the limb bud relies on at least two

highly specified cellular regions; namely, the apical ectodermal ridge (AER) and the zone of polarizing activity (ZPA). Both compartments depend on each other through a positive signaling feedback loop consisting of Fgfs and morphogens such as Shh. Experimental perturbations in either compartment result in limb malformations in both mouse and chicken models.

1.4.1 Proximal-distal growth

The AER is positioned along the dorsal-ventral boundary of the ectodermal layer of the limb bud and is the source of Fgfs, the primary driver of limb bud growth and patterning (reviewed in Pownall and Isaacs 2010). In the mouse, the dorsal-ventral boundary is shaped by two polarizing signals En1 and Wnt7a in the dorsal and ventral ectoderm, respectively. As a result of the loss of En1 which allows for the dorsal formation of ventral structures and the production of more than one AER in the limb bud, En1 restricts the expression of Wnt7a to the ventral ectoderm (Loomis et al., 1998).

Limb bud growth in the proximal-distal direction is mainly driven at the AER by two key fibroblast growth factors, Fgf4 and Fgf8. Fgf8 is associated throughout the AER and Fgf4 is expressed in the posterior half. The removal of the AER leads to a severe limb truncation which can be rescued by replacing the AER with Fgf soaked beads (Niswander et al., 1993). The Fgfs originating from the AER maintains the undifferentiated and proliferative state of the underlying limb mesenchyme. Although *Fgf8* expression is correlated with the physical appearance of the AER, the loss of *Fgf8* and/or conditional loss of *Fgf8*:*Fgf4* still results in the formation of a distinct AER (Sun et al., 2002). However, AER formation is dependent upon FGF10 expression in the early

limb mesenchyme of the ventral ectoderm, as *Fgf10* null embryos fail to develop an AER and have no *Fgf8* expression (Ohuchi et al., 1997; Sekine et al., 1999).

Early seminal work performed by Saunders (1948) and Summerbell and Wolpert (1973) in chicken embryos has demonstrated the necessity of the AER in properly forming the wing in a proximal-distal axis. They discovered that manipulations of the AER at different timepoints resulted in an ordered truncation of skeletal elements in a proximodistal axis; specifically, early excision resulted in the loss of very proximal skeletal elements such as the humerus while late excision resulted in the loss of more distal skeletal elements. Furthermore, the AER drives the proliferation of the inner mesenchymal cell mass through a positive feedback loop of Fgf8:Fgf10 signaling (Ohuchi et al., 1997; Sekine et al., 1999) which is mediated through the fibroblast growth factor receptor 2 (FgfR2). The conditional loss of *FgfR2* after limb bud initiation results in the formation of forelimbs without the distal skeletal elements (Lu et al., 2008), similar to the early observation seen when the AER was excised at later timepoints. Taken together these results support limb specification and patterning akin to the progress zone model of limb growth which was initially proposed by Summerbell and Wolpert (1973). As the limb grows outward, cells sequentially leave the mesenchymal progress zone, differentiate and first give rise to the proximal then distal skeletal structures. Thus digit formation under the progress zone model is specified at a relatively later developmental stage.

1.4.2 Anterior-posterior growth

The AER also contributes to limb growth in the anterior-posterior axis through interactions with the underlying posterior mesenchymal region of the limb bud which is

the zone of polarizing activity (ZPA). The AER and ZPA interact through signaling networks such as the Fgf:Wnt:β-catenin pathways (reviewed in Rabinowitz and Volkes, 2012). The ZPA is a source Shh which forms a morphogen gradient of high expression in the posterior with decreasing expression towards the anterior of the limb mesenchyme. The regulation of *Shh* expression is mainly achieved by its transcriptional regulators *Hox* and *Hand2* (Capellini et al., 2006; Galli et al., 2010), which in turn are both regulated by Gli3 (Litingtung et al., 2002; te Welscher et al., 2002). In the absence of Shh, Gli3 acts as a repressor of *Hand2*, *Gremlin* and *Hox* genes in the anterior limb mesenchyme. In contrast, the presence of Shh signal in the posterior compartment maintains the long activated form of Gli3. Hox5 aids in restricting Shh expression to the posterior compartment through its interaction with tumor repressor Plzf (Xu et al., 2013). The restrictive expression of Shh in the posterior limb is also under the influence of Fgfs through two ETS-box transcription factors; i.e., Etv4 and Etv5 (Mao et al., 2009, Zhang et al., 2009). As such, restrictive and permissive positional information in the limb mesenchyme allows for the patterning and the growth of the skeletal elements. Loss of *Shh* function results in the absence of posterior skeletal elements (Chiang et al., 2001; Kraus et al., 2001). Excising and re-transplanting the AER from a posterior to an anterior location on the chicken limb bud will result in the mirror image of the distal bones (Tickle et al., 1975) which suggests the developmental program for specifying the digits are located in the posterior-distal section of the limb bud. Thus Shh is an important specification factor for digit identity and limb mesenchymal proliferation through the formation and maintenance of the ZPA. In line with the discovery of the Shh morphogen gradient, several groups such as Tickle and Wolpert (2002) and Dudley et al. (2002)

proposed the early specification model for limb growth and patterning; i.e. the French Flag Model. The model suggests that limb mesenchymal cells are positioned and specified based on their exposure to morphogen concentration gradients.

1.5 Endochondral ossification

The skeletal system develops through one of two processes, either by intramembranous or endochondral ossification. Intramembranous ossification, a process which does not require a cartilage template (anlagen) to form bone, results in the formation of flat bones, such as the clavicles and the cranial bones of the skull, and contributes to fracture healing. It requires the direct differentiation of clustered mesenchymal cells within a fibrous connective tissue into osteoblasts which eventually forms an ossification center within a newly secreted and encapsulated bone matrix (reviewed in Franz-Odendaal et al., 2006). Long or tubular bones, such as those found in the hands, develop through the process of endochondral ossification (Figure 1.6). Through endochondral ossification, undifferentiated mesenchymal cells of the growing limb condense to form a primary scaffold which serves as a cartilaginous template for the future bone (reviewed in Mackie et al., 2011). At this stage, the essential transcriptional regulator of chondrogenesis is the SRY-box gene *Sox9*, whose inactivation in mice results in the absence of cartilaginous structures (Bi et al., 1999). This observation is complemented by the discovery of *SOX9* mutations in patients with campomelic dysplasia (MIM #114290), a severe chondrodysplasia with sex reversal (Foster et al., 1994; Kwok et al., 1995). At the core of the anlagen, chondroprogenitors eventually

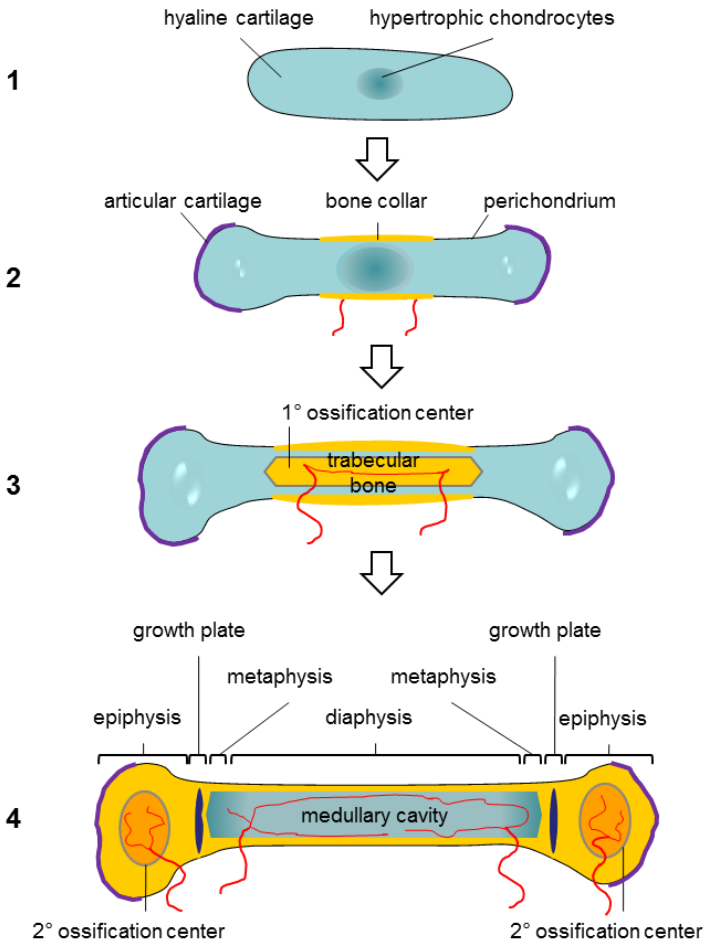

Figure 1.6. Bone development through endochondral ossification. Adapted from Pearson Education, Inc; Anatomical and histological organization of endochondral ossification; retrieved from http://www.slideshare.net/TheSlaps/dr-b-ch-05lectureresentation on September 20, 2014. **1.** Mesenchymal cells condense and differentiate into chondrocytes which secrete a cartilaginous matrix to form the hyaline cartilage template of the future bone. Chondrocytes found within the center of the template begin to enlarge (hypertrophy). **2.** As the chondrocytes continue to enlarge, osteoblasts found at the periphery of the cartilage begin to form the osteoid or bone collar. Blood vessels (red) begin to penetrate through the bone collar which allows osteoblasts and osteoclasts to enter into the diaphysis. Whereas the perichondrium encases the cartilage adjacent to the bone collar, the epiphyses are lined with articular cartilage. **3.** The primary ossification center is established when the hypertrophic chondrocytes undergo apoptosis and are replaced by the invading osteoblasts which then secrete a calcified matrix to from trabecular bone. **4.** Secondary ossification centers are established at the epiphyses of the growing bone. The growth plate becomes the only active region for bone growth. In adulthood, the growth plate becomes fused with the metaphysis and growth has ceased. The medullary cavity is highly vascularized and provides nutrients to and from the bone.

differentiate into chondrocytes and begin to secrete an extracellular matrix primarily consisting of collagen type 2 alpha 1 (Col2a1) and aggrecan. The specification of the core mesenchymal cells, destined to become chondroprogenitors, appears to be influenced by several restrictive signals originating from the dorsal-ventral ectoderm (Hurle and Gañan, 1986; Witte et al., 2009). Repressive WNT signals are also present at the interdigital space to contain chondrogenesis within the anlagen. Meanwhile, the cells at the periphery differentiate to establish a protective sheath, known as the perichondrium. The core and the periphery of the cartilage template contribute to the longitudinal and radial growth. Bone morphogenetic proteins, notably Bmps 2, 4 and 7, are positive regulators of patterning and condensation. They are mostly expressed in the interdigital space and their receptors are located in the mesenchymal condensations. Mutations which affect the members of the BMP family, their regulator Noggin and receptors Bmpr1b and Bmpr1a, interfere with chondrogenesis.

Chondrogenesis leads to the early formation of the primary ossification center of the developing bone (Figure 1.6). The proliferating chondrocytes at the center of the cartilage template eventually exit the cell cycle and differentiate into pre-hypertrophic chondrocytes. As the cartilage template elongates, the pre-hypertrophic chondrocytes enlarge and differentiate into hypertrophic chondrocytes. These terminally differentiated chondrocytes begin to secrete calcified matrix which triggers the invasion of blood vessels and osteoblasts from the perichondrium. The hypertrophic chondrocytes eventually undergo apoptosis and the calcified matrix is replaced by trabecular bone, giving rise to the diaphysis or shaft of the long bone. The chondrocytes at the distal ends of the cartilage template still maintain a proliferative state which allows for the growth of

the developing bone. Secondary ossification centers will eventually form at the distal ends of the long bone. At this stage, the longitudinal growth of the bone is restricted to the epiphyseal growth plate which is found between the primary and the secondary ossification centers until it finally fuses with the underlying metaphysis and calcifies at puberty.

1.6 Growth plate dynamics

The growth plate is organized into five histologically-defined compartments (Figure 1.7). At the distal ends of the long bone are reservoirs of resting chondrocytes, followed by a zone of proliferating chondrocytes, a compacted zone of pre-hypertrophic chondrocytes, a zone of hypertrophic chondrocytes, and finally the region known as spongy or trabecular bone. The key molecular markers that define these zones are illustrated in Figure 1.7 and reviewed in Kronenberg (2003) and Mackie et al. (2011).

One of the key paracrine regulators of bone development is Ihh. It coordinates chondrocyte differentiation and proliferation, as well as osteoblast differentiation. Ihh is mainly expressed in prehypertrophic chondrocytes and acts distally at the resting chondrocyte zone where its cognate receptor Ptch1 is expressed. In the absence of Ihh, Ptch1 inhibits the G-protein coupled receptor Smoothened (Smo). When Ihh is bound to Ptch1, Smo is de-repressed and activates downstream signaling events via the Gli family of transcription factors which lead to increased Pthlh expression (St. Jacques et al., 1999). Pthlh is expressed at the articular chondrocytes and diffuses across the growth plate to promote the proliferation of chondrocytes and to inhibit the differentiation of the prehypertrophic chondrocytes (Vortkamp et al., 1996; Kronenberg, 2003). As the bone

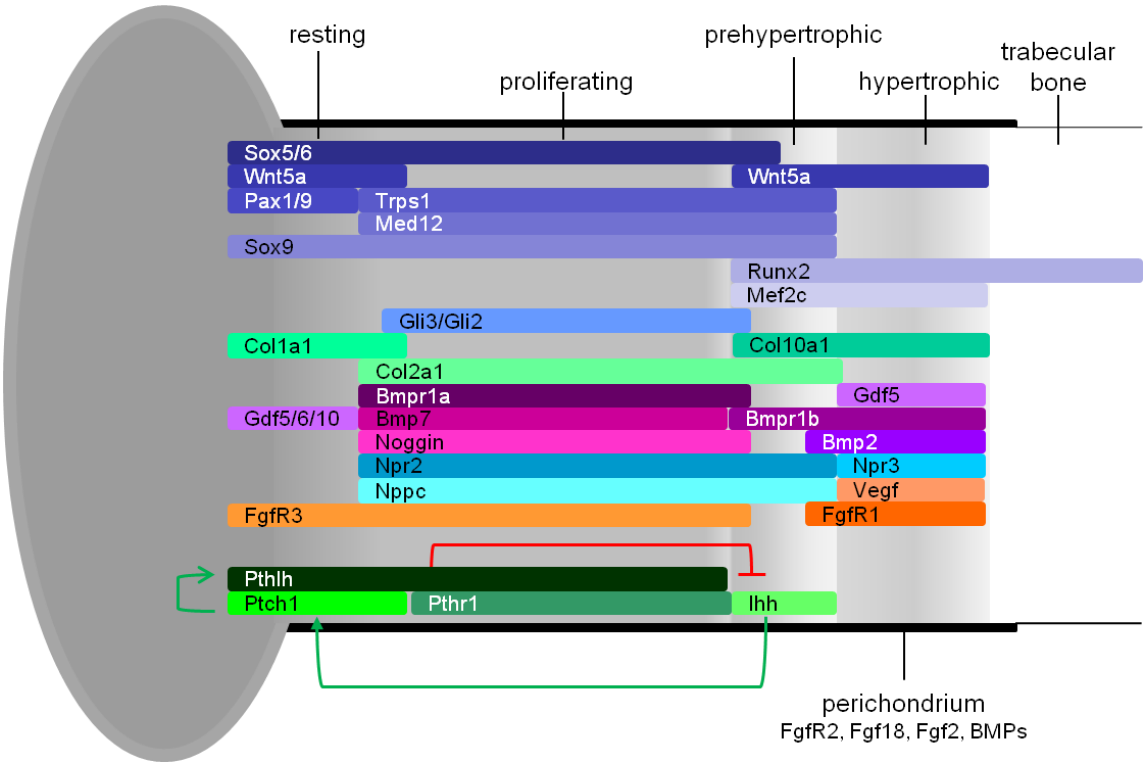

Figure 1.7. Expression profile of the growth plate. A longitudinal view of the growth plate showcasing several molecular markers that are primarily associated with the four chondrocyte zones (resting, proliferating, prehypertrophic, hypertrophic). The Ihh-Pthlh negative feedback loop which is a key component of bone growth is illustrated in green at the bottom section of the diagram. Ihh is produced in prehypertrophic chondrocytes, secreted, and targeted to Ptch1-expressing cells in the resting zone (green arrow). This elicits the secretion of Pthlh which binds to its receptor Pthr1 in the proliferating zone where it maintains the chondrogenic proliferative state and represses the production of Ihh (red line). As the bone lengthens through chondrocyte proliferation the Ihh signal weakens as the distance to its receptor in the resting zone increases, causing the release of the negative feedback loop on Ihh. The local expression of Ihh subsequently induces terminal differentiation into hypertrophic chondroctyes which eventually contributes to the formation of trabecular bone through apoptosis and osteoblast replacement.

lengthens the effect of Ihh-Pthlh negative feedback loop on distal chondrocytes decreases and triggers its differentiation into hypertrophic chondrocytes.

Not only do BMPs modulate the size of mesenchymal condensations, but they are also important regulators of chondrocyte proliferation and differentiation within the growth plate, specifically upregulating *Ihh* expression in prehypertrophic chondrocytes (Minina et al., 2001). In promoting *Ihh* expression, they inhibit FGF signaling by downregulating *FgfR1* in mice (Yoon et al., 2006). Similarly, a shift in the balance from differentiation to proliferation is achieved through the FGFs themselves. For example, FGFs 1, 2, 17 and 19 are predominantly expressed in human fetal growth plates and, with the exception of FGF-19, are capable of inhibiting chondrocyte proliferation via FGFR3 (Krejci et al., 2007). The essential role of FGFs in governing the size of the adult skeleton was proposed by Lazarus et al. (2007) when they identified increased *FGFR3* expression in older rat postnatal tibial growth plates.

The natriuretic peptide system also plays an important role in regulating bone growth. Natriuretic peptide C (Nppc) and its preferential receptor natriuretic peptide receptor 2 (Npr2) are expressed throughout the growth plate. Nppc promotes chondrogenesis in mesenchymal condensations by stimulating the synthesis of glycosaminoglycans (Woods et al., 2007). Moreover, *Nppc* null mice exhibit achondroplasia which mimics the human condition of severe dwarfism due to impaired endochondral ossification (Chushoo et al., 2001). The defect in mice can be reversed by the targeted overexpression of Nppc in an activated *FgfR3* mouse model of achondroplasia (Yasoda et al., 2004). Inactivating mutations in *NPR2* result in acromesomelic dysplasia of Maroteaux type (AMDM; MIM #602875), an autosomal

recessive skeletal dysplasia. *Npr2* null mice showed impaired endochondral ossification which resulted in severe reduction in vertebral and limb lengths (Tamura et al., 2004). Hume et al. (2009) suggested that *NPR2* missense mutations in patients with AMDM behaved as null alleles resulting from the failure of the protein's ability to travel across the endoplasmic reticulum.

1.7 Human digit formation

Human skeletal maturity can be assessed by the stage of ossification of the epiphyses of the hand bones (Gilsanz and Ratib, 2005). Each tubular bone of the hand contains two ossification centers, one located at the diaphysis and the other the epiyhysis. In the human embryo, all of the diaphyses of the tubular bones have calcified and only the epiphyses remain cartilaginous. At birth, ossification centers first appear at the wrist bones. The ossification centers at the epiphyses of the tubular bones generally appear in a predictable pattern at 10 months to 4 years of age; first, the proximal phalanges; second, the metacarpals; third, the middle phalanges and fourth, the distal phalanges. At the pre-pubertal phase, epiphyseal fusion to the metaphysis is first observed at the distal phalanges, then the metacarpals, followed by the proximal phalanges and finally the middle phalanges. Whereas the metacarpals of digits 2-5 exhibit ossification at its distal ends, ossification of the remaining tubular bones of the hands including the first metacarpal occurs at the proximal ends. By 19 years of age all of the hand bones have calcified and growth has ceased.

1.8 Digit development and the current model for BDA1

The developmental programs (reviewed in Suzuki, 2013) which govern the specification, patterning and identity of the digits are mainly driven by the co-linear expression of the *Hoxd10-Hoxd13* transcription factor gene cluster (Montavon et al., 2008 and 2011) which regulates the expression of Shh in the ZPA. The Shh gradient across the posterior-anterior plane is also involved in the early patterning and specificity of the digits (Ahn and Joyner, 2004; Towers et al., 2008). However, reaction-diffusion systems and Turing patterns, specifically looking at BMP-receptor dynamics, have been seriously considered as an alternative model to morphogen gradients for digit pattern formation (Badugu et al., 2012) because Turing patterns are not constrained to the domain size problem encountered with the morphogen gradient model. In contrast, digit elongation primarily depends on BMP-SMAD signaling at the digit crescent or phalanx forming region (PFR) to drive chondrogenesis in phalangeal condensations located behind this cellular compartment (Montero et al., 2008; Suzuki et al., 2008). Human mutations in the protein components of the BMP-SMAD signaling pathway support its role in phalangeal elongation as demonstrated by their association with the brachydactylies. Transgenic mouse models for BDA1 and BDB1 (MIM #113000) have further elucidated the roles of IHH and ROR2 in maintaining or forming the PFR by acting upstream of BMP signaling (Witte et. al., 2010). Thus the current model of BDA1 centers on the BMP-SMAD signaling pathway, and genetic perturbations associated with BDA1 result in reduced PFRs and mesenchymal condensations (Figure 1.8).

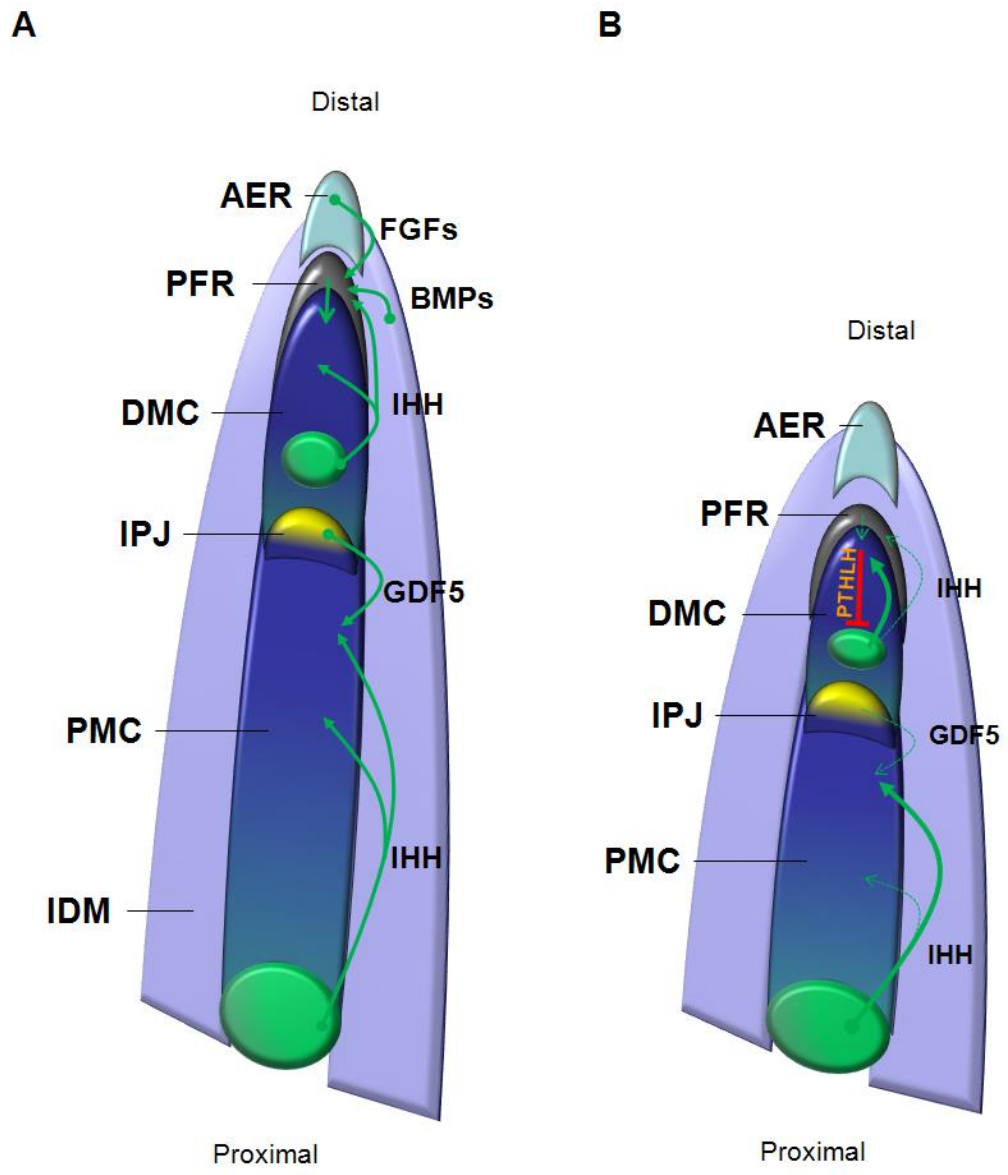

Figure 1.8. Digit formation and elongation model. (A) The primary driver for digit formation and elongation is the BMP-SMAD pathway at the phalanx forming region (PFR). BMPs from the interdigital mesenchyme (IDM), FGFs from the apical ectodermal ridge (AER), and IHH from prehypertrophic centers (green ovals) maintain the PFR. GDF5, located at the interphalangeal joint mesenchyme (IPJ), and IHH promote chondroprogenitor proliferation in the proximal and distal mesenchymal condensations (PMC and DMC, respectively). **(B)** BDA1-causing mutations in either IHH or GDF5 result in decreased proliferation in the PMC and DMC. Mutant IHH reduces the size of the PFR thereby decreasing the commitment of cells at the DMC. It further reduces the DMC size through its limited short range but enhanced long range signaling effects on PTHLH. The increased dose of PTHLH strongly inhibits IHH production. Green dashed arrows reflect positive but reduced effects.

1.9 The current state-of-the-art detection of Mendelian traits

Traditional positional cloning strategies, which use linkage analyses on multigenerational families, have elucidated many phenotype-genotype associations for Mendelian-based disorders. The catalogue of mutations causing human disorders and malformations in OMIM is a testament of the success of utilizing this approach. The current state-of-the-art of identifying Mendelian traits now rely upon microarray for copy number determination and the use of targeted genome enrichment of the whole exome, partial exome, such as in a disease gene panel, or a chromosomal region that is linked to a trait, coupled to a high-throughput sequencing (HTS) platform (reviewed in Carter, 2007; Lam et al., 2010; Metzker, 2010; Koboldt et al., 2012; Rabbani et al., 2012; Boycott et al., 2013). These technologies have garnered much interest in studying both Mendelian based disorders and in complex diseases because of the success in identifying coding and noncoding variants without heavily relying upon large kindreds for linkage analyses.

Although current technologies have improved upon the amount of sequence reads generated, the bioinformatics tools needed to align and identify disease-causing variants are still evolving. As the data culminated from sequenced personal genomes and exomes increases, there is also a need to classify sequence variants as rare, private or polymorphic and to annotate them with key genomic features in order to prioritize them as candidate functional variants. Genetic studies which involve Mendelian-based disorders can leverage the inheritance pattern, dominant or recessive, of a specific trait to aid in the identification of a candidate sequence variant present in either a heterozygous or homozygous state.

Chapter 2. Project goals

2.1 Rationale

Skeletal development is a complex and highly regulated process which involves the coordination of many regulatory networks in a spatiotemporal fashion. Congenital limb malformations can result from a molecular defect in any of these networks. Genetic manipulations in model organisms have revealed the conservation of various regulatory networks across vertebrates and the key signaling pathways at various stages of limb development, yet many human congenital limb malformations and joint disorders still have an unknown molecular cause. The formation of the distal skeletal elements is of interest to this thesis given the middle phalanges of the hands and/or feet are primarily the affected tissue compartments seen in BDA1. The study of human variation offers an opportunity to examine genotype-phenotype relationships and the study of Mendelian inherited traits such as BDA1 could lead to a better understanding of how specific tissue compartments and continuous traits such as digit length are impacted by mutations within a single gene. These insights could also highlight molecular pathways that are involved with diseased states, such as osteoarthritis (OA), and the normal processes of bone regeneration and healing.

2.2 Hypotheses

Current evidence suggests a convergence of the IHH and BMP signaling pathways in the pathology of brachymesophalangies. We hypothesize the association of BDA1 with mutations residing in the genes that code for receptor or secreted signaling proteins belonging to the BMP-SMAD pathway. Furthermore, we hypothesize that a novel gene within the *BDA1B* locus at chr5p13.3 is associated with this pathway.

2.3 Specific aims

1. To identify novel genes or novel mutations in either *IHH* or *GDF5* in a collection of 21 unrelated BDA1-affected families.
2. To identify the causative gene for BDA1 within the linked region at chromosome 5p13.3.

Chapter 3. Examining the mutation spectrum of *IHH* in causing BDA1

3.1 Preface

The majority of BDA1 cases are associated with heterozygous missense mutations in *IHH*. IHH is essential for proper skeletal development and specifically with regards to its role in the pathology of BDA1, middle phalangeal formation and elongation. As described in Chapter 1, the mutation spectrum of *IHH* encompasses two human conditions, BDA1 and ACFD to date. The location of the predicted amino acid substitutions causing BDA1 are clustered within a highly conserved 60 amino acid region within the N-terminal signaling peptide of IHH. Chapter 3 is dedicated to a published report on the discovery of 3 novel *IHH* mutations in a subset of our archived BDA1 families. The expanded repertoire of published *IHH* mutations observed in individuals affected with BDA1 strengthens the role of IHH in digit development, specifically targeting the middle phalanges. This chapter also illustrates the phenotypic variability associated with BDA1 mutations in *IHH* and presents the challenges in defining genotype-phenotype relationships. The manuscript has been re-formatted for its inclusion in this thesis with its figures and tables located after cited references. I have contributed to this paper by providing intellectual input as well as the technical work to sequence the three exons of *IHH* in Families 1, 2 and 3. I also provided the bioinformatics analyses and interpretation of the sequence variants found with the mutation screening of *IHH* for Figure 3.5. Consent forms are located in Appendix A.

3.2 Manuscript No. 1

Citation: Byrnes AM, Racacho L, Grimsey A, Hudgins L, Kwan AC, Sangalli M, Kidd A, Yaron Y, Lau YL, Nikkel SM, Bulman DE. Brachydactyly A-1 mutations restricted to the central region of the N-terminal active fragment of Indian Hedgehog. Eur J Hum Genet. 2009 Sep;17(9):1112-20.

Brachydactyly A-1 mutations restricted to the central region of the N-terminal active fragment of Indian Hedgehog

Byrnes A.M.[1,2], Racacho L.[1,2], Grimsey A.[1,2], Hudgins L.[3], Kwan A.C.[3], Sangalli M.[4], Kidd A.[5], Yaron Y.[6], Lau YL [7], Nikkel S.M.[8], Bulman D.E. [1,2,9]

Affiliations:

1 – Ottawa Health Research Institute, and the University of Ottawa Center for Neuromuscular Disease, Ottawa, Ontario, Canada
2 – Department of Biochemistry, Microbiology and Immunology, University of Ottawa, Ottawa, Ontario, Canada
3 – Department of Pediatrics, Division of Medical Genetics, Stanford University School of Medicine, Stanford, California
4 – Department of Obstetrics, Wellington Hospital, Wellington, New Zealand
5 – Central and Southern Regional Genetics Services, Wellington Hospital, Wellington, New Zealand
6 - Genetic Institute, Tel Aviv Sourasky Medical Center, Tel Aviv, Israel.
7 - Department of Paediatrics and Adolescent Medicine, University of Hong Kong, Hong Kong, China
8 – Department of Genetics, Children's Hospital of Eastern Ontario
9 – Department of Medicine, Division of Neurology, University of Ottawa, Ottawa, Ontario, Canada

Key words: Brachydactyly, Indian Hedgehog, mutational clustering

3.3 Manuscript Abstract

Mutations in the gene Indian Hedgehog (*IHH*) which cause brachydactyly A-1 (BDA1) have been restricted to a specific region of the N-terminal active fragment of Indian Hedgehog involving codons 95, 100, 131 and 154. We describe two novel mutations in codons 128 and 130, not previously implicated in BDA1. Furthermore, we identified an independent mutation at codon 131 and we also describe a New Zealand family which carries the "Farabee" founder mutation and haplotype. All of the identified BDA1 mutations occur in a restricted area of the N-terminal active fragment of IHH and are in contrast to those mutations causing autosomal recessive acrocapitofemoral dysplasia whose mutations are located at the distal N- and C-terminal regions of IHH-N and are physically separated from the BDA1 causing mutations. With multiple independent mutations in codons 95, 100 and now 131, this would implicate a discrete function to this region of the protein. Finally, we present a clinical review of all reported and confirmed cases of BDA1, highlighting features of the disorder which add to the spectrum of *IHH* mutations.

3.4 Introduction

Type A1 brachydactyly (BDA1 MIM 112500) is characterized by shortness of all middle phalanges of the hands and toes, occasional terminal symphalangism, shortness of the proximal phalanges of the first digit, and short stature. While BDA1 can occur as an isolated malformation [1-7], it has also been described as part of complex syndromes, with some of the most commonly reported associated disorders being nystagmus [8,9], developmental delay, mental retardation [8-10], and scoliosis [8,11,12].

BDA1 has the distinction of being the first disorder to be described as an autosomal dominant Mendelian trait in humans[13]. Mutations in the Indian Hedgehog gene (*IHH*) were initially identified in three Chinese BDA1 families[14], and a second locus has been mapped to 5p13.3-p13.2 [15] (MIM 607004). Furthermore, both *IHH* and the chromosome 5p13.3-p13.2 region were excluded in at least one other BDA1-affected family, implicating at least one additional locus in the development of BDA1 [16]. In addition to dominant mutations causing BDA1, recessive mutations in *IHH* cause acrocapitofemoral dysplasia (ACFD; MIM 607778) [17]. These patients presented with short stature, BDA1, and cone-shaped epiphyses of the tubular bones of the hands and the proximal end of the femur [17]. The cone-shaped epiphyses appeared early in childhood and disappeared with premature fusion of the growth plate.

In the *Ihh*$^{-/-}$ mouse, the loss of Ihh signaling results in a limb reduction phenotype with a complete lack of osteoblast development in all bones that develop by endochondral ossification [18], highlighting the role played by Ihh in cartilage differentiation and bone formation. Furthermore, an inversion of the sonic hedgehog

locus has been shown to yield a murine brachydactyly phenotype in heterozygotes via a gain of function effect [19].

In 1903, Farabee described a large family from Pennsylvania with BDA1 [13] and a few years later, three additional BDA1-affected families of English ancestry were described by Drinkwater [2-4]. Descendants of Farabee's original family and two of the Drinkwater families were found to share a common *IHH* mutation resulting in a p.Asp100Asn amino acid substitution. In addition, these families shared a common haplotype flanking *IHH*, indicating that they share a common founder [20,21].

The only reported BDA1-causing mutation not restricted to codons 95, 100 and 131 of *IHH*, is p.Thr154Ile [22]. All four of these codons are highly conserved (Figure 3.1). Multiple mutations in codons 95 and 100 indicate that these codons may be mutational hot spots; moreover, their proximity to one another suggests that they may reside in a region of IHH that is of particular importance responsible for the normal functioning of the growth plate during bone development.

3.5 Materials and Methods

Four BDA1-affected families of diverse ethnic and regional backgrounds were studied. In all cases, the disease was inherited as an autosomal dominant trait. Diagnosis was based on physical examination, radiographic findings when available, and family history. The study was approved by the Children's Hospital of Eastern Ontario Ethics Review Committee. After receiving informed consent, genomic DNA was extracted from peripheral venous blood or saliva samples with a QIAamp DNA blood mini-kit

(Qiagen, Valencia, California) or an Oragene DNA self-collection kit (DNA Genotek, Ottawa, Ontario).

Sequence analysis

All three exons of *IHH,* including flanking splice sites and untranslated regions, were amplified by PCR and sequenced using primers and conditions described previously [20]. The single-exon gene *NOGGIN* was amplified and sequenced as described above. All primers and optimized conditions are described in Supplementary Table S3.1.

Restriction enyme digestion

To detect the c.383G>A or the c.389C>A nucleotide change in the *IHH* gene, exon 2 was amplified by PCR and subsequently digested, according to manufacturer's instructions, with *Pst*I or *BstE*II respectively. Products were loaded onto a 1.5% agarose gel containing ethidium bromide, electrophoresed for 40 minutes at 100 V, and photographed under UV light. This procedure was repeated with 200 control DNA samples for both c.383G>A and c.389C>A.

Microsatellite markers

Seven markers from Marshfield's sex-averaged genetic map were examined (D2S2250, D2S433, D2S163, D2S1242, D2S424, D2S1323, and D2S126) along with two single nucleotide polymorphisms (SNPs) located upstream of exon 1 (rs437512, rs1960326) and 3 SNPs in exon 3 (rs3731881, rs394452, rs3099) of *IHH*. Genotyping was performed as described previously [20].

3.6 Results

Individuals from four families of diverse ethnic and regional backgrounds were examined for mutations within *IHH*. While sporadic cases of BDA1 have been reported, all of the families presented here show an autosomal dominant pattern of inheritance.

Family 1

Four members of an American family with BDA1 segregating in at least four generations were examined. The family's ancestors are of German, Scottish and Irish descent, with most of the migrants settling in the southern U.S. The family was ascertained when an ultrasound revealed short limbs in a third-trimester fetus. The family was referred to Stanford University Medical Center where the proband (individual 1-01 in Figure 3.2), the 43-year-old father of the fetus, was diagnosed with BDA1 on the basis of clinical and radiographic evaluations (Figure 3.3). The middle phalanges were very short, especially those in digits two and five. The proximal phalange of digit one was also quite short. The proband had short arms, but normal stature at 5'10" (175 cm) tall. Other phenotypic findings included limited dorsiflexion of the feet and tarsal coalition. The proband's father (individual 1-03 in Figure 3.2) and the father's sibling were also reportedly affected with BDA1. The father's sibling had an affected child, who in turn had three affected children. One of the children was reported to have a "problem with the palate" that did not require repair. No further abnormalities were described in the family.

The presence of tarsal coalition in the proband drew attention to the candidate gene *NOGGIN*, but no polymorphisms or sequence variants were identified in the proband's DNA. However, sequencing of the *IHH* gene revealed a novel heterozygous

c.383G>A nucleotide change in the DNA of individuals 1-01 and 1-03 (Figure 3.4A). Only the affected family members carried this nucleotide change, which results in a p.Arg128Gln amino acid substitution. The c.383G>A nucleotide change, which creates a *Pst*I restriction site, was not observed in any of the 400 control chromosomes evaluated.

Family 2

Three members of a family of Indian descent with BDA1 segregating in at least three generations were examined. The proband (individual 2-01 in figure 3.2) was referred to the University of Hong Kong's Queen Mary Hospital, where he was diagnosed with BDA1 based on clinical evaluations. Radiographs were not available. The middle phalanges were described as being very short, and images of the proband's flexed hands revealed that the middle phalanges in digits two and five were likely missing or fused to the terminal phalange as only one interdigital joint was visible. This individual had a more severe form of BDA1 associated with distal symphalangism, scoliosis, and club foot. Interestingly, all of the proband's blood relatives on his father's side were reported to have BDA1. DNA was obtained from the proband, his affected brother, and an affected cousin (individuals 2-02 and 2-03 in Figure 3.2).

A novel heterozygous c.389C>A nucleotide change was identified in the DNA of individual 2-01 (Figure 3.4B). To determine if this change co-segregated with affected status in this family, the DNA of all three available family members was screened by restriction digest with *BstE*II. Analysis revealed that all affected individuals carried the c.389C>A nucleotide change, which results in p.Thr130Asn amino acid substitution. The c.389C>A nucleotide change was not observed in any of the 400 control chromosomes evaluated.

Family 3

Three members of an Ashkenazi Jewish family residing in Israel with BDA1 reportedly segregating in at least four generations were examined. The family was ascertained when the 34-year-old female proband (individual 3-01 in Figure 3.2) was referred to the Tel Aviv Sourasky Medical Center in Tel Aviv, Israel for preimplantation genetic diagnosis of BDA1 prior to undergoing *in vitro* fertilization. The proband was diagnosed with BDA1 based on clinical and radiological findings (Figure 3.3). The middle and distal phalanges were replaced with a single small chess-pawn shaped bone in digits 2-5, and she had very short proximal and distal phalanges in digit one. Her mother was also affected. No further abnormalities were described in this family. In *IHH* a heterozygous c.391G>A nucleotide change was observed in the DNA of 3-01 (Figure 3.4C). Sequence analysis revealed that only the affected individuals carried the nucleotide change, which results in a p.Glu131Lys amino acid substitution. As this nucleotide change has been previously associated with BDA1 in a Chinese family [14], no control individuals were screened for this change.

Family 4

Seven members of a New Zealand family with BDA1 segregating as an autosomal dominant, fully penetrant disorder in at least eight generations were examined. The family's ancestors originated from England, with branches of the family settling in both Australia and New Zealand. The 35-year-old female proband (individual 4-01 in Figure 3.2) initially came to attention following a referral to the genetics clinic for evaluation of her short fingers. Radiographic analysis revealed absent middle phalanges in digits 2-5 in both the hands and feet, as well as shortened proximal phalanges in digit one (Figure 3.3).

There was a single interphalangeal joint in each digit, and the proband could not bend her thumbs. Other clinical findings included syndactyly of the second and third toes, aching back and knees, hallux vulga, and absent lateral incisors. Her height was 163cm, 25th-50th percentile.

On examination at 59 years of age, the proband's affected mother (individual 4-02 in Figure 3.4) presented with pain in the lower back, knees, toes and arches of feet. Other clinical features observed in the extended family included lumbar lordosis, extra teeth, and a shortened fifth metacarpal (Table 3.1). Within *IHH* a heterozygous c.298G>A nucleotide change was present in the DNA of individuals 4-01 and 4-02. All six affected family members were found to be carrying the c.298G>A change (Figure 3.4D), which results in a p.Asp100Asn amino acid substitution. As this mutation has been previously reported in the Farabee [21] and Drinkwater [20] pedigrees, no control individuals were screened. Based on reports that the family's ancestors were from England, a possible association of the New Zealand kindred to the Drinkwater and Farabee families was addressed by evaluating whether affected members carried the same ancestral haplotype. Seven polymorphic markers and five SNPs spanning a 4.82 cM region flanking the *IHH* gene were studied. When compared to the DNA of the Drinkwater and Farabee families, a common shared haplotype was observed between markers D2S2250 and D2S1323 (data not shown). Three synonymous exonic polymorphisms were detected in the sequence, all of which were present in the NCBI single nucleotide polymorphism (SNP) database (Build 129).

3.7 Discussion

Indian hedgehog is best known for its role in mediating condensation, growth and differentiation of long bone cartilage templates [23] and mutations in the gene are known to cause the dominant and recessive disorders BDA1 and ACFD, respectively. We have investigated the possibility that mutations in *IHH* were responsible for BDA1 in four families of diverse geographical and ethnic origins presenting with varying phenotypes.

We identified a novel heterozygous c.383G>A mutation in family 1. This nucleotide change causes a novel p.Arg128Glu amino acid substitution. Individual 1-01 presented with a complex BDA1 phenotype that included short arms, tall stature, tarsal coalition and limited dorsiflexion, none of which were seen in the other three families described here. Tall stature with BDA1 has been previously described (Table 3.1) [11]. Mesomelic shortening of the limbs has also been described in a family with Osebold-Remondini Syndrome, also referred to as brachydactyly type A6 (MIM 112910) [24]. Affected individuals in the family had small or absent middle phalanges, radial deviation of index fingers, and abnormal carpal and tarsal bones. In addition to investigating *IHH*, the candidate gene *NOGGIN* was excluded in this family. Heterozygous missense and nonsense *NOGGIN* mutations have been found to cause multiple synostoses syndrome, proximal symphalangism, and carpal-tarsal coalition syndrome, all of which present clinically with symphalangisms and/or carpal-tarsal fusions [25-28]. A phenotype of BDA1, normal stature and short arms seen with a novel p.Arg128Glu mutation indicates that the BDA1 phenotype associated with *IHH* mutations may not be restricted to the middle phalanx.

We also identified a novel heterozygous c.389C>A mutation in family 2, a family of Indian descent. This mutation co-segregated with the BDA1 phenotype in the family, and causes a novel p.Thr130Asp amino acid substitution. However, the proband also presented with distal symphalangism, scoliosis, and club foot. Interestingly, a heterozygous c.391G>A mutation was identified in family 3, a family of Ashkenazi Jewish descent residing in Israel. An identical nucleotide change has been previously reported in a Miao Chinese kindred affected with BDA1 [14]. The nucleotide change causes a p.Glu131Lys amino acid substitution in a residue which is highly conserved in many hedgehog proteins (Figure 3.1). As these two families hail from different regional and ethnic backgrounds, it seems unlikely that this mutation is the result of a common ancestor. Rather, the variant likely occurred independently resulting in BDA1 in both families, indicating that c.389C may represent a mutational hot spot in *IHH*. Affected individuals in the Chinese family were reported to be missing the middle phalanges in digits 2-5, and radiographs show the presence of the same chess pawn-shaped distal bone observed in affected individuals in the Israeli family. This phenotype, which is common to both families, suggests a particularly important role for Glu131 in IHH function throughout skeletal development.

In 1933, Nissen reported a BDA1 family that emigrated from England to Australia around 1840 [29], with one branch subsequently migrating to New Zealand around 1850. Members of this branch were examined and found to have characteristic deformities similar to Drinkwater and Farabee's families [29]. The proband's aunt (family 4) was described at age 5 by Nissen, establishing that the remaining individuals examined here are descendants of that family [29]. Interestingly, affected members of the family

presented with remarkable phenotypic heterogeneity. All six affected members examined were shorter in stature than their unaffected siblings. Radiographs were not available for all members, but the degree of shortening of the middle phalanges and the presence or absence of distal symphalangism presumably account for some of the phenotypic heterogeneity observed in the family. Four of the six affected individuals examined had 2-3 syndactyly of the toes. Affected individuals 4-01 and 4-02 were missing lateral incisors, while affected individual 4-03 was reported to have extra teeth. Supernumerary teeth and dental anomalies have been previously described in conjunction with brachydactyly types B and E, angel-shaped phalangoepiphyseal dysplasia (ASPED), and autosomal recessive and dominant Robinow syndromes [30-33], but have not been associated with BDA1 to date. Interestingly, sonic hedgehog and its downstream targets Ptc and Gli1 have been clearly implicated in both murine and fish tooth development [34,35], however no role for IHH has been delineated. Family 4 was found to carry the historic c.298G>A (p.Asp100Asn) mutation, as well as the haplotype flanking the *IHH* gene common to the two Drinkwater families and the Farabee family, indicating that these families share a common founder [20,21]. This founder mutation is speculated to have originated at least twelve generations ago. To date, three other BDA1-affected families of Italian, American and Chinese descent have been found to share this same *IHH* mutation [21,36,37]. While it remains possible that the families of Italian and American descent may have originated from this same common founder, the Chinese mutation was found to be flanked by a different haplotype [37]. Another mutation affecting the same codon, c.300C>A, has also been associated with BDA1 in another Chinese family [14]. This nucleotide change caused a p.Asp100Glu amino acid substitution. The existence of

at least three independent mutations in this codon suggests that p.Asp100 may also represent a mutational hot spot.

With the exception of p.delE95 [7], all of the BDA1-causing *IHH* mutations are missense and are limited to a 59 amino acid region of the N-terminal active fragment (IHH-N) spanning codons 95 to 154. Including the two novel mutations described here, p.Arg128Glu and p.Thr130Asp, the three dimensional structure of IHH-N reveals that all of the BDA1-causing *IHH* mutations are restricted to the central region of IHH-N (Figure 3.5). In addition, the limited number of codons involved in the disease, borne out by multiple independent mutations in codons 95, 100 and now 131, suggests a discrete function for this region of the protein. This is in contrast to the *IHH* mutations known to cause autosomal recessive acrocapitofemoral dysplasia, which are located at the distal N- and C-terminal regions of IHH-N and are physically separated from the BDA1-causing *IHH* mutations (Figure 3.5). A phenotype of BDA1, average stature and short arms seen with a novel p.Arg128Glu mutation indicates that the phenotype of BDA1 may not be restricted to the middle phalanx. In a review of the published cases of BDA1 with *IHH* mutations (see Table 3.1), shortening of the middle phalanges of the hands was the mildest phenotype. In one family, the feet were reported to be normal, however lower limb x-rays were not provided in the paper [22]. The involvement of the phalanges and metacarpals (metatarsals) is quite variable even within the same family. Shortening of the first metacarpal, which is typically a distinguishing feature of brachydactyly type C, is a rare, but reported finding [37]. Generalized musculoskeletal complaints including arthritis were often reported as well as the more specific findings of clubfoot and scoliosis. The family described by Raff *et al.,* has not had a mutation reported to date,

but the x-rays and clinical photos of the hands clearly demonstrate BDA1 [12]. Their family has associated abnormal menisci and scoliosis that was well documented. The identification of the causative gene in this family may provide insight to the phenotypic variability in some of the other families. In the extended Dutch family with ACFD [17], the carrier parents were noted to have phalangeal shortening when formally measured. The pattern would be consistent with a mild BDA1. Although short stature has been used in the definition of BDA1, in reviewing the reported cases, this is clearly not always the case. Farabee had noted the short stature in his initial paper, however in later generations, the height of affected family members is unremarkable in comparison to their unaffected relatives.

3.8 Acknowledgements

The authors would like to thank the families for their participation and Dr. John Christodoulou for his help in arranging the examination of two patients. This work was funded by the Canadian Institutes of Health Research (DEB). LR is funded by an Ontario Graduate Studentship.

3.9 Cited References

1 Armour CM, Bulman DE, Hunter AG: Clinical and radiological assessment of a family with mild brachydactyly type A1: the usefulness of metacarpophalangeal profiles. *J. Med. Genet.* 2000; **37**: 292-296.

2 Drinkwater H: An Account of a Brachydactylous Family. *Proc. Roy. Soc. Edin.* 1908; **28**: 35-57.

3 Drinkwater H: Account of a family showing minor brachydactyly. *J. Genet.* 1912; **2**: 21-40.

4 Drinkwater H: A second brachydactylous family. *J. Genet.* 1915; **4**: 323-339.

5 Haws DV, McKusick VA: Farabee's brachydactylous kindred revisited. *Bull. Johns Hopkins Hosp.* 1963; **113**: 20-30.

6 Yang X, She C, Guo J *et al*: A locus for brachydactyly type A-1 maps to chromosome 2q35-q36. *Am. J. Hum. Genet.* 2000; **66**: 892-903.

7 Lodder EM, Hoogeboom AJ, Coert JH, de Graaff E: Deletion of 1 amino acid in Indian hedgehog leads to brachydactylyA1. *Am. J. Med. Genet. A* 2008; **146A**: 2152-2154.

8 Slavotinek A, Donnai D: A boy with severe manifestations of type A1 brachydactyly. *Clin. Dysmorphol.* 1998; **7**: 21-27.

9 Tsukahara M, Azuno Y, Kajii T: Type A1 brachydactyly, dwarfism, ptosis, mixed partial hearing loss, microcephaly, and mental retardation. *Am. J. Med. Genet.* 1989; **33**: 7-9.

10 Grange DK, Balfour IC, Chen SC, Wood EG: Familial syndrome of progressive arterial occlusive disease consistent with fibromuscular dysplasia, hypertension, congenital cardiac defects, bone fragility, brachysyndactyly, and learning disabilities. *Am. J. Med. Genet.* 1998; **75**: 469-480.

11 Sillence DO: Brachydactyly, distal symphalangism, scoliosis, tall stature, and club feet: a new syndrome. *J. Med. Genet.* 1978; **15**: 208-211.

12 Raff ML, Leppig KA, Rutledge JC, Weinberger E, Pagon RA: Brachydactyly type A1 with abnormal menisci and scoliosis in three generations. *Clin. Dysmorphol.* 1998; **7**: 29-34.

13 Farabee WC. Hereditary and sexual influences in meristic variation: A study of digital malformations in man: Anthropology. Boston, Harvard University, 1903.

14 Gao B, Guo J, She C *et al*: Mutations in IHH, encoding Indian hedgehog, cause brachydactyly type A-1. *Nat. Genet.* 2001; **28**: 386-388.

15 Armour CM, McCready ME, Baig A, Hunter AG, Bulman DE: A novel locus for brachydactyly type A1 on chromosome 5p13.3-p13.2. *J. Med. Genet.* 2002; **39**: 186-188.

16 Kirkpatrick TJ, Au KS, Mastrobattista JM, McCready ME, Bulman DE, Northrup H: Identification of a mutation in the Indian Hedgehog (IHH) gene causing brachydactyly type A1 and evidence for a third locus. *J. Med. Genet.* 2003; **40**: 42-44.

17 Hellemans J, Coucke PJ, Giedion A *et al*: Homozygous mutations in IHH cause acrocapitofemoral dysplasia, an autosomal recessive disorder with cone-shaped epiphyses in hands and hips. *Am. J. Hum. Genet.* 2003; **72**: 1040-1046.

18 St-Jacques B, Hammerschmidt M, McMahon AP: Indian hedgehog signaling regulates proliferation and differentiation of chondrocytes and is essential for bone formation. *Genes Dev.* 1999; **13**: 2072-2086.

19 Niedermaier M, Schwabe GC, Fees S *et al*: An inversion involving the mouse Shh locus results in brachydactyly through dysregulation of Shh expression. *J. Clin. Invest.* 2005; **115**: 900-909.

20 McCready ME, Sweeney E, Fryer AE *et al*: A novel mutation in the IHH gene causes brachydactyly type A1: a 95-year-old mystery resolved. *Hum. Genet.* 2002; **111**: 368-375.

21 McCready ME, Grimsey A, Styer T, Nikkel SM, Bulman DE: A century later Farabee has his mutation. *Hum. Genet.* 2005; **117**: 285-287.

22 Liu M, Wang X, Cai Z *et al*: A novel heterozygous mutation in the Indian hedgehog gene (IHH) is associated with brachydactyly type A1 in a Chinese family. *J. Hum. Genet* .2006; **51**: 727-731.

23 Vortkamp A, Lee K, Lanske B, Segre GV, Kronenberg HM, Tabin CJ: Regulation of rate of cartilage differentiation by Indian hedgehog and PTH-related protein. *Science* 1996; **273**: 613-622.

24 Osebold WR, Remondini DJ, Lester EL, Spranger JW, Opitz JM: An autosomal dominant syndrome of short stature with mesomelic shortness of limbs, abnormal carpal and tarsal bones, hypoplastic middle phalanges, and bipartite calcanei. *Am J. Med. Genet.* 1985; **22**: 791-809.

25 Dixon ME, Armstrong P, Stevens DB, Bamshad M: Identical mutations in NOG can cause either tarsal/carpal coalition syndrome or proximal symphalangism. *Genet. Med*. 2001; **3**: 349-353.

26 Gong Y, Chitayat D, Kerr B *et al*: Brachydactyly type B: clinical description, genetic mapping to chromosome 9q, and evidence for a shared ancestral mutation. *Am. J. Hum. Genet.* 1999; **64**: 570-577.

27 Mangino M, Flex E, Digilio MC, Giannotti A, Dallapiccola B: Identification of a novel NOG gene mutation (P35S) in an Italian family with symphalangism. *Hum. Mutat.* 2002; **19**: 308.

28 Takahashi T, Takahashi I, Komatsu M *et al*: Mutations of the NOG gene in individuals with proximal symphalangism and multiple synostosis syndrome. *Clin. Genet.* 2001; **60**: 447-451.

29 Nissen KI: A Study in Inherited Brachydactyly. *Annals of Eugenics* 1933; **5**: 281-301.

30 Gorlin RJ, Sedano HO, Odont: Cryptodontic brachymetacarpalia. *Birth Defects Orig. Artic. Ser.* 1971; **7**: 200-203.

31 Holder-Espinasse M, Escande F, Mayrargue E *et al*: Angel shaped phalangeal dysplasia, hip dysplasia, and positional teeth abnormalities are part of the brachydactyly C spectrum associated with CDMP-1 mutations. *J. Med. Genet.* 2004; **41**: e78.

32 Hunter AG, McAlpine PJ, Rudd NL, Fraser FC: A 'new' syndrome of mental retardation with characteristic facies and brachyphalangy. *J. Med. Genet.* 1977; **14**: 430-437.

33 Robinow M, Silverman FN, Smith HD: A newly recognized dwarfing syndrome. *Am. J. Dis. Child*. 1969; **117**: 645-651.

34 Cobourne MT, Miletich I, Sharpe PT. Restriction of sonic hedgehog signalling during early tooth development. *Development* 2004; **131**: 2875-2885.

35 Fraser GJ, Bloomquist RF, Streelman JT: A periodic pattern generator for dental diversity. *BMC Biol.* 2008; **6**: 32.

36 Giordano N, Gennari L, Bruttini M *et al*: Mild brachydactyly type A1 maps to chromosome 2q35-q36 and is caused by a novel IHH mutation in a three generation family. *J. Med. Genet.* 2003; **40**: 132-135.

37 Zhu G, Ke X, Liu Q *et al*: Recurrence of the D100N mutation in a Chinese family with brachydactyly type A1: Evidence for a mutational hot spot in the Indian hedgehog gene. *Am. J. Med. Genet. A* 2007; **143**: 1246-1248.

3.10 Manuscript Figures, Tables and Legends

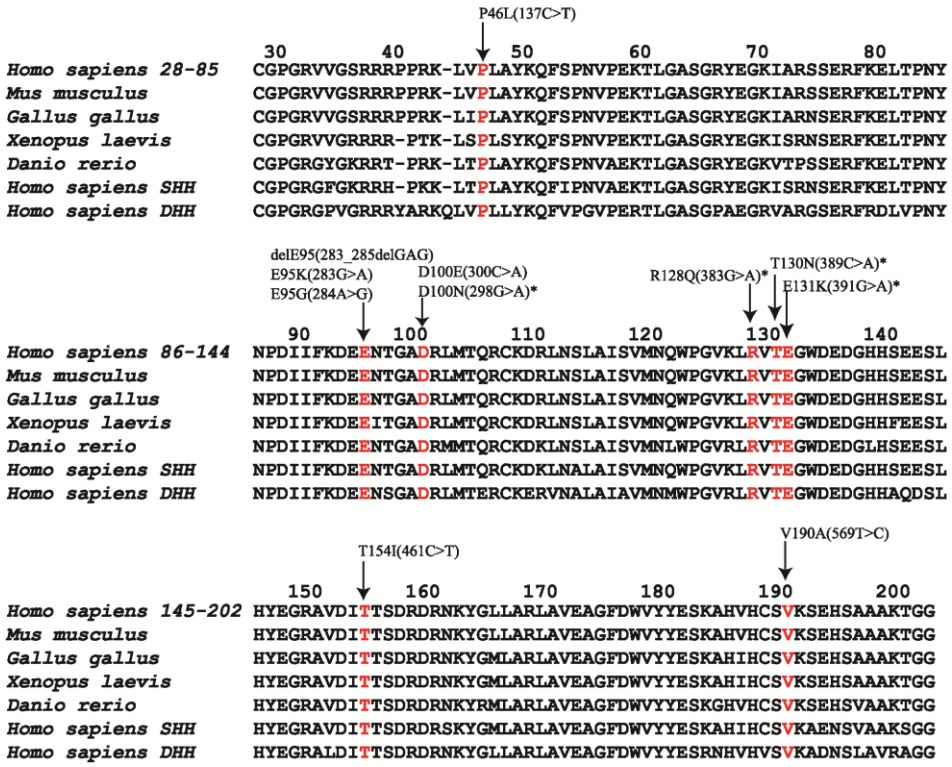

Figure 3.1. Alignment of the amino acid sequence of IHH with those of other species, as well as with human SHH and DHH. The amino acid sequence of human IHH was aligned with those of mouse Ihh, chicken Ihh, African clawed frog (banded hedgehog) and zebrafish (echidna hedgehog). The alignment has been anchored to the *Homo sapien* IHH amino acid sequence and the amino acid numbers are listed above. These were further aligned with the amino acid sequences of human SHH and DHH. Residues associated with disease are indicated by an arrow and by the wild type amino acids in red. Heterozygous mutations p.D100N, p.R128Q, p.T130N and p.E131K are associated with BDA1 in this study (denoted by an asterisk). Other BDA1-causing heterozygous mutations p.E95K, p.D100E, and p.E131K were described by Gao et al (2001); p.D100N was described by McCready et al (2002), Giordano et al (2003), and McCready et al (2005); p.E95G was described by Kirkpatrick et al (2003); p.T154I was described by Liu et al (2006); and p.delE95 was described by Lodder et al (2008). Homozygous mutations P46L and p.V190A were described by Hellemans et al (2003) and are associated with ACFD.

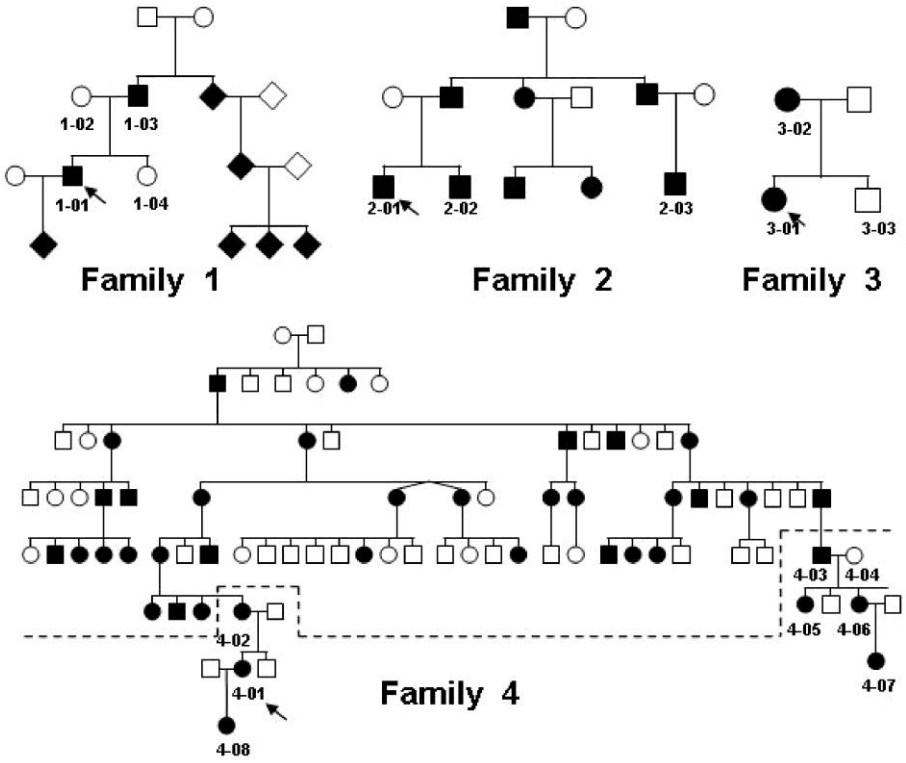

Figure 3.2. Pedigrees of four families with BDA1. Brachydactyly type A1 is transmitted as an autosomal dominant trait in all families. Probands are denoted by arrows. Numbers represent the sample number assigned to the DNA of individuals who participated in this study. Those members of family four above the dashed line represent members previously described by Nissen (1933).

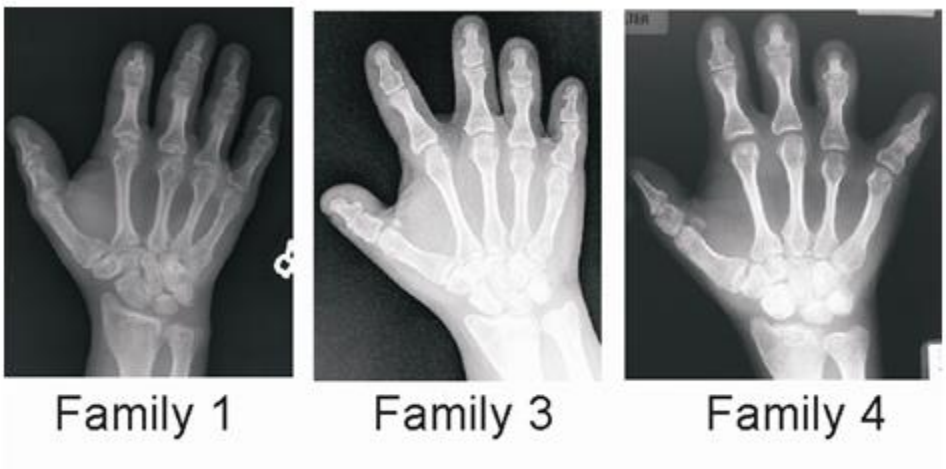

Figure 3.3. Hand radiographs of affected members of families 1, 3 and 4.

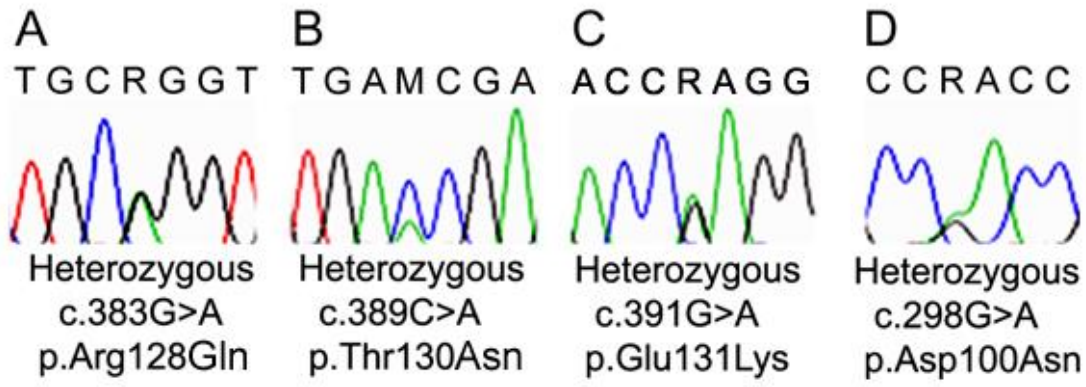

Figure 3.4. Mutations in IHH. (A) Family 1, c.383G>A; (B) Family 2, c.389C>A; (C) Family 3 c.391G>A; (D) Family 4, c.298G>A.

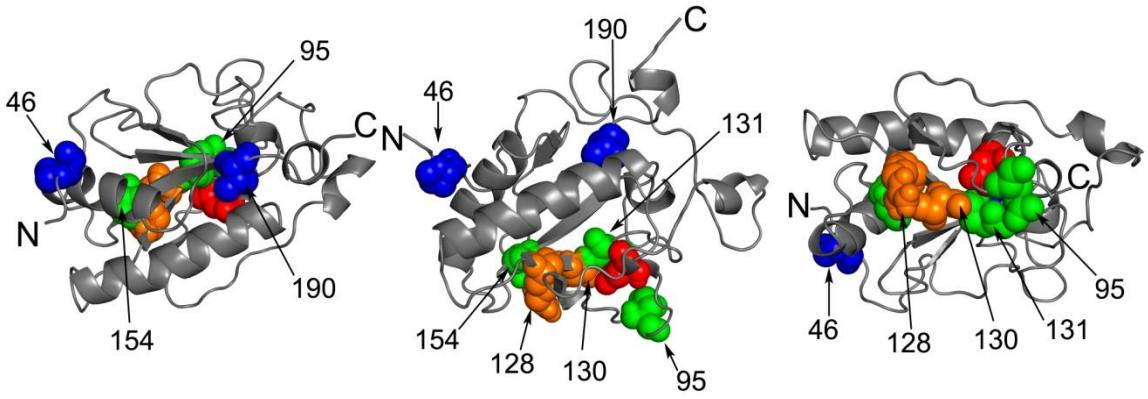

Figure 3.5. Three-dimensional reconstruction of the N-terminal active fragment of Indian hedgehog defining the positions of the amino acids whose mutation have been implicated in Brachydactyly type A1 or Acrocapitofemoral dysplasia pathogenesis. To compare the locations of the Indian Hedgehog mutations, the crystal structure of the amino-terminal domain of mouse Shh (1VHH.pdb) was used due to the its high similarity to IHH. The equivalent positions were utilized. Numbers indicate the amino acid positions. Shown: ACFD mutations (blue); BDA1 mutations at codon 100 (red), codons 95, 131 and 154 (green), and codons 128, 130 (orange). Amino-terminus (N) and carboxy-terminus (C) are indicated. The ribbons represent alpha-helices. The three representations are shown from a perspective where the N- and C-termini are: (A) closest to the viewer; (B) at the top of the molecule and; (C) furthest away from the viewer, projecting into the page. All of the BDA1 mutations appear to cluster in the central portion of IHH-N.

Table 3.1. Summary of mutations and clinical presentation in families with brachydactyly A-1. Allelic variants reported as of June 2009.

Mutation	Ethnic origin	Diagnosis	Associated unique or rare findings seen in some but not all family members	Reference:
c.283G>A p.E95K	Chinese	BDA1[a]	Severe shortening of distal phalanges	Gao et al. 2001/Yang et al. 2000 – family 1
c.284A>G p .E95G	Mexican	BDA1	nil	Kirkpatrick et al. 2003
c.298G>A p.D100N	British New Zealand Chinese Italian	BDA1 BDA1 BDA1 BDA1	Initial reports suggested short stature, not seen in later generations Non-specific knee and hip problems Non-specific musculoskeletal issues of lower limbs and back Short first metacarpal Short stature (not in all)	McCready et al. 2002/2005 (Farabee/Drinkwater family) This paper Family 4 (related to above) Zhu et al. 2007 Giordano et al. 2003
c.300C>A p.D100E	Chinese	BDA1	All affected of shorter stature	Gao et al. 2001 – family 3
c.383G>A p.R128Q	American	BDA1	Tarsal coalition Short arms with normal height	This paper Family 1
c.389C>A p. T130D	Indian	BDA1	Scoliosis and club foot	This paper Family 2
c.391G>A p. E131K	Chinese Ashkenazi Jewish	BDA1 BDA1		Gao et al. 2001/ Yang et al. 2000 family 2 This paper Family 3
c.461C>T p. T154I	Chinese	BDA1	Normal feet	Liu et al. 2006
?	American	BDA1	Discoid meniscus, scoliosis, degenerative arthritis of knees	Raff et al. 1998
c.137C>T p. P46L	Belgian	ACFD[b]	Hands resembling BDA1 Hand x-ray of carrier parent showing no obvious differences, but metacarpal-phalangeal profile not done	Hellemans et al. 2003/ Mortier et al. 2003 Family 1
c.569T>C p. V190A	Dutch	ACFD	More generalized Brachydactyly (all tubular bones involved)	Hellemans et al. 2003/ Mortier et al. 2003 Family 2

[a] BDA1 - Brachdactyly type A1 - defined as hypoplasia of middle phalanges of hands and feet with short proximal phalange of the first digit. The spectrum can include symphalangism of distal and middle phalanges and shortening of various metacarpals and metatarsals (typically 2-5)

[b] ACFD - Acrocapitofemoral Dysplasia – defined as short stature with Brachydactyly, narrow thorax, relative macrocephaly, cone shaped epiphyses, egg-shaped femoral head with short femoral neck

3.11 Manuscript Supplementary Information

Supplementary Table S3.1. **Oligonucleotide primer sequences** and amplification conditions for the genes Indian Hedgehog and Noggin.

***IHH* Exon**	**Primer Name**	**Primer Sequence**	**Primer Annealing Temperature**	**Final [$MgCl_2$] (mM)**	**Additive**	**PCR Product Size**
Upstream of exon 1	IHHsnp12-F	CGCACAGGGAGGAAAGG	60	1.5	---	237 bp
	IHHsnp12-R	GCAGGAGTGTCGGCATC				
1	IHHx1F	TGCCCATCAGCCCACCAG	62	1.5	Betaine	470 bp
	IHHx1R	GAGCGTGCCAGCCAGTCG	(40 cycles)			
2	IHHx2F	CGGCTGATTTCGCTCTG	63	1.5	---	394 bp
	IHHx2R	GGCGGGCTCTTCACCTT				
3	IHHx3.1F	AAGGGAGGGTCGTTGTG	65	1.5	---	494 bp
	IHHx3.1R	TTGTGAGCGGGGCGTAG				
3	IHHx3.2F	TGCTCTTTACGGCTGACAATC	64	1.5	---	531 bp
	IHHx3.2R	CAGAGGAGATGGCAGGAG				
3	IHHx3.3F	TGGGGCGTCTCCTGCTA	58	1.5	---	491 bp
	IHHx3.3R	GCATCGGGTCCAGCCAGA				
3	IHHx3.10F	GTATGGGTTCAAGCCTGCAT	50	1.5	---	569bp
	IHHx3.10R	GCCACGTGTGTAGAGACAGC	(Touchdown)			
***Noggin* Exon**	**Primer Name**	**Primer Sequence**	**Primer Annealing Temperature**	**Final [$MgCl_2$] (mM)**	**Additive**	**PCR Product Size**
5'UTR, Exon 1	Nog F2	ACCTCATCGAACACCCAGAC	60	1.5	---	572bp
	Nog R1.2e	CCGAGTTCTAGCACGAGCA				
Exon 1, 3'UTR	Nog CDS F	GCCAACTTGTGTGCCTTTCT	55	1.5	6% DMSO	999 bp
	Nog CDS R	GAGCGTGCCAGCCAGTCG				
	Nog R1*	AGCCCTCGGAGAACTCTAGC				
	Nog F2*	ACCTCATCGAACACCCAGAC				

Chapter 4. Examining the genetic contribution of *GDF5* in BDA1

4.1 Preface

The involvement of the *IHH* gene in causing BDA1 was first established by Gao et al (2001). Since then many others including our lab have associated *IHH* mutations with families diagnosed with BDA1. In this chapter, I describe our published report of a novel gene, *GDF5*, as a cause of BDA1 in a single consanguineous family. The identification of *GDF5* as another gene involved in BDA1 connects two signaling pathways, the IHH-PTHLH and the BMP-SMAD pathways. The manuscript has been re-formatted for its inclusion in this thesis with its figures and tables located after cited references. I have contributed to this publication through co-authorship, intellectual input, the sequencing of *GDF5* in our BDA1 cohort and in controls, the bioinformatics analyses and its interpretation. Consent forms are located in Appendix A.

4.2 Manuscript No. 2

Citation: Byrnes AM, Racacho L, Nikkel SM, Xiao F, MacDonald H, Underhill TM, Bulman DE. Mutations in GDF5 presenting as semidominant brachydactyly A1. Hum Mutat. 2010 Oct;31(10):1155-62.

Mutations in *GDF5* presenting as semi-dominant brachydactyly A1.

Ashley M. Byrnes[1,2], Lemuel Racacho[1,2], Sarah M Nikkel[4,5], Fengxia Xiao[1], Heather MacDonald[1], T. Michael Underhill[6], Dennis E. Bulman[1-3]

Affiliations:

1 – Department of Regenerative Medicine, Ottawa Hospital Research Institute, and the University of Ottawa Centre for Neuromuscular Disease, Ottawa, ON, Canada
2 – Department of Biochemistry, Microbiology and Immunology, University of Ottawa, Ottawa, ON, Canada
3 – Department of Medicine, Division of Neurology, University of Ottawa, Ottawa, ON, Canada
4 – Department of Genetics, Children's Hospital of Eastern Ontario, ON, Canada
5 – Department of Pediatrics, University of Ottawa, Ottawa, ON, Canada
6 – Department of Cellular & Physiological Sciences, University of British Columbia, Vancouver, BC, Canada

Key Words: Brachydactyly A1, GDF5, IHH, semi-dominant

4.3 Manuscript Abstract

Brachydactyly A1 (BDA1) is an autosomal dominant disorder characterized by shortness of all middle phalanges of the hands and toes, shortness of the proximal phalanges of the first digit, and short stature. Missense mutations in the Indian Hedgehog (*IHH*) gene are known to cause BDA1, and a second locus has been mapped to chromosome 5p. In a consanguineous French Canadian kindred with BDA1, both *IHH* and the 5p locus were excluded. Microsatellites flanking *GDF5* on chromosome 20q were found to cosegregate with the disease. Sequencing of the *GDF5* coding region revealed that a mildly affected individual in the family was heterozygous and that all of the severely affected individuals were homozygous for a novel missense c.1195C>T mutation that predicts a p.Arg399Cys substitution at a highly conserved amino acid. Functional analysis demonstrated that while the p.Arg399Cys mutant is able to stimulate chondrogenesis, it is much less effective than wild-type GDF5. This data confirms genetic heterogeneity in BDA1, demonstrates that mutations upstream of *IHH* can result in BDA1 and shows that BDA1 can result from semi-dominant mutations in *GDF5*.

4.4 Introduction

Brachydactyly type A1 (BDA1; OMIM 112500) was the first disorder described in terms of autosomal dominant inheritance in man [Farabee, 1903] and is characterized by shortness of all middle phalanges of the hands and feet. While all of the small tubular bones tend to be reduced in size, there is a disproportionate and significant shortness of the middle phalanges and the proximal first phalanges. The 2nd and 5th middle phalanges tend to be the most severely affected, while the 4th and 5th are the most likely of the metacarpals and metatarsals to be involved [Armour, et al., 2000]. To date, BDA1 has been described as a fully penetrant, autosomal dominant condition. Mutations have been identified in the gene Indian hedgehog (*IHH*) [Byrnes, et al., 2009; Gao, et al., 2001; Giordano, et al., 2003; Kirkpatrick, et al., 2003; Liu, et al., 2006; McCready, et al., 2005; McCready, et al., 2002; Stattin, et al., 2009; Zhu, et al., 2007], whose protein product is critical for growth and differentiation of long bone cartilage templates [Vortkamp, et al., 1996]. However mutations in *IHH* account for approximately 40% of the cases of BDA1. A second locus for BDA1 was reported at chromosome 5p13.3-13.2 (designated BDA1B; OMIM 607004) in a large Canadian family [Armour, et al., 2002]. Furthermore, an inversion of the Sonic hedgehog (*Shh*) locus has yielded a murine BDA1 phenotype in heterozygous *Short digits* (*Dsh*/+) mice [Niedermaier, et al., 2005].

Brachydactyly type A2 (BDA2; OMIM 112600) is characterized by the shortening of the middle phalange in digit 2 and to a variable degree clinodactyly of the fifth finger. Recently, it has been shown that mutations in growth/differentiation factor 5 (*GDF5*) and its receptor, bone morphogenetic receptor 1B (*BMPR1B*), both cause autosomal dominant BDA2 [Kjaer, et al., 2006; Lehmann, et al., 2003]. Brachydactyly type C (BDC; OMIM

113100) is similar to brachydactyly types A1 and A2 in that they each involve malformation of various middle phalanges, however in BDC, the fourth finger is spared; the primary characteristics observed are shortening of the middle phalanges in digits 2, 3, and 5, and of the first metacarpal. Mutations in *GDF5* have been shown to cause both autosomal dominant and semi-dominant BDC [Polinkovsky, et al., 1997; Schwabe, et al., 2004].

4.5 Materials and Methods

DNA collection and extraction

Genomic DNA was extracted from peripheral venous blood or saliva samples using the QIAamp DNA blood mini-kit and the Oragene DNA self-collection kit (Qiagen, Mississauga, Ontario; DNA Genotek, Ottawa, Ontario).

Sequencing

The primer sequences and conditions for the screening of *IHH* can be found elsewhere [McCready, et al., 2002]. Exons of the *GDF5* gene were amplified by PCR using oligonucleotide primers described in Table 4.1. The PCR products were treated with ExoSAP-IT™ (USB, Cleveland, Ohio) and were sequenced in both directions with primers from Table 1 and the BigDye™ v3.1 terminator cycle sequencing kit (Applied Biosystems, Foster City, California).

Genome screening

An autosomal 25 cM genome-wide scan was initiated using 208 primer sets from the MapPairs™ polymorphic microsatellite marker set (Research Genetics, Huntsville,

Alabama). Nine additional markers from Marshfield's sex-averaged genetic map were examined (D20S471, D20S912, D20S486, D20S601, D20S106, D20S914, D20S870, D20S865, and D20S834). Each locus was amplified in 10 µl volumes with 100 ng of genomic DNA, 1.5 mM $MgCl_2$, 10 mM Tris-HCl (pH 8.3), 0.2 mM dNTP, 0.12 µM M13-tailed forward primer, 0.12 µM reverse primer, 0.12 µM IRD-700 labeled M13 primer (LI-COR, Lincoln, NE), and 1 Unit *Taq* enzyme. Products were separated on 8% acrylamide gels using the LI-COR DNA sequencer model 4000 (LI-COR, Lincoln, Nebraska) and analyzed with LI-COR's Saga Generation 2 software.

Linkage analysis

Linkage analysis was performed using the MLINK program of the LINKAGE package (version 4.0). Due to the consanguineous nature of the family, lod scores were calculated using an autosomal recessive model with a penetrance of 100%, disease allele frequency of 0.000001, and equal recombination frequencies between males and females was assumed. At that time, individual VI-1 was thought to be unaffected.

Allele specific oligohybridization

ASOH was performed as previously described [Scoggan, et al., 2001] using γ-^{32}P - radiolabeled oligonucleotides specific for the mutant and wild-type alleles. Blots were probed with mutant probe (5'-CTTAAGGCTTGCTGCAGT- 3') at 54°C, or wild type probe (5'-CTTAAGGCTCGCTGCAGT- 3') at 56°C.

Site directed mutagenesis

To generate a form of *GDF5* incorporating the p.Arg399Cys mutation, the cDNA clone BC032495 was obtained from The Center for Applied Genomics, Toronto, Canada.

Mutagenesis was performed with the QuikChange II Site-Directed Mutagenesis Kit (Stratagene, La Jolla, California) using the primer R399C-F (5' – GCAAGAACCTTAAGGCTTGCTGCAGTCGGAAGGC– 3') for *GDF5* according to the manufacturer's suggested protocol.

Cells and transfection

Murine C3H10T1/2 mesenchymal stem cells were cultured in Dulbecco's modified Eagle's medium supplemented with 2 mM GlutaMAX, 10% fetal bovine serum, 50 U/ml Penicillin and 50 μg/ml Streptomycin. One day prior to transfection, cells were seeded at a density of 5000 cells/well in 96-well plates in growth medium without antibiotics. They were transiently transfected with 0.2 μg of pCMV-sport6 expression vector for the human full-length wild-type and mutant *GDF5* cDNA (NM_000557.2) and 0.5 μl of Lipofectamine reagent according to the manufacturer's protocol (Invitrogen).

Alkaline phosphatase and Sox 5/6/9 reporter assay

Alkaline phosphatase (ALP) activity of transfected C3H10T1/2 cells was measured 5 days after transfection with wild-type *GDF5* or *GDF5*$^{p.Arg399Cys}$ as recommended [Guo, et al., 2010]. These experiments were repeated three additional times on different days.

Wild-type and mutant expression plasmids were also transfected into primary limb mesenchymal cells harvested from CD-1 embryonic age (E) 11.5 mouse limb buds. Primary limb mesenchymal cultures from CD-1 embryonic age (E) 11.5 mouse limb buds were established as previously described [Weston, et al., 2000]. Briefly, cells were harvested from dispase-treated E11.5 whole limb buds, strained through a 40 um cell strainer (Becton-Dickinson, Franklin Lakes, New Jersey) and resuspended at a density of

2.0 X 10^7 cells/ml. Expression plasmids containing genes encoding GDF5 or variants thereof were co-transfected along with a SOX5/6/9-responsive *Col2-Luc* reporter gene at Day 0 of culture as described previously [Hoffman, et al., 2006]. Analysis of firefly and renilla luciferase activity was carried out on extracts collected on Day 2 of culture. All luciferase assays were performed in triplicate and repeated using three distinct preparations of primary cells. Student's t-test was used to compare the effects of wild-type *GDF5* and *GDF5* $^{p.Arg399Cys}$ on the SOX5/6/9 reporter.

4.6 Results

4.6.1 Clinical characterization

We studied 8 members of a family with BDA1 segregating as a semi-dominant syndrome. The classification of BDA1 was described by Temtamy and McKusick [Temtamy and McKusick, 1978] and we included metacarpophalangeal profiles (MCPP) [Garn, et al., 1972; Poznanski, et al., 1972], which has proven to be useful in identifying mildly affected individuals [Armour, et al., 2000]. The proband of this family came to attention after her daughter was referred to the Genetics Clinic for an unrelated condition. The proband was born to reportedly unaffected French-Canadian parents who were second cousins (Figure 4.1A). The family history revealed that a brother and sister had similar findings, and that there were two unaffected sisters. Another brother, who passed away at an early age, may have had brachydactyly. Among her siblings, the proband was the only affected individual to have children. Photographs and radiographs of the hands and feet of the proband and her son were obtained for detailed examination (Figure 4.1B to 4.1C). Bone lengths were measured in the phalanges and metacarpals, and metacarpal

phalangeal profiles were performed as previously described [Armour, et al., 2000]. Metacarpophalangeal profiles (MCPP) [Garn, et al., 1972; Poznanski, et al., 1972] of the proband and her son were completed by the physician using the ANTRO computer program [Hosenfeld, et al., 1991]. The radiographs and MCPP of the proband demonstrated significantly shortened middle phalanges of digits 2-5 along with the first distal phalanx, all of which are below −2.0 SD (Figures 4.2A and 4.2B). A very short first metacarpal was observed, giving the appearance of a proximally placed thumb (Figure 4.1B). The third to fifth metacarpals showed less marked shortening and the feet were likewise affected. The ulnar styloid process was truncated. Additionally, the two affected sisters who were both 5 feet tall (5^{th} centile) were treated for clubfeet as children and their X-rays did not demonstrate fibula hypoplasia. Their affected brother was 5 feet 6 inches (10^{th} centile). All affected siblings are shorter than their unaffected sisters. There are no other health concerns in the family.

4.6.2 Exclusion and linkage analysis

The family members described were found not to have mutations in *IHH*. We also excluded *SHH* and the *BDA1B* locus as candidates using linkage analysis (data not shown), indicating further genetic heterogeneity of the disorder. Subsequently, a genome-wide linkage screen was performed to identify the disease locus in the family. The study was approved by the Children's Hospital of Eastern Ontario Ethics Review Committee, and informed consent was obtained for all participants. A locus for BDA1 was mapped to a 2.1-centimorgan region between markers D20S486 and D20S834 in our family (Table 4.2). The highest maximum lod score obtained for the entire genome screen was found at marker D20S870 (Zmax = 2.15 at $\theta = 0.00$). The linked genetic

interval contains the *GDF5* gene (Figure 4.3) which drew immediate interest as it has a known role in limb development.

4.6.3 Evaluation of *GDF5*

Exons of the *GDF5* gene were amplified by PCR and sequenced using the BigDye™ v3.1 terminator cycle sequencing kit (Applied Biosystems, Foster City, California) and sequencing of *GDF5* revealed a homozygous c.1195C>T transition in the proband (reviewed but not shown), resulting in an arginine to cysteine amino acid substitution (p.Arg399Cys). Nucleotide numbering reflects the cDNA numbering with +1 corresponding to the A of the ATG translation initiation codon in the reference sequence NM_000557.2. Sequence analysis confirmed that this homozygous nucleotide change was present exclusively in the affected siblings (V-1, V-5 and V-6). The 2 unaffected siblings (V-2 and V-3) did not carry a mutated allele, however the proband's son (VI-1) was found to be heterozygous for the c.1195C>T mutation. VI-1 was noted to be of average height and his hands and feet appeared unremarkable; at the time of the linkage study, he was thought to be unaffected. Subsequently, radiographic results were consistent with a diagnosis of BDA1 as his hands revealed subtle but significant changes; his MCPP revealed that the middle phalanges of the second to fifth digits were short and below -2 S.D. when controlled for age and sex. His first metacarpal was also short (Figure 4.2).

Allele-specific oligonucleotide hybridization (ASOH) was performed on all family members and 200 control individuals to confirm genotypes and eliminate the possibility that the change was a rare polymorphism. The *GDF5* c.1195C>T nucleotide change was not detected in 400 control chromosomes.

4.6.4 Expression of wild-type and mutant GDF5

Wild-type *GDF5* and *GDF5* $^{p.Arg399Cy}$ under the control of a CMV promoter was transfected into C3H10T1/2 cells and alkaline phosphatase (ALP) activity was measured. A significant increase of ALP activity in the wild-type *GDF5* transfected cells was found at day 5 which is consistent with findings from a recent study [Gao, et al., 2009] and is in contrast with results of cells transfected with an empty control vector or mutant *GDF5* $^{p.Arg399Cys}$ ($p< 0.05$, see Figure 4.4A).

We also used a more sensitive functional assay employing a SOX5/6/9-responsive reporter construct [Weston, et al., 2002] to evaluate BMP signaling as was done to examine the effects of *GDF6* mutations [Asai-Coakwell, et al., 2009]. Relative to the transfected vector only, wild-type GDF5 was significantly better at inducing SOX5/6/9 activity than the p.Arg399Cys mutant construct ($p=0.01$) (Figure 4B). In general, the p.Arg399Cys mutation is able to stimulate chondrogenesis as measured by an increase in SOX5/6/9 activity; however, it is significantly less effective than wild-type GDF5.

4.7 Discussion

GDF5 is a member of the bone morphogenetic protein (BMP) and transforming growth factor β (TGF-β) families. All BMP family members contain an Arg-X-X-Arg cleavage site and a 6-7-cysteine motif, both of which are critical for the proper folding, dimerization, and subsequent cleavage of the mature molecule [Chang, et al., 1994; Massague and Wotton, 2000; Storm, et al., 1994; Thomas, et al., 1997]. All but one of the highly conserved cysteines are involved in the formation of intra-chain disulfide bonds, while the other cysteine forms a disulfide bond with another monomer, forming a

homo- or hetero-dimer [Massague, 1990]. Subsequent cleavage of the prodomains by subtilisin-like proteases forms the mature, active dimer [Schreuder, et al., 2005]. *GDF5* is expressed predominantly at sites of cartilage differentiation and future joint space in the developing limbs [Chang, et al., 1994; Storm, et al., 1994; Thomas, et al., 1997]. Overexpression of *GDF5* in the developing chick wing led to an increase in length and width of skeletal elements, as well as fused joints [Francis-West, et al., 1999]. Moreover, *in vitro* micromass cultures have shown that GDF5 increases chondrogenesis in a dose-dependent manner [Francis-West, et al., 1999]. This gene-dose sensitivity may account for the varying severity of diseases caused by mutations in *GDF5* in humans and mice. *GDF5* was first identified because of its association with the *brachypodism* (*bp*) mouse, as 3 strains with functionally null *GDF5* mutants display a phenotype of shortened limbs, metacarpals, metatarsals, and absent middle phalanges [Storm, et al., 1994].

Several human mutations in *GDF5* have since been associated with numerous skeletal disorders characterized by abnormal limb development. Of particular interest are the heterozygous mutations in *GDF5* which have been found to cause Brachydactyly types-A2 (BDA2) and -C (BDC) [Kjaer, et al., 2006; Lehmann, et al., 2007; Polinkovsky, et al., 1997; Schwabe, et al., 2004]. BDA1, BDA2 and BDC while clinically distinct, have been referred to as being part of a "molecular disease family" because of their common deregulation of the BMP pathway [Mundlos, 2009]. Additionally, mutations in *GDF5* are also responsible for angel-shaped phalangeal dysplasia (ASPED), multiple synostoses syndrome (SYNS1 and SYNS2), proximal symphalangism (SYM1) and congenital vertical talus (CVT) [Akarsu, 1999; Dawson, et al., 2006; Dobbs, et al., 2005; Holder-Espinasse, et al., 2004; Seemann, et al., 2005]. Furthermore homozygous and

compound heterozygous mutations in *GDF5* have been found to cause BDC, as well as more severe chondrodysplasias such as Hunter-Thompson type, Grebe type, and Du Pan syndrome [Faiyaz-Ul-Haque, et al., 2002; Schwabe, et al., 2004; Stelzer, et al., 2003; Thomas, et al., 1997; Thomas, et al., 1996].

The mutation presented here is predicted to cause an arginine to cysteine amino acid substitution at position 399 in the active region of GDF5 and this residue is conserved across species and among other GDF family members (Figure 4.3D). Moreover, the p.Arg399Cys amino acid change adds an eighth cysteine to the mature active region of the GDF5 monomer. There have been other reports of altered GDF5 activity with the addition or removal of a critical cysteine residue. A p.Arg438Cys mutation was shown to hinder monomer dimerization and secretion of the mature GDF5 protein *in vitro* [Dawson, et al., 2006; Everman, et al., 2002]. Although the precise effect of this additional cysteine is not known, the mutant protein is thought to lead to functional haploinsufficiency in heterozygotes, causing BDC, clinodactyly, or congenital vertical talus phenotypes [Dobbs, et al., 2005; Everman, et al., 2002]. In a consanguineous family with a p.Cys400Tyr substitution in GDF5, homozygotes have chondrodysplasia Grebe type, while heterozygote carriers have brachydactyly phenotypes [Thomas, et al., 1997]. Also, a heterozygous p.Cys498Ser substitution was found to cause BDC in one family [Everman, et al., 2002]. For both p.Cys substitutions, *in vitro* data showed that the mutant monomers were present in cell extracts, but neither mutant is secreted as a mature, active dimer [Everman, et al., 2002; Thomas, et al., 1997]. Furthermore, the p.Cys400Tyr mutant can have a dominant-negative effect on other TGF-β family

members, inhibiting the secretion of wild-type GDF5, BMP-2, BMP-3 and activin [Thomas, et al., 1997].

We hypothesize that the presence of this additional cysteine in the active region of GDF5 may affect the formation of the intra- or inter-chain disulfide bonds, inhibiting proper dimerization and cleavage of GDF5 precursor proteins. This could interfere with signaling by preventing the formation and secretion of mature, active GDF5 dimers. Furthermore, based on the evidence that mutant GDF5 can heterodimerize with other TGF- β family members, the mutant GDF5 may further impede chondrogenesis by sequestering other TGF-β family members to form non-functional heterodimers.

Forty percent of BDA1 patients have mutations in *IHH* and display a phenotype of short middle phalanges in digits 2-5 and a short proximal phalange in digit 1. However, one case has been described where the proximal phalange of digit 1 is spared [Liu, et al., 2006]. Terminal symphalangism, in which a rudimentary middle phalange is fused to the distal phalange, has been described in many cases of BDA1 [Gao, et al., 2001; Giordano, et al., 1997; Liu, et al., 2006; McCready, et al., 2005; McCready, et al., 2002; Yang, et al., 2000]. Individuals linked to the *BDA1B* critical region displayed a similar phenotype, though in a milder form [Armour, et al., 2000]. Metacarpophalangeal profiles revealed shortening of all phalanges and metacarpals in affected individuals, especially the middle phalanges. Similarly, BDA2-affected individuals homozygous for the c.1195C>T (p.Arg399Cys) mutation display a phenotype of very short middle phalanges in digit 2-5 with no terminal symphalangism. They also lacked the shortening of the first proximal phalange typically seen in the majority families with *IHH* mutations. In addition, they had a very short first metacarpal, giving the appearance of a proximally placed thumb

which has also been described in some patients with *IHH* mutations [Gao, et al., 2001]. This latter feature is commonly observed in BDC, suggesting that GDF5 plays an important role in development of the first metacarpal. Common features described in the *GDF5* homozygous individuals are short stature with no disproportion of the axial versus appendicular skeleton and a truncated ulnar styloid process, both of which have been described in some families with *IHH* mutations [Gao, et al., 2001; Giordano, et al., 2003; Temtamy and McKusick, 1978]. Interestingly, two affected individuals in our family had club feet, the occurrence of which may be coincidental; alternatively, this phenotype may be due to incomplete expressivity as seen with mutations in *GDF5* causing BDC [Savarirayan, et al., 2003]. The MCPP of the one heterozygous *GDF5* individual examined clinically displayed the same general pattern as homozygous individuals, but with a lesser degree of shortening of the middle phalanges and first metacarpal. Mutations in *IHH*, *GDF5*, and the 5p13.3-p13.2 critical region can cause the same general BDA1 phenotype, with additional associated features depending on the causative gene in each family.

Extensive phenotypic heterogeneity, in which mutations in the same gene yield a range of phenotypes, has been observed in families with *GDF5* mutations [Wolf, 1997]. The specific feature shared by families with *GDF5* mutations reported to date is malformations of the appendicular skeleton, with the distal skeletal elements generally most severely affected. The brachydactylies, chondrodysplasias, and ASPED are all likely the result of haploinsufficiency, null, or dominant-negative mutations leading to impaired bone formation [Polinkovsky, et al., 1997; Thomas, et al., 1997; Thomas, et al., 1996]. In contrast, the synostoses and joint fusion phenotypes are thought to arise from

gain of function mutations, which somehow increase GDF5 signaling and prevent the formation of certain joints [Dawson, et al., 2006; Seemann, et al., 2005].

This consanguineous French Canadian family represents the first case of true BDA1 reported to be caused by mutations in *GDF5*. Severely affected individuals had very short middle phalanges in digits 2-5, the hallmark feature of BDA1. Although the middle phalanges are affected in all cases, this BDA1 phenotype differs from other *GDF5* families described with BDC, in which the fourth middle phalange is spared, and *GDF5* families described with BDA2, in which only middle phalanges of digits 2, and sometimes 5, are affected [Dobbs, et al., 2005; Everman, et al., 2002; Galjaard, et al., 2001; Holder-Espinasse, et al., 2004; Kjaer, et al., 2006; Polinkovsky, et al., 1997; Savarirayan, et al., 2003; Seemann, et al., 2005; Szczaluba, et al., 2005].

A comparison of the homozygote and heterozygote phenotypes provides information regarding the nature of the abnormal course of embryonic development, resulting in the complete syndrome [Beighton, 1997]. The three severely affected siblings of this BDA1 family embody only the second report of a homozygous *GDF5* mutation causing a brachydactyly phenotype; heterozygous mutation carriers have a very mild phenotype [Schwabe, et al., 2004]. Due to the existence of a mild phenotype in heterozygous carriers in both families, the disease transmission was described as semi-dominant.

Reporter assays indicate that *IHH* is up-regulated in embryonic cells upon treatment with BMPs [Seki and Hata, 2004] including GDF5 [Storm and Kingsley, 1996]. The BDA1 phenotype resulting from a *GDF5* mutation would be consistent with the reduced

induction of *IHH* and is consistent with the view that reduced IHH signaling at the digit tip results in shortened cartilage elements [Gao, et al., 2009].

In summary, we present clinical, radiological, and molecular data on a consanguineous family with BDA1 and demonstrate that a mutation in *GDF5* is the cause of this disorder. *In vitro* studies demonstrate that mutant GDF5 was not able to induce chondrogenesis to the same extent as its wild-type counterpart. We hypothesize that this mutation, which is predicted to disrupt the highly-conserved 7-cysteine motif critical for the dimerization and maturation of GDF5, led to the development of the phenotype in this family. A more severe phenotype observed in homozygous individuals suggests that the mutation affects BDA1 development in a dose-dependent manner.

4.8 Acknowledgements

The authors would like to thank the members of the family for their participation. Funding for this work was provided by an operating grant (DEB) from the Canadian Institutes of Health Research.

4.9 Online Resources

Accession numbers and URLs for data presented herein are as follows:

GenBank, http://www.ncbi.nlm.nih.gov/Genbank/ (for *GDF5* [accession number BC032495])

Online Mendelian Inheritance in Man (OMIM), http://www.ncbi.nlm.nih.gov/Omim/ (for BDA1, BDA1B, BDA2, BDB, BDC)

4.10 Cited References

Akarsu ANR, T; Demirtas, M.; Farhud, D.D.; Sarfarazi, M. 1999. Multiple synostosis type 2 (SYNS2) maps to 20q11.2 and is caused by a missense mutation in the growth/differentiation factor 5 (GDF5). Am. J. Hum. Genet. Suppl. 65:A281.

Armour CM, Bulman DE, Hunter AG. 2000. Clinical and radiological assessment of a family with mild brachydactyly type A1: the usefulness of metacarpophalangeal profiles. J.Med.Genet. 37(4):292-296.

Armour CM, McCready ME, Baig A, Hunter AG, Bulman DE. 2002. A novel locus for brachydactyly type A1 on chromosome 5p13.3-p13.2. J Med Genet 39(3):186-8.

Asai-Coakwell M, French CR, Ye M, Garcha K, Bigot K, Perera AG, Staehling-Hampton K, Mema SC, Chanda B, Mushegian A and others. 2009. Incomplete penetrance and phenotypic variability characterize Gdf6-attributable oculo-skeletal phenotypes. Hum Mol Genet 18(6):1110-1121.

Beighton P. 1997. Heterozygous manifestations in the heritable disorders of the skeleton. Pediatr Radiol 27(5):397-401.

Byrnes AM, Racacho L, Grimsey A, Hudgins L, Kwan AC, Sangalli M, Kidd A, Yaron Y, Lau YL, Nikkel SM et al. 2009. Brachydactyly A-1 mutations restricted to the central region of the N-terminal active fragment of Indian Hedgehog. Eur J Hum Genet. 2009 17(9):1112-1120.

Chang SC, Hoang B, Thomas JT, Vukicevic S, Luyten FP, Ryba NJ, Kozak CA, Reddi AH, Moos M, Jr. 1994. Cartilage-derived morphogenetic proteins. New members of the transforming growth factor-beta superfamily predominantly expressed in long bones during human embryonic development. J Biol Chem 269(45):28227-28234.

Dawson K, Seeman P, Sebald E, King L, Edwards M, Williams Iii J, Mundlos S, Krakow D. 2006. GDF5 Is a second locus for multiple-synostosis syndrome. Am J Hum Genet 78(4):708-712.

Dobbs MB, Gurnett CA, Robarge J, Gordon JE, Morcuende JA, Bowcock AM. 2005. Variable hand and foot abnormalities in family with congenital vertical talus and CDMP-1 gene mutation. J Orthop Res 23(6):1490-1494.

Everman DB, Bartels CF, Yang Y, Yanamandra N, Goodman FR, Mendoza-Londono JR, Savarirayan R, White SM, Graham JM, Jr., Gale RP and others. 2002. The mutational spectrum of brachydactyly type C. Am J Med Genet 112(3):291-296.

Faiyaz-Ul-Haque M, Ahmad W, Wahab A, Haque S, Azim AC, Zaidi SH, Teebi AS, Ahmad M, Cohn DH, Siddique T and others. 2002. Frameshift mutation in the cartilage-derived morphogenetic protein 1 (CDMP1) gene and severe acromesomelic

chondrodysplasia resembling Grebe-type chondrodysplasia. Am J Med Genet 111(1):31-37.

Farabee WC. 1903. Hereditary and sexual influences in meristic variation: A study of digital malformations in man. [Ph.D.]. Boston: Harvard University.

Francis-West PH, Abdelfattah A, Chen P, Allen C, Parish J, Ladher R, Allen S, MacPherson S, Luyten FP, Archer CW. 1999. Mechanisms of GDF-5 action during skeletal development. Development 126(6):1305-1315.

Galjaard RJ, van der Ham LI, Posch NA, Dijkstra PF, Oostra BA, Hovius SE, Timmenga EJ, Sonneveld GJ, Hoogeboom AJ, Heutink P. 2001. Differences in complexity of isolated brachydactyly type C cannot be attributed to locus heterogeneity alone. Am J Med Genet 98(3):256-262.

Gao B, Guo J, She C, Shu A, Yang M, Tan Z, Yang X, Guo S, Feng G, He L. 2001. Mutations in IHH, encoding Indian hedgehog, cause brachydactyly type A-1. Nat Genet 28(4):386-388.

Gao B, Hu J, Stricker S, Cheung M, Ma G, Law KF, Witte F, Briscoe J, Mundlos S, He L and others. 2009. A mutation in Ihh that causes digit abnormalities alters its signalling capacity and range. Nature 458(7242):1196-2000.

Garn SM, Hertzog KP, Poznanski AK, Nagy JM. 1972. Metacarpophalangeal length in the evaluation of skeletal malformation. Radiology 105(2):375-381.

Giordano N, Gennari L, Bruttini M, Mari F, Meloni I, Baldi C, Capoccia S, Geraci S, Merlotti D, Amendola A and others. 2003. Mild brachydactyly type A1 maps to chromosome 2q35-q36 and is caused by a novel IHH mutation in a three generation family. J Med Genet 40(2):132-135.

Giordano N, Senesi M, Battisti E, Mattii G, Gennari C. 1997. Weill-Marchesani syndrome: report of an unusual case. Calcif Tissue Int 60(4):358-360.

Guo S, Zhou J, Gao B, Hu J, Wang H, Meng J, Zhao X, Ma G, Lin C, Xiao Y and others. 2010. Missense mutations in IHH impair Indian Hedgehog signaling in C3H10T1/2 cells: Implications for brachydactyly type A1, and new targets for Hedgehog signaling. Cell Mol Biol Lett 15(1):153-176.

Hoffman LM, Garcha K, Karamboulas K, Cowan MF, Drysdale LM, Horton WA, Underhill TM. 2006. BMP action in skeletogenesis involves attenuation of retinoid signaling. J Cell Biol 174(1):101-113.

Holder-Espinasse M, Escande F, Mayrargue E, Dieux-Coeslier A, Fron D, Doual-Bisser A, Boute-Benejean O, Robert Y, Porchet N, Manouvrier-Hanu S. 2004. Angel shaped

phalangeal dysplasia, hip dysplasia, and positional teeth abnormalities are part of the brachydactyly C spectrum associated with CDMP-1 mutations. J Med Genet 41(6):e78.

Hosenfeld D, Hosenfeld F, Schaefer E, Grote W. 1991. IBM-PC compatible software for establishing metacarpophalangeal pattern profiles. Clin Genet 39(5):396-400.

Kirkpatrick TJ, Au KS, Mastrobattista JM, McCready ME, Bulman DE, Northrup H. 2003. Identification of a mutation in the Indian Hedgehog (IHH) gene causing brachydactyly type A1 and evidence for a third locus. J Med Genet 40(1):42-44.

Kjaer KW, Eiberg H, Hansen L, van der Hagen CB, Rosendahl K, Tommerup N, Mundlos S. 2006. A mutation in the receptor binding site of GDF5 causes Mohr-Wriedt brachydactyly type A2. J Med Genet 43(3):225-231.

Lehmann K, Seemann P, Silan F, Goecke TO, Irgang S, Kjaer KW, Kjaergaard S, Mahoney MJ, Morlot S, Reissner C and others. 2007. A New Subtype of Brachydactyly Type B Caused by Point Mutations in the Bone Morphogenetic Protein Antagonist NOGGIN. Am J Hum Genet 81(2):388-396.

Lehmann K, Seemann P, Stricker S, Sammar M, Meyer B, Suring K, Majewski F, Tinschert S, Grzeschik KH, Muller D and others. 2003. Mutations in bone morphogenetic protein receptor 1B cause brachydactyly type A2. Proc Natl Acad Sci U S A 100(21):12277-12282.

Liu M, Wang X, Cai Z, Tang Z, Cao K, Liang B, Ren X, Liu JY, Wang QK. 2006. A novel heterozygous mutation in the Indian hedgehog gene (IHH) is associated with brachydactyly type A1 in a Chinese family. J Hum Genet 51:1083-1086.

Massague J. 1990. The transforming growth factor-beta family. Annu Rev Cell Biol 6:597-641.

Massague J, Wotton D. 2000. Transcriptional control by the TGF-beta/Smad signaling system. Embo J 19(8):1745-1754.

McCready ME, Grimsey A, Styer T, Nikkel SM, Bulman DE. 2005. A century later Farabee has his mutation. Hum Genet 117(2-3):285-287.

McCready ME, Sweeney E, Fryer AE, Donnai D, Baig A, Racacho L, Warman ML, Hunter AG, Bulman DE. 2002. A novel mutation in the IHH gene causes brachydactyly type A1: a 95-year-old mystery resolved. Hum Genet 111(4-5):368-375.

Mundlos S. 2009. The brachydactylies: a molecular disease family. Clin Genet 76(2):123-136.

Niedermaier M, Schwabe GC, Fees S, Helmrich A, Brieske N, Seemann P, Hecht J, Seitz V, Stricker S, Leschik G and others. 2005. An inversion involving the mouse Shh locus

results in brachydactyly through dysregulation of Shh expression. J Clin Invest 115(4):900-909.

Polinkovsky A, Robin NH, Thomas JT, Irons M, Lynn A, Goodman FR, Reardon W, Kant SG, Brunner HG, van der Burgt I and others. 1997. Mutations in CDMP1 cause autosomal dominant brachydactyly type C. Nat Genet 17(1):18-19.

Poznanski AK, Garn SM, Nagy JM, Gall JC, Jr. 1972. Metacarpophalangeal pattern profiles in the evaluation of skeletal malformations. Radiology 104(1):1-11.

Savarirayan R, White SM, Goodman FR, Graham JM, Jr., Delatycki MB, Lachman RS, Rimoin DL, Everman DB, Warman ML. 2003. Broad phenotypic spectrum caused by an identical heterozygous CDMP-1 mutation in three unrelated families. Am J Med Genet 117A(2):136-142.

Schreuder H, Liesum A, Pohl J, Kruse M, Koyama M. 2005. Crystal structure of recombinant human growth and differentiation factor 5: evidence for interaction of the type I and type II receptor-binding sites. Biochem Biophys Res Commun 329(3):1076-1086.

Schwabe GC, Turkmen S, Leschik G, Palanduz S, Stover B, Goecke TO, Mundlos S. 2004. Brachydactyly type C caused by a homozygous missense mutation in the prodomain of CDMP1. Am J Med Genet 124A(4):356-363.

Scoggan KA, Chandra T, Nelson R, Hahn AF, Bulman DE. 2001. Identification of two novel mutations in the CACNA1A gene responsible for episodic ataxia type 2. J Med Genet 38(4):249-253.

Seemann P, Schwappacher R, Kjaer KW, Krakow D, Lehmann K, Dawson K, Stricker S, Pohl J, Ploger F, Staub E and others. 2005. Activating and deactivating mutations in the receptor interaction site of GDF5 cause symphalangism or brachydactyly type A2. J Clin Invest 115(9):2373-2381.

Seki K, Hata A. 2004. Indian hedgehog gene is a target of the bone morphogenetic protein signaling pathway. J Biol Chem 279(18):18544-18549.

Stattin EL, Linden B, Lonnerholm T, Schuster J, Dahl N. 2009. Brachydactyly type A1 associated with unusual radiological findings and a novel Arg158Cys mutation in the Indian hedgehog (IHH) gene. Eur J Med Genet 52(5):297-302.

Stelzer C, Winterpacht A, Spranger J, Zabel B. 2003. Grebe dysplasia and the spectrum of CDMP1 mutations. Pediatr Pathol Mol Med 22(1):77-85.

Storm EE, Huynh TV, Copeland NG, Jenkins NA, Kingsley DM, Lee SJ. 1994. Limb alterations in brachypodism mice due to mutations in a new member of the TGF beta-superfamily. Nature 368(6472):639-643.

Storm EE, Kingsley DM. 1996. Joint patterning defects caused by single and double mutations in members of the bone morphogenetic protein (BMP) family. Development 122(12):3969-3979.

Szczaluba K, Hilbert K, Obersztyn E, Zabel B, Mazurczak T, Kozlowski K. 2005. Du Pan syndrome phenotype caused by heterozygous pathogenic mutations in CDMP1 gene. Am J Med Genet A 138(4):379-383.

Temtamy SA, McKusick VA. 1978. Brachydactyly as an Isolated Malformation. In: Bergsma D, Mudge JR, Paul KW, editors. The Genetics of Hand Malformations. New York: Alan R. Liss. p 187-197.

Thomas JT, Kilpatrick MW, Lin K, Erlacher L, Lembessis P, Costa T, Tsipouras P, Luyten FP. 1997. Disruption of human limb morphogenesis by a dominant negative mutation in CDMP1. Nat Genet 17(1):58-64.

Thomas JT, Lin K, Nandedkar M, Camargo M, Cervenka J, Luyten FP. 1996. A human chondrodysplasia due to a mutation in a TGF-beta superfamily member. Nat Genet 12(3):315-317.

Vortkamp A, Lee K, Lanske B, Segre GV, Kronenberg HM, Tabin CJ. 1996. Regulation of rate of cartilage differentiation by Indian hedgehog and PTH-related protein. Science 273(5275):613-622.

Weston AD, Chandraratna RA, Torchia J, Underhill TM. 2002. Requirement for RAR-mediated gene repression in skeletal progenitor differentiation. J Cell Biol 158(1):39-51.

Weston AD, Rosen V, Chandraratna RA, Underhill TM. 2000. Regulation of skeletal progenitor differentiation by the BMP and retinoid signaling pathways. J Cell Biol 148(4):679-690.

Wolf U. 1997. Identical mutations and phenotypic variation. Hum Genet 100(3-4):305-321.

Yang X, She C, Guo J, Yu AC, Lu Y, Shi X, Feng G, He L. 2000. A locus for brachydactyly type A-1 maps to chromosome 2q35-q36. Am J Hum Genet 66(3):892-903.

Zhu G, Ke X, Liu Q, Li J, Chen B, Shao C, Gong Y. 2007. Recurrence of the D100N mutation in a Chinese family with brachydactyly type A1: Evidence for a mutational hot spot in the Indian hedgehog gene. Am J Med Genet A 143(11):1246-1248.

4.11 Manuscript Figures, Tables and Legends

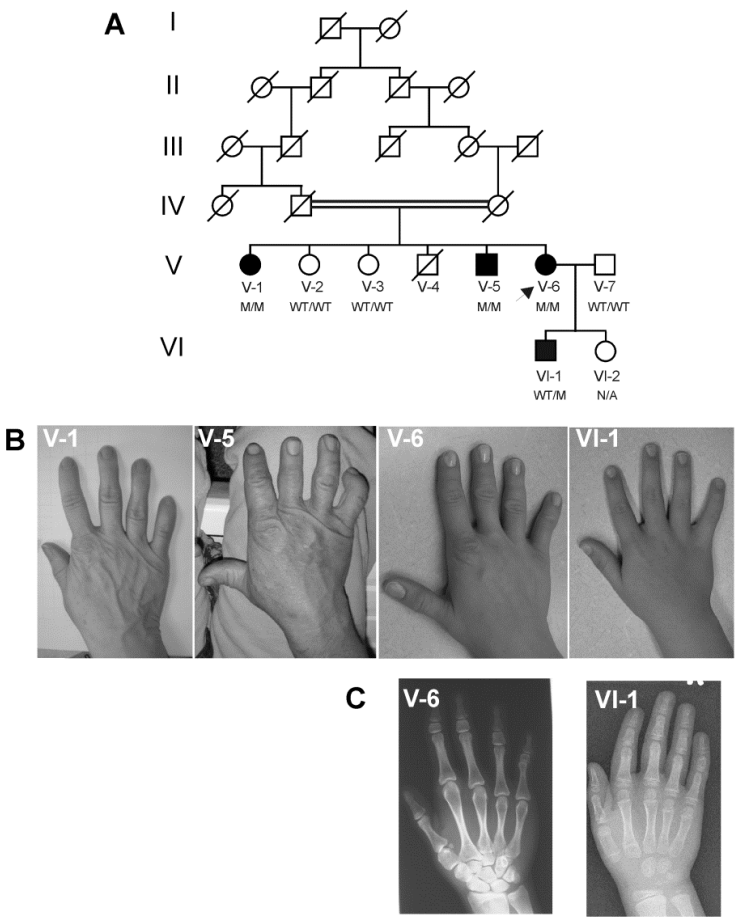

Figure 4.1. (A) Pedigree of the consanguineous family with BDA1, which is transmitted as a semi-dominant trait. Affected individuals are indicated by filled symbols. Squares – males; Circles – females; Arrowhead indicates the proband. Numbered individuals indicate those who participated in this study, with the exception of V-4. M/M indicates those who were homozygous for the p.Arg399Cys mutation, WT/M indicates those who are heterozygous and homozygous wild type (WT/WT) are also indicated. VI-2 did not participate in the genetic analysis at the request of the family. (**B)** Photographs of the right hand V-1, V-5 and V-6 indicate a proximally-placed thumb and short middle phalanges, while VI-1 has short middle phalanges. (**C)** X-rays of the right hand of individual V-6, show a very small first metacarpal and very small middle phalanges in digits 2-5, leading to the appearance of short fingers and a proximally-placed thumb, while that of VI-1, who was 9 years old at the time, has small middle phalanges. The X-ray of VI-1 is consistent with appropriate bone age.

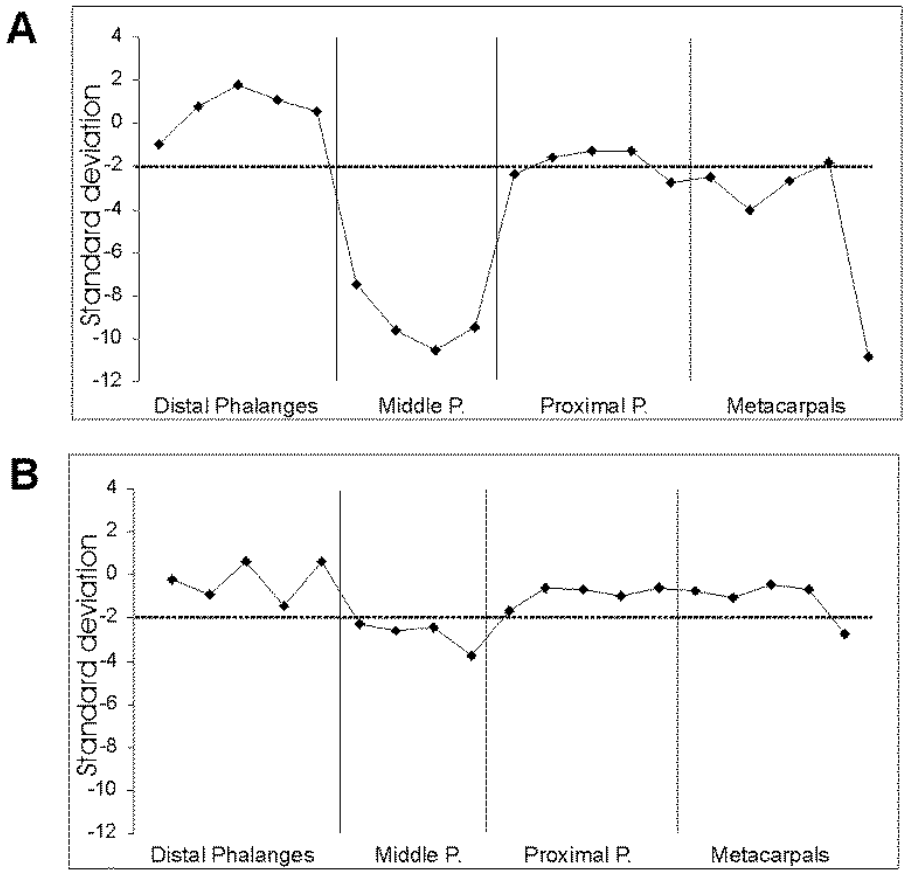

Figure 4.2. Metacarpophalangeal profiles (MCPP) of individuals (A) V-6 and (B) VI-1. The horizontal dashed line indicates -2 standard deviations. The bone lengths are depicted on the graph measured in standard deviations from normal age and sex matched controls in the sequence of distal phalanges (order digits 5-1), middle phalanges (order digits 5-2), proximal phalange (order digits 5-1), and metacarpals (order digits 5-1). The MCPP of individual V-6 shows an extremely short first metacarpal and middle phalanges and first metacarpal. Individual VI-1 shows the same general pattern as V-6 but is a much less severe case.

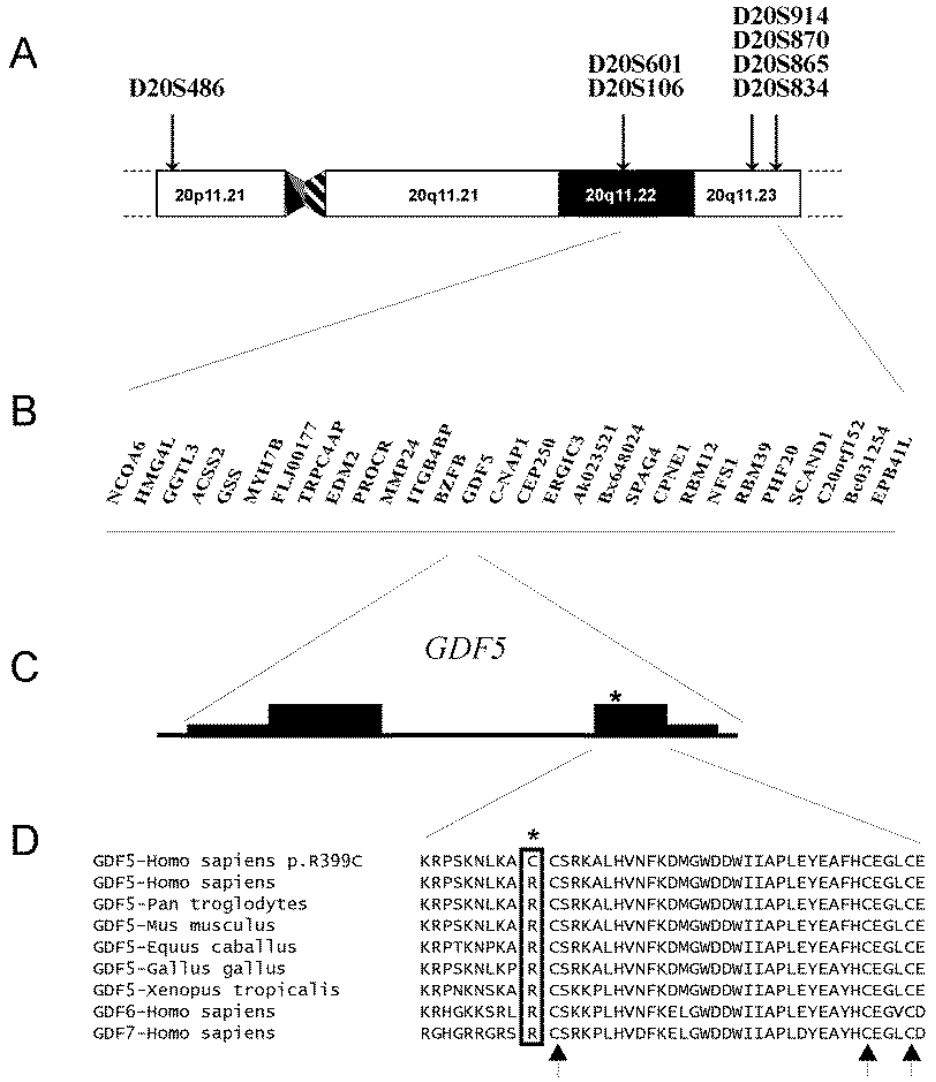

Figure 4.3. (A) Schematic representation of the microsatellite markers bounding the region of potential linkage to BDA1 located on chromosome 20q11, including genes within the candidate region (**B)**. The structure of the candidate gene *GDF5*, and a partial amino acid sequence alignment, are also shown (**C & D)**. Upward arrows indicate the position of conserved cysteine residues. The amino acid sequence of the mutant p.Arg399Cys mutation (denoted by an asterisk and box) was aligned with human wild-type *GDF5* and with those of other species, as well as with human *GDF6* and *GDF7*. The p.Arg399Cys mutation, which is conserved across species, is associated with BDA1 in this study.

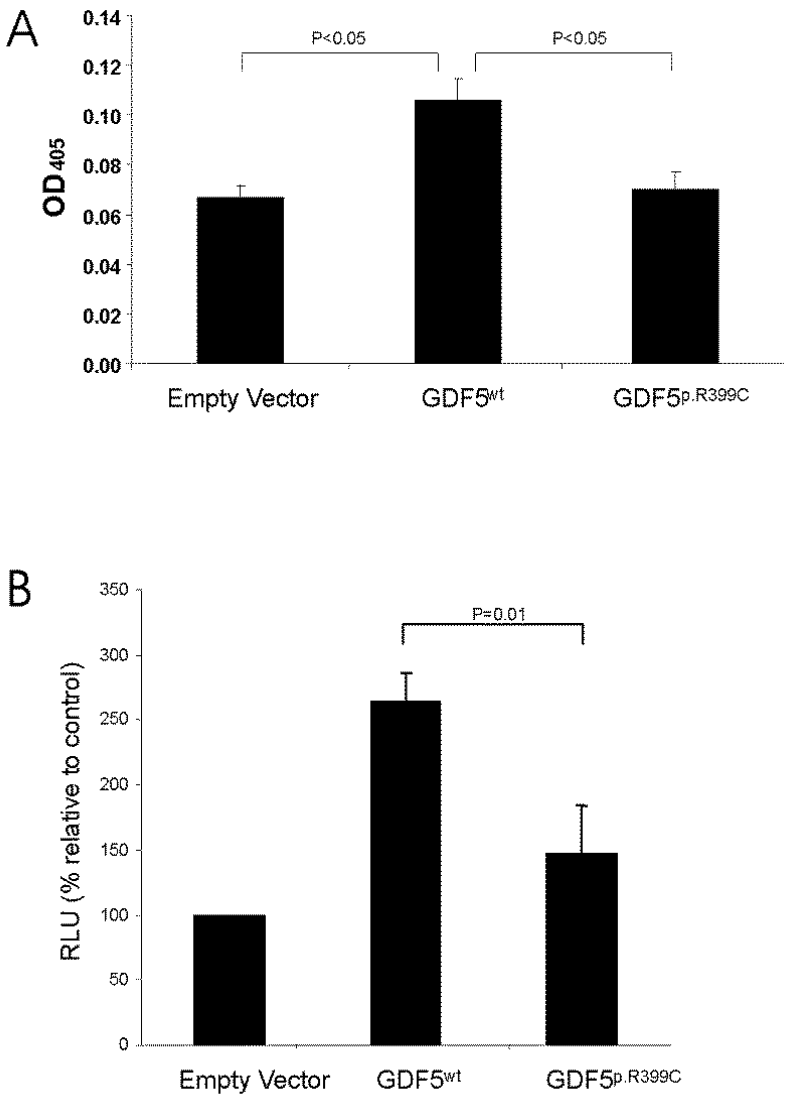

Figure 4.4. **Analysis of the human *GDF5* gene upon osteogenic differentiation in C3H10T1/2 cells. (A)** The alkaline phosphatase activity in transfected C3H10T1/2 cells is represented by Optical Density at 405 nm (OD_{405}). The data are the means of four individual values ± SE. The T-Test (Paired Two Sample for Means) is used for the significance of difference between the means of the empty vector, WT and mutant *GDF5* vectors. $p < 0.05$. **(B)** Induction of Sox5/6/9 activity by wildtype and mutant GDF5. Relative to the transfected vector only (control), wild-type GDF5 was significantly better at inducing SOX5/6/9 activity than the p.Arg399Cys mutant construct (p=0.01).

Table 4.1. Sequence of primers and conditions used to amplify and sequence the *GDF5* gene.

GDF5 Exon	Primer Name	Primer Sequence	Primer Annealing Temperature	Final $[MgCl_2]$ (mM)	PCR Product Size
5' UTR	GDF5x1F1	CGCCATTCTTCCTTCTTGG	60	1.5	391 bp
	GDF5x1R1	AGAAAGTGAGGAGTTTGGGG			
Exon 1	GDF5x1F2	TGCTGCCGCTGTTCTCTTTG	65	1.5	425 bp
	GDF5x1R2	TGTCCTTTTGGGGTCACAGTCC			
Exon 1	GDF5x1F3	CCAAACAAGGCAGGCTACAG	65	1.5	403 bp
	GDF5x1R3	ATGCACACAGTGTCTCCCAC			
Exon 2	GDF5x2F1b	TGGTGAGGTTGCAGGGAATG	68	2.0	382 bp
	GDF5x2R1b	TCCAGATGTCGAACACCTCC			
Exon 2	GDF5x2F2	TGGGAGGTGTTCGACATCTG	68	1.5	414 bp
	GDF5x2R2	GTGGAAAGCCTCGTACTCAAG			
Exon 2	GDF5x2F3	GGAAGGCACTGCATGTCAAC	62	1.5	406 bp
	GDF5x2R3	TGTGTAGATGCTCCTGCCAC			
Exon 2	GDF5x2F4	TCCTGCACTCCTGGAATCAC	60	1.5	421 bp
	GDF5x2R4	CTCTTCTCTCCCACTCTTGC			
Exon 2	GDF5x2F6	AAGAAGCCCTCGGACACG	58	1.5	700 bp
	GDF5x2R6	GGATGCTGATGGGACTCAG			
3' UTR	GDF5x2F5	CTCCTCAAATCACATTTGTGC	58	1.5	388 bp
	GDF5x2R5	TTTGGAAGGAACAGGAATGC			

Table 4.2. Two-point lod scores surrounding the region of chromosome 20. At the time of linkage analysis, individual VI:1 was not thought to be affected.

Marker	Map position	0.00	0.01	0.05	0.10	0.20	0.30	0.40
D20S482	13.21	-∞	-3.59	-1.66	-0.95	-0.39	-0.15	-0.03
D20S851	24.70	-∞	-2.36	-1.05	-0.56	-0.19	-0.06	-0.02
D20S604	32.94	-∞	-0.48	0.10	0.25	0.26	0.16	0.06
D20S470	39.25	-∞	-2.07	-0.79	-0.34	-0.03	0.02	0.01
D20S471	42.28	-∞	-1.72	-0.48	-0.08	0.13	0.11	0.04
D20S912	46.71	-∞	-1.55	-0.32	0.08	0.26	0.21	0.08
D20S486	49.22	-∞	-0.25	0.27	0.36	0.28	0.15	0.05
D20S601	50.81	2.06	2.01	1.82	1.59	1.11	0.64	0.22
D20S106	50.81	1.48	1.44	1.28	1.08	0.71	0.38	0.13
D20S914	50.81	0.26	0.25	0.20	0.15	0.08	0.03	0.01
D20S870	50.81	2.15	2.10	1.91	1.66	1.17	0.68	0.24
D20S865	50.81	1.63	1.59	1.41	1.19	0.78	0.43	0.14
D20S834	51.36	-∞	-1.89	-0.65	-0.23	0.01	0.05	0.03
D20S478	54.09	-∞	-1.82	-0.58	-0.17	0.06	0.07	0.04
D20S481	62.32	-∞	-1.76	-0.52	-0.12	0.09	0.09	0.05
D20S480	79.91	-∞	-0.68	-0.11	0.03	0.07	0.04	0.01
D20S171	95.70	-3.12	-1.13	-0.49	-0.25	-0.08	-0.03	-0.01
Theoretical Maximum[1]	-	2.15	2.10	1.91	1.66	1.17	0.68	0.28

[1] The theoretical maximum lod score attainable.

Chapter 5. Examining the genetic contribution of *BMPR1B* in BDA1

5.1 Preface

The work presented in this chapter has been accepted for publication and is in press for the European Journal of Human Genetics (2015). I have contributed to this work through primary authorship, artwork, intellectual input, experimental design, bioinformatics analyses and its interpretation, and the sequencing of *GDF5* in both families. Consent forms are located in Appendix A.

5.2 Manuscript No. 3

Two disease causing variants in *BMPR1B* are associated with brachydactyly type A1

Racacho L.[1,6], Byrnes A.M.[1,3], MacDonald H.[3], Nikkel S.M.[2,4], Allanson J.[4], Rosser E.[5], Bulman D.E.[1,2,6‡]

Affiliations:

1. Department of Biochemistry, Microbiology and Immunology, Faculty of Medicine, University of Ottawa, ON, Canada.
2. Department of Pediatrics, Faculty of Medicine, University of Ottawa, ON, Canada
3. Regenerative Medicine Program, Ottawa Hospital Research Institute, Ottawa, ON, Canada.
4. Department of Genetics, Children's Hospital of Eastern Ontario, Ottawa, ON, Canada.
5. Clinical Genetics Unit, Great Ormond Street Hospital for Children NHS Trust, London, UK.
6. Children's Hospital of Eastern Ontario Research Institute, Ottawa, ON, Canada.

‡ Corresponding Author

Keywords: Brachydactyly A1, BMPR1B, GDF5, BMP-SMAD

5.3 Manuscript Abstract

Brachydactyly type A1 (BDA1, MIM #112500) is an autosomal dominant brachymesophalangy, primarily characterized by hypoplasia/aplasia of the middle phalanges of digits 2-5. There is considerable overlap in the affected bone patterns of the brachymesophalangies. Human and mouse genetic perturbations in the BMP-SMAD signaling pathway have been associated with many brachymesophalangies, including BDA1, as mutations in *IHH* and *GDF5* have been previously identified in BDA1 cases. GDF5 interacts directly as the preferred ligand for the BMP type 1 receptor BMPR1B and are important for both chondrogenesis and digit formation. We report pathogenic variants in *BMPR1B* which are associated with complex BDA1. A c.975A>C (p.Lys325Asn) was identified in the first patient displaying absent middle phalanges and shortened distal phalanges of the toes in addition to the shortening of middle phalanges in digits 2, 3 and 5 of the hands. The second patient displayed a combination of brachydactyly and arachnodactyly. The sequencing of *BMPR1B* in this individual revealed a novel c.447-1G>A at a canonical acceptor splice site of exon 8 which is predicted to create a novel acceptor site, thus leading to a frameshift. Both mutations are most likely to act in a dominant negative fashion, similar to the effects observed in *BMPR1B* mutations that cause BDA2. These findings demonstrate that *BMPR1B* is another gene involved with the pathogenesis of BDA1 and illustrates the continuum of phenotypes between BDA1 and BDA2.

5.4 Introduction

The brachydactylies constitute a collection of human digit phenotypes characterized by varying patterns of bone hypoplasia and malformed interphalangeal joints which leads to shortened or absent tubular bones in the hands and/or feet. Genetic studies in humans and mice have revealed that most brachydactylies are attributed to perturbations in the bone morphogenetic protein (BMP) signaling pathway, specifically targeting the ligands, their antagonists and cognate receptors at the cell surface (Stricker and Mundlos, 2011).

Although the brachydactylies are isolated traits, there is considerable overlap in the pattern of the affected bones. For example, Ploger et al. (2008) described a BDA2 (MIM #112600) family where some of its affected members displayed shortened middle phalanges of digit 2, a classic BDA2 feature, along with various degrees of shortening of the middle phalanges of digits 3 and 4. Seemann et al. (2005) described another variation where in some patients the shortening of the middle phalange of digit 2, and to a lesser extent digit 5, resembled Temtamy-type BDA4 (MIM %112800) (Temtamy and McKusick, 1978). The phenotypic overlap is suggestive of a common genetic pathway in phalangeal and metacarpal bone development. The work performed by described in Chapter 4, Byrnes et al., (2010) and Degenkolbe et al. (2012) illustrated this point through the discovery of missense mutations in the growth differentiation factor 5 gene (*GDF5*) in patients diagnosed with BDA1, an autosomal dominant brachymesophalangy usually associated with mutations clustered in the central region of the N-terminal signaling fragment of Indian hedgehog (*IHH*) (see Chapter 3 and Byrnes et al., 2009). Dominant mutations in *GDF5* were previously associated with four human conditions;

i.e., angel-shaped phalango-epiphysea dysplasia (ASPED; MIM 105835) (Gutierrez-Amavizca et al., 2012; Holder-Espinasse et al., 2004), BDA2 (Seemann et al., 2005; Kjaer et al., 2006; Plöger et al., 2008), BDC (MIM #113100) (Polinkovsky et al., 1997; Thomas et al., 1997; Everman et al., 2002; Schwabe et al., 2004; Savarirayan et al. 2003), multiple synostosis (SYNS2; MIM #610017) (Dawson et al., 2006; Degenkolbe et al., 2013) and symphalangism proximal 1B (SYM1B; MIM #185800) (Seemann et al., 2005; Wang et al., 2006; Yang et al., 2008), whereas severe chondrodysplasias of the Hunter-Thomson (MIM #201250) (Thomas et al., 1996), Grebe (MIM #200700) (Thomas et al., 1997; Faiyaz-Ul-Haque et al., 2002; Al-Yahyaee et al., 2003), and Du Pan (MIM #228900) (Faiyaz-Ul-Haque et al., 2002) types were attributed to homozygous loss-of-function mutations.

The GDFs, like the bone morphogenetic proteins (BMPs), belong to the TGF-β superfamily of secretory signaling molecules which have diverse biological functions such as embryonic development and patterning, tissue homeostasis, immune response, reproduction and skeletal formation (reviewed in Massague, 2012). GDF5 is a well established osteo- and chondroinductive cytokine which preferentially binds with higher affinity to BMP receptor type-1B (BMPR1B) than to receptor type-1A (BMPR1A) (Kotzsch et al., 2009; Mueller and Nickel, 2012). These transmembrane serine-threonine kinase receptors belong to the TGF-β receptor superfamily. The mammalian BMP receptors are subclassified into 7 BMP type-1 receptors and 5 BMP type-2 receptors. BMPR1A and BMPR1B closely resemble the amino acid composition of the activin receptor class 1 (ACVR1/ALK2), the gene responsible for fibrodysplasia ossificans progressive (Shore et al., 2006; Lin et al., 2006; Nakajima et al., 2007; Furuya et al.,

2008; Bocciardi et al., 2009; Kaplan et al., 2009; Petrie et al., 2009; Barnett et al., 2011). Phylogenetic analyses of the BMP type-1 receptor family suggest that both BMPR1B and BMPR1A co-evolved and are derived from the drosophila thickveins receptor (TKV) (Schmierer and Hill, 2007), a receptor essential for visceral mesoderm patterning (Affolter et al., 1994).

Bmpr1a null mice are not viable, but mice carrying the inactivated *Bmpr1a* allele in chondrocytes exhibited hypoplasia of the long bones (Yoon et al., 2005). The skeletal defects of *Bmpr1b* null mice were restricted to the phalanges which displayed brachydactyly (Baur et al., 2000; Yi et al., 2000; Yoon et al., 2005), similar to the *GDF5* null mutant brachypodism mouse (Storm et al., 1994). Yoon et al. (2005) demonstrated the functional redundancy of Bmpr1a and Bmpr1b in chondrogenic differentiation by comparing the skeletal phenotypes in $Bmpr1a^{CKO}$, $Bmpr1b^{-/-}$, and $Bmpr1a^{CKO}$; $Bmpr1b^{-/-}$ mice. The latter resulted in the absence of skeletal elements normally formed through endochondral ossification. Bmpr1b is the major transducer of BMP signals in early limb mesenchymal condensations (Zou et al., 1997). Upon ligand binding, heterotetrameric formation of BMP type-1 and BMP type-2 receptors occurs at the cell surface. This event triggers the intracellular transphosphorylation of the BMP type-1 receptor which results in the phosphorylation of intracellular receptor-regulated SMADS (R-SMADS) causing it to translocate to the nucleus where it regulates transcriptional targets (Nohe et al., 2004, Schmierer and Hill, 2007). Dominant mutations in the *BMPR1B* gene are associated with BDA2, BDC-SYM1 (Lehmann et al., 2003 and 2006), and idiopathic pulmonary arterial hypertension (IPAH) (Chida et al., 2012) whereas homozygous loss-

of-function mutations cause acromesomelic chondrodysplasia (Demirhan et al., 2005 and Graul-Neumann et al., 2014).

We have a collection of BDA1 probands that do not carry any mutations in either *GDF5* or *IHH* and have been excluded for linkage to the *BDA1* locus at chromosome 5p13.3 (BDA1B; MIM %607004). Since GDF5 interacts directly with BMPR1B, we tested whether a subset of the probands in our cohort had mutations in the *BMPR1B* gene. We report the identification of two novel mutations in *BMPR1B* which are associated with BDA1.

5.5 Materials and Methods

Ethics approval

This study was approved by the research ethics boards of the Ottawa Hospital and the Children's Hospital of Eastern Ontario. Genetic testing required voluntary informed consent by the patient or his/her legal guardians.

Clinical assessment

A collection of genomic DNA (gDNA) from individuals presenting with BDA1 features and who were previously found not to have BDA1-causing mutations in *IHH* and *GDF5* were assessed for BDA1-causing mutations in the candidate gene *BMPR1B*. When possible, molecular and clinical assessments of additional family members were performed.

Metacarpophalangeal pattern profile (MCPP)

MCPPs were performed on standardized hand radiographs by SN. The length of each hand bone, excluding the wrist bones, were measured using the software ANTRO (Hosenfeld et al., 1991) and adjusted for age and sex as described in Armour et al., (2000). Tubular hand bones with a SD $\leq$ -2 were classified as being disproportionately short, whereas those with a SD $\geq$ +2 indicated disproportionately long bones.

Molecular analyses

Genomic DNA was extracted and column purified from whole blood using QIA Blood Mini Kit (Qiagen) as per manufacturer protocol. Whole blood was obtained by venipuncture into EDTA vacutainers (Becton-Dickenson). Purified genomic DNA from each patient was amplified with primer pairs specific to each exon of *BMPR1B*. Each primer pair was designed by ExonPrimer (www.ihg.gsf.de/ihg/ExonPrimer.html) to flank at least 50 bases from each intron-exon boundary as listed in Supplementary Table S5.1. Amplification with each primer pair was performed in a 50 µl reaction as follows: 50 ng template, 10 µM forward and reverse primer, 10 mM dNTPs (Roche), 2.0 mM $MgCl_2$ (Sigma-Aldrich), 10X PCR buffer (100 mM Trizma®-HCl pH 8.3, 500 mM KCl; Sigma-Adrich) and 1U r*Taq* (Sigma-Aldrich). Cycling conditions were set at 95°C 5 min initial denaturation, followed by 30 cycles of 95°C 45 s denaturation, 55°C 30 s annealing, 72°C 30 s extension, and a final extension at 72°C for 10 min. All PCR samples were analyzed on a 2% agarose gel and stained with 5 mg/ml EtBr. PCR samples were either treated with ExoSap-It (USB) or isolated and purified with QIAquick Gel Extraction Kit (Qiagen). A 2 µl aliquot sample was prepared for BigDyeV3.1 terminator sequencing on an AB 3730*xl* genetic analyzer (Life Technologies) as described in Byrnes et al., (2010).

Amplification primers were used for sequencing in both directions. Unincorporated dye-terminators were either removed from each sequencing reaction by ethanol precipitation or by SPRI magnetic beads (Agencourt® CleanSeq®) on a Biomek® FX automated workstation (Beckman Coulter).

In-silico analyses

All electropherograms were generated and viewed individually using Sequencing Analysis Software (Applied Biosystems) or uploaded onto FinchTV (Geospiza, Inc) to examine sequence quality. Each sequence was aligned to the human reference build HG18 using BLAT (UCSC Genome Browser Tools) to identify any sequence mismatches. A novel sequence variant was defined as not being present in dbSNP142, Genome Variants, Human Gene Mutation Database or Exome Variant Server. Sequence variants meeting this criterion were evaluated for pathogenicity using PolyPhen-2 V2.2.2 (Adzhubei et al., 2010) and SIFT (Kumar et al., 2009). Sequence variants that aligned within annotated splice sites were evaluated with online web services Human Splice Finder V2.4.1 (Desmet et al., 2009), SplicePort (Dogan et al., 2007) and Alternative Splice Site Prediction (Wang and Marin, 2006). ENSEMBL Transcript ID: ENST00000515059 was used as input sequence for all of the splice prediction services. Sequence variants were deposited at http://database.LOVD.nl/. Multiple sequence alignment of BMPR1B from human (AAH47773.1), mouse (AAH65106.1), sheep (NP_990463.1), and chicken (NP_001009431.1) was performed using ClustalOmega with default parameters. Cn3D v4.3 (NCBI tools) was used to visualize the location of *BMPR1B* mutations superimposed on the crystal structure of BMPR1B (PDB ID:

3MDY_A). VAST (NCBI tools) was used to align structure neighbors (PDB IDs: 4C02_A and 1B6C_B).

5.6 Results

5.6.1 Clinical findings

Family-1

The proband was a well, developmentally normal 16 month old Caucasian female, the first child born to a pair of healthy and unrelated parents (Figure 5.1A). No complications were noted during the pregnancy and she was born at term with a birth weight of 3410 g and length of 52 cm. Both parents appeared normal and did not exhibit any hand or foot anomalies. The proband's stature was average (height 75th percentile, head circumference 50th percentile), but her index fingers were very short and the fifth fingers were slightly short with ulnar curvature (Supplementary Figure S5.1A). The face appeared square with a small chin. The eyebrows were dramatic as they extended further laterally. The nose displayed a broad root, scooped bridge and small upturned tip. The philtrum had a very mild groove and the vermilion borders of the lips appeared normal. The thorax and abdomen appeared emaciated with thin skin, prominent vascular patterning, rounded shoulders, abdominal protrusion and an umbilical hernia. There was no indication of organomegaly. The genitalia and anus appeared normal. The hands and feet, however, displayed remarkable bone anomalies. The palmar creases were normal but digital creases were reduced at the distal interphalangeal joints. Examination of the feet revealed shortened big toes. The second toes were very long with moderate syndactyly between toes 2 and 3. Hand radiographs showed a slightly reduced size of the

terminal phalanx of the thumbs (S. Nikkel, personal communication, 2010). The index fingers lacked middle phalanges and the fifth digits had very small middle phalanges. Radiographs of the feet displayed two phalanges in all of the toes, the terminal phalanges being very short (S. Nikkel, personal communication). The MCPP revealed the presence of a short distal and proximal phalange of both thumbs, a shortening of the terminal and middle phalanges of digit 3, severe shortening of the middle phalanges of digit 2, and a slight shortening of the middle phalanges of digit 5 (Figure 5.1A). The bones that make up digit 4 appeared to be normal. Cytogenetic analysis revealed a normal karyotype; i.e. 22 autosome pairs and one sex pair of XX.

Family-2

The proband who was of African descent born to healthy and unrelated parents (Figure 5.2A) was initially seen at 11 months of age. The child sat, unsupported at 7 months, stood with supports at 11 months and walked at 14 months of age. Mild developmental delay was noted with speech and toileting delay, poor motor coordination and brachydactyly of the hands. All fingernails were present and there was no facial dysmorphology. A younger brother who had normal hands and feet also had speech delay. By age 9 years, the proband was doing well at school with extra support, had good hand function and was not dysmorphic. A hand radiograph taken from the proband displayed small cube-shaped middle phalanges of digit 2 and small trapezoid-shaped middle phalanges of digit 5 in both hands (Figure 5.2B). The middle phalange of digit 2 displayed a socket-like groove for the epiphysis of the proximal phalange. Clinodactyly in both the fifth digits and the right thumb was observed in the proband. There were no remarkable hand bone features in the parents (Supplementary Figure S5.1B). The MCPP

from both hands revealed moderate shortening of the distal phalanges of digits 1 and 2, shortened proximal phalange of digit 1, and severe shortening of the middle phalanges of digits 2 and 5 (Figure 5.2C). The proband had a normal karyotype and was excluded for Fragile X.

5.6.2 Two novel sequence variants in *BMPR1B* are associated with BDA1-like phenotypes

The 16 month old female patient in Family-1 did not carry a mutation in either IHH or GDF5. Sequencing of the *BMPR1B* gene revealed a novel heterozygous c.975A>C (p.(Lys325Asn)) in her, but the variant was not found in the mother. The biological father was reported to have no hand or feet anomalies, but was unavailable to study. The sequence variant was not identified in any of the public variant databases including dbSNP142, Personal Genomes, HGMD and Exome Variant Server. Moreover, we sequenced 100 controls which comprised of healthy Canadian individuals and did not identify this variant in exon 10 of *BMPR1B*. The asparagine substitution at residue position 325 was predicted by both SIFT (score = 0) and PolyPhen-2 (score = 1) to be pathogenic. A ClustalOmega multiple alignment of the peptide sequence of BMPR1B from human, mouse, chicken and sheep positioned Lys325 within a highly conserved region of the cytoplasmic protein kinase domain (Figure 5.3).

We also report on an individual of African descent with a mix BDA1-arachnodactyly condition. All three family members did not have a mutation in either *IHH* or *GDF5*. The sequencing of *BMPR1B* revealed a heterozygous c.447-1G>A (HG19 NC000004.11:g.96046133G>A) in only the proband and mother. The sequence variant was not observed in 100 sequenced controls nor in any public variant databases.

The nucleotide substitution occurred in a constitutive acceptor splice site for exon 8 of *BMPR1B* where the last two nucleotides **AG** are highly conserved in the consensus acceptor splice site sequence $YYTT(Y)_6NC\mathbf{AG}\,|\,G$ (Senapathy et al., 1990). The G to A transition was predicted to abolish the 3' splice site and to create a novel 3' site just one nucleotide downstream at position c.447 (Table 5.1). This would result in a translational frameshift of one nucleotide which in turn produced a truncated peptide of 162 amino acids (Figure 5.7). The two novel sequence variants as described above were deposited at the LOVD database with LOVD ID numbers 0000053136 (c.9775A>C) and 00029686 (c.447-1G>A).

5.6.3 Mutation distribution of BMPR1B

BMPR1B encodes for a 502 amino acid protein with three main functional domains, an extracellular ligand binding domain; namely, a single transmembrane domain, and an intracellular protein kinase domain. We found that the majority of mutations that have been shown to be associated with brachymesophalangies in *BMPR1B* resided within the protein kinase domain (Figures 5.3 and 5.4). The superimposition of missense mutations onto the 3D model of BMPR1B suggest that mutations which are associated with BDA1 and BDA2 are found on the surface of the cytoplasmic region of BMPR1B, whereas the mutation that is associated with IPAH is buried within the core of 4 alpha helices (Figure 5.5).

5.6.4 BMPR1B^{Lys325Asn} resides in a structural conserved motif

A VAST structure alignment of closely related cytoplasmic peptide chains revealed a conserved stretch of 23 residues: TQGKPAIAHRDLKSKNILVKKNG (Figure

5.6). This motif in BMPR1B was also observed in ACVR1 and TGF-β type-1 receptors, and corresponded to an outward facing beta strand at the kinase domain containing the predicted p.(Lys325Asn) (Figures 5.4 and 5.5).

5.7 Discussion

Mutations in either *IHH* or *GDF5* have been previously shown to be associated with BDA1. In this study we describe two novel sequence variants in the human BMP receptor type-1B gene (*BMPR1B*) that are associated with BDA1-like conditions in two unrelated individuals. In the first BDA1-like case, a c.975A>C is predicted to cause a p.(Lys325Asn) substitution next to the serine-threonine kinase active site in the C-terminal domain of BMPR1B. The lysine substitution was predicted to be pathogenic. It is possible that the exchange of a positively charged amino acid like lysine for an uncharged asparagine residue could result in a loss of kinase activity, similar to the effect observed in the study describing the BDA2-causing mutation p.Ile200Lys (Lehmann et al., 2003). In the same study, a recombinant chicken Bmpr1b expression vector containing the BDA2-causing mutation p.R486W was found to retain normal kinase activity despite a demonstrated strong inhibitory effect on chondrogenesis in micromass cultures. The serine-threonine domain of BMP type-1 receptors serves two purposes in establishing the proper intracellular response upon ligand binding: 1) phosphorylation of the R-SMADs, and 2) proper complex formation between type-1 and type-2 receptors (Nohe et al., 2002, Ehrlich et al., 2012). Thus, an alternative pathogenic mechanism to consider is the disruption of the formation of the heterotetrameric complex. The BDA1-associated variant c.975A>C (p.(Lys325Asn)) was located in a highly conserved structure

motif (Figure 5.6) where exact function, and may well involve receptor complex formation. The proper formation of the complex has been shown to affect the avidity for ligands (Sebald et al., 2004) and it is possible that p.(Lys325Asn) could disrupt the strength of ligand binding to receptor complexes which include BMPR1B and BMPR1A. Recently, it has been shown that *in-vitro* SMAD reporter assays of BDA1-causing mutations in GDF5, p.Arg399Cys and p.Trp414Arg resulted in a more severe reduction in BMPR1A signal as compared to BMPR1B (Degenkolbe et al., 2013). The authors suggested that a disruptive BMPR1A signaling could be the key pathogenic feature involved with causing BDA1. An evaluation of the effects of p.(Lys325Asn) in SMAD signaling could further support the group's model.

The second BDA1 case carried a novel heterozygous substitution, c.447-1G>A, within a canonical acceptor splice site of exon 8 of *BMPR1B*. Mutations within acceptor splice sites have been previously shown to cause exon skipping and intron retention which could translate into a truncated peptide (Licatolosi and Darnell, 2010). The predicted consequence of c.447-1G>A on the splicing of *BMPR1B* pre-mRNA would be the creation of an adjacent acceptor splice site at c.447 (Table 5.1, Figure 5.7). Since the predicted resulting transcript would encode only 13 additional codons before premature termination, it could be subjected to nonsense mediated decay (Maquat, 2004). If this is the case, then the BDA1 condition of the proband would be a result of haploinsufficiency of BMPR1B. Alternatively c.447-1G>A could act as a hypomorphic allele similar to what was described in a mouse mutant Ali30 carrying a T to G transversion in the splice donor site of exon 10 of *Bmpr1b* (Graw et al., 2012). These mutant mice exhibited brachydactyly in addition to retinopathy. Although the mother carried the c.450-1G>A

variant, she did not exhibit the brachydactyly features observed in her son. It is possible that the environment and/or genes other than *IHH* and *GDF5* could have modified the expression. Interestingly, the proband exhibited restricted arachnodactyly features. Contractual arachnodactyly combined with brachydactyly and sensoneural hearing loss has been primarily reported in a single case study (Alpteken et al., 2005), but our patient's hearing was unremarkable. Further, there were no indications of visual impairment as seen in the mouse mutant Ali30. Long skeletal elements are classical features of Marfan syndrome (MIM #154700) which has been previously linked to mutations in the fibrilin-1 gene (Collod-Beroud et al., 2003). It is unclear if the splice sequence variant in this family is contributing to the disproportionate lengthening of digits 3 and 4. Further functional characterization is needed to address this concern.

We did note the remarkable similarity in MCPP of both probands. There are also phenotypic similarities between our patient and the ones described with BDA2-causing mutations in *BMPR1B*. Our patient with the c.975A>C (p.(Lys325Asn)) variant has a similar missing middle phalange of digit 2 as does the BDA2 patient with the p.Ile200Lys mutation (Lehmann et al., 2003). Unlike the reported BDA2 cases, both of our patients displayed the shortening of the proximal and distal phalange of the thumb which is also distinct from BDC. These differences could be attributed to the position of the mutations within *BMPR1B*, similar to what has been observed in GDF5 for BDA1, BDA1/SYNS2, and BDA2 (Degenkolbe et al., 2013).

In summary, we identified two novel sequence variants in *BMR1B* which are associated with BDA1-like phenotypes. These variants were positioned in or near the coding region for the intracellular region of BMPR1B. Their effects are predicted to

disrupt SMAD signaling either in a dominant-negative fashion (c.975A>C) as a result of disrupting the formation of a receptor complex with the wildtype protein, or by haploinsufficiency (c.447-1G>A) as a result of nonsense mediated decay. Hence, our study further supports the role of the BMP-SMAD pathway in brachymesophalangies and partially reveals the nature of structurally conserved domains of BMPR1B.

5.8 Acknowledgements

The authors would like to thank the members of the families for their participation. Funding for this work was provided by an operating grant (DEB) from the Canadian Institutes of Health Research.

5.9 Online Resources

ASSP: wangcomputing.com/assp/
CLUSTALW: www.ebi.ac.uk/Tools/msa/clustalo/
ENSEMBL: www.ensembl.org/
ExomeVariant Server: evs.gs.washington.edu/
ExonPrimer: www.ihg.gsf.de/ihg/ExonPrimer.html
HGMD: www.hgmd.org/
HumanSpliceFinder: www.umd.be/HSF/
PolyPhen-2: genetics.bwh.harvard.edu/pph2/
SIFT: sift.jcvi.org/
SplicePort: spliceport.cbcb.umd.edu/
UCSC Genome Browser: https://genome.ucsc.edu/
VAST: http://structure.ncbi.nlm.nih.gov/Structure/VAST/

5.10 Cited References

Adzhubei, I.A., Schmidt, S., Peshkin, L., Ramensky, V.E., Gerasimova, A., Bork, P., Kondrashov, A.S., Sunyaev, S.R. (2010). A method and server for predicting damaging missense mutations. Nat. Methods *7*, 248-249.

Affolter, M., Nellen, D., Nussbaumer, U., Basler, K. (1994). Multiple requirements for the receptor serine/threonine kinase thick veins reveal novel functions of TGF beta homologs during Drosophila embryogenesis. Development *120*, 3105-3117.

Alptekin, N., Ozturk, E.A., Gok, H., Yalcin, P., Tekin, M. (2005). Congenital contractural arachnodactyly, brachydactyly and sensorineural hearing loss: an unusual association. Genet. Couns. *16*, 421-423.

Al-Yahyaee, S. A.S., Al-Kindi, M.N., Habbal, O., Kumar, D.S. (2003). Clinical and molecular analysis of Grebe acromesomelic dysplasia in an Omani family. Am. J. Med. Genet. *121A*: 9-14.

Armour, C.M., Bulman, D.E., Hunter, A.G. (2000). Clinical and radiological assessment of a family with mild brachydactyly type A1: the usefulness of metacarpophalangeal profiles. J. Med. Genet. *37*, 292-296.

Barnett, C. P., Dugar, M., Haan, E. A. (2011). Late-onset variant fibrodysplasia ossificans progressiva leading to misdiagnosis of ankylosing spondylitis. Am. J. Med. Genet. *155A*, 1492-1495.

Baur, S.T., Mai, J.J., Dymecki, S.M. (2000). Combinatorial signaling through BMP receptor IB and GDF5: shaping of the distal mouse limb and the genetics of distal limb diversity. Development *127*, 605-619.

Bocciardi, R., Bordo, D., Di Duca, M., Di Rocco, M., Ravazzolo, R. (2009). Mutational analysis of the ACVR1 gene in Italian patients affected with fibrodysplasia ossificans progressiva: confirmations and advancements. Eur. J. Hum. Genet. *17*, 311-318.

Byrnes, A.M., Racacho, L., Grimsey, A., Hudgins, L., Kwan, A.C., Sangalli, M., Kidd, A., Yaron, Y., Lau, Y.L., Nikkel, S.M., Bulman, D.E. (2009). Brachydactyly A-1 mutations restricted to the central region of the N-terminal active fragment of Indian Hedgehog. Eur. J. Hum. Genet. *17*, 1112-1120.

Byrnes, A.M., Racacho, L., Nikkel, S.M., Xiao, F., MacDonald, H., Underhill, T.M., Bulman, D.E. (2010). Mutations in GDF5 presenting as semidominant brachydactyly A1. Hum. Mutat. *31*, 1155-1162.

Chida, A., Shintani, M., Nakayama, T., Furutani, Y., Hayama, E., Inai, K., Saji, T., Nonoyama, S., Nakanishi, T. (2012). Missense mutations of the BMPR1B (ALK6) gene in childhood idiopathic pulmonary arterial hypertension. Circ. J. *76*, 1501-1508.

Collod-Beroud, G., Le Bourdelles, S., Ades, L., Ala-Kokko, L., Booms, P., Boxer, M., Child, A., Comeglio, P., De Paepe, A., Hyland, J.C., Holman, K., Kaitila, I., Loeys, B., Matyas, G., Nuytinck, L., Peltonen, L., Rantamaki, T., Robinson, P., Steinmann, B., Junien, C., Béroud, C., Boileau, C. (2003). Update of the UMD-FBN1 mutation database and creation of an FBN1 polymorphism database. Hum. Mutat. *22*, 199-208.

Dawson, K., Seeman, P., Sebald, E., King, L., Edwards, M., Williams, J., III, Mundlos, S., Krakow, D. (2006). GDF5 is a second locus for multiple-synostosis syndrome. Am. J. Hum. Genet. *78*, 708-712.

Degenkolbe, E., König, J., Zimmer, J., Walther, M., Reißner, C., Nickel, J., Plöger, F., Raspopovic, J., Sharpe, J., Dathe, K., Hecht, J.T., Mundlos, S., Doelken, S.C., Seemann, P. (2013). A GDF5 point mutation strikes twice--causing BDA1 and SYNS2. PLoS Genet. *9*, e1003846.

Demirhan, O., Türkmen, S., Schwabe, G.C., Soyupak, S., Akgül, E., Tastemir, D., Karahan, D., Mundlos, S., Lehmann, K. (2005). A homozygous BMPR1B mutation causes a new subtype of acromesomelic chondrodysplasia with genital anomalies. J. Med. Genet. *42*, 314 – 317.

Desmet, F.O., Hamroun, D., Lalande, M., Collod-Béroud, G., Claustres, M., Béroud, C. (2009). Human Splicing Finder: an online bioinformatics tool to predict splicing signals. Nucleic Acids Res. *37*, e67.

Dogan, R.I., Getoor, L., Wilbur, W.J., Mount, S.M. (2007). SplicePort--an interactive splice-site analysis tool. Nucleic Acids Res. *35* (Web Server issue), W285-W291.

Ehrlich, M., Gutman, O., Knaus, P., Henis, Y.I. (2012). Oligomeric interactions of TGF-β and BMP receptors. FEBS Lett. *586*, 1885-1896.

Everman, D.B., Bartels, C.F., Yang, Y., Yanamandra, N., Goodman, F.R., Mendoza-Londono, J.R., Savarirayan, R., White, S.M., Graham, J.M., Jr., Gale, R. P., Svarch, E., Newman, W.G., Kleckers, A.R., Francomano, C.A., Govindaiah, V., Singh, L., Morrison, S., Thomas, J.T., Warman, M.L. (2002). The mutational spectrum of brachydactyly type C. Am. J. Med. Genet. *112*, 291-296.

Faiyaz-Ul-Haque, M., Ahmad, W., Zaidi, S.H.E., Haque, S., Teebi, A.S., Ahmad, M., Cohn, D.H., Tsui, L.C. (2002). Mutation in the cartilage-derived morphogenetic protein-1 (CDMP1) gene in a kindred affected with fibular hypoplasia and complex brachydactyly (DuPan syndrome). Clin. Genet. *61*, 454-458.

Furuya, H., Ikezoe, K., Wang, L., Ohyagi, Y., Motomura, K., Fujii, N., Kira, J., Fukumaki, Y. (2008). A unique case of fibrodysplasia ossificans progressiva with an ACVR1 mutation, G356D, other than the common mutation (R206H). Am. J. Med. Genet. *146A*, 459-463.

Graul-Neumann, L.M., Deichsel, A., Wille, U., Kakar, N., Koll, R., Bassir, C., Ahmad, J., Cormier-Daire, V., Mundlos, S., Kubisch, C., Borck, G., Klopocki, E., Mueller, T.D., Doelken, S.C., Seemann, P. (2014). Homozygous missense and nonsense mutations in BMPR1B cause acromesomelic chondrodysplasia-type Grebe. Eur. J. Hum. Genet. *22*, 726-733.

Graw, J., Puk, O., Weber, S., Wagner, S., Thiele, F., Przemeck, G., Hrabé de Angelis, M. (2012). Bmpr1b splice site mutation leads to optic nerve head degeneration in the mouse. Invest. Ophthalmol. Vis. Sci. *53*, E-Abstract 1534.

Gutierrez-Amavizca, B.E., Brambila-Tapia, A.J., Juarez-Vazquez, C.I., et al. (2012). A novel mutation in CDMP1 causes brachydactyly type C with "angel-shaped phalanx". A genotype-phenotype correlation in the mutational spectrum. Eur. J. Med. Genet. *55*, 611-614.

Holder-Espinasse, M., Escande, F., Mayrargue, E., et al. (2004). Angel shaped phalangeal dysplasia, hip dysplasia, and positional teeth abnormalities are part of the brachydactyly C spectrum associated with CDMP-1 mutations. J. Med. Genet. *41*, e78.

Hosenfeld, D., Hosenfeld, F., Schaefer, E., Grote, W. (1991). IBM-PC compatible software for establishing metacarpophalangeal pattern profiles. Clin. Genet. *39*, 396-400.

Kaplan, F.S., Xu, M., Seemann, P., Connor, J.M., Glaser, D.L., Carroll, L., Delai, P., Fastnacht-Urban, E., Forman, S.J., Gillessen-Kaesbach, G., Hoover-Fong, J., Koster, B., Pauli, R. M., Reardon, W., Zaidi, S.A., Zasloff, M., Morhart, R., Mundlos, S., Groppe, J., Shore, E.M. (2009). Classic and atypical fibrodysplasia ossificans progressiva (FOP) phenotypes are caused by mutations in the bone morphogenetic protein (BMP) type I receptor ACVR1. Hum. Mutat. *30*, 379-390.

Kjaer, K.W., Eiberg, H., Hansen, L., van der Hagen, C.B., Rosendahl, K., Tommerup, N., Mundlos, S. (2006). A mutation in the receptor binding site of GDF5 causes Mohr-Wriedt brachydactyly type A2. J. Med. Genet. *43*, 225-231.

Kotzsch, A., Nickel, J., Seher, A., Sebald, W., Müller, T.D. (2009). Crystal structure analysis reveals a spring-loaded latch as molecular mechanism for GDF-5-type I receptor specificity. EMBO J. *28*, 937-947.

Kumar, P., Henikoff, S., Ng, P.C. (2009). Predicting the effects of coding non-synonymous variants on protein function using the SIFT algorithm. Nat. Protoc. *4*, 1073-1081.

Lehmann, K., Seeman, P., Stricker, S., Sammar, M., Meyer, B., Süring, K., Majewski, F., Tinschert, S., Grzeschik, K.H., Müller, D, Knaus, P., Nürnberg, P., Mundlos, S. (2003). Mutations in bone morphogenetic protein receptor 1B cause brachydactyly type A2. Proc. Natl. Acad. Sci. USA *100*, 12277–12282.

Lehmann, K., Seeman, P., Boergermann, J., Morin, G., Reif, S., Knaus, P., Mundlos, S. (2006). A novel R486Q mutation in BMPR1B resulting in either a brachydactyly type C/symphalangism-like phenotype or brachydactyly type A2. Eur. J. Hum. Genet. *14*, 1278–1254.

Licatalosi, D.D. and Darnell, R.B. (2010). RNA processing and its regulation: global insights into biological networks. Nat. Rev. Genet. *11*, 75-87.

Lin, G.T., Chang, H.W., Liu, C.S., Huang, P.J., Wang, H.C., Cheng, Y.M. (2006). De novo 617G-A nucleotide mutation in the ACVR1 gene in a Taiwanese patient with fibrodysplasia ossificans progressiva. J. Hum. Genet. *51*, 1083-1086.

Massague, J. (2012). TGFbeta signalling in context. Nat. Rev. Mol. Cell Biol. 2012; *13*: 616-630.

Mueller, T.D., and Nickel, J. (2012). Promiscuity and specificity in BMP receptor activation. FEBS Lett. *586*, 1846-1859.

Nakajima, M., Haga, N., Takikawa, K., Manabe, N., Nishimura, G., Ikegawa, S. (2007). The ACVR1 617G-A mutation is also recurrent in three Japanese patients with fibrodysplasia ossificans progressiva. J. Hum. Genet. *52*, 473-475.

Maquat, L.E. (2004). Nonsense-mediated mRNA decay: splicing, translation and mRNP dynamics. Nat. Rev. Mol. Cell Biol. *5*, 89–99.

Nohe, A., Hassel, S., Ehrlich, M., Neubauer, F., Sebald, W., Henis, Y.I., Knaus, P. (2002). The mode of bone morphogenetic protein (BMP) receptor oligomerization determines different BMP-2 signaling pathways. J. Biol. Chem. *277*, 5330-5338.

Nohe, A., Keating, E., Knaus, P., Petersen, N.O. (2004). Signal transduction of bone morphogenetic protein receptors. Cell Signal *16*, 291–299.

Petrie, K.A., Lee, W.H., Bullock, A.N., Pointon, J.J., Smith, R., Russell, R.G.G., Brown, M.A., Wordsworth, B.P., Triffitt, J.T. (2009). Novel mutations in ACVR1 result in atypical features in two fibrodysplasia ossificans progressiva patients. PLoS One *4*, e5005.

Plöger, F., Seemann, P., Schmidt-von Kegler, M., Lehmann, K., Seidel, J., Kjaer, K.W., Pohl, J., Mundlos, S. (2008). Brachydactyly type A2 associated with a defect in proGDF5 processing. Hum. Mol. Genet. *17*, 1222-1233.

Polinkovsky, A., Robin, N.H., Thomas, J.T., Irons, M., Lynn, A., Goodman, F.R., Reardon, W., Kant, S G., Brunner, H.G., van der Burgt, I., Chitayat, D., McGaughran, J., Donnai, D., Luyten, F.P., Warman, M.L. (1997). Mutations in CDMP1 cause autosomal dominant brachydactyly type C. (Letter) Nat. Genet. *17*, 18-19.

Savarirayan, R., White, S.M., Goodman, F.R., Graham, J.M., Jr., Delatycki, M.B., Lachman, R.S., Rimoin, D.L., Everman, D.B., Warman, M.L. (2003). Broad phenotypic spectrum caused by an identical heterozygous CDMP-1 mutation in three unrelated families. Am. J. Med. Genet. *117A*, 136-142.

Schmierer, B., Hill, C.S. (2007). TGFbeta-SMAD signal transduction: molecular specificity and functional flexibility. Nat. Rev. Mol. Cell Biol. *8*, 970-982.

Schwabe, G.C., Turkmen, S., Leschik, G., Palanduz, S., Stover, B., Goecke, T.O., Mundlos, S. (2004). Brachydactyly type C caused by a homozygous missense mutation in the prodomain of CDMP1 Am. J. Med. Genet. *124A*, 356-363.

Sebald, W., Nickel, J., Zhang, J.L. and Mueller, T.D. (2004). Molecular recognition in bone morphogenetic protein (BMP)/receptor interaction. J. Biol. Chem. *385*, 697–710.

Seemann, P., Schwappacher, R., Kjaer, K.W., Krakow, D., Lehmann, K., Dawson, K., Stricker, S., Pohl, J., Plöger, F., Staub, E., Nickel, J., Sebald, W., Knaus, P., Mundlos, S. (2005). Activating and deactivating mutations in the receptor interaction site of GDF5 cause symphalangism or brachydactyly type A2. J. Clin. Invest. *115*, 2373-2381.

Senapathy, P., Shapiro, M.B., Harris, N.L. (1990). Splice junctions, branch point sites, and exons: sequence statistics, identification, and applications to genome project. Methods Enzymol. *183*, 252-278.

Shore, E.M., Xu, M., Feldman, G.J., Fenstermacher, D.A., Cho, T.J., Choi, I.H., Connor, J.M., Delai, P., Glaser, D. L., LeMerrer, M., Morhart, R., Rogers, J.G., Smith, R., Triffitt, J.T., Urtizberea, J.A., Zasloff, M., Brown, M.A., Kaplan, F.S. (2006). A recurrent mutation in the BMP type I receptor ACVR1 causes inherited and sporadic fibrodysplasia ossificans progressiva. Nat. Genet. *38*, 525-527.

Storm EE, Huynh TV, Copeland NG, Jenkins NA, Kingsley DM, Lee SJ. (1994). Limb alterations in brachypodism mice due to mutations in a new member of the TGF beta-superfamily. Nature *368*, 639-643.

Stricker, S., and Mundlos, S. (2011). Mechanisms of digit formation: Human malformation syndromes tell the story. Dev. Dyn. *240*, 990-1004.

Temtamy, S.A. and McKusick, V.A. (1978). The Genetics of Hand Malformations. Birth Defects Original Article Series (New York: Daniel Bergsma Publisher) *14*, i-xviii, 1-619.

Thomas, J.T., Lin, K., Nandedkar, M., Camargo, M., Cervenka, J., Luyten, F.P. (1996). A human chondrodysplasia due to a mutation in a TGF-beta superfamily member. Nat. Genet. *12*, 315-317.

Thomas, J. T., Kilpatrick, M. W., Lin, K., Erlacher, L., Lembessis, P., Costa, T., Tsipouras, P., Luyten, F. P. (1997). Disruption of human limb morphogenesis by a dominant negative mutation in CDMP1. Nat. Genet. *17*, 58-64.

Wang, M., and Marín, A. (2006). Characterization and prediction of alternative splice sites. Gene *366*, 219-227.

Wang, X., Xiao, F., Yang, Q., Liang, B., Tang, Z., Jiang, L., Zhu, Q., Chang, W., Jiang, J., Jiang, C., Ren, X., Liu, J.Y., Wang, Q.K., Liu, M. (2006). A novel mutation in GDF5

causes autosomal dominant symphalangism in two Chinese families. Am. J. Med. Genet. *140A*, 1846-1853.

Wu, M.Y., and Hill, C.S. (2009). Tgf-beta superfamily signaling in embryonic development and homeostasis. Dev. Cell *16*, 329-343.

Yang, W., Cao, L., Liu, W., Jiang, L., Sun, M., Zhang, D., Wang, S., Lo, W.H.Y., Luo, Y., Zhang, X. (2008). Novel point mutations in GDF5 associated with two distinct limb malformations in Chinese: brachydactyly type C and proximal symphalangism. J. Hum. Genet. *53*, 368-374.

Yi, S.E., Daluiski, A., Pederson, R., Rosen, V., Lyons, K.M. (2000). The type I BMP receptor BMPRIB is required for chondrogenesis in the mouse limb. Development *127*, 621-630.

Yoon, B.S., Ovchinnikov, D.A., Yoshii, I., Mishina, Y., Behringer, R.R., Lyons, K.M. (2005). Bmpr1a and Bmpr1b have overlapping functions and are essential for chondrogenesis in vivo. Proc. Nat. Acad. Sci. USA *102*, 5062-5067.

Zou, H., Wieser, R., Massagué, J., Niswander, L. (1997). Distinct roles of type I bone morphogenetic protein receptors in the formation and differentiation of cartilage. Genes Dev. *11*, 2191-2203.

5.11 Manuscript Figures, Tables and Legends

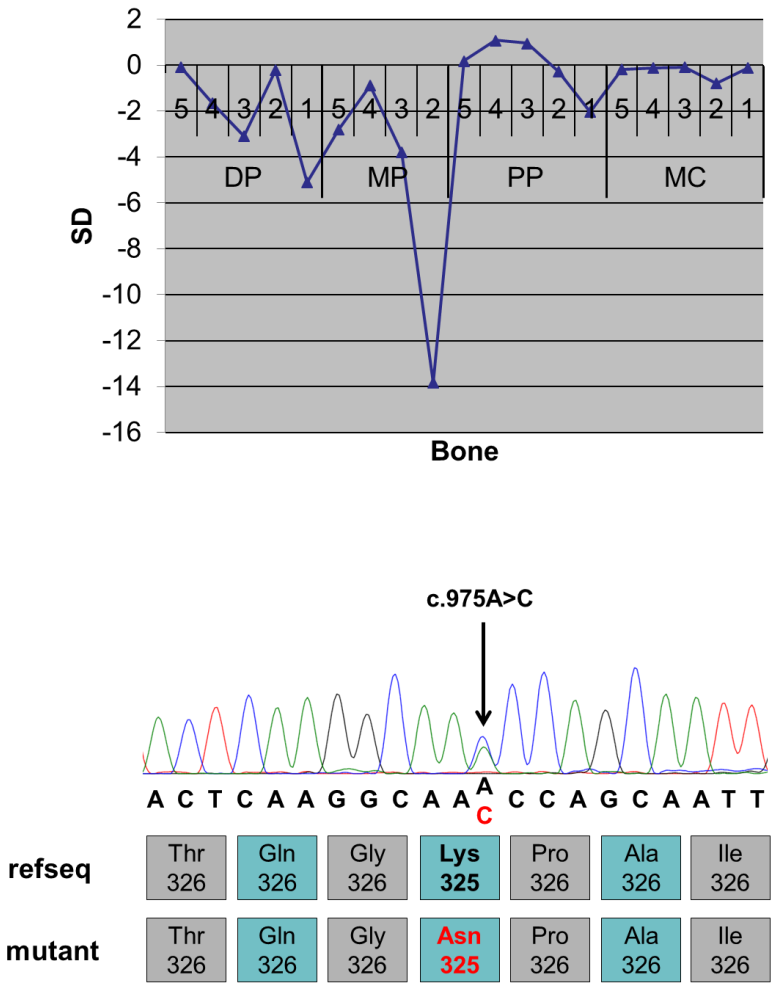

Figure 5.1. BMPR1B^{Lys325Asn} is associated with BDA1. **(A)** Results of the MCPP are plotted as the standard deviation (SD) for each hand bone measured in the proband. MCPP of the hands indicate the shortening (SD ≤ -2) of the proximal and distal phalange of digit 1, the distal and middle phalange of digit 3, and the middle phalange of digits 2 and 5. Distal phalange (DP). Middle phalange (MP). Proximal phalange (PP). Metacarpal (MC). Standard deviation (SD). **(B)** The sequencing of *BMPR1B* in the proband revealed a heterozygous c.975A>C (p.(Lys325Asn)). The mutation is highlighted in red font which is displayed in the sequence below the electropherogram and in the partial peptide sequence.

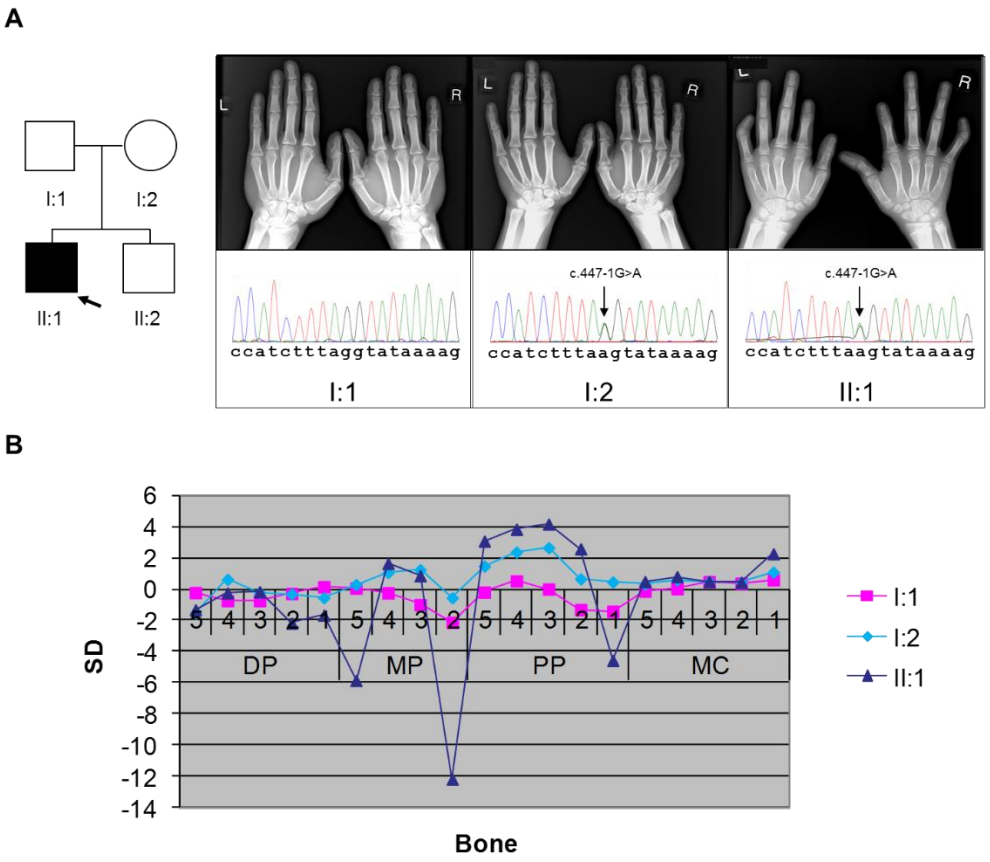

Figure 5.2. A donor splice site variant c.447-1G>A is associated with a complex BDA1 condition. (A) The sequencing of *BMPR1B* in three family members revealed a c.447-1G>A in the proband (II:1; marked with a black arrow) and his mother (I:2). Hand radiographs of each family member are displayed above its respective electropherogram. A pedigree of the family is shown to the left of the hand radiographs. A filled symbol represents an affected family member with BDA1. **(B)** Results of the MCPP are plotted as the standard deviation (SD) for each hand bone measured in the father (I:1; pink), mother (I:2; light blue), and proband (II:1; dark blue). MCPP of the family members displays extreme shortening of the proximal phalange of digit 1 and of the middle phalanges of digits 2 and 5 only in the proband. There are disproportionately long proximal phalanges of digits 3 and 4 in both the proband and mother. Distal phalange (DP). Middle phalange (MP). Proximal phalange (PP). Metacarpal (MC).

Figure 5.3. Mutation distribution across the species conserved intracellular region of BMPR1B. Mutations that are associated with the human conditions BDA1, BDA2, BDC/SYM1, IPAH and acromesomelic chondrodysplasia-type Grebe are marked above their respective residue position along the multiple sequence alignment of the BMPR1B protein from human (Hs), mouse (Mm), chicken (Gg), and sheep (Oa). Pfam protein domains, Transforming growth factor beta type-1 GS-motif (PF08515.7) and Protein kinase domain (PF00069.20) and are depicted below the alignment as orange and blue bars, respectively. The high degree of amino acid sequence conservation throughout BMPR1B is indicated below the amino acid sequences by the symbol "*****", whereas any deviation from sequence identity is indicated by "**:**". The Genbank accession IDs used for the ClustalOmega alignment are AAH47773.1 (Hs), AAH65106.1 (Mm), NP_990463.1 (Gg), and NP_001009431.1 (Oa).

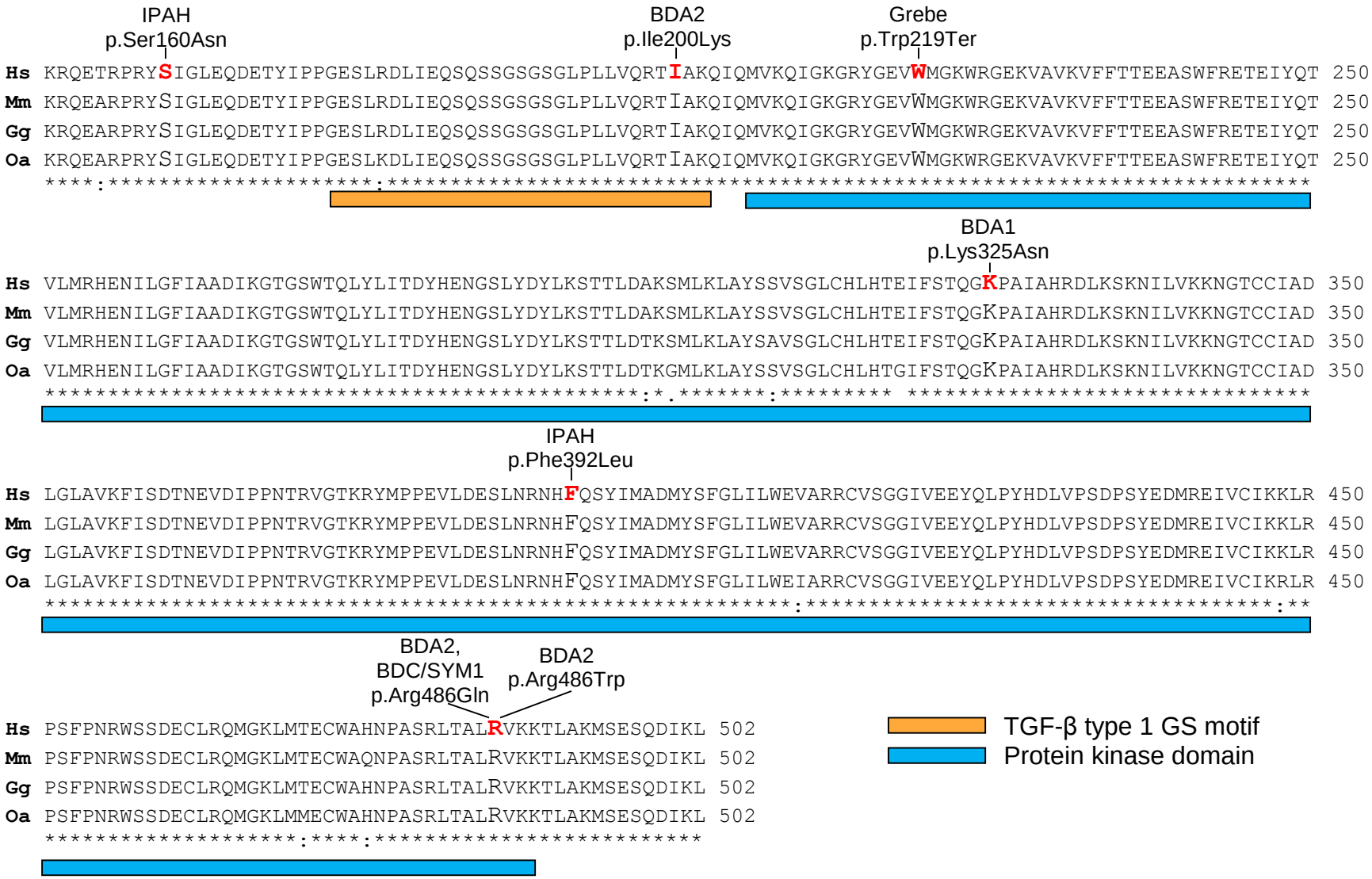
IPAH
p.Ser160Asn
BDA2
p.Ile200Lys
Grebe
p.Trp219Ter
Hs KRQETRPRYSIGLEQDETYIPPGESLRDLIEQSQSSGSGSGLPLLVQRTIAKQIQMVKQIGKGRYGEVWMGKWRGEKVAVKVFFTTEEASWFRETEIYQT 250
Mm KRQEARPRYSIGLEQDETYIPPGESLRDLIEQSQSSGSGSGLPLLVQRTIAKQIQMVKQIGKGRYGEVWMGKWRGEKVAVKVFFTTEEASWFRETEIYQT 250
Gg KRQEARPRYSIGLEQDETYIPPGESLRDLIEQSQSSGSGSGLPLLVQRTIAKQIQMVKQIGKGRYGEVWMGKWRGEKVAVKVFFTTEEASWFRETEIYQT 250
Oa KRQEARPRYSIGLEQDETYIPPGESLKDLIEQSQSSGSGSGLPLLVQRTIAKQIQMVKQIGKGRYGEVWMGKWRGEKVAVKVFFTTEEASWFRETEIYQT 250
BDA1
p.Lys325Asn
Hs VLMRHENILGFIAADIKGTGSWTQLYLITDYHENGSLYDYLKSTTLDAKSMLKLAYSSVSGLCHLHTEIFSTQGKPAIAHRDLKSKNILVKKNGTCCIAD 350
Mm VLMRHENILGFIAADIKGTGSWTQLYLITDYHENGSLYDYLKSTTLDAKSMLKLAYSSVSGLCHLHTEIFSTQGKPAIAHRDLKSKNILVKKNGTCCIAD 350
Gg VLMRHENILGFIAADIKGTGSWTQLYLITDYHENGSLYDYLKSTTLDTKSMLKLAYSAVSGLCHLHTEIFSTQGKPAIAHRDLKSKNILVKKNGTCCIAD 350
Oa VLMRHENILGFIAADIKGTGSWTQLYLITDYHENGSLYDYLKSTTLDTKGMLKLAYSSVSGLCHLHTGIFSTQGKPAIAHRDLKSKNILVKKNGTCCIAD 350
IPAH
p.Phe392Leu
Hs LGLAVKFISDTNEVDIPPNTRVGTKRYMPPEVLDESLNRNHFQSYIMADMYSFGLILWEVARRCVSGGIVEEYQLPYHDLVPSDPSYEDMREIVCIKKLR 450
Mm LGLAVKFISDTNEVDIPPNTRVGTKRYMPPEVLDESLNRNHFQSYIMADMYSFGLILWEVARRCVSGGIVEEYQLPYHDLVPSDPSYEDMREIVCIKKLR 450
Gg LGLAVKFISDTNEVDIPPNTRVGTKRYMPPEVLDESLNRNHFQSYIMADMYSFGLILWEVARRCVSGGIVEEYQLPYHDLVPSDPSYEDMREIVCIKKLR 450
Oa LGLAVKFISDTNEVDIPPNTRVGTKRYMPPEVLDESLNRNHFQSYIMADMYSFGLILWEIARRCVSGGIVEEYQLPYHDLVPSDPSYEDMREIVCIKRLR 450
BDA2,
BDC/SYM1
p.Arg486Gln
BDA2
p.Arg486Trp
Hs PSFPNRWSSDECLRQMGKLMTECWAHNPASRLTALRVKKTLAKMSESQDIKL 502
Mm PSFPNRWSSDECLRQMGKLMTECWAQNPASRLTALRVKKTLAKMSESQDIKL 502
Gg PSFPNRWSSDECLRQMGKLMTECWAHNPASRLTALRVKKTLAKMSESQDIKL 502
Oa PSFPNRWSSDECLRQMGKLMMECWAHNPASRLTALRVKKTLAKMSESQDIKL 502
TGF-β type 1 GS motif
Protein kinase domain

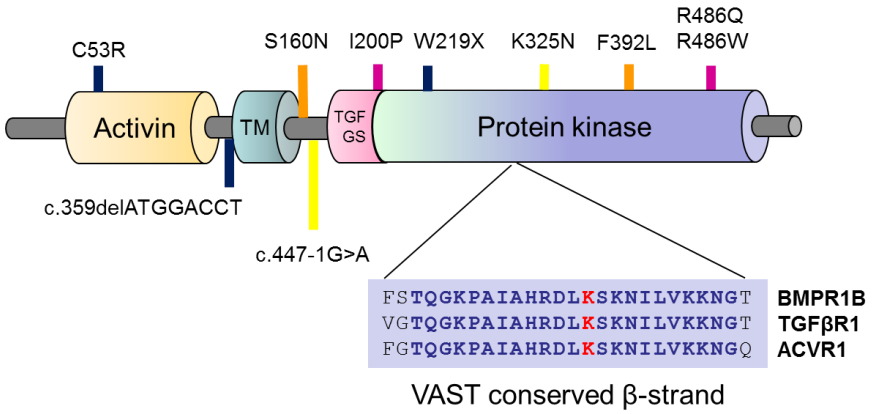

Figure 5.4. Mutation spectrum of BMPR1B. With the exception of two mutations that are associated with acromesomelic chondrodysplasia, mutations in BMPR1B are found in the intracellular signaling region. BDA1 (red font), BDA2 and BDC/SYM1 (black font), acromesomelic chondrodysplasia (dark blue font), and IPAH (purple font). Transmembrane domain (TM). TGF-GS (Transforming growth factor β GS domain). The location of a predicted VAST conserved β-strand using BMPR1B, TGFβR1 and ACVR1 as templates (also see Figure 5.6) is shown below the protein kinase domain.

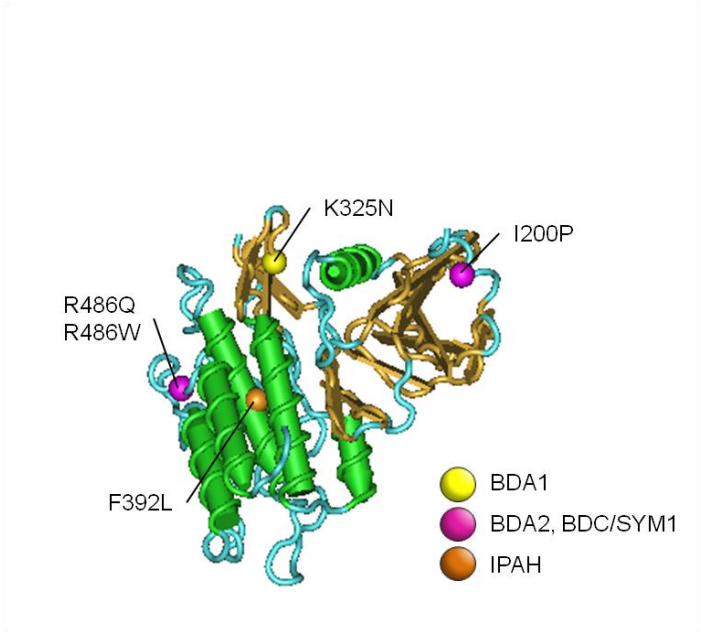

Figure 5.5. BDA1 and BDA2 mutations are found on the outer edge of the intracellular region of BMPR1B. A Cn3D (v4.3) tube view of the intracellular region of BMPR1B (PDB ID: 3MDY_A). Secondary structures are colored as follows: Alpha helices in green and beta strands in brown. Amino acid substitutions are described next to each colored ball for a specific human condition; yellow represents BDA1 p.(K325N), purple is for BDA2 (p.I200P, p.R486Q and p.R486W) and BDC/SYM1 (p.R486Q), and orange is associated with IPAH (p.F392L).

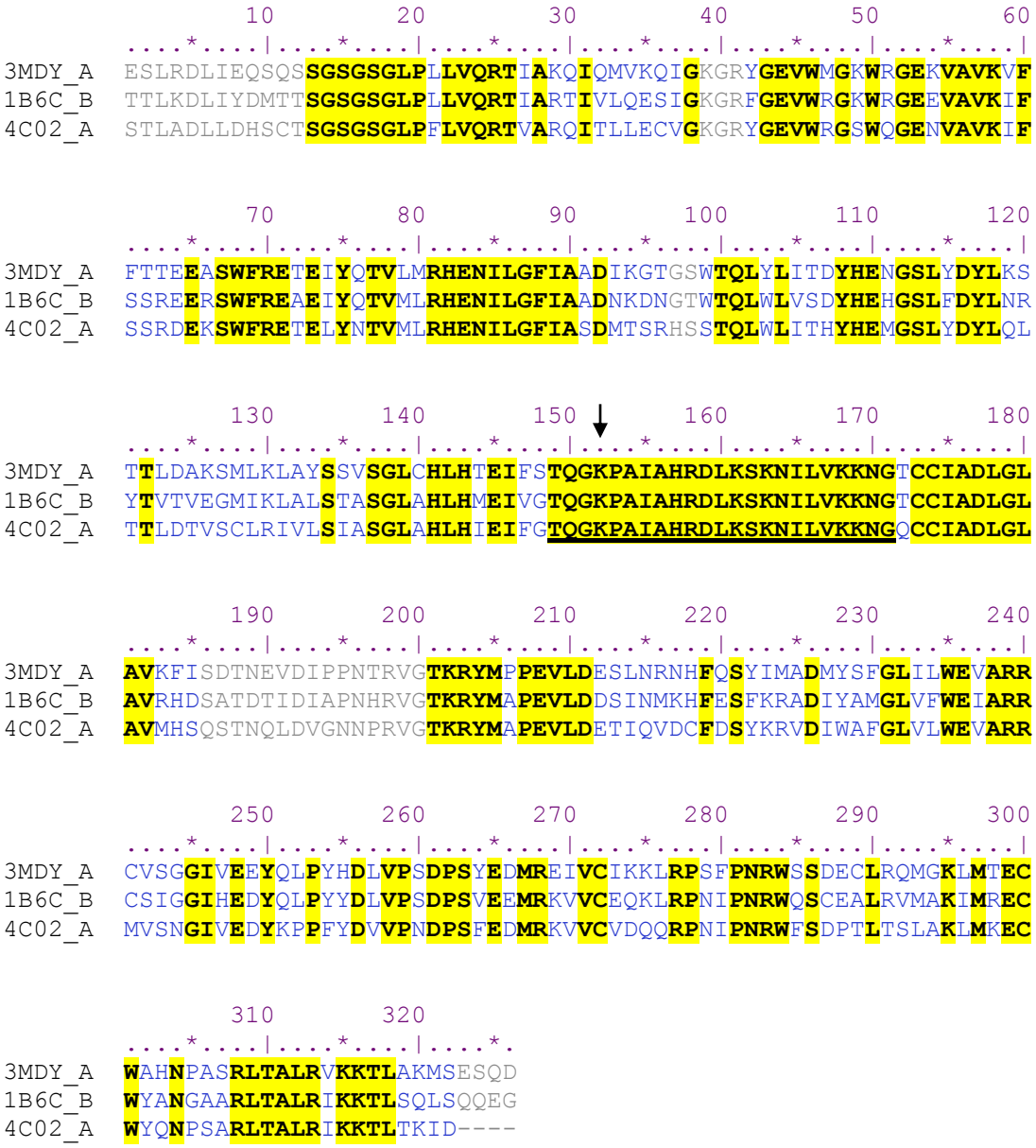

Figure 5.6. BMPR1B^{Lys325Asn} resides in a conserved structural motif. Three peptide chains from BMPR1B (3MDY_A.pdb), TGF-β Superfamily Receptor 1 (1B6C_B.pdb), and ACVR1/ALK2 (4C02_A.pdb) were aligned using VAST (NCBI Tools) to identify structural similarities in their 3D conformations. The numbering above the aligned sequences refers to the starting position of the alignment of all three peptide chains. The BDA1 mutation p.(Lys325Asn) (black arrow) is located in a structural conserved region (underlined amino acids) starting at the VAST alignment position 149 and ending at position 171. Identical residues within conserved structures are highlighted in yellow. Blue colored letters represent aligned but non-identical residues. Unaligned residues are colored in grey.

Table 5.1. Partial list of splice site predictions on mutant c.447-1G>A. Three online splicing prediction services, Alternative Splice Site Prediction (ASSP), Human Splice Finder (HSF) and SplicePort (SP) were used to evaluate the genomic region (HG19 NC000004.11) inclusive of *BMPR1B* exons 7-9 for c.447-1G>A. The mutant acceptor site was predicted to create a novel acceptor site at c.447. HSF consensus values greater than 80 were displayed except in the case of the mutant sequence. Variation values between wild-type and mutant sequences are expressed in percentages and are displayed within parentheses. N/A = not identified by prediction.

Putative splice site	Position	Sequence	ASSP		HSF		SP
			Score	Conf.	Cons. Value	MaxEnt	Score
Cryptic acceptor	c.447-112	tattatatttagGT	4.396	0.528	81.30	7.18	-1.0843
Constitutive acceptor	c.447-12	atccatctttagGT	8.856	0.451	83.39	10.56	1.14746
Mutant acceptor	c.447-1	atccatctttaagTA	3.291	0.709	77.85 (59.2%)	5.55 (332.22%)	-0.147124
Cryptic acceptor	c.447	acctcgatacagCA	N/A	N/A	82.57	N/A	-3.19676
Cryptic acceptor	c.558	ctcagagctcagGA	N/A	N/A	83.9	N/A	-4.45218
Constitutive donor	c.586	CTGgtatga	9.500	0.347	84.11	6.69	-0.245188
Cryptic acceptor	c.588+104	agctctatgcagTC	N/A	N/A	82.68	3.34	-4.23626

A

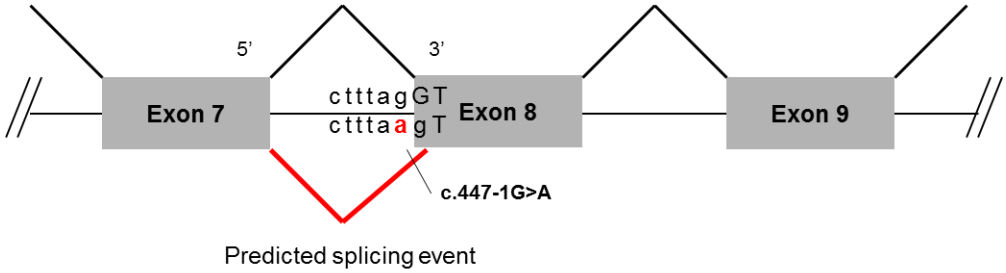

B

```
1....MLLRSAGKLNVGTKKEDGESTAPTPRPKVLRCKCHHHCPEDSVNNICSTD....50
51...GYCFTMIEEDDSGLPVVTSGCLGLEGSDFQCRDTPIPHQRRSIECCTERN....100
101..ECNKDLHPTLPPLKNRDFVDGPIHHRALLISVTVCSLLLVLIILFCYFRI....150
151..KDKKPDLDTALG*....162
```

Figure 5.7. Predicted splicing event for c.447-1G>A at exon 8 results in truncated peptide. (A) Selective view of exons 8, 9 and 10 of *BMPR1B*. Constitutive splicing is illustrated with black lines above the introns. The predicted splicing event for c.447-1G>A in intron 7 is highlighted in red resulting in exon 7 splicing into exon 8 at c.447. **(B)** The abnormal splicing event would cause a frameshift, adding 13 residues (grey highlight) before premature termination.

5.12 Manuscript Supplementary Information

Supplementary Table S5.1. Primer details for *BMPR1B*. Primer sequences were designed by ExonPrimer to amplify each exon of *BMPR1B* in human gDNA. Ta = anneling temperature.

Exon	Amplicon length (bp)	Ta (°C)	Forward sequence	Reverse sequence
1	225	62	AGCCGAGGAGCGAGAGG	CTCGGGAACTCGGCCAC
2	262	55	ATGTATTACCATGATTCTGC	TCTGTTAACTTCAGCATACC
3	295	55	GTAACATGCACACAGAGG	TCATTAGCTTTGACATGC
4	331	55	AATGTAATCTCATGTTTTCG	GTTCTTTGAAACACTAGCC
5	302	55	GCAATAAAACAAATGATACAC	AAAAGAATGGTTTTATCTTG
6	324	55	GTGTTTGAGTGAAATTGTTAG	TGGTACAGGTAGATTGAGAG
7	274	55	ATTTTGTGCGTGATACTTAG	GGCAAAAGCAGAATATTAG
8	296	55	GTGATTACCATTTTAGTTGC	TAAGTGAAACCCCATATTC
9	368	55	CAGTAATCGTTTCTTCTCTG	AGACAGATGAGTTAACATGC
10	495	55	AATTGAATGAAATGCTAAAC	TATCCTAGAAGCACTGCG
11	368	55	CTAACTAAAGCCATTGTTTC	AACCAGATCTTATAGACAGTATG
12	293	55	TCCTTTGAGAACTGTGTTAG	TCAATATGTGGAATTTTAGC
13_a	638	55	CAAACTTAATGAACCTAAAAC	TTAATTTACCTTCCAGCAG
13_b	631	55	TTTGCCAAAATAAAACAG	TTACCTCTATTTGAAAGCAC
13_c	623	55	CATCTCTTTCATGGTAAAAC	AATAGTGAATTGAGCATCAC
13_d	605	55	TAAAATCAATATGGTTGGAG	GATTCTCCCAAACTGTAAG
13_e	630	55	AACATTTTCCTCACTTCTG	GCTTAATTTCAAATCATCAC
13_f	635	55	ATCATCTACAAAACAACAGG	ACTCTTCTTAGTCTTTGAAATAG
13_g	617	55	AAAATTTCTAGTGGCTCAG	AATGAATATGTATGACTGTAGG
13_h	633	55	AATGAATATGTATGACTGTAGG	CAATGGGATATTTTCAAAG

Chapter 6. Evaluation of the *BDA1B* locus on chromosome 5p13.3

6.1 Preface

Cis-regulatory elements control the expression of developmental genes both spatially and temporally. Traditional positional cloning strategies for Mendelian based disorders mainly focus on identifying causal variants in the coding sequences. In this chapter I describe the evidence for an intergenic *cis*-regulatory variant which eluded detection in our earlier mutation screening strategies. The work described in this chapter has been submitted for publication. The paper has been formatted for this thesis and includes additional work related to the project. Additional investigation and data not included in the manuscript but still pertinent to the project was included as Supplementary Figures and Tables which is located after the cited references. Primer sequences which were used for the initial characterization of the *BDA1B* locus are listed in Appendix B. I have contributed to this work through primary authorship, artwork, targeted enrichment design, aCGH design, and all bioinformatics analyses. I have also performed all of the Sanger sequencing of transcriptional units, which were not assessed by previous students, preceding the high-throughput resequencing of the *BDA1B* locus, all *in-vitro* reporter assays and real-time quantitative PCR assays. Furthermore, I have contributed to the sectioning and photography work of the transgenic embryos. Consent forms are located in Appendix A.

6.2 Manuscript No. 4

An intergenic 9.5 kb duplication at chromosome 5p13.3 is associated with BDA1

Lemuel Racacho[1], Sarah M. Nikkel[2,3], Jennifer MacKenzie[4], Christine M. Armour, M[2,3]. Elizabeth McCready[5], Yves De Repentigny[6], Rashmi Kothary[6], Len A. Pennacchio[7,8], Dennis E. Bulman[1,2,3,9]‡

Affiliations:

1. Department of Biochemistry,Microbiology and Immunology, Faculty of Medicine, University of Ottawa, ON, Canada
2. Department of Pediatrics, Faculty of Medicine, University of Ottawa, ON, Canada
3. Department of Genetics, CHEO Research Institute, Children's Hospital of Eastern Ontario, Ottawa, ON, Canada
4. Department of Pediatrics, Kingston General Hospital, Queen's University, Kingston, ON, Canada
5. Pathology and Molecular Medicine, McMaster University, Hamilton, ON, Canada
6. Regenerative Medicine Program, Ottawa Hospital Research Insitute, Ottawa, ON, Canada
7. Genomics Division, Lawrence Berkeley National Laboratories, Berkeley, CA, USA
8. US Department of Energy Joint Genome Institute, Walnut Creek, CA, USA
9. Newborn Screening Ontario, Ottawa, ON, Canada

‡ Corresponding Author

Keywords: *Cis*-regulatory, brachydactyly A1, microduplication, phalanges, autosomal dominant

6.3 Manuscript Abstract

Brachydactyly type A1 (BDA1; MIM #11250) is a rare autosomal dominant trait primarily characterized by bilateral hypoplastic/aplastic middle phalanges. We previously mapped a locus for BDA1 to 11 cM at chromosome 5p13.3 (BDA1B; MIM %607004) in a single 7 generation Canadian family. We hypothesized that a gene within the *BDA1B* critical region was necessary for phalangeal formation and elongation. The subsequent sequencing of all protein coding genes in the linked region did not reveal a BDA1 causal variant. Furthermore, we did not identify any large genomic rearrangements across the region as determined by 3-color FISH, nor did we detect copy number changes using whole genome 500K SNP array. To provide a higher sensitivity of mutation detection, we performed a targeted high-throughput sequencing of the *BDA1B* locus. Here we report that a novel 9.5 kb microduplication downstream of *NPR3*, which codes for the natriuretic peptide clearance receptor, is associated with BDA1 in two unrelated families. Noncoding conserved sequence elements located within the microduplication behaved as temporal and tissue specific enhancers in an *in-vivo* reporter assay. We also showed an upregulation of *NPR3* and *PDZD2* expression in patients' fibroblasts, suggesting distal enhancer effects on dosage sensitive genes.

6.4 Introduction

Vertebrate skeletal development involves the precise orchestration of many complex signaling networks across specific tissue compartments at specific developmental timepoints. Genetic network maps have been instrumental in describing the interaction between signaling pathways and several key regulators of skeletal

development, such as BMPs and FGFs. Although there has been progress in characterizing many of the key molecules in skeletal formation, the spatial and temporal regulation of these factors in phalangeal formation and elongation are not fully understood.

The human genome is composed of 98% non-protein coding sequence (Gregory, 2005), of which as much as 3.5% is highly conserved (Bejerano et al., 2004, 2005). Some of these conserved sequences elicit robust reporter activity in specific mouse tissues (Pennacchio et al., 2006), demonstrating a selective pressure to retain these elements for the preservation of regulatory circuitry across species. Many of the conserved noncoding sequences are enriched in developmental genes (Visel et al., 2008). Although sequence conservation is often considered as indication of functional relevance, the deletion of some ultra-conserved elements result in viable mice with no overt phenotypes (Ahituv et al., 2007). Recently, distal enhancers which contribute to the development and morphology of the craniofacial bones in mouse have been identified (Attanasio et al., 2013). The ENCODE project has compiled a compendium of functional elements mapping to 80% of the human genome, many of which are not associated with protein coding sequences (ENCODE Project Consortium, 2012). Given our current understanding of the dynamic nature of the human genome, these noncoding conserved sequences could result in human malformations when perturbed. For example, point mutations in regulatory sequences (Lettice et al., 2003; Wierczorek et al., 2010) and intergenic copy number variations (CNVs) such as deletions (Staehling-Hampton et al., 2002; Coutton et al., 2014) and duplications (Dathe et al., 2009; Kurthe et al., 2009;

Wierczorek et al., 2010; Klopocki et al., 2011; Yuksel-Apak et al., 2012; Lohan et al., 2014) have been implicated in causing congenital human limb malformations.

Brachydactyly type A1 (BDA1, MIM #112500) was the first reported autosomal dominant trait in humans (Farabee et al., 1903). It is a rare congenital hand malformation primarily characterized by the bilateral shortening of the middle phalanges of digits 2-5 and the proximal phalanges of the thumbs. There is some evidence to support a broader effect of genetic perturbation in BDA1 as it can be associated with short stature and with non-skeletal clinical manifestations. Thus far only *IHH*, *GDF5* and now *BMPR1B* (see Chapter 5) have been associated with BDA1 where the mutations affect the encoded proteins' ability to bind to its receptor, resulting in a loss of downstream signaling (Gao et al., 2009; Byrnes et al., 2010; Degenkolbe et al., 2013). In 2002, we reported a single 7 generation family cosegregating an autosomal dominant BDA1 trait (Figure 6.1A) to an 11 cM region at chromosome 5p13.3 through linkage analyses (BDA1B; MIM %607004) (Armour et al., 2002). The critical region was further refined to a 2.8 Mb region (Figure 6.2A) yet the subsequent sequencing of the exons of all contained protein coding genes did not reveal a causal variant (McCready, 2004; Grimsey, 2006). In order to obtain higher resolution analysis of for detecting a mutation in the *BDA1B* critical region, we performed the integrative genomics strategy built on the hybridization enrichment of the locus in two affected family members followed by high-throughput sequencing (HTS). We report the identification of a novel intergenic 9.5 kb microduplication 265 kb downstream of *NPR3*. Our findings in this report imply the dysregulation of tissue specific *cis*-regulatory sequences as a mechanism of causing BDA1.

6.5. Materials and Methods

Ethics statement

The current study was approved by the research ethics boards of the Ottawa Hospital and the Children's Hospital of Eastern Ontario. Genetic testing required voluntary informed consent by the patient or his/her legal guardians.

Patients

Selected members of a seven generation Canadian family (Family-1) that displayed a mild form of BDA1 (Armour et al., 2002), were evaluated for causal sequence variants in novel exons and noncoding RNAs within the 2.8 Mb critical region prior to executing the targeted sequencing of the entire *BDA1B* locus in two family members. New members of Family-1 were examined by S. Nikkel and genotyped with microsatellite markers within the *BDA1B* haplotype as defined by Armour et al. (2002), McCready (2004) and Grimsey (2006). In addition to Family-1, we have established a BDA1 collection of BDA1-affected individuals consisting of 28 families. Of the 28, 9 probands who did not have mutations in *IHH*, *GDF5* or *BMPR1B*, and were thus assessed for any candidate causal variant resulting from the targeted sequencing of the *BDA1B* locus. Hand radiographs were available for many indiviudals of our BDA1 collection.

Nucleic acids extraction and isolation

Genomic DNA (gDNA) was isolated, as per the manufacturer's protocol, from either whole blood, spit or primary fibroblasts using QIAmp DNA Blood Mini Kit (Qiagen), Oragene·DNA (DNA Genotek) and QIAmp DNA Mini Kit (Qiagen), respectively. DNA was purified using ethanol precipitation after extraction with

Oragene·DNA Kit. All PCR products were isolated and purified using QIAquick Gel Extraction Kit (Qiagen). RNA isolation was performed as recommended by the manufacturer with either QIAquick RNAeasy Kit (Qiagen), Purelink® RNA Mini Kit (Ambion) or TRIzol® (Invitrogen). All RNA preparations were treated with DNAse I. DNA was quantified with a NanoDrop 1000 (Thermo Fisher). RNA quality was assessed with a 2100 Bioanalyzer (Agilent Technologies) and only a RIN >8.0 was used for downstream applications.

Fluorescence-based capillary electrophoresis

PCR products were preprocessed with either a QIAquick Gel Extraction Kit (Qiagen) or treated with ExoSap-It® (USB) as per the manufacturers' protocols. Sequencing in both directions was performed on each amplicon with BigDye® Terminator V3.1 as previously described (Byrnes et al., 2010). Amplification primers were used as sequencing primers unless specified (Supplementary Table S6.1 and Appendix B). Excess dye-terminators were removed with either Sephadex®-G50 or by ethanol precipitation. The sequencing reactions were loaded onto a 3130*xl* Genetic Analyzer (Applied Biosystems). ABI formatted electropherograms were manually inspected for read quality with Sequencing Analysis Software (Applied Biosystems) and FinchTV (Geospiza, Inc), followed by BLAT alignment to human reference build hg19 (UCSC Genome Browser Tools). A bonafide sequence variant was defined as a nucleotide mismatch or gap relative to the human reference sequence, and validated in both forward and reverse sequencing reads.

Analyses for large genomic rearrangements

Three color fluorescent *in-situ* hybridization (3-color FISH) was performed by TCAG (The Hospital for Sick Children, Toronto, ON) as a clinical cytogenetic service on an immortalized lymphoblastoid cell line from an affected individual of Family-1 (P1-74). Six BAC probe combinations were tested for any deviation in the physical order and copy number across the critical region (Supplementary Figure S6.1A). The critical region was also evaluated for copy number using an Affymetrix GeneChip® Mapping 500K Set on an affected individual from Family-1 (P1-09). This was performed as a clinical diagnostic service by TCAG. A custom high-resolution NimbleGen array comparative hybridization (aCGH) was performed by Roche-NimbleGen (Iceland) to assess copy number across a 2.2 Mb region at chromosome 5p13.3 in a panel of twelve test samples which consisted of two affected members of Family-1 (P1-26 and P1-64), nine unrelated BDA1 patients (P6-01, P9-01, P11-01, P15-01, P19-01, P24-02, P26-01, P27-01, and P28-01) and one unrelated and unaffected female control sample. To maximize the available microarray surface for testing, we chose a 2.2 Mb region which contains the duplicated interval. A NimbleGen custom 135K x 12 array was used to hybridize 1 μg of Cy-3 labelled test gDNA and 1 μg of Cy-5 labelled male reference DNA per array according to the manufacturer's protocol. A high density arrangement of probes (n = 134245) with an average spacing of 10 bp (median = 9 bp) were designed to hybridize gDNA fragments originating from a 2.2 Mb target region at chromosome 5p13.3 with hg19 genomic coordinates g.32567043 to g.34764243. The relative probe signal ratios of patient versus the reference were plotted on a $\log_2$ scale. The $\log_2$ ratios were calculated as averaged normalized probe ratios in a 100 bp window with the CGH-

segMNT algorithm (Roche-NimbleGen) and visualized using DEVA V1.2 software (Roche-NimbleGen).

High-throughput sequencing of targeted *BDA1B* locus

Approximately 1 μg of gDNA from affected patients P1-06 and P1-64 were individually fragmented and separately hybridized to a custom solid support NimbleGen array. The 2.8 Mb critical region (hg19:g.31896378-34721586) was extended on both sides to achieve a total of 3.2 Mb (hg19:g.31634243-34834243) for enrichment with probes (3 probe redundancy) designed to give an expected coverage of 74%. The probe design and hybridization service was provided by Roche-NimbleGen (Madison,WI). Fragmented gDNA was polished then ligated with Roche 454 sequencing adapters. As such, NimbleGen enriched fragments were primed for pyrosequencing using Titanium™ reagents on a Roche 454 FLX platform. The sequencing was performed as a service by TCAG (Toronto, ON). Sequencing reads were automatically assembled into contigs with GS De Novo Assembler (Roche) and aligned to human reference hg19 with GS Reference Mapper (Roche) after adapter trimming.

Breakpoint analyses

A PCR-based assay to evaluate the breakpoints in patients and controls was achieved by designing outwardly facing primers (Supplementary Table S6.1) positioned at the junction as illustrated in Figure 6.4a). Multiplex PCR on gDNA was performed in a 50 μl reaction volume as follows: 50 ng template, 10X PCR buffer (200 mM Tris-HCl pH8.4, 500 mM KCl; Invitrogen), 2.5 mM $MgCl_2$ (Invitrogen), 10 mM dNTPs (Roche), 10 μM each primers, 1U r*Taq* (Invitrogen). PCR cycling conditions on a Hybaid MBS 0.2G thermal cycler (ThermoFisher) were 95°C 5 min, 30 cycles of 95°C 30 s, 55°C 30 s,

72°C 40 s, with a final 72°C extension for 10 min. Similarly, single PCR was performed with each primer pair. The PCR products were loaded onto a 1% agarose gel and electrophoresed using a Mini-Gel Sub System (BioRad) at constant voltage (65 V). Amplified products were visualized with EtBr staining under UV. DNA fragments were isolated and column purified after electrophoresis with QIAquick Gel Extraction Kit (Qiagen) in accordance to the manufacturer's instructions. Expand 20 kb PLUS PCR System (Roche) was performed as instructed by the manufacturer to estimate the size of the duplication in a junction-positive patient. Long range PCR was performed on 50 ng of gDNA with primers extending approximately 1 kb upstream and downstream of the donor region (Supplementary Table S6.1). PCR cycling conditions were 92°C 2 min, 10 cycles of 92°C 10s, 55°C 30s, 68°C 18 min, followed by 20 cycles of 92°C 10s, 55°C 30s, 68°C 18 min with subsequent extension at 10 s/cycle, and ending with a final 68°C extension for 7 min. Human β-globin primers from the kit allowed for the amplification of a 23 kb fragment. Amplified products were electrophoresed at constant voltage (50 V) on a 0.8% low melt agarose gel and visualized with EtBr staining under UV.

Cell cultures

Primary dermal fibroblasts and human osteosarcoma U2OS cells (kind gift from Dr. Michael Huh) were cultured on 100 mm culture plates in growth media (DMEM: 1 mM Glutamine/1 mM Glucose; 10% FBS; 5000 Units/ml penicillin-streptomycin), in a humidified incubator at 37°C with 5% CO_2. Patient fibroblasts from Family-1 and Family-24 were derived from 5 mm skin punctures. A healthy female donor of age 40 years with no clinical features of BDA1, mentioned herein as our study's age-matched control, provided a dermal sample.

The skin punctures were immediately placed in DMEM supplemented with 50 U/ml penicillin-streptomycin (Invitrogen). All of the skin punctures were sectioned into 1 mm pieces, placed in the center of a 35 mm culture dish and covered with a 10 mm sterile glass coverslip. Growth media was carefully added to the tissue explants and left undisturbed for 3-4 days. Coverslips were removed by sterile forceps after 7 days and the cultures were allowed to grow for another 7 days before its expansion onto a 60 mm culture dish. Primary fibroblasts were grown to 70-80% confluency before expanding 1:3 onto 100 mm culture dishes. All cultures were harvested with 1% TrypLE trypsin (Invitrogen) after 2 washes in calcium and magnesium free 1X PBS (Invitrogen). Growth media was replaced every 2 days after one wash with sterile 1X PBS.

Reverse transcriptase quantitative PCR

First strand synthesis was generated with SuperScript® Vilo™ (Invitrogen) on 1 μg of human primary fibroblast total RNA as per the manufacturer's instructions and a two-step reverse transcriptase quantitative PCR (RT-qPCR) was performed to evaluate gene expression. FAM™ dye-labeled TaqMan® pre-validated assays for *PDZD2* (Hs00389477_m1), *NPR3* (Hs01099009_m1), *LOC34011* (Hs03657763_m1), *TARS* (Hs01080958_m1), and *RAI14* (Hs00210238_m1) were evaluated for relative gene expression in patients (P1-12 and P24-02) versus control. The TaqMan® assays were chosen to detect a specific exon-exon junction. Each target probe was individually mixed in a 20 μl reaction consisting of 100 ng of cDNA, VIC® dye-labeled primer limiting endogenous control *ACTB* (Hs99999903_m1) or *TBP* (Hs99999910_m1) and TaqMan® Gene Expression Master Mix. Each target assay was performed in 3 technical replicates in standard mode on an Applied Biosystem® HT4500 Fast Real-Time PCR System.

Relative quantification of gene expression to the age-matched control using the ΔΔCt relative quantitation method was calculated for each target assay. Fold change was calculated as $2^{-\Delta\Delta Ct}$.

Generation of reporter expression vectors

Primers at 0.5 μM were designed to flank potential regulatory elements (RE) within the donor region for amplification in 100 ng human gDNA, 200 μM dNTPs, 1 X Phusion® HF buffer and 0.02 U/μl Phusion® High-Fidelity DNA Polymerase (NEB). The junction amplicon [B-A] was amplified from the gDNA of a junction-positive BDA1 patient. Individual restriction endonuclease recognition sites for *Kpn*I, *Nhe*I and *Sac*I (NEB) were added to the 5'-end of each primer as described in Supplementary Table S6.1. PCR cycling conditions on a Hybaid MBS 0.2G thermal cycler (ThermoFisher) were 98°C 30 s, 30 cycles of 98°C 5 s, 60-65°C 30 s, 72°C 45 s, with a final 72°C extension for 10 min. PCR products were electrophoresed in an EtBr-preloaded 1.2% agarose gel and briefly visualized under UV. Each purified fragment was subjected to double digestion with the appropriate restriction endonucleases (*Kpn*I-*Sac*I: [RE2], [RE4], [RE5], [B-A], [RE6]; *Kpn*I-*Nhe*I: [RE1]; *Nhe*I-*Sac*I: [RE3]) and Buffer 1 (NEB) in a 100 μl reaction volume at 37°C for at least 3 hours. The purified inserts were ligated with T4 DNA ligase (NEB) into the multiple cloning site of the reporter pGL-4.26 [*Luc2*/*minP*/*Hygro*] (Promega) at an insert to vector ratio of 3:1. Ligation products (25-50 ng) were transformed into 100 μl of DH5α competent cells (Invitrogen) in a 17 x 100 mm polypropylene tube (BD Falcon) by first incubating the mixture on ice for 10 min, heat-shocking at 42°C for 45 s, chilling on ice for 2 min and then incubation in freshly prepared SOC media at 37°C for 1 hour. The transformed cells were plated on 100

mg/ml ampicilin LB plates and grown at 37°C overnight. Ampicilin resistant colonies were picked and grown overnight at 37°C in 5 ml LB. Reporter plasmids for each test insert were extracted and column purified using QIAprep Spin Miniprep kit (Qiagen) as per the manufacturer's protocol. Each reporter expression vector was verified by sequencing with primers listed in Supplementary Table S6.1.

Cell based reporter assay

U2OS cells were seeded onto a 6 well culture plate at a density of 2.0 x 10^5 cells per well 24 hours before the co-transfection of 1 μg test and 100-500 ng pGL4.74[pRluc-TK] transfection control reporters with transfection media (Genejuice® or Nanojuice® (Novagen) transfection reagent diluted in Opti-Mem® (Invitrogen)). Transfection media was replaced with complete growth media after 6-8 hours. The Dual-Luciferase® Reporter Assay (DLR™) (Promega) was performed after 24 hours of transfection according to the manufacturer's instructions. Briefly using reagents from the DLR™ kit, 500 μl of 1X Passive Lysis Buffer was added to each well and 20 μl aliquots were added to 100 μl of LARII solution in a 1.5 ml microcentrifuge tube. 100 μl Stop & Glo® solution was added after the first fluorescent reading. All fluorescent readings were performed as a single assay on a 20/20n luminometer (Turner Biosystems). At least three independent experiments for each assay were performed.

Mouse transgenic reporter assay

An *in-vivo* evaluation of the conserved elements in the donor region was performed as described by Pennacchio et al. (2006). Briefly, two nonoverlapping test fragments, [RE7] and [RE8], were individually generated by the amplification of human gDNA with primers (Supplementary Table S6.2) for Gateway® cloning into pENTRO/D-

TOPO vector (Invitrogen). Entry clones were transferred via LR clonase™ into the destination reporter vector containing a Gateway® cassette and a basal *Hsp68* promoter coupled to *LacZ*. Plasmid DNA was linearized with either *Xho*I or *Hind*III and purified by Montage® PCR centrifugal filters and Micropure-EZ enzyme remover (Millipore) before pronuclear injections of 1.5-2 ng/μl plasmid into FVB/N embryos. Transgenic embryos were harvested at E11.5 and E13.5 and prepared before staining by three 30 min cleansings with wash buffer (2 mM $MgCl_2$, 0.01% deoxycholate, 0.02% NP-40, 100 mM phosphate buffer at pH 7.3). Embryos were incubated at room temperature for 24 hours in staining solution (wash buffer supplemented with 0.8 mg/ml X-gal, 4 mM potassium ferrocyanide, 4 mM potassium ferricyanide, and 20 mM Tris at ph 7.5) followed by 3 rinses in 1X PBS and fixed in 4% paraformaldehyde. Whole-mounted embryos were photographed with a Nikon Coolpix E4500 digital camera which was mounted on a Leica MZ95 light microscope with an Intralux 5000-1 as a light source.

Bioinformatics

GS Referene Mapper (Roche) was used to identify sequence variants by mapping 454 sequence flowgrams, also known as sff files, to the hg18 reference genome. The genomic coordinates of each variant was converted to hg19 coordinates by UCSC Liftover (UCSC Genome Tools). A separate analysis on NextGENe® software (SoftGenetics) was performed on the 454 formatted sff sequence reads. The pipeline consisted of a series of preprocessing, starting with the removal of sequencing adapters, followed by the removal of low quality reads (QV < 20) and 3' end soft trimming (details described in Supplementary Materials and Methods). Reads less than 50 bases were finally removed before hg19 reference genome alignment at 80% of the read length.

Sequence variants meeting the criteria of 100% and > 20% mutation call rate, were binned into homozygous and heterozygous variants, respectively. Each patient's variants list were annotated and filtered for known sequence variants from Exome Variant Server (http://evs.gs.washington.edu/EVS/), our chr5p13.3 sequence variant catalogue (Appendix C) and UCSC Genome Browser Annotation data tracks dbSNP142 and Personal Genome Variants (Karolchik et al., 2014). This was followed by genome coordinate intersection to identify novel and shared sequence variants. Sequence variants sharing the same genomic coordinates with known variants but having a different annotated nucleotide change were included as novel sequence variants. The variants were then annotated with genome features derived from UCSC Table Browser (Karolchik et al., 2004, 2014) and prioritized for further validation and verification. Pooled single-end reads from P1-06 and P1-64 were analyzed by NextGENe® software (SoftGenetics) to identify large (≥ 100 bp) structural sequence variants by creating pseudo paired-end reads or split-reads. These were derived from first aligning the reads at 30% with seed length at 22 bases to the reference genome. The split-reads were aligned back to the reference genome at 90% match. Structural sequence variants were filtered against DGV (Iafrate et al., 2004; Zhang et al., 2006; MacDonald et al., 2014), DECIPHER (Firth et al., 2009), human chained self aligned regions (Schwartz et al., 2003), segmental duplications (Bailey et al., 2001, 2002), and repetitive elements (http://repeatmasker.org).

UCSC Genome Browser (GRCh37/hg19) (Kent et al., 2002) was used to visualize ENCODE tracks (Rosenbloom et al., 2013) to identify various epigenetic marks and ChIP-seq signatures within the donor region. UCSC Table Browser (Karolchik et al.,

2004) were used in conjunction with Galaxy (Giardine et al., 2005; Blankenberg, et al., 2010; Goecks et al., 2010), to analyze and format data.

Potential regulatory elements (RE) within the donor region were defined by PhyloP subtrack (Pollard et al., 2010; Karolchik et al., 2014) and ENCODE/BROAD Institute DNase I hypersensitive sites (Release 3, August 2012) (Mikkelsen et al., 2007; Ernst et al., 2011; Rosenbloom et al., 2013) on UCSC Genome Browser. Predicted human enhancer blocks within microduplications which are associated with digit malformations were downloaded from EnhancerFinder (Erwin et al., 2014). The identification of motif blocks within multiple aligned sequences was performed using MEME and MAST V4.9.1 with max motifs = 3, min motif width = 6, max motif width = 50, and occurrence of motif = zero or one per sequence (Bailey et al., 1994, 1998 and 2006). Each FASTA sequence was masked for repetitive elements by RepeatMasker (http://repeatmasker.org) before submission into MEME. TOMTOM V4.9.1 (Gupta et al., 2007) was used to find similar matches of position-specific scoring matrices (PSSMs) between each motif and a vertebrate transcription factor binding site (TFBS) in three databases, JASPAR 2014 (Sandelin et al., 2004; Mathelier et al., 2014), UniPROBE Mouse (Newburger and Bulyk, 2009) and Human and Mouse Jolma2013 (Jolma et al., 2013). Predicted TFBS were also identified with rVISTA (Loots and Ovcharenko, 2004) after enriching for sequence conservation via ECRBrowser (Ovcharenko et al., 2004) at DCODE (www.dcode.org, NCBI).

Statistical analyses

Multiple group comparisons for the dual luciferase reporter assays were analyzed using the non-parametric Kruskal-Wallis *H* test followed by post hoc pairwise

comparisons using the Dunn's test with corrected p values at $\alpha = 0.05$. Data are presented as mean ± SD. Statistical significance was claimed at $p < 0.05$. The statistical analysis of relative gene expression was performed by BootstRatio, an online statistical package which utilizes a combination of bootstrap and permutation tests to specifically assess normalized RE derived from very small sample sizes (Clèries et al., 2011).

6.6 Results

6.6.1 Assessment of the *BDA1B* locus

As a result of the dynamic annotation level of the human reference genome, we screened for candidate BDA1-causal variants in novel protein-coding exons, ESTs and miRNAs which were annotated at the critical region. The sequencing of these features in several affected Family-1 members did not reveal a BDA1-causal variant (Supplementary Table S6.3). Although previous students managed to narrow the critical region by genotyping the family with additional polymorphic genetic markers, the inclusion of two additional family members prompted us to evaluate them for any potential recombination events which could have further narrowed the region. However, no novel recombination events were identified as the genotyping of the two new members of Family-1 with suspected mild BDA1 resulted in both having no carrier status of the *BDA1B* haplotype (Supplementary Figure S6.2). The evaluation of potential large genomic rearrangements at the critical region by 3-color FISH in an affected Family-1 individual resulted in a potential inversion event located between BACs RP11-78O23 and RP11-684I7 (Supplementary Figure S6.1B and Table S6.2). However another experiment, utilizing a closer anchored probe RP11-78O23 with RP11-208F4 and RP11-1149M13, yielded

expected middle probe ratios and thus did not support the initial finding (Supplementary Figure S6.1B and Table S6.2).

6.6.2 Evaluation of HTS of the targeted *BDA1B* locus

A total of 449965 reads with an average read length of 224 bp were aligned to the 2.8 Mb critical region, resulting in an average of 36X coverage. Simple sequence variants were defined as a variant belonging to the group of single nucleotide substitutions, insertions, deletions or any indel of less than 50 bp. A total of 3172 and 2860 simple sequence variants were identified in P1-06 and P1-64, respectively, by GS Reference Mapper (Figure 6.2B). Further filtering with dbSNP142, Personal Genome Variants, Exome Variant Server, and our own chr5p13.3 catalogue of variants retained only 94 shared variants of which 91 were identified within chained self aligned regions or segmental duplications. The remaining 3 variants were found within intergenic regions (Supplementary Table S6.4). Forty-nine large structural variants of greater or equal to 100 bp were identified in a separate analysis (Figure 6.2C). The split-reads analyses on both patients revealed a suspicious alignment at hg19 coordinates g.33057268 and g.33066676 (Figure 6.3A). The presence of wildtype sequence reads at both breakpoints suggested the presence of a heterozygous novel tandem duplication of a 9469 bp donor sequence. The nearest protein coding genes, *NPR3* and *TARS*, flanked the donor region 265 kb and 374 kb upstream and downstream, respectively (Figure 6.3A). A genome view of the donor region revealed only two DGV annotated deletions, one spanning the entire donor region (nsv523429) and the other overlapping the proximal breakpoint by 59 bp (nsv881181) (Figure 6.3B). The alignment of the reference sequences to the junction sequence revealed two pairs of direct repeats at the duplication breakpoint sites and

several dinucleotide microhomology sites including a $(A)_2$ at the breakpoint (Figure 6.3C).

Sequence conservation as determined by PhyloP in 100 vertebrates (UCSC Genome Browser) revealed several conserved elements across the donor region with some elements overlapping annotated DNase I hypersensitive sites (Figures 6.6C and Supplementary Figure S6.3). A specific DNase I hypersensitive site contained within RE2 was positioned over an ENCODE annotated polycomb segment and an L1 retrotransposon of the L1PA2 family. RNA-seq evidence suggests the region is actively transcribed. The position of the ENCODE ChIP-seq peaks in osteoblasts and adult human dermal fibroblasts for H2A.Z, a histone variant involved with chromatin dynamics such as compaction, and H3K4me1, a histone marker associated with poised enhancers, overlapping with RE5 (SupplementaryFigure 6.3).

6.6.3 Verification reveals a similar breakpoint in another BDA1 family

As illustrated in Figure 6.4A, a junction amplification product should only exist if primers B and A are juxtaposed as a result of a tandem duplication. A single fragment migrating between 200-300 bp was observed in the two BDA1 patients, P1-06 and P1-64, who were previously shown by HTS to harbor the breakpoints (Figure 6.4B). The expected size of the junction amplicon was 266 bp. The same fragment size was observed in the remaining affected Family-1 members and was not detected in unaffected related individuals and in 300 controls. PCR was performed with DNA from affected individual P1-26 with primer pair A and B yielding a single amplicon between 200-300 bp. The sequencing of this amplicon and its BLAT alignment to the HG19 human reference verified the breakpoint at g.33057268 and g.33066676 (Figure 6.4C). The

additional screening for the junction amplicon in our BDA1 panel resulted in its detection in an unrelated BDA1 individual P24-02 (Figure 6.4B). Family-24 consisted of three BDA1-affected individuals (Figure 6.1B). The proband was an 8 year old female presenting with short fingers and severe inflammation of the interphalangeal joints. Her hand radiographs displayed short middle phalanges in all of the digits and a short metacarpal of digit 5. Her mother and brother also displayed similar hand features. A slight distal radial deviation of digit 3 was observed in the proband. Her brother also presented with distal radial deviation but in digit 4. The mother reported finger joint stiffness with mild pain. Unlike Family-1 there was no indication of asthma in Family-24.

We further verified the length of the suspected tandem duplication by long range PCR with primers designed to flank the donor region. The amplification of gDNA from a junction-positive patient with these primers resulted in two amplicons, one migrating around 12 kb and the other at a similar position as the 23 kb control β-globin fragment (Figure 6.4D). The expected size of an amplified wildtype allele is 12864 bp whereas the size of a mutant amplicon in the junction-positive sample is expected to be 22334 bp. An unaffected Family-1 member who tested negative for the junction amplicon only displayed a single fragment migrating around 12 kb.

6.6.4 Screening BDA1 probands for copy number variation

Since the design of the junction amplicon and long range PCR assays were specific in their evaluation of the breakpoints, any other duplication which might overlap the duplicated interval would not be detected by these methods. Thus, our panel of 9 BDA1 probands including three junction-positive individuals, P1-26, P1-64 and P24-02,

were assessed for copy number across a 2.2 Mb region with high density aCGH. A plot of the $\log_2$ probe ratios confirmed a gain of one genome copy at the expected coordinates for the duplicated region in three junction-positive individuals (Figure 6.5). However, we did not identify any duplication which spans the donor region in the remaining patient samples (Supplementary Figure S6.4). Initially we did not detect copy number change across the critical region by means of a whole genome 500K SNP array as there was only one probe featured in the donor region (Supplementary Table S6.5).

Thus far, 16 of 28 families in our BDA1 collection have a known gene or locus associated with BDA1. A summary of the clinical manifestations and molecular findings in our BDA1 collection is presented in Supplementary Table S6.6.

6.6.5 Cell based assessment of potential regulatory elements

We tested individual REs, which were mapped to the donor region (Figure 6.6B), for enhancer activity in a human bone derived cell line. We noticed a very significant fold change of reporter activity in U2OS cells (H (7) = 24.35, p = 0.000989, Figure 6.6A). Moreover, a post hoc Dunn's test on separate pairwise comparisons of reporter inserts [RE4], [RE5] and the junction amplicon [B-A] to empty vector revealed a significant increase in fold change activity (Z = 23.49, one-tailed, p = 0.0018) (Figure 6.6A and B). Two test inserts, one labeled [RE2] which overlaps a DNAse I hypersensitive site within a nonconserved and fast evolving region as indicated by the plotted negative phyloP scores in red, and the other labeled [RE3] elicited stronger reporter activity than the neighboring conserved elements (Figure 6.6A). We also tested two potential regulatory elements mapped outside the donor region, an upstream promoter element [RE1] and a downstream enhancer element [RE6]. These sequence elements were not annotated by

EnhancerFinder but showed typical ENCODE histone modification marks for promoters, such as H3Kme3, and enhancers, such as H3Kme1. Although both test elements elicited strong reporter activity, only [RE6] displayed a similar positive effect as [RE2] and [RE3] (Figure 6.6A).

6.6.6 *In-vivo* evaluation of potential enhancers in mouse

Since *IHH* is known to be expressed at the limb buds at E11.5, we individually tested RE7 and RE8 in an *in-vivo* transgene reporter assay at this developmental timepoint. The testing of RE8 did not result in any transgene reporter expression at E11.5, resulting in our decision not to further test this fragment at E13.5. The X-gal staining of whole-mounted E11.5 transgenic embryos displayed reporter expression for only the RE8 transgene. We observed a consistent staining pattern at the shoulder crest and the spinal cord (n=4/8) as represented by Embryo-1 and -2 (Figure 6.6D). In one embryo, namely Embryo-2, we noted a strong and distinct staining at the dorsal-posterior region of the limb bud. At E13.5, the RE8 transgene elicited more tissue expression with a consistent staining pattern at the hindlimbs, pelvis and shoulders (n=7/10) as represented by Embryo-3 and -4 (Figure 6.6D). The forelimb, hindlimb, zygomatic arch, dorsal segment of the rib cage, shoulder and pelvis showed strong X-gal staining (n=2/10) (Figure 6.6D and E). We observed focal staining next to the hindpaws which might refer to the knees. The forelimb and forepaw displayed diffuse staining on the dorsal plane (Figure 6.6E [i]). Upon higher magnification of the palm, the perichondrium of the future metacarpals of digits 2, 3, and 4 were outlined with X-gal staining with exception at its distal ends or epiphyses (Figure 6.6E [vi,vii] and Supplementary Figure S6.5). We also observed a thin layer of staining at the outer edges of the developing

forepaw with strong intensity at each digit tip (Figure 6.6E [vii] and Supplementary Figure S6.5).

6.6.7 Identifying regulatory motifs *in-silico*

Although we observed the absence of ENCODE transcription factor ChIP-seq peaks at the donor region, we specifically focused our *in-silico* search for predicted TFBS at conserved sequences within Fragment-2. Among the list of predicted TFBS at RE3, RE4 and RE5 were sites for SMAD4, Gli, Sox and pioneer factors Oct and Nanog (Figure 6.7C, Supplementary Figure S6.6 and Supplementary Tables S6.8 and S6.9), which are all mediators of chondrogenesis (Chimal-Monroy et al., 2003; Liu et al., 2009; Bénazet et al., 2012; Hojo et al., 2013). Interestingly, we identified a high scoring predicted Mef2C binding site at the junction (Figure 6.7D). Furthermore, we asked whether paralogous regulatory sequences for specific digit expression could be identified by comparing the sequences of various copy number variants which were found to be in association with human digit malformations. We specifically searched for shared motifs within functionally validated enhancer blocks in the SHH-ZRS core (Lettice et al., 2003), the BDA2 microduplication (Dathe et al., 2009; Su et al., 2011; Liu et al., 2014), and RE8 using MEME and MAST. All three predicted motifs were clustered at RE5 with only one motif positioned at RE3 (Figure 6.7A and B).

6.6.8 Evaluation of *cis*-distal gene expression

Since there was no obvious transcriptional unit originating from within the donor region, we considered whether the expression levels of *cis*-distal genes could be affected in the two unrelated junction-positive patients relative to an age-matched control. Genes which flank the tandem duplication were assayed for differential expression in two

junction-positive BDA1 patients, P1-12 and P24-02. We observed a significant increase in the fold change of *NPR3* expression at $p < 0.05$ for P1-12 and at $p < 0.001$ for P24-02 (Figure 6.8A) relative to its expresseion in the age-matched control. However, *TARS* which is located approximately 374 kb downstream of the donor region did not show a significant change in relative gene expression for both patients ($p > 0.1$). Although endogenous control gene *ACTB* was readily detected, we did not detect the expression of noncoding gene *LOC340113* in any of our fibroblast samples (data not shown). We also evaluated for differential expression of genes located at the boundaries of the *BDA1B* critical region. At the centromeric boundary of the critical region, the *RAI14* gene which is approximately 1.5 Mb downstream of the duplication only showed a significant increase in gene expression for P1-12 ($p < 0.05$). A significant increase in fold change was observed for *PDZD2*, a gene located approximately 1 Mb upstream of the duplication event, in both junction-positive patients ($p < 0.001$, Figure 6.8B). Moreover, we observed a 6 fold increase in *PDZD2* expression (Median = 19.71) when compared to *NPR3* expression (Median = 3.48) for P24-02. The increase in *PDZD2* (Median = 136.53) is even more dramatic for P1-02 with a 29 fold change when compared to *NPR3* (Median = 4.65).

6.7. Discussion

Intergenic regions have been largely overlooked in mutation screening strategies despite evidence showing an abundance of noncoding transcriptional units and potential *cis*-regulatory sequences at these regions. In this study we report the identification of a novel intergenic 9.5 kb tandem duplication at the *BDA1B* locus which was previously described in a genetic linkage study by Armour et al. (2002). We also demonstrated

through the use of orthogonal assays another independent family sharing a similar microduplication, possibly due to a founder effect. It is unclear if both families share an identical proximal breakpoint within an $(A)_5$ homopolymer string. Since we have allelic information from Family-1 we would genotype Family-2 to evaluate whether both families share an identical affected haplotype. Despite our previous efforts to identify copy number changes via a whole genome 500K SNP array in an affected Family-1 member, we were not able to detect the microduplication as only one probe was positioned within the donor region. The resolution offered by the high-throughput sequencing of the targeted locus enabled us to precisely identify the breakpoints by examining the split alignments of each read at these locations. The absence of flanking low copy repeats and the presence of a dinucleotide microhomology site at the junction suggest either non-homologous end-joining (NHEJ) or fork stalling and template switching (FoSTeS) (Lee et al., 2007; Zhang et al., 2009; Lieber, 2010) as the mechanism for giving rise to the tandem duplication.

Human noncoding conserved sequences have been shown to regulate distal gene expression in a spatial and temporal fashion (Sakabe et al., 2012). Our *in-vivo* transgene reporter assay demonstrated that the distal half of the donor region is capable of eliciting tissue and temporal reporter activity. Although the pattern of reporter expression at E13.5 was consistently observed at the pelvis and shoulder, we also noticed expression at the digits which suggests regulatory elements can drive expression here. The posterior position of the X-gal staining of transgene RE8 at the E11.5 limb bud suggests the presence of a limb bud enhancer element in RE8 behaving in a similar spatiotemporal fashion as the SHH regulatory region, SHH-ZRS, as described by Lettice et al., (2003).

Interestingly, transgene RE7 did not display reporter activity at E11.5 despite *in-vitro* results demonstrating strong luciferase expression for RE2. It is possible, given the heterologous nature of our reporter constructs, that any *cis*-regulatory elements found within this fragment are dependent on its target endogenous promoter. Alternatively, the individual component when removed out of its endogenous position could explain this discrepancy, especially given that RE7 harbors the majority of an ENCODE annotated polycomb segment. The polycomb repressive complexes PRC1 and PRC2 are involved with transcriptional silencing and chromatin compaction (Francis et al., 2004; Margueron and Reinberg, 2012). Although the polycomb segment partially extends into the proximal region of RE8, it does not appear to affect reporter expression *in-vivo*. Our *in-vivo* and *in-vitro* results support the presence of cartilage/bone enhancer elements within RE8 as demonstrated by the transgene expression domains at various cartilage/bone compartments. The embryonic expression pattern for RE8 is progressive from E11.5 to E13.5 with the appearance of more stained tissue compartments. The difference in reporter activity suggests that regulatory elements in RE8 are responsive to tissue specific transcription factors, such as Gli and Sox, in a temporal manner. Our *in-silico* evaluation of predicted TFBS in paralogous motifs highlighted odd-skipped regulatory 1 (Osr1), a regulator of phalangeal joint formation (Gao et al., 2011), as a potential regulator (Figure 6.7B). ChIP assays in either primary human cells or cartilage/bone cell lines are needed to determine if any of these factors can directly bind to the motifs. In order to fully evaluate the extent of regulatory activity at the microduplication, we would need to create a transgenic knockin of the tandem duplication in mouse.

Enhancers can regulate distal gene expression even as far away as 1 Mb (Lettice et al., 2003). We identified the upregulation of two distal genes, *NPR3* and *PDZD2*, in two patient fibroblast samples. The *NPR3* gene codes for a clearance receptor for natiruretic peptides NPPA, NPPB and NPPC, all of which are involved in maintaining blood pressure and volume (Matsukawa et al., 1999). Our patients did not exhibit any clinical features suggestive of either hyper- or hypotension when they were examined at the onset of this study. However, many of the BDA1-affected members of Family-1 were reported by Armour et al., (2002) to be of short stature. This additional phenotype is of interest to our study given that whole genome-wide association studies have associated three human height variation alleles at the *NPR3* gene, namely rs10472828 (Estrada et al., 2009), rs3792752 (Lango Allen et al., 2010), rs6450922 and rs9292468 (Berndt et al., 2013). Moreover, *NPR3* has an important role in skeletal development as demonstrated by the skeletal overgrowth phenotypes seen in *Npr3* null mouse mutants (Jaubert et al., 1999) and in an ENU-induced variant carrying a missense mutation in the extracelluar domain of Npr3 in the homozygous state (Dauphinee et al., 2013). A similar skeletal overgrowth phenotype is observed in patients with an activating mutation in *NPR2* (Hannema et al., 2013), whereas the opposite effect is seen in loss-of-function mutations which cause acromesomelic dysplasia, type Maroteux (Bartels et al., 2004). Yasoda et al. (2004) have previously shown that overexpression of Nppc, the preferred natriuretic peptide for Npr2, can rescue the mouse model of achondroplasia. Furthermore, Nppc has been shown to stimulate chondrogenic condensations in micromass limb bud cultures (Woods et al., 2007) and to induce *Npr3* expression in mouse tibial hypertrophic chondrocytes where it regulates local natriuretic peptide concentrations (Agoston et al.,

2007). Taken together, the upregulation of *NPR3* could reduce local Nppc concentrations thereby decreasing the size of digit mesenchymal condensations and the hypertrophic zone of the growth plate.

PDZD2 is a secreted multi-PDZ domain protein (sPDZD2) with multiple tissue expression (Yeung et al., 2003). Unlike NPR3, there is paucity in the literature regarding PDZD2's role in chondrogenesis. Tsang et al. (2010) have demonstrated a physiological role for Pdzd2 in regulating insulin secretion. Although the report did not describe any skeletal defects in the *Pdzd2* null mouse, a recent study shows that *Pdzd2* is expressed in the limb bud and in the digits (Tsui, 2013). Interestingly, the digit pattern of *Pdzd2* expression at E13.5 is similar to our *in-vivo* X-gal staining of the digit mesenchyme, particularly at the metacarpals and digit tips (Tsui, 2013, Figure 3.8 A and B). Through a series of overexpression studies in neural tubes and the characterization of the compound mutant $Ihh^{+/E95K}$:$Pdzd2^{+/-}$, the author proposed that Pdzd2 negatively regulates and restricts Ihh signaling range such that a loss of *Pdzd2* would extend Ihh's range in a similar fashion as described in the $Ihh^{E95K/E95K}$ BDA1 model by Gao et al. (2009). We observed an increased expression of *PDZD2* in our patients which is contrary to what would be expected given that the reported loss of *Pdzd2* in mice resulted in a BDA1-like phenotype, albeit within a BDA1 mutant background. Although counterintuitive, the overexpression of a gene product could lead to a similar phenotype as loss-of-function mutations by interfering with the stoichiometry of a protein needed complex (Sopko et al., 2006). Since PDZ domain containing proteins are known to bind transmembrane or ion channel receptors (Kim et al., 2004) the overexpression of PDZD2 could interfere with BMP receptor complexes, IHH's receptor PTCH1 or its modulator HHIP.

Our evaluation of the duplicated interval for regulatory activity in the mouse has revealed a specific expression domain located at the metacarpal perichondrium of digits 2, 3 and 4. The perichondrium consists of an outer fibrous layer and inner chondroprogenitor layer, which provides cellular appositional growth through the deposition of cells and matrix over the existing mesenchymal core. This process contributes to the lateral or widthwise growth of bone. Several genetic factors contributing to the width of metacarpals of digits 2, 3, and 4 have been identified by genome wide quantitative trait loci (QTL) mapping in humans (Karasik et al., 2008). Although the genes residing at the *BDA1B* locus were not implicated as QTL for metacarpal size, another independent genetic study could reveal additional QTL. Alternatively, the reassessment through imputation, the inference of ungentoyped alleles in linkage disequilibrium with gentoyped SNPs, of the genome wide study by Karasik et al. (2008) could identify QTL at the *BDA1B* locus. Although a transcriptome analysis of the chicken tibial inner periosteum layer revealed the expression of *Rai14* (Bandyopadhyay et al., 2008), we did not see a significant difference in its expression in our tested junction-positive patients when compared to the age-matched and unaffected sample. However, we noticed the RNA *in-situ* expression for *Npr3* (transverse section 12-14) and *Pdzd2* (transverse section 22) at the digit perichondrium of E14.5 mouse embryos (www.eurexpress.org). Since there is no clinical standardized measurement for the width of hand bones, it is unclear if our BDA1 patients have altered hand bone thickness. Interestingly enough, Fitch (1979) noted that the epiphysis of the metacarpals were broad while the diaphyses appeared thin in many BDA1 patients.

The current model for distal *cis*-regulation is through chromatin looping of the enhancer(s) to the target promoter (Sanyal et al., 2012; DeMare et al., 2013; Wouter de Laat et al., 2013). The duplication of enhancers results in the overexpression of target genes such as those described in microduplications associated with *SOX9* (Akiyamaet al., 2007; Kurth et al., 2009) and *BMP2* (Dathe et al., 2009). We propose that *NPR3* and *PDZD2* are dose sensitive genes which can be regulated by enhancer elements at the donor region by chromatin looping to both promoters (Figure 6.9). The location of the microduplication coincides with weak ChIP-seq signals for enhancer signatures, such as H3Kme1 and H3K27ac. As such, extra copies of these elements could act synergistically to increase the dose of transcriptional activity for its target gene(s) and/or direct ectopic expression similar to what was observed in a microduplication syndrome involving *GREM1* (Jaeger et al., 2012). As the junction sequence was slightly able to drive luciferase expression in U2OS cells, we predict the creation of a novel regulatory element could also drive ectopic expression of a target gene. Although we did not test this sequence *in-vivo*, we identified a predicted Mef2c binding site spanning the junction. Mef2c, a MADS box transcription factor, is expressed in prehypertrophic and hypertrophic chondrocytes where it co-regulates the expression of *Col10a1* with *Sox9* (Dy et al., 2011).

In summary, we have provided evidence for a gain-of-function mechanism in causing BDA1 in at least two families through the duplication of tissue specific long-range *cis*-regulatory elements resulting in the overexpression of *PDZD2* and *NPR3*. This is significant because we've identified a *cis*-regulatory logic in a previously poorly annotated intergenic region. In addition, this finding has opened a new door for further

investigative work and discovery in three notable areas. First, it remains to be seen if both genes showing increased expression act together or alone to cause BDA1 and the evaluation of chromatin looping at the microduplication could provide the answer. Nonetheless, our finding supports a role for PDZD2 and NPR3 in restricting and/or inhibiting chondrogenesis (Figure 6.10). Second, given the socioeconomic burden of (OA) it would be desirable to evaluate the overexpression of both genes in articular cartilage especially in light of current evidence showing increased *NPR3* expression in OA cartilage (Peake et al., 2013). Lastly, the screening of the duplicated region in other brachydactyly families would help to determine the clinical spectrum attributed by copy number variation at this region.

6.8 Acknowledgements

The authors would like to thank the members of the families for their participation. Funding for this work was provided by an operating grant (DEB) from the Canadian Institutes of Health Research. This study makes use of data generated by the DECIPHER Consortium. A full list of centres who contributed to the generation of the data is available from http://decipher.sanger.ac.uk and via email from decipher@sanger.ac.uk. Funding for the project was provided by the Wellcome Trust.

6.9 Online Resources

BootstRatio: http://pdo.iconcologia.net/stats/br/
ConSite: consite.genereg.net/
DCODE: www.dcode.org
ENSEMBL: http://www.ensembl.org/index.html
Eurexpress : www.eurexpress.org
Exome Variant Server: http://evs.gs.washington.edu/EVS/

JASPAR: jaspar.genereg.net/
MEME Suite: http://meme.nbcr.net/meme/
NCBI: www.ncbi.nlm.nih.gov/
NIH Roadmap Epigenomics Mapping Consortium: www.roadmapepigenomics.org/
Primer3Plus: http://www.bioinformatics.nl/cgi-bin/primer3plus/primer3plus.cgi/
RepeatMasker : www.repeatmasker.org
rVISTA: rvista.dcode.org/
UCSC Genome Browser: https://genome.ucsc.edu/

6.10 Cited References

Agoston, H., Khan, S., James, C.G., Gillespie, J.R., Serra, R., Stanton, L.A., Beier, F. (2007). C-type natriuretic peptide regulates endochondral bone growth through p38 MAP kinase dependent and -independent pathways. BMC Dev. Biol. *7*, 18.

Ahituv, N., Zhu, Y., Visel, A., Holt, A., Afzal, V., Pennacchio, L.A., Rubin, E.M. (2007). Deletion of ultraconserved elements yields viable mice. PLoS Biol. *5*, e234.

Akiyama, H., Stadler, H.S., Martin, J.F., Ishii, T.M., Beachy, P.A., Nakamura, T., de Crombrugghe, B. (2007). Misexpression of Sox9 in mouse limb bud mesenchyme induces polydactyly and rescues hypodactyly mice. Matrix Biol. *26*, 224-233.

Armour, C.M., Bulman, D.E., Hunter, A.G. (2000). Clinical and radiological assessment of a family with mild brachydactyly type A1: the usefulness of metacarpophalangeal profiles. J. Med. Genet. *37*, 292-296.

Armour, C.M., McCready, M.E., Baig, A., Hunter, A.G., Bulman, D.E. (2002). A novel locus for brachydactyly type A1 on chromosome 5p13.3-p13.2. J. Med. Genet. *39*, 186-188.

Attanasio, C., Nord, A.S., Zhu, Y., Blow, M.J., Li, Z., Liberton, D.K., Morrison, H., Plajzer-Frick, I., Holt, A., Hosseini, R., Phouanenavong, S., Akiyama, J.A., Shoukry, M. Afzal, V., Rubin, E.M., Fitzpatrick, D.R., Ren, B., Hallgrimsson, B., Pennacchio, L.A., Visel, A. (2013). Fine tuning of craniofacial morphology by distant-acting enhancers. Science *342*, 1241006.

Bailey, J.A., Yavor, A.M., Massa, H.F., Trask, B.J., Eichler, E.E. (2001). Segmental duplications: organization and impact within the current human genome project assembly. Genome Res. *11*, 1005-1017.

Bailey, J.A., Gu, Z., Clark, R.A., Reinert, K., Samonte, R.V., Schwartz, S., Adams, M.D., Myers, E.W., Li, P.W., Eichler, E.E. (2002). Recent segmental duplications in the human genome. Science *297*, 1003-1007.

Bailey, T.L., and Elkan, C. (1994). Fitting a mixture model by expectation maximization to discover motifs in biopolymers. Proc. Int. Conf. Intell. Syst. Mol. Biol. *2*, 28-36.

Bailey, T.L., and Gribskov, M. (1998). Combining evidence using p-values: application to sequence homology searches. Bioinformatics *14*, 48-54.

Bailey, T.L., Williams, N., Misleh, C., Li, W.W. (2006). MEME: discovering and analyzing DNA and protein sequence motifs. Nucleic Acids Res. (Web Server issue) *1*, W369-W373.

Bartels, C.F., Bükülmez, H., Padayatti, P., Rhee, D.K., van Ravenswaaij-Arts, C., Pauli, R.M., Mundlos, S., Chitayat, D., Shih, L.Y., Al-Gazali, L.I., Kant, S., Cole, T., Morton, J., Cormier-Daire, V., Faivre, L., Lees, M., Kirk, J., Mortier, G.R., Leroy, J., Zabel, B., Kim, C.A., Crow, Y., Braverman, N.E., van den Akker, F., Warman, M.L. (2004). Mutations in the transmembrane natriuretic peptide receptor NPR-B impair skeletal growth and cause acromesomelic dysplasia, type Maroteaux. Am. J. Hum. Genet. *75*, 27-34.

Bénazet, J.D., Pignatti, E., Nugent, A., Unal, E., Laurent, F., Zeller, R. (2012). Smad4 is required to induce digit ray primordia and to initiate the aggregation and differentiation of chondrogenic progenitors in mouse limb buds. Development *139*, 4250-4260.

Bejerano, G., Pheasant, M., Makunin, I., Stephen, S., Kent, W.J., Mattick, J.S., Haussler, D. (2004). Ultraconserved elements in the human genome. Science *304*, 1321-1325.

Bejerano, G., Siepel, A.C., Kent, W.J., Haussler, D. (2005). Computational screening of conserved genomic DNA in search of functional noncoding elements. Nat. Methods *2*, 535-545.

Berndt, S.I., Gustafsson, S., Mägi, R., Ganna, A., Wheeler, E., Feitosa, M.F., Justice, A.E., Monda, K.L., Croteau-Chonka, D.C., Day, F.R., Esko, T., Fall, T., Ferreira, T., Gentilini D, Jackson, A.U., Luan, J., Randall, J.C., Vedantam, S., Willer, C.J., Winkler, T.W., Wood, A.R., Workalemahu, T., Hu, Y.J., Lee, S.H., Liang, L., Lin, D.Y., Min, J.L., Neale, B.M., Thorleifsson, G., Yang, J., Albrecht, E., Amin, N., Bragg-Gresham, J.L., Cadby, G., den Heijer, M., Eklund, N., Fischer, K., Goel, A., Hottenga, J.J., Huffman, J.E., Jarick, I., Johansson, Å., Johnson, T., Kanoni, S., Kleber, M.E., König, I.R., Kristiansson, K., Kutalik, Z., Lamina, C., Lecoeur, C., Li, G., Mangino, M., McArdle, W.L., Medina-Gomez, C., Müller-Nurasyid, M., Ngwa, J.S., Nolte, I.M., Paternoster, L., Pechlivanis, S., Perola, M., Peters, M.J., Preuss, M., Rose, L.M., Shi, J., Shungin, D., Smith, A.V., Strawbridge, R.J., Surakka, I., Teumer, A., Trip, M.D., Tyrer, J., Van Vliet-Ostaptchouk, J.V., Vandenput, L., Waite, L.L., Zhao, J.H., Absher, D., Asselbergs, F.W., Atalay, M., Attwood, A.P., Balmforth, A.J., Basart, H., Beilby, J., Bonnycastle, L.L., Brambilla, P., Bruinenberg, M., Campbell, H., Chasman, D.I., Chines, P.S., Collins, F.S., Connell, J.M., Cookson, W.O., de Faire, U., de Vegt, F., Dei, M., Dimitriou, M., Edkins, S., Estrada, K., Evans, D.M., Farrall, M., Ferrario, M.M., Ferrières, J., Franke, L., Frau, F., Gejman, P.V., Grallert, H., Grönberg, H., Gudnason, V., Hall, A.S., Hall, P.,

Hartikainen, A.L., Hayward, C., Heard-Costa, N.L., Heath, A.C., Hebebrand, J., Homuth, G., Hu, F.B., Hunt, S.E., Hyppönen, E., Iribarren, C., Jacobs, K.B., Jansson, J.O., Jula, A., Kähönen, M., Kathiresan, S., Kee, F., Khaw, K.T., Kivimäki, M., Koenig, W., Kraja, A.T., Kumari, M., Kuulasmaa, K., Kuusisto, J., Laitinen, J.H., Lakka, T.A., Langenberg, C., Launer, L.J., Lind, L., Lindström, J., Liu, J., Liuzzi, A., Lokki, M.L., Lorentzon, M., Madden, P.A., Magnusson, P.K., Manunta, P., Marek, D., März, W., Mateo Leach, I., McKnight, B., Medland, S.E., Mihailov, E., Milani, L., Montgomery, G.W., Mooser, V., Mühleisen, T.W., Munroe, P.B., Musk, A.W., Narisu, N., Navis, G., Nicholson, G., Nohr, E.A., Ong, K.K., Oostra, B.A., Palmer, C.N., Palotie, A., Peden, J.F., Pedersen, N., Peters, A., Polasek, O., Pouta, A., Pramstaller, P.P., Prokopenko, I., Pütter, C., Radhakrishnan, A., Raitakari, O., Rendon, A., Rivadeneira, F., Rudan, I., Saaristo, T.E., Sambrook, J.G., Sanders, A.R., Sanna, S., Saramies, J., Schipf, S., Schreiber, S., Schunkert, H., Shin, S.Y., Signorini, S., Sinisalo, J., Skrobek, B., Soranzo, N., Stančáková, A., Stark, K., Stephens, J.C., Stirrups, K., Stolk, R.P., Stumvoll, M,. Swift, A.J., Theodoraki, E.V., Thorand, B., Tregouet, D.A., Tremoli, E., Van der Klauw, M.M., van Meurs, J.B., Vermeulen, S.H., Viikari, J., Virtamo, J., Vitart, V., Waeber, G., Wang, Z., Widén, E., Wild, S.H., Willemsen, G., Winkelmann, B.R., Witteman, J.C., Wolffenbuttel, B.H., Wong, A., Wright, A.F., Zillikens, M.C., Amouyel, P., Boehm, B.O., Boerwinkle, E., Boomsma, D.I., Caulfield, M.J., Chanock, S.J., Cupples, L.A., Cusi, D., Dedoussis, G.V., Erdmann, J., Eriksson, J.G., Franks, P.W., Froguel, P., Gieger, C., Gyllensten, U., Hamsten, A., Harris, T.B., Hengstenberg, C., Hicks, A.A., Hingorani, A., Hinney, A., Hofman, A., Hovingh, K.G., Hveem, K., Illig, T., Jarvelin, M.R., Jöckel, K.H., Keinanen-Kiukaanniemi, S.M., Kiemeney, L.A., Kuh, D., Laakso, M., Lehtimäki, T., Levinson, D.F., Martin, N.G., Metspalu, A., Morris, A.D., Nieminen, M.S., Njølstad, I, Ohlsson, C., Oldehinkel, A.J., Ouwehand, W.H., Palmer, L.J., Penninx, B., Power, C., Province, M.A., Psaty, B.M., Qi, L., Rauramaa, R., Ridker, P.M., Ripatti, S., Salomaa, V., Samani, N.J., Snieder, H., Sørensen, T.I., Spector, T.D., Stefansson, K., Tönjes, A., Tuomilehto, J., Uitterlinden, A.G., Uusitupa, M., van der Harst, P., Vollenweider, P., Wallaschofski, H., Wareham, N.J., Watkins, H., Wichmann, H.E., Wilson, J.F., Abecasis, G.R., Assimes, T.L., Barroso, I., Boehnke, M., Borecki, I.B., Deloukas, P., Fox, C.S., Frayling, T., Groop, L.C., Haritunian, T., Heid, I.M., Hunter, D., Kaplan, R.C., Karpe, F., Moffatt, M.F., Mohlke, K.L., O'Connell, J.R., Pawitan, Y., Schadt, E.E., Schlessinger, D., Steinthorsdottir, V., Strachan, D.P., Thorsteinsdottir, U., van Duijn, C.M., Visscher, P.M., Di Blasio, A.M., Hirschhorn, J.N., Lindgren, C.M., Morris, A.P., Meyre, D., Scherag, A., McCarthy, M.I., Speliotes, E.K., North, K.E., Loos, R.J., Ingelsson, E. (2013). Genome-wide meta-analysis identifies 11 new loci for anthropometric traits and provides insights into genetic architecture. Nat. Genet. *45*, 501-512.

Blankenberg D, Von Kuster G, Coraor N, Ananda G, Lazarus R, Mangan M, Nekrutenko A, Taylor J. (2010). Galaxy: a web-based genome analysis tool for experimentalists. Curr. Prot. Mol. Biol. Chapter 19, Unit 19. *10*, 1-21.

Bandyopadhyay, A., Kubilis, J.K., Crochiere, M.L., Linsenmayer, T.F., Tabin, C.J. (2008). Identification of unique molecular subdomains in the perichondrium and periosteum and their role in regulating gene expression in the underlying chondrocytes. Dev. Biol. *321*, 162-174.

Byrnes, A.M., Racacho, L., Nikkel, S.M., Xiao, F., MacDonald, H., Underhill, T.M., Bulman, D.E. (2010). Mutations in GDF5 presenting as semidominant brachydactyly A1. Hum. Mutat. *31*, 1155-1162.

Chimal-Monroy, J., Rodriguez-Leon, J., Montero, J.A., Gañan, Y., Macias, D., Merino, R., Hurle, J.M. (2003). Analysis of the molecular cascade responsible for mesodermal limb chondrogenesis: Sox genes and BMP signaling. Dev. Biol. *257*, 292-301.

Clèries, R., Galvez, J., Espino, M., Ribes, J., Nunes, V., de Heredia, M.L. (2012). BootstRatio: A web-based statistical analysis of fold-change in qPCR and RT-qPCR data using resampling methods. Comput. Biol. Med. *42*, 438-45.

Coutton, C., Poreau, B., Devillard, F., Durand, C., Odent, S., Rozel, C., Vieville, G., Amblard, F., Jouk, P.S., Satre, V. (2014). Currarino syndrome and HPE microform associated with a 2.7-Mb deletion in 7q36.3 excluding SHH gene. Mol. Syndromol. *5*, 25-31.

Dathe, K., Kjaer, K.W., Brehm, A., Meinecke, P., Nürnberg, P., Neto, J.C., Brunoni, D., Tommerup, N., Ott, C.E., Klopocki, E., Seemann, P., Mundlos, S. (2009). Duplications involving a conserved regulatory element downstream of BMP2 are associated with brachydactyly type A2. Am. J. Hum. Genet. *84*, 483-492.

Dauphinee, S.M., Eva, M.M., Yuki, K.E., Herman, M., Vidal, S.M., Malo, D. (2013). Characterization of two ENU-induced mutations affecting mouse skeletal morphology. G3 (Bethesda) *3*, 1753-1758.

de Laat, W., and Duboule, D. (2013). Topology of mammalian developmental enhancers and their regulatory landscapes. Nature *502*, 499-506.

DeMare, L.E., Leng, J., Cotney, J., Reilly, S.K., Yin, J., Sarro, R., Noonan, J.P. (2013). The genomic landscape of cohesin-associated chromatin interactions. Genome Res. *23*, 1224-1234.

Degenkolbe, E., König, J., Zimmer, J., Walther, M., Reißner, C., Nickel, J., Plöger, F., Raspopovic, J., Sharpe, J., Dathe, K., Hecht, J.T., Mundlos, S., Doelken, S.C., Seemann, P. (2013). A GDF5 point mutation strikes twice--causing BDA1 and SYNS2. PLoS Genet. *9*, e1003846.

Dy, P., Wang, W., Bhattaram, P., Wang, Q., Wang, L., Ballock, R.T., Lefebvre, V. (2012). Sox9 directs hypertrophic maturation and blocks osteoblast differentiation of growth plate chondrocytes. Dev. Cell *22*, 597-609.

ENCODE Project Consortium, Bernstein, B.E., Birney, E., Dunham, I., Green, E.D., Gunter, C., Snyder, M. (2012). An integrated encyclopedia of DNA elements in the human genome. Nature *489*, 57-74.

Ernst, J., Kheradpour, P., Mikkelsen, T.S., Shoresh, N., Ward, L.D., Epstein, C.B., Zhang, X., Wang, L., Issner, R., Coyne, M., Ku, M., Durham, T., Kellis, M., Bernstein, B.E. (2011). Mapping and analysis of chromatin state dynamics in nine human cell types. Nature *473*, 43-49.

Erwin, G.D., Oksenberg, N., Truty, R.M., Kostka, D., Murphy, K.K., Ahituv, N., Pollard, K.S., Capra, J.A. (2014). Integrating diverse datasets improves developmental enhancer prediction. PLoS Comput. Biol. *10*, e1003677.

Estrada, K., Krawczak, M., Schreiber, S., van Duijn, K., Stolk, L., van Meurs, J.B., Liu, F., Penninx, B.W., Smit, J.H., Vogelzangs, N., Hottenga, J.J., Willemsen, G., de Geus, E.J., Lorentzon, M., von Eller-Eberstein, H., Lips, P., Schoor, N., Pop, V., de Keijzer, J., Hofman, A., Aulchenko, Y.S., Oostra, B.A., Ohlsson, C., Boomsma, D.I., Uitterlinden, A.G., van Duijn, C.M., Rivadeneira, F., Kayser, M. (2009). A genome-wide association study of northwestern Europeans involves the C-type natriuretic peptide signaling pathway in the etiology of human height variation. Hum. Mol. Genet. 18, 3516-3524.

Firth, H.V., Richards, S.M., Bevan, A.P., Clayton, S., Corpas, M., Rajan, D., Van Vooren, S., Moreau, Y., Pettett, R.M., Carter, N.P. (2009). DECIPHER: Database of Chromosomal Imbalance and Phenotype in Humans Using Ensembl Resources. Am. J. Hum. Genet. *84*, 524-533.

Fitch, N. (1979). Classification and identification of inherited brachydactylies. J. Med. Genet. *16*, 36-44.

Francis, N.J., Kingston, R.E., Woodcock, C.L. (2004). Chromatin compactin by a polycomb group protein complex. Science *306*, 1574-1577.

Gao, B., Hu, J., Stricker, S., Cheung, M., Ma, G., Law, K.F., Witte, F., Briscoe, J., Mundlos, S., He, L., Cheah, K.S., Chan, D. (2009). A mutation in Ihh that causes digit abnormalities alters its signaling capacity and range. Nature *458*, 1196-1200.

Gao, Y., Lan, Y., Liu, H., Jiang, R. (2011). The zinc finger transcription factors Osr1 and Osr2 control synovial joint formation. Dev. Biol. *352*, 83-91.

Giardine, B., Riemer, C., Hardison, R.C., Burhans, R., Elnitski, L., Shah, P., Zhang, Y., Blankenberg, D., Albert, I., Taylor, J., Miller, W., Kent, W.J., Nekrutenko, A. (2005). Galaxy: a platform for interactive large-scale genome analysis. Genome Res. *15*, 1451-1455.

Goecks, J., Nekrutenko, A., Taylor, J. and The Galaxy Team. (2010). Galaxy: a comprehensive approach for supporting accessible, reproducible, and transparent computational research in the life sciences. Genome Biol. 11, R86.

Gregory, T.R. (2005). Synergy between sequence and size in Large-scale genomics. Nat. Rev. Genet. *6*, 699-708.

Grimsey A. (2006). Brachydactyly type A1: Identification and characterization of the genes involved. M.Sc. Thesis. University of Ottawa.

Gupta, S., Stamatoyannopoulos, J.A., Bailey, T.L., Noble, W.S. (2007). Quantifying similarity between motifs. Genome Biol. *8*, R24.

Hannema, S.E., van Duyvenvoorde, H.A., Premsler, T., Yang, R.B., Mueller, T.D., Gassner, B., Oberwinkler, H., Roelfsema, F., Santen, G.W., Prickett, T., Kant, S.G., Verkerk, A.J., Uitterlinden, A.G., Espiner, E., Ruivenkamp, C.A., Oostdijk, W., Pereira, A.M., Losekoot, M. (2013). An activating mutation in the kinase homology domain of the natriuretic peptide receptor-2 causes extremely tall stature without skeletal deformities. J. Clin. Endocrinol. Metab. *98*, E1988-E1998.

Hojo, H., Ohba, S., Taniguchi, K., Shirai, M., Yano, F., Saito, T., Ikeda T,, Nakajima, K., Komiyama, Y., Nakagata, N., Suzuki, K., Mishina, Y., Yamada, M., Konno, T., Takato, T., Kawaguchi, H., Kambara, H., Chung, U.I. (2013). Hedgehog-Gli activators direct osteo-chondrogenic function of bone morphogenetic protein toward osteogenesis in the perichondrium. J. Biol. Chem. *288*, 9924-9932.

Iafrate, A.J., Feuk, L., Rivera, M.N., Listewnik, M.L., Donahoe, P.K., Qi, Y., Scherer, S.W., Lee, C. (2004). Detection of large-scale variation in the human genome. Nat. Genet. *36*, 949-951.

Jaeger, E., Leedham, S., Lewis, A., Segditsas, S., Becker, M., Cuadrado, P.R., Davis, H., Kaur, K., Heinimann, K., Howarth, K., East, J., Taylor, J., Thomas, H., Tomlinson, I. (2012). Hereditary mixed polyposis syndrome is caused by a 40-kb upstream duplication that leads to increased and ectopic expression of the BMP antagonist GREM1. Nat. Genet. *44*, 699-703.

Jaubert, J., Jaubert, F., Martin, N., Washburn, L.L., Lee, B.K., Eicher, E.M., Guénet, J.L. (1999). Three new allelic mouse mutations that cause skeletal overgrowth involve the natriuretic peptide receptor C gene (Npr3). Proc. Natl. Acad. Sci. USA *96*, 10278-10283.

Jolma, A., Yan, J., Whitington, T., Toivonen, J., Nitta, K.R., Rastas, P., Morgunova, E., Enge, M., Taipale, M., Wei, G., Palin, K., Vaquerizas, J.M., Vincentelli, R., Luscombe, N.M., Hughes, T.R., Lemaire, P., Ukkonen, E., Kivioja, T., Taipale, J. (2013). DNA-binding specificities of human transcription factors. Cell *152*, 327-339.

Karasik, D., Shimabuku, N.A., Zhou, Y., Zhang, Y., Cupples, L.A., Kiel, D.P., Demissie, S. (2008). A genome wide linkage scan of metacarpal size and geometry in the Framingham Study. Am. J. Hum. Biol. *20*, 663-670.

Kim, E., and Sheng, M. (2004). PDZ domain proteins of synapses. Nat. Rev. Neurosci. *5*, 551-581.

Karolchik, D., Hinrichs, A.S., Furey, T.S., Roskin, K.M., Sugnet, C.W., Haussler, D., Kent, W.J. (2004). The UCSC Table Browser retrieve tool. Nucleic Acids Res. (Database issue) *32*, D493-D496.

Karolchik, D., Barber, G.P., Casper, J., Clawson, H., Cline, M.S., Diekhans, M., Dreszer, T.R., Fujita, P.A., Guruvadoo, L., Haeussler, M., Harte, R.A., Heitner, S., Hinrichs, A.S., Learned, K., Lee, B.T., Li, C.H., Raney, B.J., Rhead, B., Rosenbloom, K.R., Sloan, C.A., Speir, M.L., Zweig, A.S., Haussler, D., Kuhn, R.M., Kent, W.J. (2014). The UCSC Genome Browser database: 2014 update. Nucleic Acids Res. *42*, D764-D770.

Kent, W.J., Sugnet, C.W., Furey, T.S., Roskin, K.M., Pringle, T.H., Zahler, A.M., Haussler, D. (2002). The human genome browser at UCSC. Genome Res. *12*, 996-1006.

Klopocki, E., Lohan, S., Brancati, F., Koll, R., Brehm, A., Seemann, P., Dathe, K., Stricker, S., Hecht, J., Bosse, K., Betz, R.C., Garaci, F.G., Dallapiccola, B., Jain, M., Muenke, M., Ng, V.C., Chan, W., Chan, D., Mundlos, S. (2011). Copy-number variations involving the IHH locus are associated with syndactyly and craniosynostosis. Am. J. Hum. Genet. *88*, 70-75.

Kuhn, M., and Wit, J.M. (2013). An activating mutation in the kinase homology domain of the natriuretic peptide receptor-2 causes extremely tall stature without skeletal deformities. J. Clin. Endocrinol. Metab. *98*, E1988-E1998.

Kurth, I., Klopocki, E., Stricker, S., van Oosterwijk, J., Vanek, S., Altmann, J., Santos, H.G., van Harssel, J.J., de Ravel, T., Wilkie, A.O., Gal, A., Mundlos, S. (2009). Duplications of noncoding elements 5' of SOX9 are associated with brachydactyly-anonychia. Nat. Genet. *41*, 862-863.

Lango Allen, H., Estrada, K., Lettre, G., Berndt, S.I., Weedon, M.N., Rivadeneira, F., Willer, C.J., Jackson, A.U., Vedantam, S., Raychaudhuri, S., Ferreira, T., Wood, A.R., Weyant, R.J., Segrè, A.V., Speliotes, E.K., Wheeler, E., Soranzo, N., Park, J.H., Yang, J., Gudbjartsson, D., Heard-Costa, N.L., Randall, J.C., Qi, L., Vernon, Smith, A., Mägi, R., Pastinen,T., Liang, L., Heid, I.M., Luan, J., Thorleifsson, G., Winkler, T.W., Goddard, M.E., Sin Lo, K., Palmer, C., Workalemahu, T., Aulchenko, Y.S., Johansson, A., Zillikens, M.C., Feitosa, M.F., Esko, T., Johnson, T., Ketkar, S., Kraft, P., Mangino, M., Prokopenko, I., Absher, D., Albrecht, E., Ernst, F., Glazer, N.L., Hayward, C., Hottenga, J.J., Jacobs, K.B., Knowles, J.W., Kutalik, Z., Monda, K.L., Polasek, O., Preuss, M., Rayner, N.W., Robertson, N.R., Steinthorsdottir, V., Tyrer, J.P., Voight, B.F., Wiklund, F., Xu, J., Zhao, J.H., Nyholt, D.R., Pellikka, N., Perola, M., Perry, J.R., Surakka, I., Tammesoo, M.L., Altmaier, E.L., Amin, N., Aspelund, T., Bhangale, T., Boucher, G., Chasman, D.I., Chen, C., Coin, L., Cooper, M.N., Dixon, A.L., Gibson, Q., Grundberg, E., Hao, K., Juhani Junttila, M., Kaplan, L.M., Kettunen, J., König, I.R., Kwan, T., Lawrence, R.W., Levinson, D.F., Lorentzon, M., McKnight, B., Morris, A.P., Müller, M., Suh Ngwa, J., Purcell, S., Rafelt, S., Salem, R.M., Salvi, E., Sanna, S., Shi, J., Sovio, U., Thompson, J.R., Turchin, M.C., Vandenput, L., Verlaan, D.J., Vitart, V., White, C.C., Ziegler, A., Almgren, P., Balmforth, A.J., Campbell, H., Citterio, L., De Grandi, A.,

Dominiczak, A., Duan, J., Elliott, P., Elosua, R., Eriksson, J.G., Freimer, N.B., Geus, E.J., Glorioso, N., Haiqing, S., Hartikainen, A.L., Havulinna, A.S., Hicks, A.A., Hui, J., Igl, W., Illig, T., Jula, A., Kajantie, E., Kilpeläinen, T.O., Koiranen, M., Kolcic, I., Koskinen, S., Kovacs, P., Laitinen, J., Liu, J., Lokki, M.L., Marusic, A., Maschio, A., Meitinger, T., Mulas, A., Paré, G., Parker, A.N., Peden, J.F., Petersmann, A., Pichler, I., Pietiläinen, K.H., Pouta, A., Ridderstråle, M., Rotter, J.I., Sambrook, J.G., Sanders, A.R., Schmidt, C.O., Sinisalo, J., Smit, J.H., Stringham, H.M., Bragi Walters, G., Widen, E., Wild, S.H., Willemsen, G., Zagato, L., Zgaga, L., Zitting, P., Alavere, H., Farrall, M., McArdle, W.L., Nelis, M., Peters, M.J., Ripatti, S., van Meurs, J.B., Aben, K.K., Ardlie, K.G., Beckmann, J.S., Beilby, J.P., Bergman, R.N., Bergmann, S., Collins, F.S., Cusi, D., den Heijer, M., Eiriksdottir, G., Gejman, P.V., Hall, A.S., Hamsten, A., Huikuri, H.V., Iribarren, C., Kähönen, M., Kaprio, J., Kathiresan, S., Kiemeney, L., Kocher, T., Launer, L.J., Lehtimäki, T., Melander, O., Mosley, T.H. Jr., Musk, A.W., Nieminen, M.S., O'Donnell, C.J., Ohlsson, C., Oostra, B., Palmer, L.J., Raitakari, O., Ridker, P.M., Rioux, J.D., Rissanen, A., Rivolta, C., Schunkert, H., Shuldiner, A.R., Siscovick, D.S., Stumvoll, M., Tönjes, A., Tuomilehto, J., van Ommen, G.J., Viikari, J., Heath, A.C., Martin, N.G., Montgomery, G.W., Province, M.A., Kayser, M., Arnold, A.M., Atwood, L.D., Boerwinkle, E., Chanock, S.J., Deloukas, P., Gieger, C., Grönberg, H., Hall, P., Hattersley, A.T., Hengstenberg, C., Hoffman, W., Lathrop, G.M., Salomaa, V., Schreiber, S., Uda, M., Waterworth, D., Wright, A.F., Assimes, T.L., Barroso, I., Hofman, A., Mohlke, K.L., Boomsma, D.I., Caulfield, M.J., Cupples, L.A., Erdmann, J., Fox, C.S., Gudnason, V., Gyllensten, U., Harris, T.B., Hayes, R.B., Jarvelin, M.R., Mooser, V., Munroe, P.B., Ouwehand, W.H., Penninx, B.W., Pramstaller, P.P., Quertermous, T., Rudan, I., Samani, N.J., Spector, T.D., Völzke, H., Watkins, H., Wilson, J.F., Groop, L.C., Haritunians, T., Hu, F.B., Kaplan, R.C., Metspalu, A., North, K.E., Schlessinger, D., Wareham, N.J., Hunter, D.J., O'Connell, J.R., Strachan, D.P., Wichmann, H.E., Borecki, I.B., van Duijn, C.M., Schadt, E.E., Thorsteinsdottir, U., Peltonen, L., Uitterlinden, A.G., Visscher, P.M., Chatterjee, N., Loos, R.J., Boehnke, M., McCarthy, M.I., Ingelsson, E., Lindgren, C.M., Abecasis, G.R., Stefansson, K., Frayling, T.M., Hirschhorn, J.N. (2010). Hundreds of variants clustered in genomic loci and biological pathways affect human height. Nature 467, 832-838.

Lee, J.A., Cravalho, C.M., Lupski, J.R. (2007). A DNA replication mechanism for generating nonrecurrent rearrangements associated with genomic disorders. Cell *131*, 1235-1247.

Lettice, L.A., Heaney, S.J., Purdie, L.A., Li, L., de Beer, P., Oostra, B.A., Goode, D., Elgar, G., Hill, R.E., de Graaff, E.A. (2003). A long-range Shh enhancer regulates expression in the developing limb and fin and is associated with preaxial polydactyly. Hum. Mol. Genet. *12*, 1725-1735.

Lieber, M.R. (2010). The mechanism of double-strand DNA break repair by the nonhomologous DNA end-joining pathway. Annu. Rev. Biochem. *79*, 181-211.
Liu, T.M., Wu, Y.N., Guo, X.M., Hui, J.H., Lee, E.H., Lim, B. (2009). Effects of ectopic Nanog and Oct4 overexpression on mesenchymal stem cells. Stem Cells Dev. *18*, 1013-1022.

Liu, X., Gao, L., Zhao, A., Zhang, R., Ji, B., Wang, L., Zheng, Y., Zeng, B., Valenzuela, R.K., He, L., Ma, J. (2014). Identification of duplication downstream of BMP2 in a Chinese family with brachydactyly type A2 (BDA2). PLoS One *9*, e94201.

Lohan, S., Spielmann, M., Doelken, S.C., Flöttmann, R., Muhammad, F., Baig, S.M., Wajid, M., Hülsemann, W., Habenicht, R., Kjaer, K.W., Patil, S.J., Girisha, K.M., Abarca-Barriga, H.H., Mundlos, S., Klopocki, E. (2014). Microduplications encompassing the Sonic hedgehog limb enhancer ZRS are associated with Haas-type polysyndactyly and Laurin-Sandrow syndrome. Clin. Genet. *86*, 318-325.

Loots, G.G., and Ovcharenko, I. (2004). rVISTA 2.0: evolutionary analysis of transcription factor binding sites. Nucleic Acids Res. (Web Server Issue) *1*, W217-21.

MacDonald, J.R., Ziman, R., Yuen, R.K., Feuk, L., Scherer, S.W. (2014). The Database of Genomic Variants: a curated collection of structural variation in the human genome. Nucleic Acids Res. (Database issue) *42*, D986-D992.

Margueron, R., and Reinberg, D. (2011). The Polycomb complex PRC2 and its mark in life. Nature *469*, 343-349.

Mathelier, A., Zhao, X., Zhang, A.W., Parcy, F., Worsley-Hunt, R., Arenillas, D.J., Buchman, S., Chen, C.Y., Chou, A., Ienasescu, H., Lim, J., Shyr, C., Tan, G., Zhou, M., Lenhard, B., Sandelin, A., Wasserman, W.W. (2014). JASPAR 2014: an extensively expanded and updated open-access database of transcription factor binding profiles. Nucleic Acids Res. (Database issue) *42*, D142-D147.

Matsukawa, N., Grzesik, W.J., Takahashi, N., Pandey, K.N., Pang, S., Yamauchi, M., Smithies, O. (1999). The natriuretic peptide clearance receptor locally modulates the physiological effects of the natriuretic peptide system. Proc. Natl. Acad. Sci. USA. *96*, 7403-7408.

McCready, M. E., Sweeney, E., Fryer, A. E., Donnai, D., Baig, A., Racacho, L., Warman, M. L., Hunter, A. G. W., Bulman, D. E. (2002). A novel mutation in the IHH gene causes brachydactyly type A1: a 95-year-old mystery resolved. Hum. Genet. *111*, 368-375.

McCready, M.E. (2004). Molecular investigation into brachydactyly type A1. Ph.D. Thesis. University of Ottawa.

Mikkelsen, T.S., Ku, M., Jaffe, D.B., Issac, B., Lieberman, E., Giannoukos, G., Alvarez, P., Brockman, W., Kim, T.K., Koche, R.P., Lee, W., Mendenhall, E., O'Donovan, A., Presser, A., Russ, C., Xie, X., Meissner, A., Wernig, M., Jaenisch, R., Nusbaum, C., Lander, E.S., Bernstein, B.E. (2007). Genome-wide maps of chromatin state in pluripotent and lineage-committed cells. Nature *448*, 553-560.

Newburger, D.E., and Bulyk, M.L. (2009). UniPROBE: an online database of protein binding microarray data on protein-DNA interactions. Nucleic Acids Res. (Database issue) *37*, D77-D82.

Ovcharenko, I., Nobrega, M.A., Loots, G.G., Stubbs, L. (2004). ECR Browser: a tool for visualizing and accessing data from comparisons of multiple vertebrate genomes. Nucleic Acids Res. (Web Server issue) *32*, W280-W286.

Pennacchio, L.A., Ahituv, N., Moses, A.M., Prabhakar, S., Nobrega, M.A., Shoukry, M., Minovitsky, S., Dubchak, I., Holt, A., Lewis, K.D., Plajzer-Frick, I., Akiyama, J., De Val, S., Afzal, V., Black, B.L., Couronne, O., Eisen, M.B., Visel, A., Rubin, E.M. (2006). In vivo enhancer analysis of human conserved non-coding sequences. Nature *444*, 499-502.

Peake, N., Su, N., Ramachandran, M., Achan, P., Salter, D.M., Bader, D.L., Moyes, A.J., Hobbs, A.J., Chowdhury, T.T. (2013). Natriuretic peptide receptors regulate cytoprotective effects in a human ex vivo 3D/bioreactor model. Arthritis Res. Ther. *15*, R76.

Pollard, K.S., Hubisz, M.J., Rosenbloom, K.R., Siepel, A. (2010). Detection of nonneutral substitution rates on mammalian phylogenies. Genome Res. *20*, 110-121.

Rosenbloom, K.R., Sloan, C.A., Malladi, V.S., Dreszer, T.R., Learned, K., Kirkup, V.M., Wong, M.C., Maddren, M., Fang, R., Heitner, S.G., Lee, B.T., Barber, G.P., Harte, R.A., Diekhans, M., Long, J.C., Wilder, S.P., Zweig, A.S., Karolchik, D., Kuhn, R.M., Haussler, D., Kent, W.J. (2013). ENCODE data in the UCSC Genome Browser: year 5 update. Nucleic Acids Res. (Database issue) *41*, D56-D63.

Sakabe, N.J., Savic, D., Nobrega, M.A. (2012). Transcriptional enhancers in development and disease. Genome Biol. *13*, 238.

Sandelin, A., Alkema, W., Engström, P., Wasserman, W.W., Lenhard, B. (2004). JASPAR: an open-access database for eukaryotic transcription factor binding profiles. Nucleic Acids Res. (Database issue) *32*, D91-4.

Sanyal, A., Lajoie, B.R., Jain, G., Dekker, J. (2012). The long-range interaction landscape of gene promoters. Nature *489*, 109-113.

Schwartz, S., Kent, W.J., Smit, A., Zhang, Z., Baertsch, R., Hardison, R.C., Haussler, D., Miller, W. (2003). Human-mouse alignments with BLASTZ. Genome Res. *13*, 103-107.

Sopko, R., Huang, D., Preston, N., Chua, G., Papp, B., Kafadar, K., Snyder, M., Oliver, S.G., Cyert, M., Hughes, T.R., Boone, C., Andrews, B. (2006). Mapping pathways and phenotypes by systematic gene overexpression. Mol. Cell *21*, 319-330.

Staehling-Hampton, K., Proll, S., Paeper, B. W., Zhao, L., Charmley, P., Brown, A., Gardner, J. C., Galas, D., Schatzman, R. C., Beighton, P., Papapoulos, S., Hamersma, H.,

Brunkow, M. E. (2002). A 52-kb deletion in the SOST-MEOX1 intergenic region on 17q12-q21 is associated with van Buchem disease in the Dutch population. Am. J. Med. Genet. *110*, 144–152.

Su, P., Ding, H., Huang, D., Zhou, Y., Huang, W., Zhong, L., Vyse, T.J., Wang, Y.A. (2011). 4.6 kb genomic duplication on 20p12.2-12.3 is associated with brachydactyly type A2 in a Chinese family. J. Med. Genet. *48*, 312-316.

Tsang, S.W., Shao, D., Cheah, K.S., Okuse, K., Leung, P.S., Yoa, K.M. (2010). Increased basal insulin secretion in Pdzd2-defecient mice. Mol. Cell Endocrinol. *315*, 263-70.

Tsui, M.G. (2013). PDZD2, a candidate for Brachydactyly Type A1, encodes a secreted protein that negatively modulates Hedgehog signaling. Ph.D. Thesis. The University of Hong Kong.

Visel, A., Prabhaker, S., Akiyama, J.A., Shoukry, M., Lewis, K.D., Hot, A., Plajzer-Frick, I., Afzal, V., Rubin, E.M., Pennacchio, L.A. (2008). Ultraconservation identifies a small subset of extremely constrained developmental enhancers. Nat. Genet. *40*, 158-160.

Wieczorek, D., Pawlik, B., Li, Y., Akarsu, N.A., Caliebe, A., May, K.J., Schweiger, B., Vargas, F.R., Balci, S., Gillessen-Kaesbach, G., Wollnik, B. (2010). A specific mutation in the distant sonic hedgehog (SHH) cis-regulator (ZRS) causes Werner mesomelic syndrome (WMS) while complete ZRS duplications underlie Haas type polysyndactyly and preaxial polydactyly (PPD) with or without triphalangeal thumb. Hum. Mutat. *31*, 81-89.

Woods, A., Khan, S., Beier, F. (2007). C-type natriuretic peptide regulates cellular condensation and glycosaminoglycan synthesis during chondrogenesis. Endocrinology *148*, 5030-5041.

Yasoda, A., Komatsu, Y., Chusho, H., Miyazawa, T., Ozasa, A., Miura, M., Kurihara, T., Rogi, T., Tanaka, S., Suda, M., Tamura, N., Ogawa, Y., Nakao, K. (2004). Overexpression of CNP in chondrocytes rescues achondroplasia through a MAPK-dependent pathway. Nat. Med. *10*, 80-86.

Yeung, M.L., Tam, T.S., Tsang, A.C., Yao, K.M. (2003). Proteolytic cleavage of PDZD2 generates a secreted peptide containing two PDZ domains. EMBO Rep. *4*, 412-418.

Yuksel-Apak, M., Bögershausen, N., Pawlik, B., Li, Y., Apak, S., Uyguner, O., Milz, E., Nürnberg, G., Karaman, B., Gülgören, A., Grzeschik, K.H., Nürnberg, P., Kayserili, H., Wollnik, B. (2012). A large duplication involving the IHH locus mimics acrocallosal syndrome. Eur. J. Hum. Genet. *20*, 639-44.

Zhang, F., Khajavi, M., Connolly, A.M., Towne, C.F., Batish, S.D., Lupski, J.R. (2009). The DNA replication FoSTeS/MMBIR mechanism can generate genomic, genic and exonic complex rearrangements in humans. Nat. Genet. *41,* 849-853.

Zhang, J., Feuk, L., Duggan, G.E., Khaja, R., Scherer, S.W. (2006). Development of bioinformatics resources for display and analysis of copy number and other structural variants in the human genome. Cytogenet. Genome Res. *115,* 205-214.

6.11 Manuscript Figures, Tables and Legends

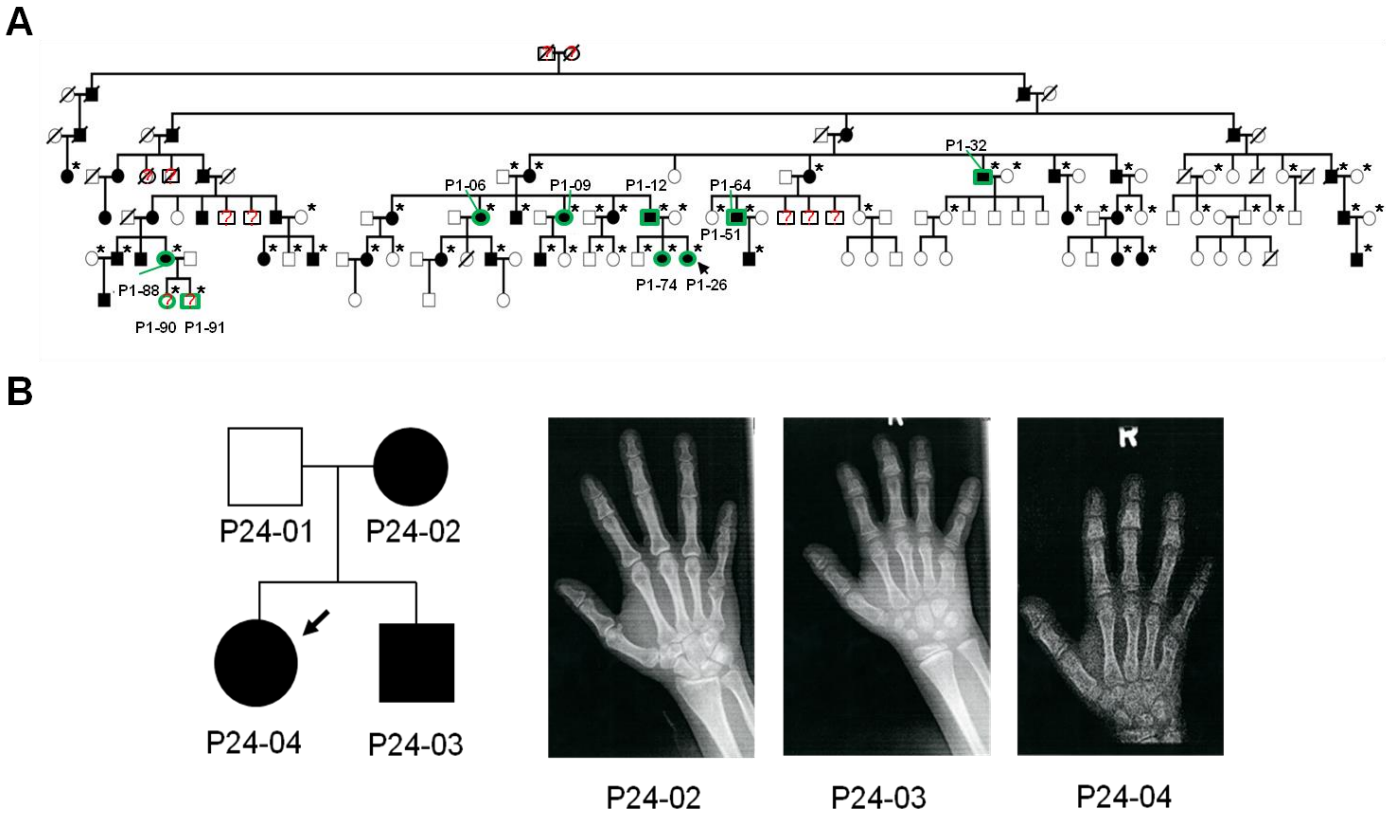

Figure 6.1. An intergenic 9.5 kb microduplication at chr5p13.3 is associated with BDA1 in two kindreds. (A) An updated version of Family-1 which was previously reported by Armour et al. (2002). Genotyped individuals are marked with an "*****". Individuals that are described in the text are highlighted in green. **(B)** Hand radiographs of the BDA1-affected members of Family-24 display remarkable shortening of the middle phalanges of digits 2-5 and of the 5th metacarpal. Probands are indicated with an arrow. Filled symbols denote a positive BDA1-affected status. Unknown affection status is marked with "**?**".

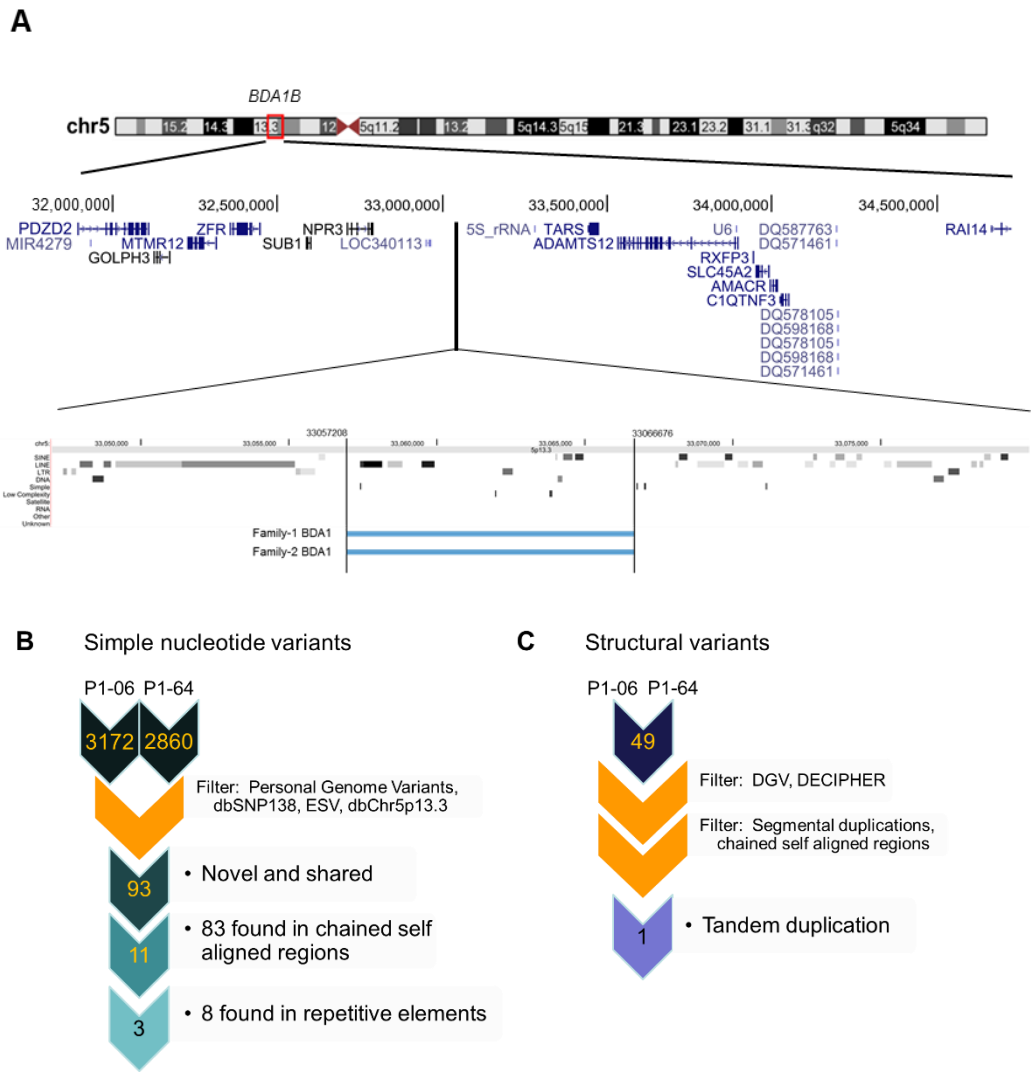

Figure 6.2. Targeted HTS of the *BDA1B* locus. (A) Schematic of the 2.8 Mb *BDA1B* locus at chr5p13.3 that encompasses 13 protein coding genes and 12 noncoding genes (UCSC Genes track). An intergenic microduplication (light blue) was identified by targeted HTS on enriched DNA libraries derived from patients P1-06 and P1-64l (see pedigree in Figure 6.2A). Family-2 was identified through PCR-based junction assay and aCGH. **(B)** Novel and shared simple sequence variants obtained after HTS reads were aligned to hg19 reference genome and excluded for polymorphic sequence variants. **(C)** Novel and shared structural sequence variants ≥ 100 bp obtained after HTS reads were aligned to hg19 reference genome and excluded for polymorphic structural variants. Yellow chevrons represent the filtering out or exclusion of sequence variants identified in the public sequence variant databases.

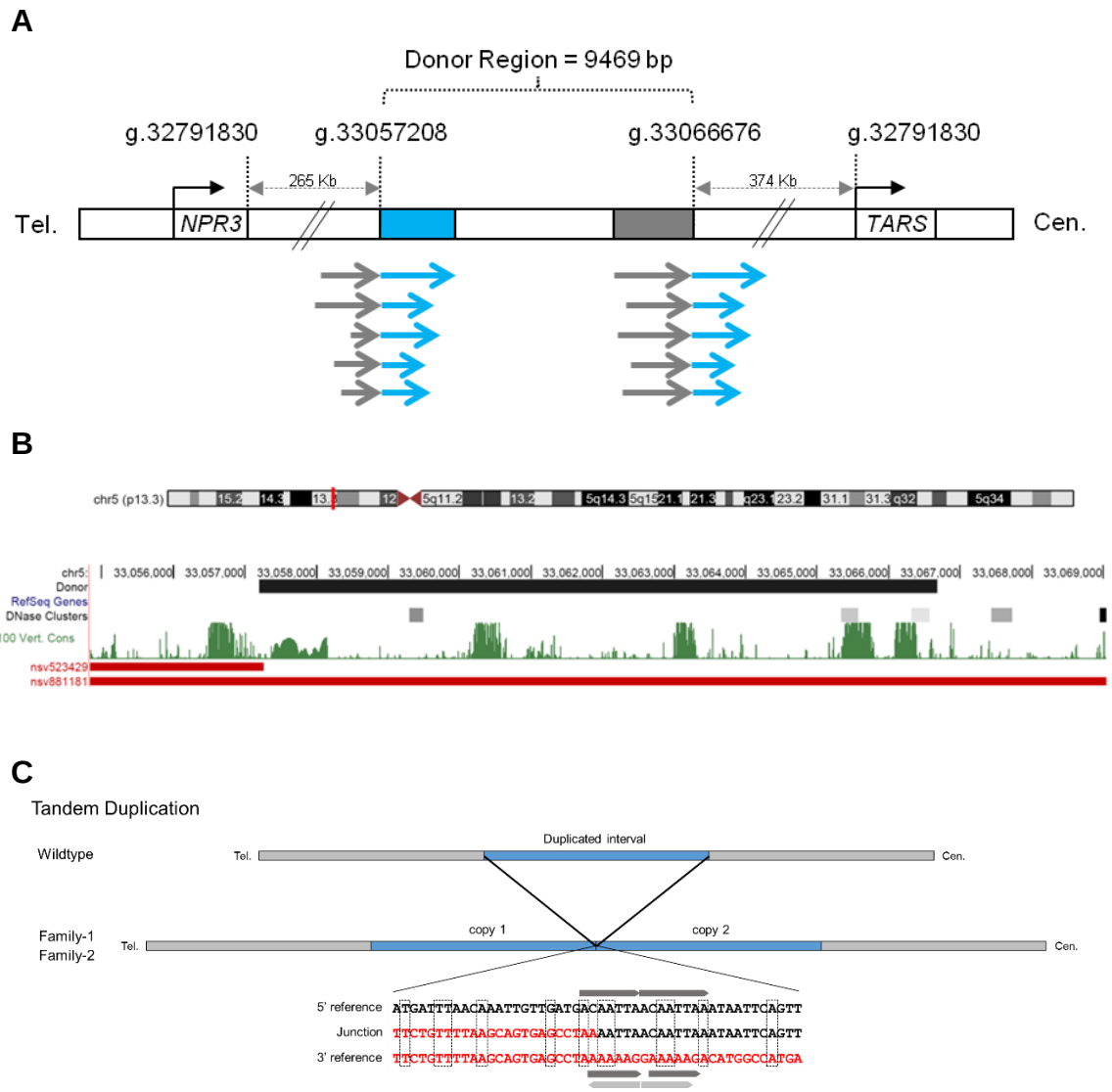

Figure 6.3. Identification of a heterozygous novel duplicated interval. (A) The alignment of HTS reads from two Family-1 members, P1-06 and P1-64, revealed two shared and novel breakpoints at hg19 chr5:g.33057208 and chr5:g.33066676. A representation of each aligned HTS read across the breakpoints are depicted as grey and blue arrows that correspond to its aligned reference genomic position shown in either a grey or blue rectangle. The donor region is the duplicated interval. **(B)** UCSC Genome Browser snapshot of the microduplication positioned within the 2.8 Mb critical region at chr5p13.3. The donor region (black bar) overlaps with two annotated deletions from DGV (red bars). Several conserved sequence elements and DNase I hypersensitive sites are depicted below the donor region. **(C)** The sequence alignment at the junction of the tandem duplication to the reference sequence displays several adjacent microhomology sites (dashed boxes) at the breakpoint. Direct and inverted repeats are shown in dark gray and light gray, respectively. The 5' reference coordinates are chr5:g.33057184-33057231. The 3' reference coordinates are chr5:g.33066653-33066700.

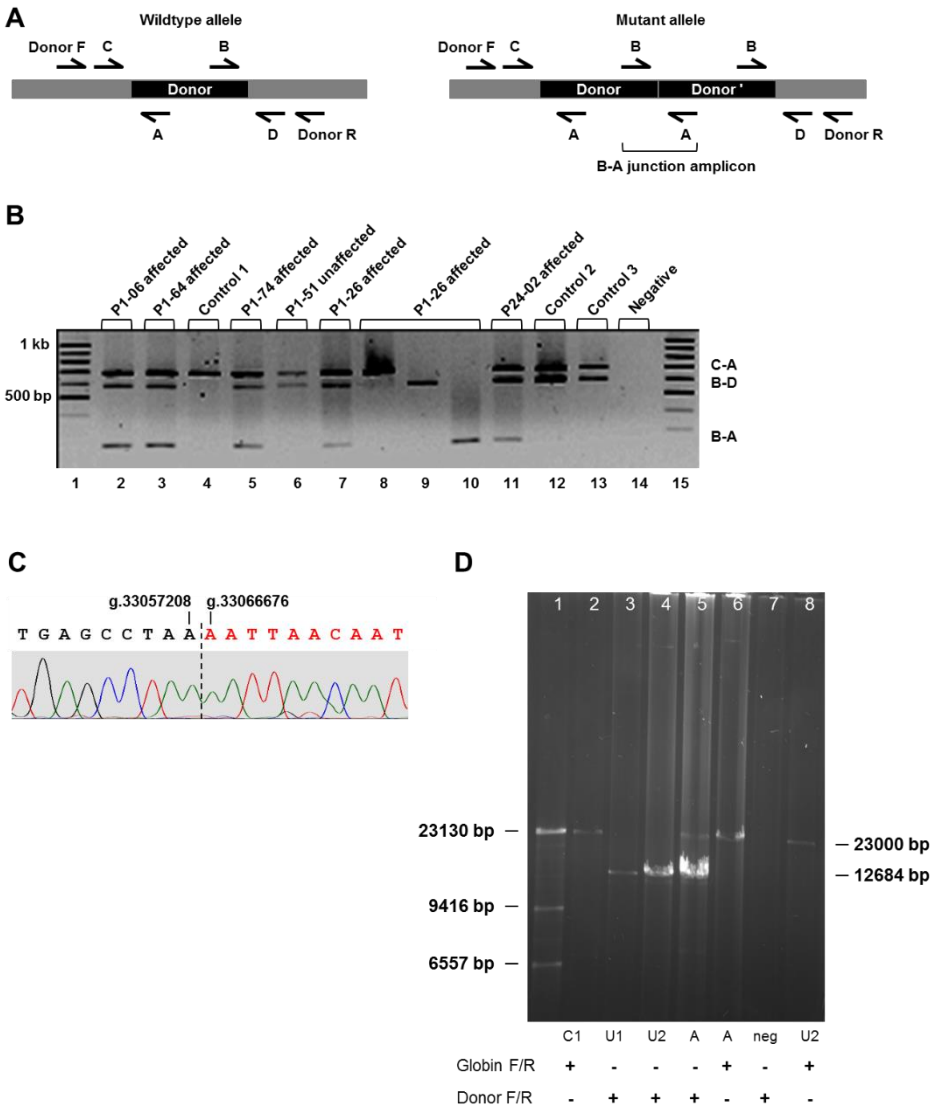

Figure 6.4. Breakpoint verification. (A) Schematic of a PCR-based assay to evaluate the junction created by the duplication of the donor region (black). **(B)** Gel agarose image of electrophoresed samples from multiplex PCR (lanes 2-7 and 11-14) and single PCR (lanes 8-10). Family-1 members (lanes 2, 3, 5-10). Unrelated controls (lanes 4, 12, and 13). Family-24 individual (lane 11). HighRanger Plus 100 bp ladder (Norgen Biotek) (lanes 1 and 15). The expected fragment sizes for amplicon C-A is 702 bp, amplicon B-D is 600 bp, and junction amplicon [B-A] is 206 bp. **(C)** Electropherogram displaying the sequence at the breakpoint the junction amplicon [B-A] of patient P1-26. **(D)** Gel agarose image of long range PCR products reveals two fragments migrating at the expected size of a tandem duplication in the junction-positive patient P1-06 (lane 5) when primer pairs flanking the donor region (Donor F/R) were used. Primer inclusions for each PCR are shown below the samples: Unrelated junction-negative (C1), related junction-negative P1-51 (U1) and P1-91 (U2), related junction-positive P1-06 (A). λ*Hind*III DNA ladder (Invitrogen) loaded onto lane 1.

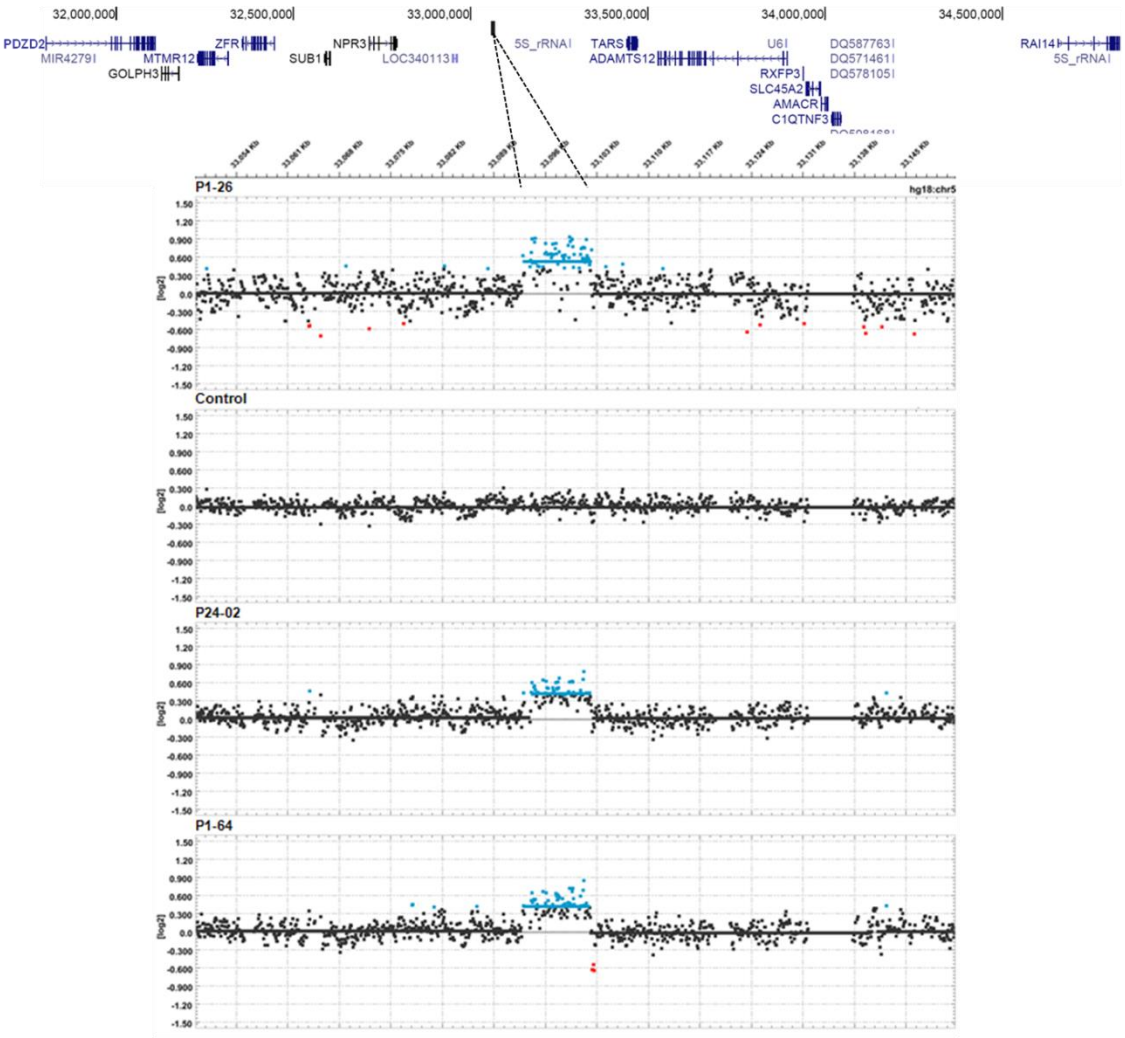

Figure 6.5. High density aCGH confirms the size of the duplicated interval. Log_2 plots of copy number changes spanning a selected view of the aCGH targeted region display a gain-of-copy (blue) at the interval suspected to harbor a tandem duplication in three junction-positive individuals (P1-26, P24-02, and P1-64). There was no deviation in copy number (black) across this region in the unaffected individual (Control). The values are derived from the CGH-segMNT analysis (Roche-NimbleGen) using a 100 bp average window across the tiling region. The log_2 ratio threshold for gain-of-copy was set at 0.40 and loss-of-copy at -0.50 (red). The aCGH were designed with hg18 probe positions. The schematic above the snapshot of aCGH plots displays the position of the duplicated interval relative to the hg19 UCSC Genes track. The UCSC LiftOver tool was used to convert the genomic coordinates from hg18 to hg19.

Figure 6.6. The BDA1-associated duplication interval harbors enhancer elements with spatiotemporal specificity. (**A,B**) *In-vitro* Dual Luciferase Reporter® assay in U2OS cells reveals enhancer activity for reporter test inserts denoted as regulatory elements [RE1], [RE2], [RE3], [RE4], [RE5], [RE6] and the junction amplicon [B-A], as shown at their hg19 genomic location in (c). Each reporter expression vector was derived from amplified human gDNA that was inserted into the multiple cloning site upstream of the minimal promoter of vector pGL-4.26 [*Luc2/minP/Hygro*]. [RE4], [RE5], and junction amplicon [B-A] expression vectors exhibited significant fold change increase when compared to control vector ($Z = 23.49$, one-tailed, $p = 0.0018$). Kruskal-Wallis test with Dunn's post hoc test, $p < 0.00l$ (***). (**C**) Schematic of the genomic positions of the *in-vitro* and *in-vivo* reporter test REs relative to the duplication breakpoints at hg19 chr5:g.33057208 and g.33066676, as well as several UCSC genome tracks namely the 100 vertebrate PhyloP conservation, ENCODE DNaseI Clusters, and enhancer histone modifications represented by ENCODE 7 cell line H3K4m1 and H3K27ac. Tested and expression not found for transgene RE7 at E11.5. (**D**) Lateral and frontal displays of selected whole-mounted embryos carrying the RE8 reporter transgene [*RE8/Hsp68/LacZ*] which were harvested and stained with X-gal at E11.5 (Embryo-1 and -2) and E13.5 (Embryo-3 and -4). Shoulder (sh) and spinal cord (sc) expression domains at E11.5 (n = 4/8); Note X-gal staining in the posterior-dorsal section of the limbud. Hindlimbs (hl), sh, and pelvis (pv) expression domains at E13.5 (n = 7/10). Forelimb (fl) and forepaw (fp) expression domains at E13.5 (n = 2/10). (**E**) Montage of close-up views of selected X-gal stained tissue compartments from Embyro-3 (i, ii) and Embryo-4 (iii-vii). Panels vi (unadjusted) and vii (adjusted: brightness 18%, contrast 76%) are palmar views of the forepaw pictured in panel v; Note the X-gal staining at all of the digit tips and at the perichondrium which outlines the metacarpals (MC) of digits 2, 3 and 4 except at its distal ends or epiphyses. Abbreviations for other highlighted mouse tissues are: Limbbud (lb), zygomatic arch (za), nasal process (np), nasal bone (nb), ribcage (rc), interdigital space 1-4 (id1-4), digit 1-4 (d1-4), proximal phalange (PP), middle phalange (MP), and distal phalange (DP).

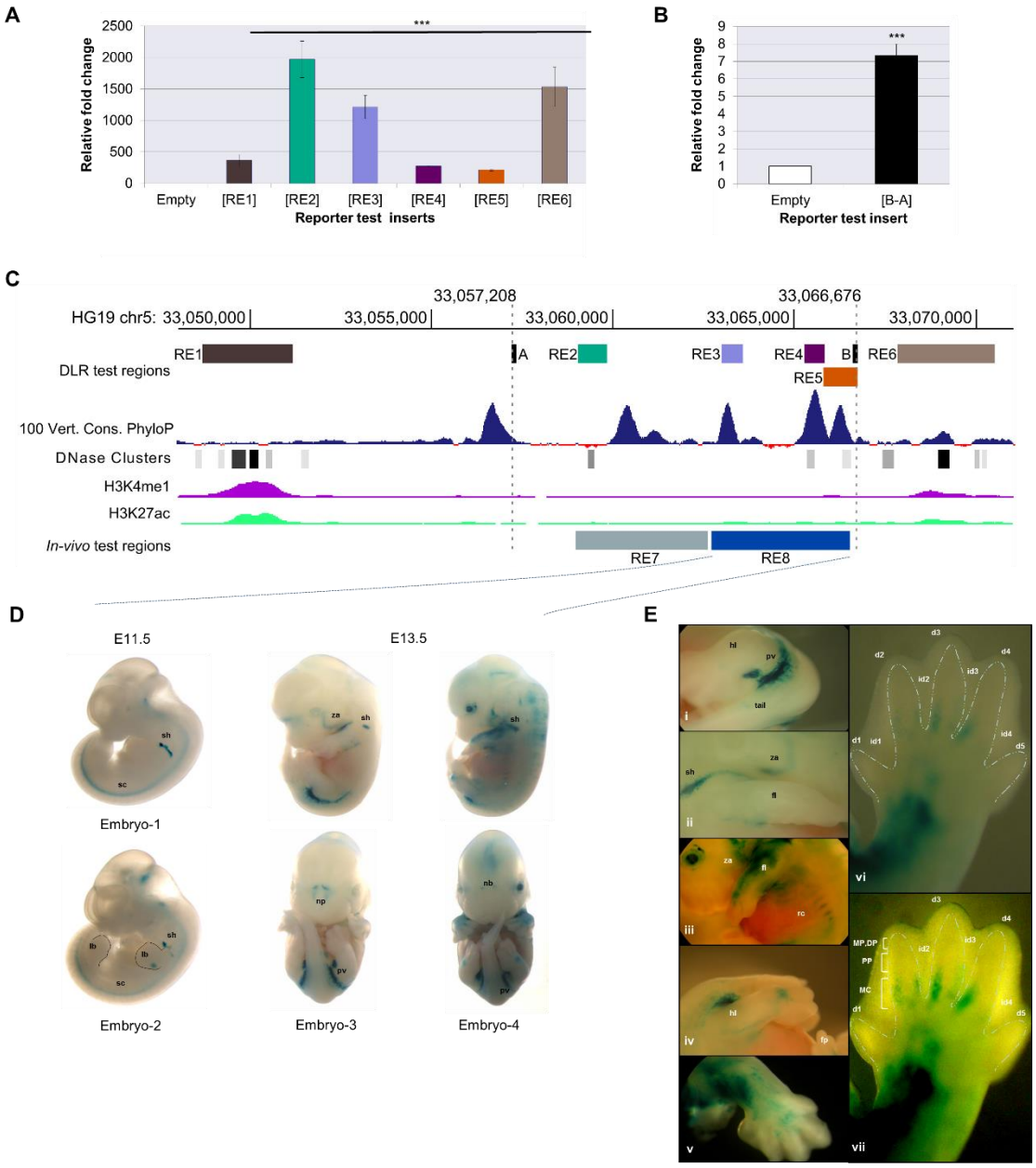
A
Relative fold change
2500
2000
1500
1000
500
0
***
Empty
[RE1]
[RE2]
[RE3]
[RE4]
[RE5]
[RE6]
Reporter test inserts
B
Relative fold change
9
8
7
6
5
4
3
2
1
0
***
Empty
[B-A]
Reporter test insert
C
HG19 chr5: 33,050,000
33,055,000
33,057,208
33,060,000
33,065,000
33,066,676
33,070,000
RE1
DLR test regions
A
RE2
RE3
RE4
B
RE5
RE6
100 Vert. Cons. PhyloP
DNase Clusters
H3K4me1
H3K27ac
In-vivo test regions
RE7
RE8
D
E11.5
E13.5
Embryo-1
Embryo-2
Embryo-3
Embryo-4
E
i
ii
iii
iv
v
vi
vii

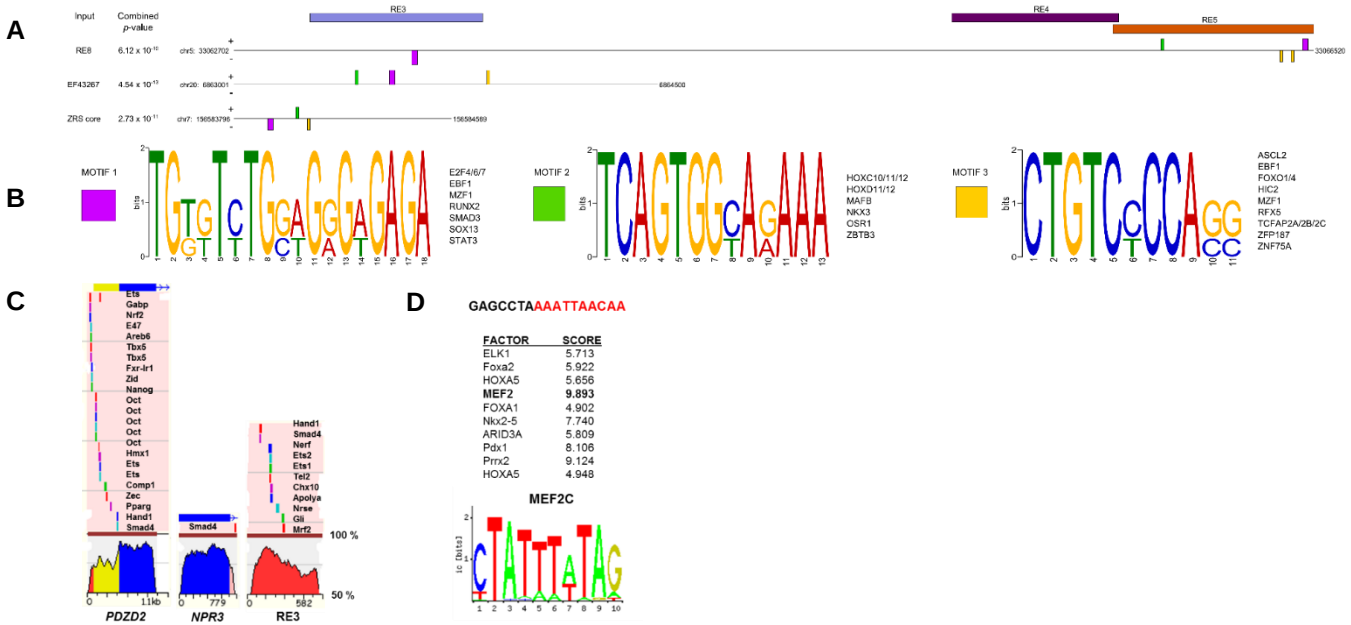

Figure 6.7. Predicted transcription factor binding sites shared between three human enhancer sequences expressed in mouse limbbuds. (A) MAST V4.9.1 block alignment of paralogous motifs within RE8 (3819 bp), BMP2 associated enhancer EF43267 (1500 bp) (Erwin et al., 2014) and ZRS-SHH core (774 bp) (Lettice et al., 2003) sequences (max motif = 3, min motif width =6, max motif width = 50, occurrence of motif = zero or one per sequence). The position of the in-vitro reporter test inserts RE3, RE4 and RE5 relative to transgene insert RE8 are shown above as colored horizontal bars. Shared motifs across the three test sequences were only located in RE3 and RE5. The hg19 genomic coordinates for the test sequences are located at their ends. **(B)** Each motif served as input for TOMTOM V.4.9.1 TFBS prediction using JASPAR 2014, UniPROBE Mouse and Human and Mouse Jolma2013 TF databases. The predicted TF binding sites are listed next to the MAST generated motif logo. **(C)** rVISTA conservation (50-100%) panels of conserved transcription factor binding sites associated with RE3 and exon 1 of *PDZD2* and *NPR3*. 3' UTR (green). CDS (blue). Noncoding (red). Only hits generated by high-specificity matrices which are optimized for function similarity (cut-off Transfac PWM similarity ≤ 0.85) are illustrated. **(D)** JASPAR predicted transcription factor binding sites associated with the junction sequence depicted above. The breakpoint is at the black/red sequence demarcation. MEF2C logo was generated by ConSite with the input junction sequence.

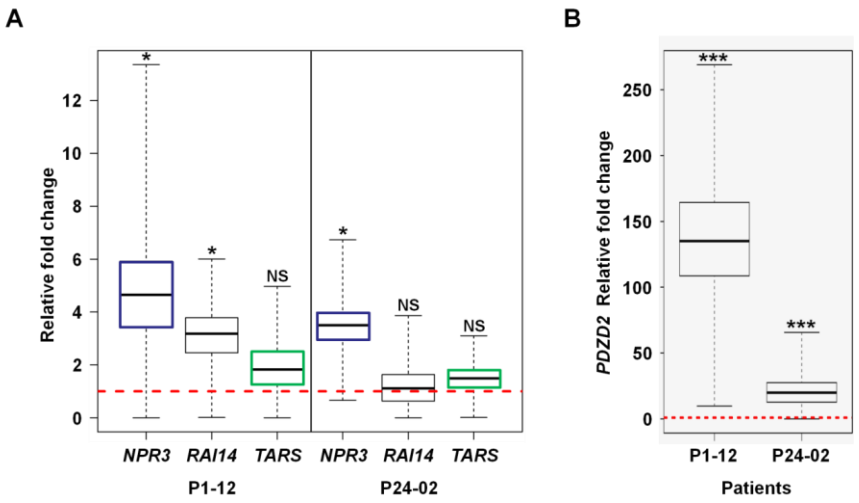

Figure 6.8. *Cis*-distal genes are misregulated in junction-positive BDA1 patients. (**A,B**) Boxplots displaying relative fold change ($2^{-\Delta\Delta Ct}$) in *PDZD2* (n = 6), *NPR3* (n = 7), *TARS* (n = 6), and *RAI14* (n = 3) expression, as measured by TaqMan pre-validated assays, in fibroblast cDNAs of junction-positive patients, P1-12 and P2-02, versus an age-matched and unrelated junction-negative control. Endogenous controls *ACTB* or *TBP* were used to normalize gene expression. P2-02 *PDZD2* expression (Median = 19.71) shows 6 fold increase relative to *NPR3* (Median = 3.48). P1-12 *PDZD2* expression (Median 136.53) shows 29 fold increase relative to *NPR3* (Median = 4.65). Box = 1st and 3rd quartile; bars = min and max values; threshold = 1 (red dashed line). BootstRatio test; $p < 0.05$ (*) and $p < 0.001$ (***). 'NS' indicates no significant difference ($p > 0.05$).

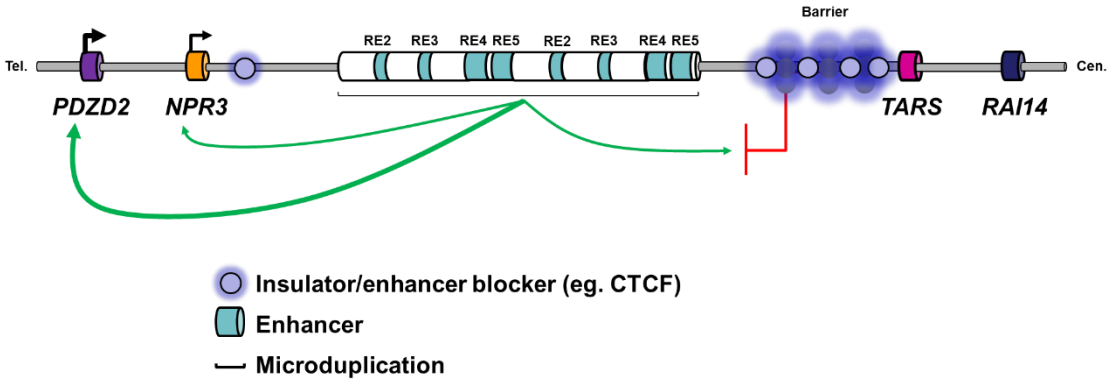

Figure 6.9. *Cis*-regulatory model. *Cis*-regulatory elements RE2-RE5 within the microduplication would interact with the promoters of *PDZD2* and *NPR3*. A cluster of CTCF ChIP-seq peaks which were identified through the ENCODE/BROAD Institute Histone Modifications track would act as a barrier for enhancer interactions with downstream transcriptional units.

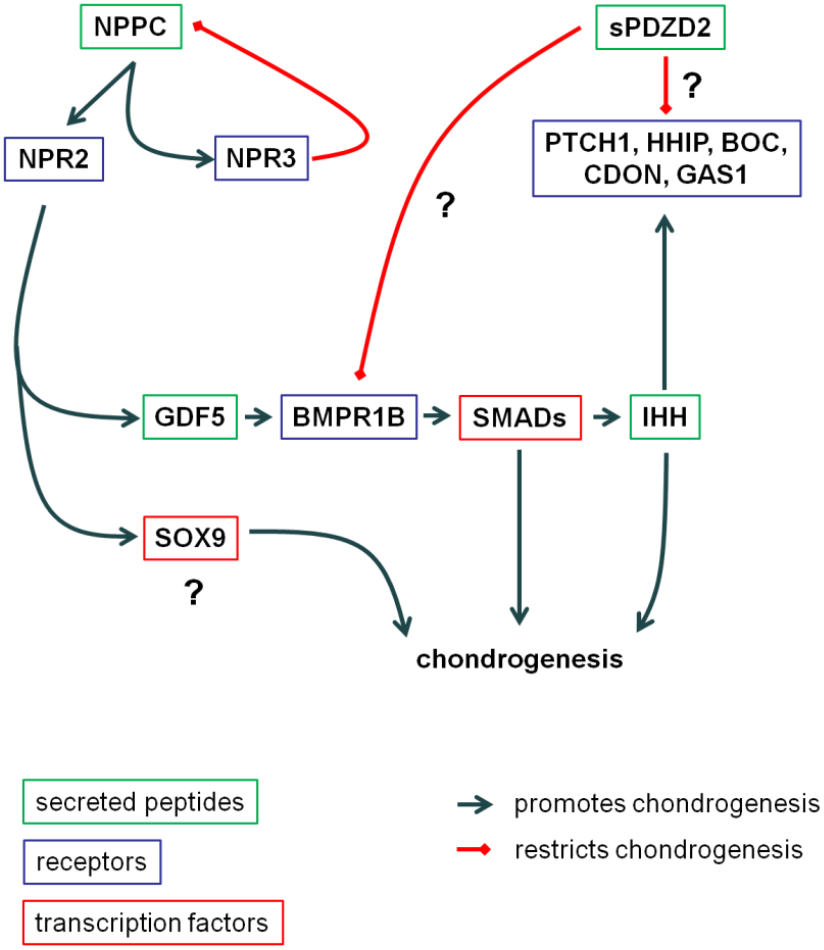

Figure 6.10. Chondrogenesis centered on the BMP-SMAD signaling pathway. NPR3 and sPDZD2 inhibits and/or restricts chondrogenesis. Suspected interactions are denoted with a "**?**".

6.12 Manuscript Supplementary Materials and Methods

Bioinformatics analyses of HTS reads.

Roche 454 sff formatted files were converted into .fna and .qual formats for downstream quality checks and processing. Sequencing adapters were removed and only reads meeting the criteria of a call base ≥ 50% and a read length ≥ 50 bases were kept for base quality value (QV) processing. Reads with an average base QV ≥ 20 were soft-clipped twice for base QV ≤ 16 in at least 3 bases within the last 20% of the read. A final soft-clipping of QV ≤ 20 in at least 3 bases within the last 20% of the read was performed before filtering reads with greater than 3 Ns. We assumed that the majority of low QVs and uncalled bases would occur at the 3'end of the sequence. In order to obtain long reads for sequence alignment to the reference, we removed reads of less than 100 bases. BWA sequence alignment to the human reference hg19 was performed under a seed length of 22 bases, minimum matching base ≥ 12 and minimum sequence identity ≥ 80% of the entire read length. The average fold coverage was calculated for total reads aligned to the *BDA1B* critical region by the following equation:

Equation 6.10.1

$$\text{Coverage} = \frac{\text{Total number reads X Average length of reads (bp)}}{\text{Target region (bp)}}$$

Sequence variants were flagged by meeting an observed base call rate ≥ 10% in at least 3 reads. This strategy allowed us to take into account potential sequence variants in regions of very low read coverage. Split-reads or pseudo paired-end reads were generated in a second alignment strategy under a seed length of 30 bases, moving window of 12 bases, minimum matching base number ≥ 12, a sequence identity of ≥ 50% of the entire read length and an allowance for multiple alignment hits. These reads were

re-mapped to the reference genome under a higher alignment stringency of ≥ 85% sequence identity.

Sequence variants from both patients were filtered for known variants which were deposited in both public datbases and our chr5p13.3 catalogue of sequence variants. Shared and novel candidate causal variants were first checked for base QV ≥ 16 then for QV at ± 3 bases from the reported nucleotide change. Next, the variants were prioritized on overlapping genomic features such as protein coding and noncoding exons. These included the exon/intron boundaries for potential variants positioned at the splice sites. These features took precedent over intergenic sequence variants for verification in family members and controls. Variants within homopolymer tracts were ignored and binned for later inspection as 454 pyrosequencing is known to carry a high error call rate at these sequences.

6.13 Manuscript Supplementary Figures, Tables and Legends

Supplementary Table S6.1. List of primer sequences.

Application	Primer	Sequence
Junction assay/sequencing	A	ACCTGAATCTGACCCCAGTG
	B	GCGGTGAAGGTGACAGAAGT
	C	CCAACGGCTAAGATTATGATGA
	D	TTGCATTTGGAACCATTCAC
Long range PCR	Donor-F	CTTCCCTATGTCAACTCTCAGGCACTTC
	Donor-R	GGGACTGTCCTCAAGTGTAGGGTAATGT
Cloning into pGL4.26	A-SacI	TCCgagctcACCTGAATCTGACCCCAGTG
	B-KpnI	GTTTAggtaccGCGGTGAAGGTGACA
	RE1-KpnI	CGGggtaccCGGGGTACCCCACGGACCAGTACCA
	RE1-NheI	CTAgctagcCTAGCTAGCGCCAGTTCAACAGAGTG
	RE2-KpnI	CGGggtaccCAACAGTCTTGACTACTGCCTA
	RE2-SacI	TCCgagctcGCTGCACCTTTCAACCCGTCA
	RE3-NheI	CTAgctagcGCACAGTAAGCTTCTTGAGA
	RE3-SacI	TCCgagctcTCTTCTGTAAGCACACTGTGGA
	RE4-KpnI	CGGggtaccGCGTGCCTGAGTCTGATCTA
	RE4-SacI	TCCgagctcCCAAGATGAGATTCCCTCCA
	RE5-KpnI	CGGggtaccTGGAGGGAATCTCATCT
	RE5-SacI	TCCgagctcCATTTCCAAGGCCATGT
	RE6-KpnI	CGGggtaccCGGGGTACCCTCAAGCACCATGTCAA
	RE6-SacI	TCCgagctcTCCGAGCTCCCTGCCTCTGTCAAATG
Sequencing pGL4.26	RVprimer3	TAGCAAAATAGGCTGTCCC
Cloning into Gateway reporter [*Hsp68*/*LacZ*]	RE7-F	CACCGACCCCAGGAGAGGAGAGTC
	RE7-R	CACCGCGATGGCTAGTTGAGATCAG
	RE8-F	CACCTGCAGAAACCCTTTTTACCC
	RE8-R	CACCCCTCCCTCCTGTTAGCCTTT

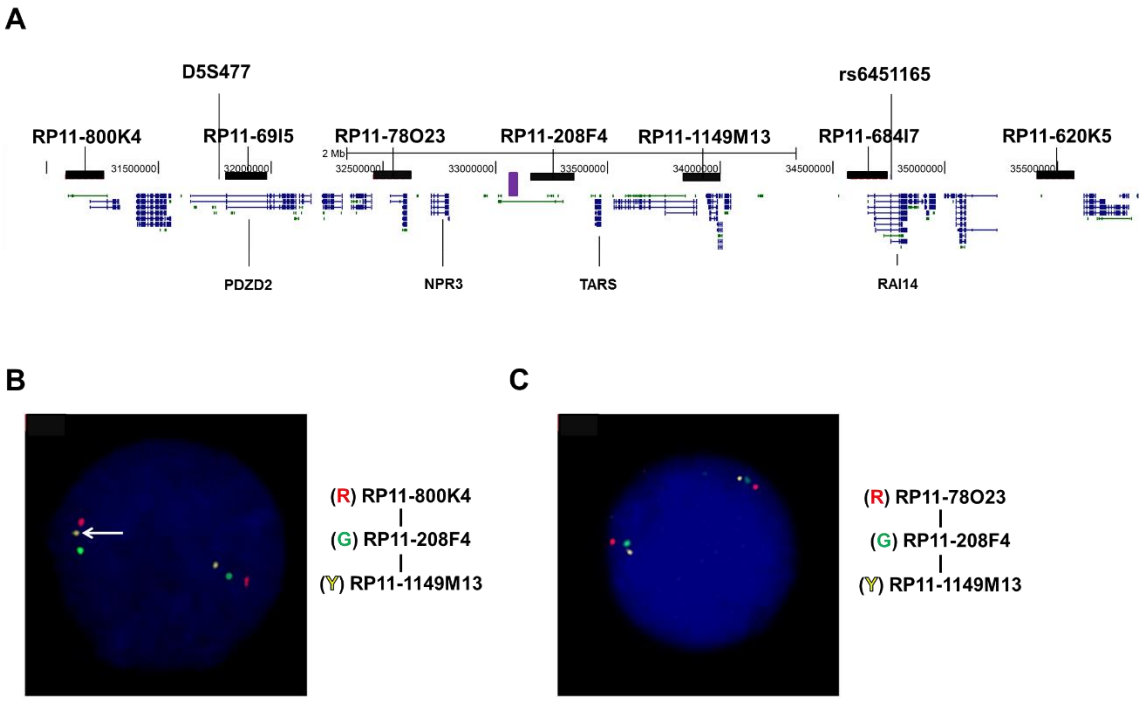

Supplementary Figure S6.1. Evaluation of the *BDA1B* locus for genomic rearrangements using 3-color FISH. (A) Schematic of the physical position for each BAC probe (black bar) used to tile the *BDA1B* locus at chr5p13.3 as defined by the recombinant makers D5S477 and rs6451165. Selected genes are highlighted below the BAC track. The purple vertical bar represents the location of the tandem duplication, subsequently identified in two BDA1 families. Protein coding (blue lines) and noncoding (green) transcripts are shown below the probes. A total of 825364 bp or 29% of the *BDA1B* locus was covered by these probes. **(B)** Lymphoblast interphase spread of an affected patient belonging to Family-1 tested with a probe combination listed on the right hand side. A potential inversion between probes RP11-208F4 (green) and RP11-1149M13 (yellow) on one allele is indicated by an arrow. **(C)** Lymphoblast interphase spread of the same individual shown in (B) with another probe combination. Probe combinations and observed frequencies are listed in Supplementary Table S6.2.

Supplementary Table S6.2. Observed frequencies of BAC probes at the middle position. All counts were performed by two observers (R1 and R2) on interphase spreads from one affected individual of Family-1 or an unaffected individual (control).

Experiment ID		Probe Combination			Total nuclei scored	Conclusion
		Probe 1	Probe 2	Probe 3		
Expt. 1		RP11-800K4	RP11-69I5	RP11-78O23	n=228	Ratios not indicative of inversion within this probe set
	R1	16	118	17		
	R2	3	63	11		
Expt. 2		RP11-1149M13	RP11-684I7	RP11-620K5	n= 249	Ratios not indicative of inversion within this probe set
	R1	15	75	17		
	R2	12	110	20		
Expt. 3		RP11-800K4	RP11-78O23	RP11-208F4	n= 242	Ratios not indicative of inversion within this probe set
	R1	14	114	29		
	R2	2	64	19		
Expt. 4		RP11-69I5	RP11-208F4	RP11-684I7	n= 271	Ratios not indicative of inversion within this probe set
	R1	18	72	19		
	R2	19	116	27		
Expt. 5		RP11-800K4	RP11-208F4	RP11-1149M13	n=223	Inversion or due to large distance between RP11-208F4 & RP11-1149M13
	R1	4	60	40		
	R2	6	65	48		
Expt. 5 (repeat)		RP11-800K4	RP11-208F4	RP11-1149M13	n=227	Inconclusive
	R1	2	89	35		
	R2	1	70	30		
Expt. 6		RP11-78O23	RP11-208F4	RP11-1149M13	n=138	Ratios not indicative of inversion with this probe set
	R1	11	54	16		
	R2	7	39	11		
Expt. 6 Control		RP11-78O23	RP11-208F4	RP11-1149M13	n=201	Ratios not indicative of inversion with this probe set
	R1	24	74	19		
	R2	13	53	18		

Supplementary Table S6.3. Mutation screening of novel exons within the *BDA1B* critical region. These genomic features were not assessed by previous students. All of the identified sequence variants were already annotated in the public databases, such as dbSNP142.

Category	Identifier	Targeted Region	Identified SNPs
Gene	*SUB1*	exon 6	rs1458047
	NPR3	promoter	rs3762988, rs3834818, rs3762989
	c5orf23 (NPR3)	entire exon	rs3214434, rs1173756, rs1173757
	C1QTNF3	3'UTR	rs840387, rs60561051
mRNA, EST	BU171287	all exons	rs35172885
	AK127389	exon 2	rs299608
	AW268575	exon 2	rs1530507
	AF138859	entire exon	rs1429007
	BU626326	exon 2	rs10057069, rs11750438
	CF130386	entire exon	rs57544432
Long ncRNA	AK022112	all exons	rs7702240, rs7379804, rs12656221, rs1994934, rs7735012, rs7710613, rs7714776
Small ncRNA	ENSG00000210286	entire exon	none
	ENSG00000210296	entire exon	none
	ENSG00000210290	entire exon	none
	ENSG00000200065	entire exon	none
	ENSG00000199731	entire exon	rs1678887
	ENSG00000207052	entire exon	rs1142605
	ENSG00000210335	entire exon	rs444815, rs414372, rs399608
	ENSG00000201623	entire exon	none
rRNA	28S-rRNA-related	entire exon	rs7712366

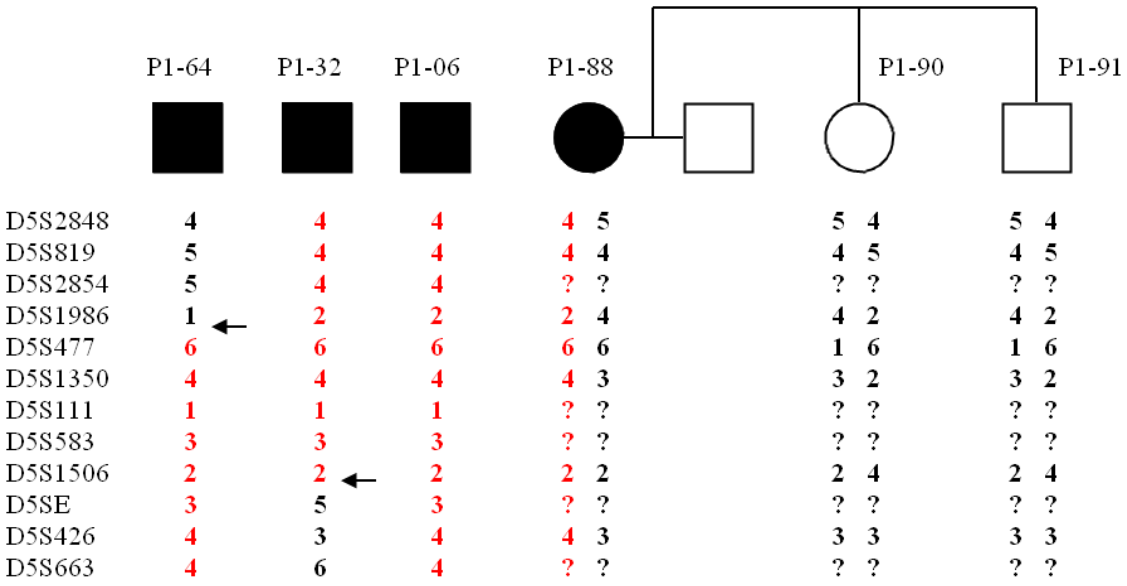

Supplementary Figure S6.2. Genotyping of additional Family-1 members, P1-90 and P1-91. P1-90 and P1-91 were clinically observed as potentially having short fingers. No hand radiographs were obtained for these individuals. Filled symbols represent individuals who were diagnosed with BDA1. Polymorphic microsatellite markers used for genotyping are listed in the first column. The numbers in red font represent the affected haplotype. The arrows point to a recombination event. Unknown genotypes are represented with a question mark "**?**".

Supplementary Table S6.4. Shared and novel sequence variants between individuals P1-06 and P1-64. Hg19 coordinates are listed in the first column.

Genome position	Reference Allele	Observed Allele	Features
g.32707998-32707999	TA	-	EST intron
g. 33258283-33258283	G	A	EST intron
g. 34523122-34523124	CTT	-	$(CTT)_3$ tract

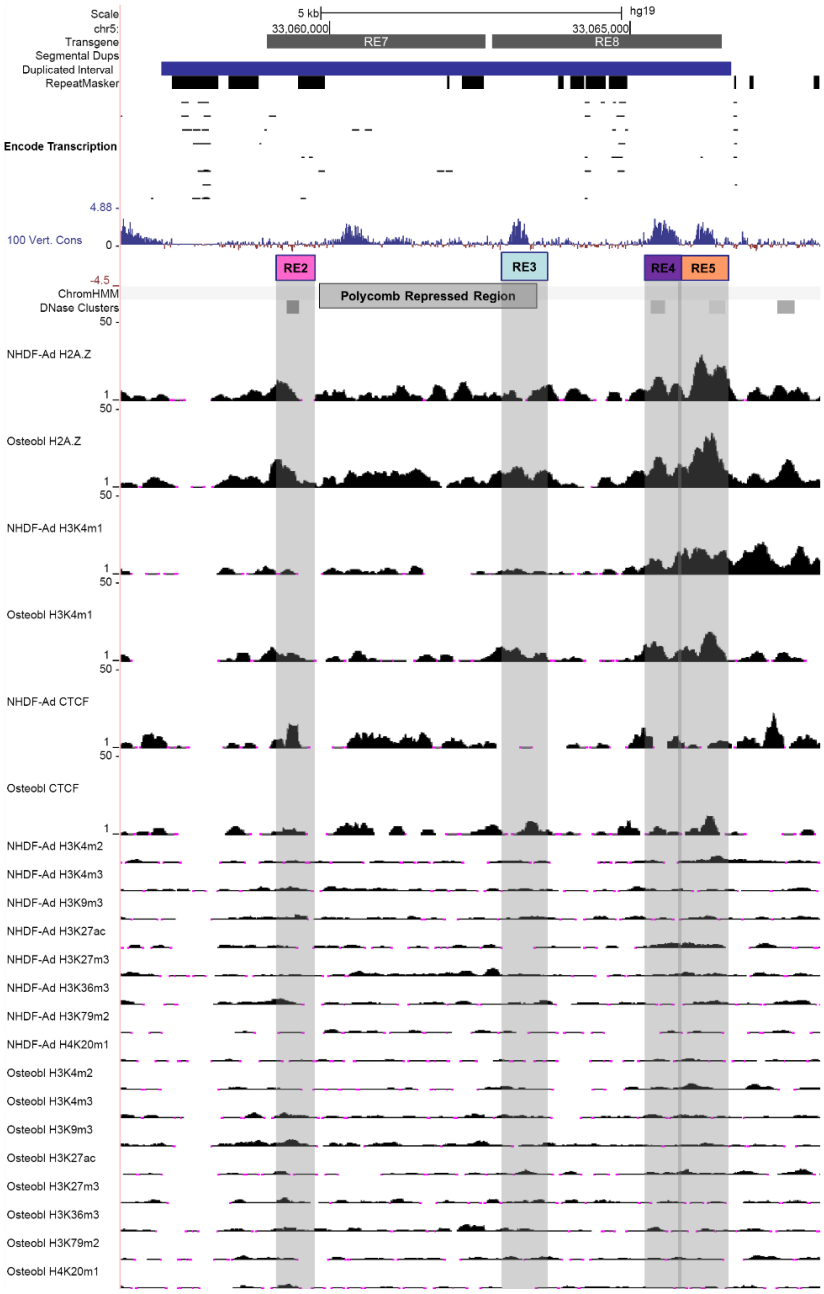

Supplementary Figure S6.3. Hg19 genome view of chromatin landmarks relative to the duplicated interval. Reporter inserts, labeled RE, are shown below the 100 vertebrates PhyloP track. *In-vivo* transgene reporter inserts, RE7 and RE8, are displayed above the donor region (blue bar). Displayed along the y-axis are selected UCSC Genome Browser tracks, namely Segmental Duplications, RepeatMasker, ENCODE Transcription, and ENCODE histone modification tracks for normal primary adult human dermal fibroblasts (NHDF-Ad) and primary human osteoblasts (Osteobl) such as H2A.Z, H3K4m1, CTCF, H3K4m2, H3K4m3, H3K9m3, H3K27ac, H3K27m3, H3K36m3, H3K9m2, and H4K20m1. ENCODE ChromHMM and DNaseI clusters are shown below the *in-vitro* reporter test inserts. Genome features overlapping the tested fragments are highlighted in shaded columns.

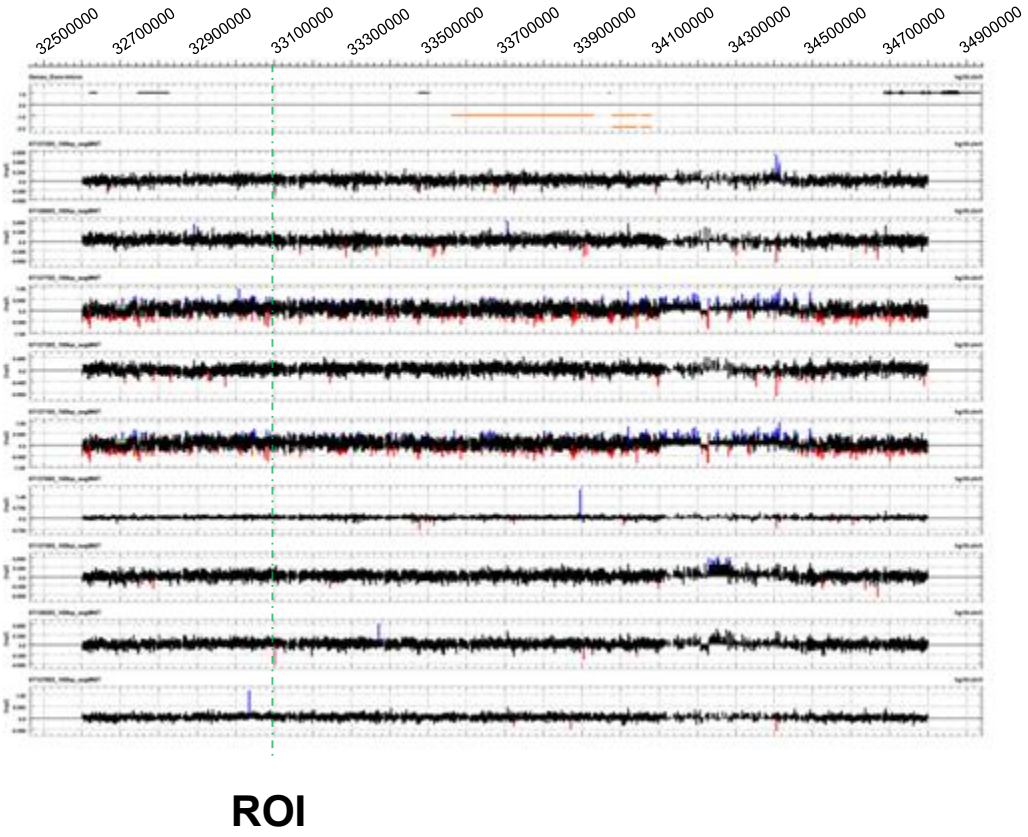

Supplementary Figure S6.4. Averaged 100 bp-segmented log_2 plots of the aCGH tested interval of 2.2 Mb for the remaining BDA1 probands. The region of interest (ROI) is positioned (green dashed line) at the same location as the detected gain-of-copy interval presented in Figure 6.5. No duplications were identified across the ROI in the same aCGH experiment as shown in Figure 6.5. The aCGH probe design was originally based on hg18 reference genomic coordinates as indicated above.

Supplementary Table S6.5. Affymetrix Human Mapping 500K SNP probes. The gray highlighted row refers to a probe within the donor region. Hg19 genomic coordinates are displayed for each probe.

500K SNP	Start	End	Probe	Strand	Ref/Obs	rs ID
Affy250Nsp	33074501	33074502	SNP_A-1810147	+	C/T	rs16890624
Affy250Sty	33091536	33091537	SNP_A-2147631	-	A/G	rs1428217
Affy250Sty	33095739	33095740	SNP_A-2207409	-	C/T	rs3860750
Affy250Sty	33103631	33103632	SNP_A-2088527	-	A/G	rs2619864
Affy250Nsp	33104736	33104737	SNP_A-2313621	-	A/C	rs2619861

Supplementary Table S6.6. Clinical manifestations of probands in our BDA1 cohort. Phalangeal bones: Distal (DP), Middle (MP), Proximal (PP). Metacarpals (MC) and metatarsals (MT). Digit # in parentheses. [Extra features]. * denotes this thesis.

Family	Origin	Gene	Mutation	Clinical manifestations
1	Canada	*PDZD2,NPR3*	chr5:g.33055760_33066676dup*	BDA1 [Short: DP (2-5), MP (2-5), PP (2-5), MC (3-5); Cone-shaped epiphyses]
2	England	*IHH*	p.Asp100Asn	BDA1
3	England	*IHH*	p.Asp100Asn	BDA1
4	USA	*IHH*	p.Glu95Gly	BDA1
5	N. Zealand	?	?	BDA1 [Developmental delay, renal anomaly]
6	England	*IHH*	p.Asp100Asn	BDA1
7	Canada	*BMPR1B*	p.Lys325Asn*	BDA1 [Short: DP (3), MP (2,3,5), PP (1)]
8	Canada	?	?	BDA1 [Hands: Distal fusion (2,5), short MC (1,3,4); Feet: Syndactyly]
9	USA	*IHH*	p.Asp100Asn*	BDA1
10	Scotland	?	?	BDA1 [Short & absent phalanges]
11	USA	?	?	BDA1 [LH: Absent MP (2-5), short square PP (1); RH: Square MP (2-5)]
12	Canada	*GDF5*	p.Lys244Ter	BDA1/BDC
13	USA	*IHH*	p.Asp100Asn	BDA1
14	USA	?	?	BDA1
15	N. Zealand	*IHH*	p.Asp100Asn*	BDA1
16	Africa	*BMPR1B*	c.450-1G>A*	BDA1 [Short: DP (1,2), MP (2,5), PP (1); Long: PP (2-5), MC (1); Radial deviation DP (5)]
17	Canada	*GDF5*	p.Arg399Cys*	BDA1
18	Canada	?	?	BDA1
19	USA	*IHH*	p.Arg128Glu*	BDA1
20	USA	?	?	BDA1
21	India	*IHH*	p.Thr130Asn*	BDA1
22	Israel	*IHH*	p.Glu131Lys*	BDA1
23	Mexico	?	?	BDA1 [Hands: Brachydactyly (2,5), camptodactyly (3), polydactyly; Feet: Syndactyly (3-5)]
24	Canada	*PDZD2,NPR3*	chr5:g.33055760_3306667dup*	BDA1 [Short: Square MP (2-5); Radial clinodactyly (3); Joint inflammation]
25	Italy	?	?	BDA1
26	England	?	?	BDA1 [Hands: Short MP (2,5), PP (3), MC (1); LH absent MP (3); Feet: Distal fusion (2-5)]
27	France	?	?	BDA1 [Hands: Short MP (2,4,5), MC (1,3,4); Feet: MT (1,4,5); Short humerus]
28	Canada	?	?	BDA1 [Short: MP (2-5); Joint hypermobility]

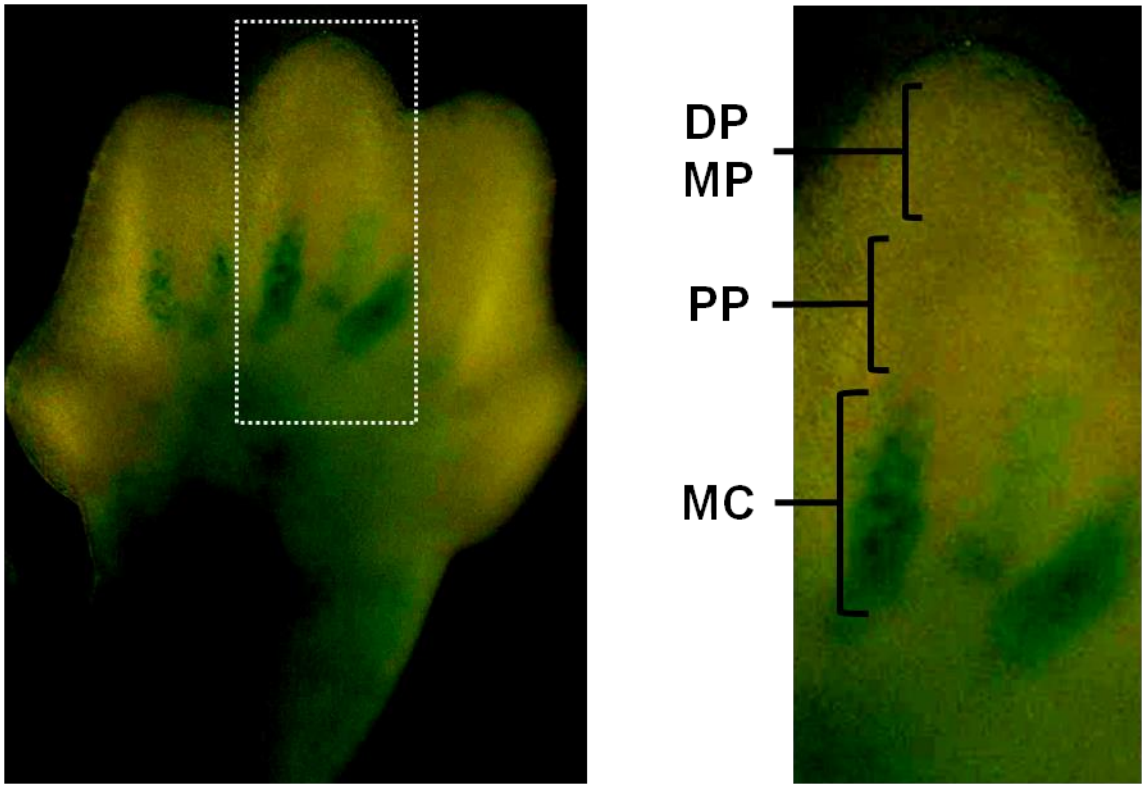

Supplementary Figure S6.5. X-gal staining of E13.5 forepaw. Palmar view of the left forepaw and close-up of the boxed section. Metacarpal (MC). Proximal phalanx (PP). Middle phalanx (MP). Distal phalanx (DP). Note the staining of the perichondrium at the metacarpals and at the digit tips.

Supplementary Table S6.7. Predicted conserved TFBS located across RE3. Transfac Professional V.10.2 matrices with cut-off similarity score ≥ 85 are only listed.

Matched Matrix	Strand	Human ECR Position	Human ECR Sequence	Mouse ECR Position	Mouse ECR Sequence	Cut-off similarity score
VSHAND1E47_01	-	95-110	aattCCAGAcattctt	489-504	aagaatgTCTGGaatt	100
VSSMAD_Q6_01	+	96-106	attcCAGACat	493-503	atGTCTGgaat	100
VSNERF_Q2	+	170-187	tacTAGGAAGtaattagg	411-428	cctaattaCTTCCTActa	100
VSETS2_B	+	171-184	acTAGGAAgtaatt	414-427	aattacTTCCTAct	100
VSETS1_B	+	172-186	cTAGGAAGTAATTag	412-426	ctAATTACTTCCTAc	100
VSTEL2_Q6	-	173-182	TAGGAAGTAa	416-425	tTACTTCCTA	100
VSCHX10_01	+	177-190	aagTAATTAGGcgt	408-421	acgCCTAATTActt	100
VSAPOLYA_B	-	181-195	aATTAGGCGTTGATG	403-417	CATCAACGCCTAATt	100
VSNRSE_B	-	224-244	GTTGAGGGCCTTGGAGCTGAg	355-375	cCCAGCTCCTCGGCCTTCAGC	85
VSGLI_Q2	-	271-282	aGACCACCCAca	317-328	tgTGGGTGGTCt	95
VSMRF2_01	+	276-289	accCACAATATCAG	310-323	CTGGTCTTGTGggt	95

Supplementary Figure S6.6. rVISTA conserved TFBS across RE4 to RE5. rVISTA panel of conserved transcription factor binding sites (Transfac Professional V.10.2 similarity cut-off score ≥ 85) across the sequence represented by RE4-RE5.

Supplementary Table S6.8. Predicted conserved TFBS across RE4 to RE5. Transfac Professional V.10.2 matrices with cut-off similarity score ≥ 85 are only listed.

Matched Matrix	Strand	Human ECR Position	Human ECR Sequence	Mouse ECR Position	Mouse ECR Sequence	Cut-off similarity score
VSETS_Q4	+	111-122	tatgg**CTTCCT**g	1334-1345	c**AGGAAG**tcata	85
VSCETS1P54_03	-	111-126	tatggct**TCCT**gtatg	1330-1345	aattc**AGGA**agtcata	85
VSETS2_B	-	111-124	tatggc**TTCCTG**ta	1332-1345	tt**CAGGAA**gtcata	85
VSCETS1P54_01	-	114-123	ggct**TCCTG**t	1333-1342	t**CAGGA**agtc	85
VSETS_Q6	+	115-122	gc**TTCC**tg	1334-1341	ca**GGAA**gt	85
VSHSF1_Q6	-	175-191	taa**GAATCTTCCAAAT**a	1285-1301	c**ATTTGGAAAGTTC**ttc	80
VSHSF1_01	-	177-186	a**GAATCTTC**c	1290-1299	g**GAAAGTTC**t	80
VSALX4_01	+	256-268	**CCTGAGTCTGATC**	1215-1227	**GATCAAACTCAGG**	80
VSPBX_Q3	+	347-358	**GATTTA**ttgtcc	1119-1130	ggacaa**TAAATC**	90
VSMRF2_01	-	400-413	**TCTGTAATGTG**gtc	1064-1077	gac**CACATTACAGA**	95
VSSOX_Q6	+	437-449	c**TCTTTGAT**atct	1028-1040	agat**ATCAAAGA**g	100
VSGR_01	+	438-464	tctttgatatctttta**TGTTCT**taacat	1013-1039	atgtta**AGAACA**taaagatatcaaaga	100
VSPR_01	+	438-464	tctttga**TATCTTTATGTTCT**taacat	1013-1039	atgttaA**GAACATAAAGATA**tcaaaga	100
VSGR_Q6	+	442-460	tgatatctttta**TGTTC**tta	1017-1035	taa**GAACA**taaagatatca	100
VSAR_Q2	+	444-458	**ATATCTTTATGTTCT**	1019-1033	**AGAACATAAAGATAT**	100
VSGR_Q6	+	451-458	ta**TGTTC**t	1019-1026	a**GAACA**ta	100
VSRP58_01	+	458-469	tt**AACATCTGC**a	1008-1019	t**GCAGATGTT**aa	100
VSE2F_03	-	538-549	cagc**CCTCCAAA**	928-939	**TTTGGAGG**gctg	100
VSE2F_Q6_01	+	539-550	agcc**CTCCAA**aa	927-938	tt**TTGGAG**ggct	100
VSE2F_Q4_01	+	540-550	gcc**CTCCAAA**a	927-937	t**TTTGGAG**ggc	100
VSE2F1_Q4_01	-	541-549	cc**CTCCAAA**	928-936	**TTTGGAG**gg	100
VSE2F_Q3_01	-	541-549	cc**CTCCAAA**	928-936	**TTTGGAG**gg	100
VSE2F1_Q4	-	542-549	**CCTCCAA**a	928-935	t**TTGGAGG**	100
VSPBX1_01	+	582-590	**ATTAATCA**t	887-895	a**TGATTCAT**	90
VSPAX3_01	+	871-883	**TCCTCACAT**ttta	613-625	tgaa**ATGTGAGGA**	90
VSHES1_Q2	-	1052-1066	ttttg**CACCAG**actt	435-449	aagt**CTGGTG**caaaa	100
VSTCF11_01	-	1076-1088	gtcacaac**ATGAC**	413-425	**GTCAT**gttgtgac	100
VSAP1_Q6_01	+	1084-1092	a**TGACTTA**a	409-417	t**TAAGTCA**t	100
VSAP1_Q4_01	+	1084-1091	a**TGACTTA**	410-417	**TAAGTCA**t	100
VSOCT1_05	-	1095-1108	ag**TTTGAAAAT**gag	393-406	ctc**ATTTTCAAA**ct	100
VSOCT_C	-	1096-1108	gt**TTGAAAATGA**g	393-405	c**TCATTTTCAA**ac	100
VSNANOG_01	-	1100-1111	**GAAAATGAGC**cc	390-401	gg**GCTCATTTTC**	100
VSHNF4_Q6	-	1133-1141	g**TGGCC**ttt	360-368	aaa**GGCCA**c	95
VSYY1_Q6	-	1156-1164	aa**AGATGGA**	337-345	**TCCATCT**tt	100
VSPBX_Q3	+	1159-1170	**GATGGA**atgtct	331-342	agacat**TCCATC**	100
VSCEBP_01	-	1233-1245	aat**TCACCA**aact	230-242	agtt**TGGTGA**gtt	100
VSBARBIE_01	-	1237-1251	**CACCAAACTTT**tcat	224-238	atga**AAAGTTTGGTG**	100
VSMTF1_Q4	+	1274-1287	tc**TGCACAGGGC**ca	188-201	tg**GCCGCGTGCA**ga	85
VSNFY_Q6_01	+	1279-1291	acaggg**CCAAT**ca	184-196	tg**GTTGG**ccgcgt	85
VSCAAT_C	+	1284-1308	g**CCAATCACCAAGCCAAACTCATCT**	167-191	**AGATGAGGTTGGCTTAGTGGTTGG**c	95

Chapter 7 - General discussion

7.1 Scope of discussion

Studies on human genetic variation continue to explore the relationship between genotype and phenotype. In response to the advances in mutation detection strategies, the resurgence of genetic studies on rare orphan disorders and malformations have culminated in the increased reporting of mutations for these Mendelian inherited conditions. Although rare and benign, BDA1 is a good candidate for examination of the genetic perturbations underlying phenotypic variability in the human population.

The work presented in this thesis has improved our understanding of the molecular pathways and its regulation in phalangeal development by expanding the repertoire of mutations associated with a variety of BDA1 clinical manifestations. It has provided strong evidence to support a common genetic pathway in phalangeal development.

7.2 Distribution of *IHH* mutations

The contribution of *IHH* mutations which are associated with BDA1 was confirmed by performing the PCR-based sequencing of the *IHH* gene in our collection of BDA1 families. In Chapter 3, I describe the identification of three novel missense mutations in *IHH*. The position of these mutations is clustered with other BDA1 mutations along a stretch of 60 highly conserved amino acids within the central region of the N-terminal signaling peptide. It is unclear as to why specific amino acid positions in

IHH are prone to multiple mutations. These positions could represent mutation hotspots. Further functional studies are needed to determine if the three novel mutations affect IHH's biological function by impairing its cleavage, lipid modification, or secretion, or by docking to PTCH1 or to its modulators such as HHIP. The majority of published BDA1 families have mutations in *IHH* which highlights its important role in middle phalangeal formation and elongation.

7.3 Genetic heterogeneity of BDA1

In addition to the recent identification of the BDA1 mutation on chromosome 5p13.3 (Chapter 6) mutations in *IHH* account for 36% of our documented BDA1 cases. This motivated us to explore additional genes involved in causing BDA1. Fortunately, as described in Chapter 4, we were able to use linkage analysis to identify a BDA1 linked region at chromosome 20q11.2 in one consanguineous family. The subsequent sequencing of the coding region for *GDF5* in three affected family members revealed a novel mutation, thereby establishing it as another BDA1 gene. As a result of this finding, I proposed that a common genetic pathway which involves the BMP-SMAD signaling axis is perturbed in BDA1. In Chapter 5, I presented evidence to further support this concept by identifying two novel mutations in *BMPR1B*, the gene which codes for the preferred receptor of GDF5, in two BDA1 families. The missense mutation could act in a dominant negative fashion, similar to heterozygous *BMPR1B* mutations which cause BDA2, whereas the splice site mutation could act as a loss of function. Both mutations are predicted to cause reduced downstream SMAD signaling. In order to determine the effects of both mutations on the activity of BMPR1B and SMAD signaling, additional

characterization into their function is currently underway in the laboratory of Dr. Michael Underhill (University of British Columbia).

7.4 Genotype-phenotype relationship

The clinical spectrum of BDA1 ranges from the complete absence of to the intermediate or mild shortening of the middle phalanges. Heterozygous *IHH* mutations which are associated with classical BDA1 tend to favor severe shortening of the middle phalanges of digits 2-5 and the proximal phalange of digit 1, or the complete absence of the middle phalanges of digits 2-5 due to symphalangism of the middle and distal bones. There is no clear association between the severity of the phenotype and the position of the mutations in *IHH*. Extreme shortening of the middle phalanges of digits 2-5 with a shortening of the first metacarpal was also described in two siblings who harbored a homozygous missense mutation in *GDF5* (see Chapter 4). This specific mutation did not appear to disrupt the function of GDF5's role in interphalangeal joint formation in these patients as we did not observe hypersegmentation or symphalangism which is commonly seen in BDC, whereas cone-shaped epiphyses of the middle phalanges, due to premature epimetaphyseal fusion, and metacarpal shortening are features found in mild BDA1 cases, such as the family described in Chapter 6. Although intra- and interfamilial variability exists, the most consistent pattern associated with the BDA1 families described in this thesis is the shortening of the middle phalanges of digits 2 and 5. It is tempting to conclude that specific genes when mutated will account for all of the variations in BDA1 phenotypes. However, there is considerable functional redundancy in the pathways and other genetic and/or environmental factors could modify the

expression of the phenotype. As such, it is still important to continue examining the genotype-phenotype relationship in Mendelian inherited traits that could reveal the molecular underpinnings of complex disorders.

7.5 Tissue specific noncoding *cis*-regulatory elements

The disruption of long-range cis-regulatory elements by point mutation, translocation, inversion, deletion and duplication are some of the mechanisms leading to misregulated gene expression (Kleinjan and Coutinho, 2009). Identifying these types of mutations is an ongoing challenge as targeting genomic regions enriched in highly repetitive sequences, poorly mapped regions, areas of sequence bias, and hypervariable regions represent the obstacles for any mutation detection platform to overcome. In Chapter 6, I described the identification of a novel intergenic 9.5 kb microduplication within the *BDA1B* critical region by performing HTS on a locus enriched DNA library from two affected family members. An independent family also harbored a similar breakpoint and copy number change. I have shown that conserved sequence elements in the duplicated interval behave like enhancers with temporal and tissue specificity. In addition, the expression of transgene RE8 at the perichondrium of the metacarpals suggests a putative role in controlling gene expression that facilitates the developmental growth program for hand bone width and length. These *cis*-regulatory elements could act on distal and dose sensitive genes by chromatin looping. *PDZD2* and *NPR3* could represent these genes as I have demonstrated an increase in its gene expression in affected individuals carrying the microduplication. Thus unlike the loss-of-function and dominant-negative mutations described in Chapters 3 to 5, I proposed that a gain-of-

function mechanism is the most likely cause of BDA1 in these two families. It is unclear if the upregulation of one or both genes are needed to elicit the BDA1 phenotype. Further functional characterization of the enhancer looping model to its target gene(s) is currently underway in the laboratory of Dr. Dennis Bulman.

7.6 A common genetic pathway involved with phalangeal development and elongation

I have provided evidence that supports Stricker and Mundlos' model of phalangeal development (2011) by identifying *IHH*, *GDF5* and *BMPR1B* as key mediators of BDA1. These three genes are all found within the BMP-SMAD pathway. In conjunction with the other genes in this pathway, they contribute towards the pathogenesis of approximately 53% of the isolated brachydactylies. In addition, I have introduced PDZD2 and NPR3 as candidate interactants within the BMP-SMAD signaling axis. Although the natriuretic peptide system has been associated with bone growth, there is paucity in the literature on the role of PDZD2 in cartilage and bone development. That said, the work presented in the Ph.D. thesis of Tsui (2013) has shown strong evidence to support the role of Pdzd2 in phalangeal development and elongation in mice. A revised BDA1 genetic model that considers NPR3 and PDZD2 in this network is displayed in Figure 6.10.

7.7 Conclusion

By identifying the genetic perturbations which result in human malformations, we can form a map of genetic interactions that might prove useful for clinical diagnosis and

genetic screening. This strategy was implemented in my thesis and has successfully revealed at least three important signaling networks, i.e. IHH, GDF5 and natriuretic peptide, converging at the SMAD signaling axis for phalangeal development. Moreover, it has partially revealed a *cis*-regulatory logic in an intergenic region at chromosome 5p13.3 for specific tissue expression. Noncoding mutations still represent a challenge in defining the molecular mechanisms underlying human conditions, as functional characterization still lacks the tools to properly assess their biological consequence. While these tools continue to evolve, genetic studies should still employ orthogonal mutation detection assays to identify causal variants in noncoding sequences for Mendelian inherited traits.

References

Ahn, S., and Joyner, A.L. (2004). Dynamic changes in the response of cells to positive hedgehog signaling during mouse limb patterning. Cell *118*, 505-516.

Anderson, E., Peluso, S., Lettice, L.A., Hill, R.E. (2012). Human limb abnormalities caused by disruption of hedgehog signaling. Trends Genet. *28*, 364-373.

Armour, C.M., Bulman, D.E., Hunter, A.G. (2000). Clinical and radiological assessment of a family with mild brachydactyly type A1: the usefulness of metacarpophalangeal profiles. J. Med. Genet. *37*, 292-296.

Armour, C.M., McCready, M.E., Baig, A., Hunter, A.G., Bulman, D.E. (2002). A novel locus for brachydactyly type A1 on chromosome 5p13.3-p13.2. J. Med. Genet. *39*, 186-188.

Badugu, A., Kraemer, C., Germann, P., Menshykau, D., Iber, D. (2012). Digit patterning during limb development as a result of the BMP-receptor interaction. Sci. Rep. *2*, 991.

Baker, F. (1888). Anthropological notes on the human hand. American Anthropol. *1*, 51–75.

Bamford, S., Dawson, E., Forbes, S., Clements, J., Pettett, R., Dogan, A., Flanagan, A., Teague, J., Futreal, P.A., Stratton, M.R., Wooster, R. (2004). The COSMIC (Catalogue of Somatic Mutations in Cancer) database and website. Br. J. Cancer. *91*, 355-358.

Bell, J. (1951). On brachydactyly and symphalangism. In Treasury of Human Inheritance, L.S, Penrose, ed. (London, Cambridge University Press), pp. 1-31.

Bejerano, G., Pheasant, M., Makunin, I., Stephen, S., Kent, W.J., Mattick, J.S., Haussler, D. (2004). Ultraconserved elements in the human genome. Science *304*, 1321-1325.

Bénazet, J.D., and Zeller, R. (2009). Vertebrate limb development: moving from classical morphogen gradients to an integrated 4-dimensional patterning system. Cold Spring Harb. Perspect. Biol. *1*, a001339.

Bi, W., Deng, J.M., Zhang, Z., Behringer, R.R., de Crombrugghe, B. (1999). Sox9 is required for cartilage formation. Nat. Genet. *22*, 85-89.

Boycott, K.M., Vanstone, M.R., Bulman, D.E., MacKenzie, A.E. (2013). Rare-disease genetics in the era of next-generation sequencing: discovery to translation. Nat. Rev. Genet. *14*, 681-691.

Briscoe, J., and Thérond, P.P. (2013). The mechanisms of Hedgehog signaling and its roles in development and disease. Nat. Rev. Mol. Cell Biol. *14*, 416-429.

Byrnes, A.M., Racacho, L., Grimsey, A., Hudgins, L., Kwan, A.C., Sangalli, M., Kidd, A., Yaron, Y., Lau, Y.L., Nikkel, S.M., Bulman, D.E. (2009). Brachydactyly A-1 mutations restricted to the central region of the N-terminal active fragment of Indian Hedgehog. Eur. J. Hum. Genet. *17*, 1112-1120.

Byrnes, A.M., Racacho, L., Nikkel, S.M., Xiao, F., MacDonald, H., Underhill, T.M., Bulman, D.E. (2010). Mutations in GDF5 presenting as semidominant brachydactyly A1. Hum. Mutat. *31*, 1155-1162.

Cantagrel, V., Lossi, A.M., Lisgo, S., Missirian, C., Borges, A., Philip, N., Fernandez, C., Cardoso, C., Figarella-Branger, D., Moncla, A., Lindsay, S., Dobyns, W.B., Villard, L. (2007). Truncation of NHEJ1 in a patient with polymicrogyria. Hum. Mutat. *28*, 356-364.

Capellini, T.D., Di Giacomo, G., Salsi, V., Brendolan, A., Ferretti, E., Srivastava, D., Zappavigna, V., Selleri, L. (2006). Pbx1/Pbx2 requirement for distal limb patterning is mediated by the hierarchical control of Hox gene spatial distribution and Shh expression. Development *133*, 2263-2273.

Carter, N.P. (2007). Methods and strategies for analyzing copy number variation using DNA microarrays. Nat. Genet. *39*, S16-S21.

Chiang, C., Litingtung, Y., Harris, M.P., Simandl, B.K., Li, Y., Beachy, P.A., Fallon, J.F. (2001). Manifestation of the limb prepattern: limb development in the absence of sonic hedgehog function. Dev. Biol. *236*, 421-435.

Chusho, H., Tamura, N., Ogawa, Y., Yasoda, A., Suda, M., Miyazawa, T., Nakamura, K., Nakao, K., Kurihara, T., Komatsu, Y., Itoh, H., Tanaka, K., Saito, Y., Katsuki, M., Nakao, K. (2001). Dwarfism and early death in mice lacking C-type natriuretic peptide. Proc. Natl. Acad. Sci. USA *98*, 4016-4021.

Cushing, H. (1916). Hereditary anchylosis of proximal phalangeal joints (symphalangism). Genetics *1*, 90-106.

Deardorff, M.A., Bando, M., Nakato, R., Watrin, E., Itoh, T., Minamino, M., Saitoh, K., Komata, M., Katou, Y., Clark, D., Cole, K.E., De Baere, E., Decroos, C., Di Donato, N., Ernst, S., Francey, L.J., Gyftodimou, Y., Hirashima, K., Hullings, M., Ishikawa, Y., Jaulin, C., Kaur, M., Kiyono, T., Lombardi, P.M., Magnaghi-Jaulin, L., Mortier, G.R., Nozaki, N., Petersen, M.B., Seimiya, H., Siu, V.M., Suzuki, Y., Takagaki, K., Wilde, J.J., Willems, P.J., Prigent, C., Gillessen-Kaesbach, G., Christianson, D.W., Kaiser, F.J., Jackson, L.G., Hirota, T., Krantz, I.D., Shirahige, K. (2012). HDAC8 mutations in Cornelia de Lange syndrome affect the cohesion acetylation cycle. Nature *489*, 313-317.

Degenkolbe, E., König, J., Zimmer, J., Walther, M., Reißner, C., Nickel, J., Plöger, F., Raspopovic, J., Sharpe, J., Dathe, K., Hecht, J.T., Mundlos, S., Doelken, S.C., Seemann, P. (2013). A GDF5 point mutation strikes twice--causing BDA1 and SYNS2. PLoS Genet. *9*, e1003846.

den Hollander, N.S., Hoogeboom, A.J., Niermeijer, M.F., Wladimiroff, J.W. (2001). Prenatal diagnosis of type A1 brachydactyly. Ultrasound Obstet. Gynecol. *17*, 529-530.

Dijkstra, P.F. and Venema, H.W. (1991). Metacarpophalangeal pattern profiles: Q-score for ages from birth to 7 years. Am. J. Med. Genet. *40*, 107-114.

Dijkstra, P.F. and Venema, H.W. (1992). Metacarpophalangeal pattern profiles: Q-score for ages 3 years to adult with epiphyses: an update. Am. J. Med. Genet. *43*, 1041-1043.

Drinkwater, H. (1908). An account of a brachydactylous family. Proc. Royal Soc. Edin. *28*, 35-57.

Drinkwater, H. (1912). Account of a family showing minor-brachydactyly. J. Genet. *2*, 21-40.

Drinkwater, H. (1914). A second brachydactylous family. J. Genet. *4*, 323-339.

Duboc, V. and Logan, M.P. (2011). Regulation of limb bud initiation and limb-type morphology. Dev. Dyn. *240*, 1017-1027.

Dudley, A.T., Ros, M.A., Tabin, C.J. (2002). A re-examination of proximodistal patterning during vertebrate limb development. Nature *418*, 539-544.

Ecker, A. (1875). Einige Bemerkungen über einen Schwankenden Charakter in den Hand des Menschen [Some remarks about a varying character in the hand of humans]. Archiv. fur Anthropologie *8*, 68–74.

Farabee, W.C. (1903). Hereditary and sexual influence in meristic variation: a study of digital malformations in man. Ph.D. Thesis: Harvard University.

Farabee, W.C. (1905). Inheritance of Digital Malformations in Man. Papers of the Peabody Museum of the American Archaeology and Ethnology *3*, 65-78.

Fitch, N. (1979). Classification and identification of inherited brachydactylies. J. Med. Genet. *16*, 36-44.

Foster, J.W., Dominguez-Steglich, M.A., Guioli, S., Kwok, C., Weller, P.A., Stevanović, M., Weissenbach, J., Mansour, S., Young, I.D., Goodfellow, P.N., Brook, J.D., Schafer, A.J. (1994). Campomelic dysplasia and autosomal sex reversal caused by mutations in an SRY-related gene. Nature *372*, 525-530.

Franz-Odendaal, T.A., Hall, B.K., Witten, P.E. (2006). Buried alive: How osteoblasts become osteocytes. Dev. Dyn. *235*, 176-190.

Fukushima, Y., Ohashi, H., Wakui, K., Nishimoto, H., Sato, M., Aihara, T. (1995). De novo apparently balanced reciprocal translocation between 5q11.2 and 17q23 associated with Klippel-Feil anomaly and type A1 brachydactyly. Am. J. Med. Genet. *57*, 447-449.
Gallet, A. (2011). Hedgehog morphogen: from secretion to reception. Trends Cell Biol. *21*, 238-246.

Galli, A., Robay, D., Osterwalder, M., Bao, X., Bénazet, J.D., Tariq, M., Paro, R., Mackem, S., Zeller, R. (2010). Distinct roles of Hand2 in initiating polarity and posterior Shh expression during the onset of mouse limb bud development. PLoS Genet. *6*, e1000901.

Gao, B., Guo, J., She, C., Shu, A., Yang, M., Tan, Z., Yang, X., Guo, S., Feng, G., He, L. (2001). Mutations in IHH, encoding Indian hedgehog, cause brachydactyly type A-1. Nat. Genet. *28*, 386-388.

Gao, B., Hu, J., Stricker, S., Cheung, M., Ma, G., Law, K.F., Witte, F., Briscoe, J., Mundlos, S., He, L., Cheah, K.S., Chan, D. (2009). A mutation in Ihh that causes digit abnormalities alters its signaling capacity and range. Nature *458*, 1196-1200.

Gilsanz, V., and Ratib, O. (2005). Hand Bone Age: A Digital Atlas of Skeletal Maturity. (Germany, Springer-Verlag Berlin Heidelberg New York), pp 1-95.

Giordano, N., Gennari, L., Bruttini, M., Mari, F., Meloni, I., Baldi, C., Capoccia, S., Geraci, S., Merlotti, D., Amendola, A., Martini, G., Nuti, R., Gennari, C., Renieri, A. (2003). Mild brachydactyly type A1 maps to chromosome 2q35-q36 and is caused by a novel IHH mutation in a three generation family. J. Med. Genet. *40*, 132-135.

Girirajan, S., and Elsea, S.H. (2005). Brachydactyly A1: new relatives for old families? J. Genet. *84*, 95-98.

Grange, D.K., Balfour, I.C., Chen, S.C., Wood, E.G. (1998). Familial syndrome of progressive arterial occlusive disease consistent with fibromuscular dysplasia, hypertension, congenital cardiac defects, bone fragility, brachysyndactyly, and learning disabilities. Am. J. Med. Genet. *75*, 469-480.

Grimsey, A. (2006). Brachydactyly type A1: Identification and characterization of the genes involved. M.Sc. Thesis. University of Ottawa.

Haws, D.V., and McKusick, V.A. (1963). Farabee's brachydactylous kindred revisited. Bull. Johns Hopkins Hosp. *113*, 20-30.

Hellemans, J., Coucke, P.J., Giedion, A., De Paepe, A., Kramer, P., Beemer, F., Mortier, G.R. (2003). Homozygous mutations in IHH cause acrocapitofemoral dysplasia, an

autosomal recessive disorder with cone-shaped epiphyses in hands and hips. Am. J. Hum. Genet. *72*, 1040-1046.

Hoefnagel, D., and Gerald, P.S. (1966). Hereditary brachydactyly. Ann. Hum. Genet. *29*, 377-382.

Holder-Espinasse, M., Escande, F., Mayrargue, E., Dieux-Coeslier, A., Fron, D., Doual-Bisser, A., Boute-Benejean, O., Robert, Y., Porchet, N., Manouvrier-Hanu, S. (2004). Angel shaped phalangeal dysplasia, hip dysplasia, and positional teeth abnormalities are part of the brachydactyly C spectrum associated with CDMP-1 mutations. J. Med. Genet. *41*, e78.

Huber, C., and Cormier-Daire, V. (2012). Ciliary disorder of the skeleton. Am. J. Med. Genet. C Semin. Med. Genet. *160C*, 165-174.

Hume, A.N., Buttgereit, J., Al-Awadhi, A.M., Al-Suwaidi, S.S., John, A., Bader, M., Seabra, M.C., Al-Gazali, L., Ali, B.R. (2009). Defective cellular trafficking of missense NPR-B mutants is the major mechanism underlying acromesomelic dysplasia-type Maroteaux. Hum. Mol. Genet. *18*, 267-277.

Hurle, J.M., and Gañan, Y. (1986). Interdigital tissue chondrogenesis induced by surgical removal of the ectoderm in the embryonic chick leg bud. J. Embryol. Exp. Morphol. *94*, 231-244.

Jaubert, J., Jaubert, F., Martin, N., Washburn, L.L., Lee, B.K., Eicher, E.M., Guénet, J.L. (1999). Three new allelic mouse mutations that cause skeletal overgrowth involve the natriuretic peptide receptor C gene (Npr3). Proc. Natl. Acad. Sci. USA *96*, 10278-10283.

Karp, S.J., Schipani, E., St-Jacques, B., Hunzelman, J., Kronenberg, H., McMahon, A.P. (2000). Indian hedgehog coordinates endochondral bone growth and morphogenesis via parathyroid hormone related-protein-dependent and -independent pathways. Development *127*, 543-548.

Kirkpatrick, T.J., Au, K.S., Mastrobattista, J.M., McCready, M.E., Bulman, D.E., Northrup, H. (2003). Identification of a mutation in the Indian Hedgehog (IHH) gene causing brachydactyly type A1 and evidence for a third locus. J. Med. Genet. *40*, 42-44.

Kleinjan, D.J. and Coutinho, P. (2009). Cis-ruption mechanisms: disruption of cis-regulatory control as a cause of human genetic disease. Brief. Funct. Genomic Proteomic *8*, 317-332.

Klopocki, E., Lohan, S., Brancati, F., Koll, R., Brehm, A., Seemann, P., Dathe, K., Stricker, S., Hecht, J., Bosse, K., Betz, R.C., Garaci, F.G., Dallapiccola, B., Jain, M., Muenke, M., Ng, V.C., Chan, W., Chan, D., Mundlos, S. (2011). Copy-number variations involving the IHH locus are associated with syndactyly and craniosynostosis. Am. J. Hum. Genet. *88*, 70-75.

Kobayashi, T., Chung, U.I., Schipani, E., Starbuck, M., Karsenty, G., Katagiri, T., Goad, D.L., Lanske, B., Kronenberg, H.M. (2002). PTHrP and Indian hedgehog control differentiation of growth plate chondrocytes at multiple steps. Development *129*, 2977-2986.

Koboldt, D.C., Larson, D.E., Chen, K., Ding, L., Wilson, R.K. (2012). Massively parallel sequencing approaches for characterization of structural variation. Methods Mol. Biol. *838*, 369-384.

Kraus, P., Fraidenraich, D., Loomis, C.A. (2001). Some distal limb structures develop in mice lacking Sonic hedgehog signaling. Mech. Dev. *100*, 45-58.

Krejci, P., Krakow, D., Mekikian, P.B., Wilcox, W.R. (2007). Fibroblast growth factors 1, 2, 17, and 19 are the predominant FGF ligands expressed in human fetal growth plate cartilage. Pediatr. Res. *61*, 267-272.

Kronenberg, H.M. (2003). Developmental regulation of the growth plate. Nature *423*, 332-336.

Kwok, C., Weller, P.A., Guioli, S., Foster, J.W., Mansour, S., Zuffardi, O., Punnett, H.H., Dominguez-Steglich, M.A., Brook, J.D., Young, I.D., Goodfellow, P.N., Schafer, A.J. (1995). Mutations in SOX9, the gene responsible for Campomelic dysplasia and autosomal sex reversal. Am. J. Hum. Genet. *57*, 1028-1036.

Lacombe, D., Delrue, M.A., Rooryck, C., Morice-Picard, F., Arveiler, B., Maugey-Laulom, B., Mundlos, S., Toutain, A,, Chateil, J.F. (2010). Brachydactyly type A1 with short humerus and associated skeletal features. Am. J. Med. Genet. A. *152A*, 3016-3021.

Laporte, G., Serville, F., Peant, J. (1979). [Type A1 branchydactyly. Study of one family (author's transl)]. Nouv. Presse Med. *8*, 4095-4097.

Lam, C.W., Lau, K.C., Tong, S.F. (2010). Microarrays for personalized genomic medicine. Adv. Clin. Chem. *52*, 1-18.

Lazarus, J.E., Hegde, A., Andrade, A.C., Nilsson, O., Baron, J. (2007). Fibroblast growth factor expression in the postnatal growth plate. Bone *40*, 577-586.

Litingtung, Y., Dahn, R.D., Li, Y., Fallon, J.F., Chiang, C. (2002). Shh and Gli3 are dispensable for limb skeleton formation but regulate digit number and identity. Nature *418*, 979-983.

Liu, M., Wang, X., Cai, Z., Tang, Z., Cao, K., Liang, B., Ren, X., Liu, J.Y., Wang, Q.K. (2006). A novel heterozygous mutation in the Indian hedgehog gene (IHH) is associated with brachydactyly type A1 in a Chinese family. J. Hum. Genet. *51*, 727-731.

Lodder, E.M., Hoogeboom, A.J., Coert, J.H., de Graaff, E. (2008). Deletion of 1 amino acid in Indian hedgehog leads to brachydactylyA1. Am. J. Med. Genet. A *146A*, 2152-2154.

Loomis, C.A., Kimmel, R.A., Tong, C.X., Michaud, J., Joyner, A.L. (1998). Analysis of the genetic pathway leading to formation of ectopic apical ectodermal ridges in mouse Engrailed-1 mutant limbs. Development *125*, 1137-1148.

Lu, P., Yu, Y., Perdue, Y., Werb, Z. (2008). The apical ectodermal ridge is a timer for generating distal limb progenitors. Development *135*, 1395-1405.

Mackie, E.J., Tatarczuch, L., Mirams, M. (2011). The skeleton: a multi-functional complex organ: the growth plate chondrocyte and endochondral ossification. J. Endocrinol. *211*, 109-121.

Mao, J., McGlinn, E., Huang, P., Tabin, C.J., McMahon, A.P. (2009). Fgf-dependent Etv4/5 activity is required for posterior restriction of Sonic Hedgehog and promoting outgrowth of the vertebrate limb. Dev. Cell *16*, 600-606.

Mastrobattista, J.M., Dollé, P., Blanton, S.H., Northrup, H. (1995). Evaluation of candidate genes for familial brachydactyly. J. Med. Genet. *32*, 851-854.

McCready, M. E., Sweeney, E., Fryer, A. E., Donnai, D., Baig, A., Racacho, L., Warman, M. L., Hunter, A. G. W., Bulman, D. E. (2002). A novel mutation in the IHH gene causes brachydactyly type A1: a 95-year-old mystery resolved. Hum. Genet. *111*, 368-375.

McCready, M.E. (2004). Molecular investigation into brachydactyly type A1. Ph.D. Thesis. University of Ottawa.

McCready, M.E, Grimsey, A., Styer, T., Nikkel, S.M., Bulman, D.E. (2005). A century later Farabee has his mutation. Hum. Genet. *117*, 285-287.

McLellan, J.S., Zheng, X., Hauk, G., Ghirlando, R., Beachy, P.A., Leahy, D.J. (2008). The mode of Hedgehog binding to Ihog homologues is not conserved across different phyla. Nature *455*, 979-983.

Meiselman, S.A., Berkenstadt, M., Ben-Ami, T., Goodman, R.M. (1989). Brachydactyly type A-7 (Smorgasbord): a new entity. Clin. Genet. *35*, 261-267.

Metzker, M.L. (2010). Sequencing technologies - the next generation. Nat. Rev. Genet. *11*, 31-46.

Mic, F.A., Sirbu, I.O., Duester, G. (2004). Retinoic acid synthesis controlled by Raldh2 is required early for limb bud initiation and then later as a proximodistal signal during apical ectodermal ridge formation. J. Biol. Chem. *279*, 26698-26706.

Minina, E., Wenzel, H.M., Kreschel, C., Karp, S., Gaffield, W., McMahon, A.P., Vortkamp, A. (2001). BMP and Ihh/PTHrP signaling interact to coordinate chondrocyte proliferation and differentiation. Development *128*, 4523-4534.

Minina, E., Kreschel, C., Naski, M.C., Ornitz, D.M., Vortkamp, A. (2002). Interaction of FGF, Ihh/Pthlh, and BMP signaling integrates chondrocyte proliferation and hypertrophic differentiation. Dev. Cell *3*, 439-449.

Montavon, T., Le Garrec, J.F., Kerszberg, M., Duboule, D. (2008). Modeling Hox gene regulation in digits: reverse colinearity and the molecular origin of thumbness. Genes Dev. *22*, 346-359.

Montavon, T., Soshnikova, N., Mascrez, B., Joye, E., Thevenet, L., Splinter, E., de Laat, W., Spitz, F., Duboule, D. (2011). A regulatory archipelago controls Hox genes transcription in digits. Cell *147*, 1132-1145.

Montero, J.A., Lorda-Diez, C.I., Gañan, Y., Macias, D., Hurle, J.M. (2008). Activin/TGFbeta and BMP crosstalk determines digit chondrogenesis. Dev. Biol. *321*, 343-356.

Mortier, G.R., Kramer, P.P., Giedion, A., Beemer, F.A. (2003). Acrocapitofemoral dysplasia: an autosomal recessive skeletal dysplasia with cone shaped epiphyses in the hands and hips. J Med Genet. *40*, 201-207.

Niswander, L., Tickle, C., Vogel, A., Booth, I., Martin, G.R. (1993). FGF-4 replaces the apical ectodermal ridge and directs outgrowth and patterning of the limb. Cell *75*, 579-587.

Nord, A.S., Blow, M.J., Attanasio, C., Akiyama, J.A., Holt, A., Hosseini, R., Phouanenavong, S., Plajzer-Frick, I., Shoukry, M., Afzal, V., Rubenstein, J.L., Rubin, E.M., Pennacchio, L.A., Visel, A. (2013). Rapid and pervasive changes in genome-wide enhancer usage during mammalian development. Cell *155*, 1521-1531.

Ohuchi, H., Nakagawa, T., Yamamoto, A., Araga, A., Ohata, T., Ishimaru, Y., Yoshioka, H., Kuwana, T., Nohno, T., Yamasaki, M., Itoh, N., Noji, S. (1997). The mesenchymal factor, FGF10, initiates and maintains the outgrowth of the chick limb bud through interaction with FGF8, an apical ectodermal factor. Development *124*, 2235-2244.

Osebold, W.R., Remondini, D.J., Lester, E.L., Spranger, J.W., Opitz, J.M. (1985). An autosomal dominant syndrome of short stature with mesomelic shortness of limbs, abnormal carpal and tarsal bones, hypoplastic middle phalanges, and bipartite calcanei. Am. J. Med. Genet. *22*, 791-809.

Pepinsky, R.B., Zeng, C., Wen, D., Rayhorn, P., Baker, D.P., Williams, K.P., Bixler, S.A., Ambrose, C.M., Garber, E.A., Miatkowski, K., Taylor, F.R., Wang, E.A., Galdes,

A. (1998). Identification of a palmitic acid-modified form of human Sonic hedgehog. J. Biol. Chem. *273*, 14037-14045.

Piussan, C., Lenaerts, C., Mathieu, M., Boudailliez, B. (1983). Dominance reguliere d'une ankylose des pouces avec retard mental se transmettant sur trois generations. J. Genet. Hum. *31*, 107-114.

Porter, J.A., Young, K.E., Beachy, P.A. (1996). Cholesterol modification of hedgehog signalling proteins in animal development. Science *274*, 255-259.

Pownall, M.E., and Isaacs, H.V. (2010), FGF Signaling in Vertebrate Development. (San Rafael, CA, Morgan & Claypool Life Sciences), pp 1-75.

Poznanski, A.K., Garn, S.M., Nagy, J.M., Gall, J.C. Jr. (1972). Metacarpophalangeal pattern profiles in the evaluation of skeletal malformations. Radiology *104*, 1-11.

Rabbani, B., Mahdieh, N., Hosomichi, K., Nakaoka, H., Inoue, I. (2012). Next-generation sequencing: impact of exome sequencing in characterizing Mendelian disorders. J Hum Genet. *57*, 621-632.

Rabinowitz, A.H., and Vokes, S.A. (2012). Integration of the transcriptional networks regulating limb morphogenesis. Dev. Biol. *368*, 165-180.

Raff, M.L., Leppig, K.A., Rutledge, J.C., Weinberger, E., Pagon, R.A. (1998). Brachydactyly type A1 with abnormal menisci and scoliosis in three generations. Clin. Dysmorphol. *7*, 29-34.

Retting, K.N., Song, B., Yoon, B.S., Lyons, K.M. (2009). BMP canonical Smad signaling through Smad1 and Smad5 is required for endochondral bone formation. Development *136*, 1093-1104.

Rodrigues, R.G. (2007). Aplasia cutis congenita, congenital heart lesions, and frontonasal cysts in four successive generations. Clin. Genet. *71*, 558-60.

Ryan, K.E. and Chiang, C. (2012). Hedgehog secretion and signal transduction in vertebrates. J. Biol. Chem. *287*, 17905-17913.

Sandelin, A., Bailey, P., Bruce, S., Engström, P.G., Klos, J.M., Wasserman, W.W., Ericson, J., Lenhard, B. (2004). Arrays of ultraconserved non-coding regions span the loci of key developmental genes in vertebrate genomes. BMC Genomics *5*, 99.

Saunders, J.W. Jr. (1948). The proximo-distal sequence of origin of the parts of the chick wing and the role of the ectoderm. J. Exp. Zool. *108*, 363-403.

Seki, K. and Hata, A. (2004). Indian hedgehog gene is a target of the bone morphogenetic protein signaling pathway. J. Biol. Chem. *279*, 18544-18549.

Sekine, K., Ohuchi, H., Fujiwara, M., Yamasaki, M., Yoshizawa, T., Sato, T., Yagishita, N., Matsui, D., Koga, Y., Itoh, N., Kato, S. (1999). Fgf10 is essential for limb and lung formation. Nat. Genet. *21*, 138-141.

Sillence, D.O. (1978). Brachydactyly, distal symphalangism, scoliosis, tall stature, and club feet: a new syndrome. J. Med. Genet. *15*, 208-11.

Sillence, D., Spranger, J., Unger, S., Zabel, B., Superti-Furga, A. (2011). Nosology and classification of genetic skeletal disorders: 2010 revision. Am. J. Med. Genet. A *155A*, 943-968.

Slavotinek, A. and Donnai, D. (1998). A boy with severe manifestations of type A1 brachydactyly. Clin. Dysmorphol. *7*, 21-27.

Solomon, L.A., Russell, B.A., Watson, L.A., Beier, F, Bérubé, N.G. (2013). Targeted loss of the ATR-X syndrome protein in the limb mesenchyme of mice causes brachydactyly. Hum. Mol. Genet. *22*, 5015-5025.

St-Jacques, B., Hammerschmidt, M., McMahon, A.P. (1999). Indian hedgehog signaling regulates proliferation and differentiation of chondrocytes and is essential for bone formation. Genes Dev. *13*, 2072-2086.

Stricker, S. and Mundlos, S. (2011). Mechanisms of digit formation: Human malformation syndromes tell the story. Dev. Dyn. *240*, 990-1004.

Sugiura, Y., Tajima, Y., Suguira, I., Muaramoto, K., Wu, W.D. (1962). Abnormalities of musculo-skeletal system observed in Shizuoka school children. Jpn. J. Hum. Genet. *7*, 10-9.

Summerbell, D., and Wolpert, L. (1973). Precision of development in chick limb morphogenesis. Nature *244*, 228-230.

Sun, X., Mariani, F.V., Martin, G.R. (2002). Functions of FGF signaling from the apical ectodermal ridge in limb development. Nature *418*, 501-508.

Suzuki, T., Hasso, S.M., Fallon, J.F. (2008). Unique SMAD1/5/8 activity at the phalanx-forming region determines digit identity. Proc. Natl. Acad. Sci. USA *105*, 4185-4190.

Suzuki, T. (2013). How is digit identity determined during limb development? Dev. Growth Differ. *55*, 130-138.

Tamura, N., Doolittle, L.K., Hammer, R.E., Shelton, J.M., Richardson, J.A., Garbers, D.L. (2004). Critical roles of the guanylyl cyclase B receptor in endochondral ossification and development of female reproductive organs. Proc. Natl. Acad. Sci. USA *101*, 17300-17305.

Temtamy, S.A., and McKusick, V.A. (1978). The Genetics of Hand Malformations. (New York, Daniel Bergsma Publisher), pp 1-619.

Temtamy, S.A., and Aglan, M.S. (2008). Brachydactyly. Orphanet J. Rare Dis. *3*, 15.
te Welscher, P., Zuniga, A., Kuijper, S., Drenth, T., Goedemans, H.J., Meijlink, F., Zeller, R. (2002). Progression of vertebrate limb development through SHH-mediated counteraction of GLI3. Science *298*, 827-830.

Tickle, C., Summerbell, D., Wolpert, L. (1975). Positional signaling and specification of digits in chick limb morphogenesis. Nature *254*, 199-202.

Tickle, C., and Wolpert, L. (2002). The progress zone -- alive or dead? Nat. Cell Biol. *4*, E216-E217.

Tickle, C. (2006). Making digit patterns in the vertebrate limb. Nat. Rev. Mol. Cell Biol. *7*, 45-53.

Towers, M., Mahood, R., Yin, Y., Tickle, C. (2008). Integration of growth and specification in chick wing digit-patterning. Nature *452*, 882-886.

Tsukahara, M., Azuno, Y., Kajii, T. (1989). Type A1 brachydactyly, dwarfism, ptosis, mixed partial hearing loss, microcephaly, and mental retardation. Am. J. Med. Genet. *33*, 7-9.

Vortkamp, A., Lee, K., Lanske, B., Segre, G.V., Kronenberg, H.M., Tabin, C.J. (1996). Regulation of rate of cartilage differentiation by Indian hedgehog and PTH-related protein. Science *273*, 613-622.

Warman, M.L., Cormier-Daire, V., Hall, C., Krakow, D., Lachman, R., LeMerrer, M., Mortier, G., Mundlos, S., Nishimura, G., Rimoin, D.L., Robertson, S., Savarirayan, R., Sillence, D., Spranger, J., Unger, S., Zabel, B., Superti-Furga, A. (2011). Nosology and classification of genetic skeletal disorders: 2010 revision. Am. J. Med. Genet. A *155A*, 943-968.

Williams, K.D., Blangero, J., Cottom, C.R., Lawrence, S., Choh, A.C., Czerwinski, S.A., Lee, M., Duren, D.L., Sherwood, R.J., Dyer, T.D., Jha, B., Subedi, J., Williams-Blangero, S., Towne, B. (2007). Heritability of brachydactyly type A3 in children, adolescents, and young adults from an endogamous population in eastern Nepal. Hum. Biol. *79*, 609-622.

Witte, F., Dokas, J., Neuendorf, F., Mundlos, S., Stricker, S. (2009). Comprehensive expression analysis of all Wnt genes and their major secreted antagonists during mouse limb development and cartilage differentiation. Gene Expr. Patterns *9*, 215-223.

Witte, F., Chan, D., Economides, A.N., Mundlos, S., Stricker, S. (2010). Receptor tyrosine kinase-like orphan receptor 2 (ROR2) and Indian hedgehog regulate digit

outgrowth mediated by the phalanx-forming region. Proc. Natl. Acad. Sci. USA *107*, 14211-14216.

Woods, A., Khan, S., Beier, F. (2007). C-type natriuretic peptide regulates cellular condensation and glycosaminoglycan synthesis during chondrogenesis. Endocrinology *148*, 5030-5041.

Xu, B., Hrycaj, S.M., McIntyre, D.C., Baker, N.C., Takeuchi, J.K., Jeannotte, L., Gaber, Z.B., Novitch, B.G., Wellik, D.M. (2013). Hox5 interacts with Plzf to restrict Shh expression in the developing forelimb. Proc. Natl. Acad. Sci. USA *110*, 19438-19443.

Yang, X., She, C., Guo, J., Yu, A.C., Lu, Y., Shi, X., Feng, G., He, L. (2000). A locus for brachydactyly type A-1 maps to chromosome 2q35-q36. Am. J. Hum. Genet. *66*, 892-903.

Yasoda, A., Komatsu, Y., Chusho, H., Miyazawa, T., Ozasa, A., Miura, M., Kurihara, T., Rogi, T., Tanaka, S., Suda, M., Tamura, N., Ogawa, Y., Nakao, K. (2004). Overexpression of CNP in chondrocytes rescues achondroplasia through a MAPK-dependent pathway. Nat. Med. *10*, 80-86.

Yoon, B.S., Pogue, R., Ovchinnikov, D.A., Yoshii, I., Mishina, Y., Behringer, R.R., Lyons, K.M. (2006). BMPs regulate multiple aspects of growth-plate chondrogenesis through opposing actions on FGF pathways. Development *133*, 4667-4678.

Yuksel-Apak, M., Bögershausen, N., Pawlik, B., Li, Y., Apak, S., Uyguner, O., Milz, E., Nürnberg, G., Karaman, B., Gülgören, A., Grzeschik, K.H., Nürnberg, P., Kayserili, H., Wollnik, B. (2012). A large duplication involving the IHH locus mimics acrocallosal syndrome. Eur. J. Hum. Genet. *20*, 639-644.

Zhang, Z., Verheyden, J.M., Hassell, J.A., Sun, X. (2009). FGF-regulated Etv genes are essential for repressing Shh expression in mouse limb buds. Dev. Cell *16*, 607-613.

Zhu, G., Ke, X., Liu, Q., Li, J., Chen, B., Shao, C., Gong, Y. (2007). Recurrence of the D100N mutation in a Chinese family with brachydactyly type A1: evidence for a mutational hot spot in the Indian hedgehog gene. Am. J. Med. Genet. A *143A*, 1246-1248.

Contribution of Collaborators

My contributions for Chapters 3, 4, 5 and 6, which are fully acknowledged by my PhD supervisor Dr. Dennis E. Bulman, are mentioned at the preface of each chapter.

Dr. Sarah M. Nikkel (Children's Hospital of Eastern Ontario) performed patient examinations, MCPPs, and skin punctures.

Ashley Byrnes (MSc. student, University of Ottawa) is a co-author of the published manuscripts inserted in Chapters 3 and 4. She performed the screening of BDA1-families for mutations in *IHH* and *NOG*. She also performed the linkage analyses described in Chapter 4.

Allison Grimsey (MSc. student, University of Ottawa) helped sequence *IHH* in Chapter 3 and refined the *BDA1B* critical region in Chapter 6.

Ruobing Zou (Children's Hospital of Eastern Ontario) performed PCR and sequencing of control samples in Chapter 6, and the genotyping of families in Chapter 4.

Kelly Westaff (Ottawa Hospital Research Institute) performed the genotyping of families in Chapter 4.

Dr. Fengxia Xiao (Ottawa Hospital Research Institute) performed the site-directed mutagenesis of *GDF5* in Chapter 4.

Heather MacDonald (Ottawa Hospital Research Institute) helped construct the *GDF5* expression vector in Chapter 4.

Dr. Michael Underhill (University of British Columbia) performed chondrogenic assays on GDF5 in Chapter 4.

Dr. Len Pennacchio (Joint Genome Institute) performed the *in-vivo* transgenic reporter assay in Chapter 6.

Yves De Repentigny and Dr. Rashmi Kothary (Ottawa Hospital Research Institute) performed light microscopy and cryosectioning on the transgenic embryos in Chapter 6.

Llyold Ma and Brendan Zhao (summer students, Ottawa Hospital Research Institute) optimized PCRs for reporter inserts in Chapter 6.

Armin Yazdani (summer students, Ottawa Hospital Research Institute) optimized PCRs in Chapter 6 and updated our in-house sequence variant database in Appendix C.

Dr. Elizabeth McCready (McMaster University) refined the *BDA1B* critical region in Chapter 6.

Dr. Alexa Kidd (Central and Southern Regional Genetics Services, Wellington Hospital, Wellington, New Zealand); Dr. Hope Northrup (Shriners Hospital for Children, Houston, Texas); Dr. Louanne Hudgins (Stanford University Medical Center, Palo Alto, California); Prof. Yuval Yaron (Tel Aviv Sourasky Medical Center, Tel Aviv, Israel); Dr. Yu Lung (The University of Hong Kong's Queen Mary Hospital in Hong Kong); Dr. Elizabeth Rosser (Clinical Genetics Unit, Great Ormond Street Hospital for Children NHS Trust, London, UK); Drs. Judith Allanson and Christine Armour (Children's Hospital of Eastern Ontario) performed patient examinations and diagnosis.

Permission to Reproduce Material

JOHN WILEY AND SONS LICENSE
TERMS AND CONDITIONS
Aug 18, 2014

This is a License Agreement between Lemuel Racacho ("You") and John Wiley and Sons ("John Wiley and Sons") provided by Copyright Clearance Center ("CCC"). The license consists of your order details, the terms and conditions provided by John Wiley and Sons, and the payment terms and conditions.

All payments must be made in full to CCC. For payment instructions, please see information listed at the bottom of this form.

License Number	3398931302217
License date	May 30, 2014
Licensed content publisher	John Wiley and Sons
Licensed content publication	Human Mutation
Licensed content title	Mutations in GDF5 presenting as semidominant brachydactyly A1
Licensed copyright line	© 2010 Wiley-Liss, Inc.
Licensed content author	Ashley M. Byrnes,Lemuel Racacho,Sarah M. Nikkel,Fengxia Xiao,Heather MacDonald,T. Michael Underhill,Dennis E. Bulman
Licensed content date	Sep 7, 2010
Start page	1155
End page	1162
Type of use	Dissertation/Thesis
Requestor type	Author of this Wiley article
Format	Electronic
Portion	Full article
Will you be translating?	No
Title of your thesis / dissertation	Identifying the molecular pathways for brachydactyly type-A1
Expected completion date	Jun 2014
Expected size (number of pages)	250
Total	0.00 USD

BMJ PUBLISHING GROUP LTD. LICENSE
TERMS AND CONDITIONS

Sep 24, 2014

This is a License Agreement between Lemuel Racacho ("You") and BMJ Publishing Group Ltd. ("BMJ Publishing Group Ltd.") provided by Copyright Clearance Center ("CCC"). The license consists of your order details, the terms and conditions provided by BMJ Publishing Group Ltd., and the payment terms and conditions.

All payments must be made in full to CCC. For payment instructions, please see information listed at the bottom of this form.

License Number	3474831255704
License date	Sep 23, 2014
Licensed content publisher	BMJ Publishing Group Ltd.
Licensed content publication	Journal of Medical Genetics
Licensed content title	Clinical and radiological assessment of a family with mild brachydactyly type A1: the usefulness of metacarpophalangeal profiles
Licensed content author	C M Armour, D E Bulman, A G W Hunter
Licensed content date	Apr 1, 2000
Volume number	37
Issue number	4
Type of Use	Dissertation/Thesis
Requestor type	Individual
Format	Print and electronic
Portion	Figure/table/extract
Number of figure/table/extracts	2
Descriptionof figure/table/extracts	Figures 2 and 4
Will you be translating?	No
Circulation/distribution	10
Title of your thesis / dissertation	The Genetic Heterogeneity of Brachydactyly Type A1: Identifying the molecular pathways
Expected completion date	Oct 2014
Estimated size(pages)	230
BMJ VAT number	674738491
Billing Type	Invoice
Billing address	401 Smyth Rd. Ottawa, ON K1H8L1 Canada
Permissions Cost	0.00 GBP
VAT (0.00%)	0.00 GBP
Total	0.00 GBP

Appendix A

Patient information sheet

PATIENT INFORMATION SHEET

BRACHYDACTYLY STUDY

Below you will find a brief explanation of our study to identify the cause of Brachydactyly.

Brachydactyly type A1 (BDA-1) is a genetic disorder, which is inherited as an autosomal dominant trait. This means that an affected individual has a 50% chance of passing the disorder to their children. BDA-1 is a disorder in which one of the bones in the fingers and toes either fails to form properly or fuses to the adjacent bone. People with BDA-1 tend to be shorter on average. By studying BDA-1 we are learning about the key feature required to control bone growth. What we learn in this study may provide us with ways of treating a variety of bone disorders such as arthritis.

Our research involves the collection of a blood sample from individuals who have Brachydactyly and from other family members who may not be affected. This permits us to analyze the DNA for the presence of genes, which may confer susceptibility to this disorder. DNA is isolated from leukocytes (white blood cells), which comprise a very small fraction of total blood cells. If you are willing to participate, please sign the enclosed consent form to allow us to draw 40 ml of blood (eight teaspoons) as a one-time donation.

DNA analysis may yield information on paternity status in your family. You also agree to provide a family history to the best of your knowledge. All information derived from these studies will be confidential.

Your participation in this study is voluntary and you may refuse or withdraw consent at any time for any reason and that such action will not affect the quality of ongoing or future care. All personal information regarding your sample will be kept confidential and your name will not be used in any publication and only the overall statistical information may be published.

It is not uncommon for labs working on the same disease to share DNA samples. Should your DNA sample be shared with another lab, we will code the sample so that personal information will NOT be made available.

This protocol has been approved by the Ottawa Hospital Research Ethics Board. This committee considers the ethical aspects of all hospital research projects involving human subjects. If you wish, you may contact the Chairperson of the Committee.

Should you require more information or have any questions, please contact the principle investigator of the study, Dennis Bulman, Ph.D.

Patient consent form page 1

Children's Hospital of Eastern Ontario
Hôpital pour enfants de l'est de l'Ontario

A Study to Locate and Isolate the A1-Brachydactyly gene

Christine Armour, MD, Alasdair Hunter, MD Genetics PSU CHEO, Judith Allanson, MD Genetics PSU CHEO Sarah Nikkel, MD Genetics PSU CHEO, Dennis Bulman, Ph.D. Ottawa Health Research Institute.

I _____ understand that my/my spouse's family has been diagnosed as having a genetic (inherited) condition called **Type A1-Brachydactyly** (BDA-1). This condition is quite mild and results in certain fingers and toes being shorter than average, but they function normally. The inheritance of this condition is called autosomal dominant, which means that both males and females can be affected and that, on average, half the children born to a person with BDA-1 will also have BDA-1.

I understand that Drs. Alasdair Hunter, Judith Allanson and Sarah Nikkel of the Genetics PSU and CHEO, Dennis Bulman of the Ottawa Health Research Institute and Christine Armour, a Resident in Genetics are undertaking a project to try to find the gene that causes BDA-1. This first phase of the study will involve what is called "mapping". This allows the general location of the gene to be identified (mapped) to an area on one of the 22 different chromosomes, which may carry the gene. If we are successful, the next step will be to try to identify the actual gene. It is hoped that by finding these types of genes and understanding their function that we will learn more about the normal development of the hands as well as learn more about general bone growth.

I understand that if I am in the direct bloodline of the BDA-1 gene, that my participation will involve having an x-ray of my hands (if not already available), some simple clinical measurements, and a blood sample of about 30cc (2 tablespoons). The blood is required to isolate the genetic material (DNA). Children will be offered a local anesthetic cream (EMLA) prior to any blood sampling. If I am not in the direct blood line (i.e. a spouse) my participation is limited to a blood sample, which is needed to help with the mapping process for the family.

In agreeing to participate in the study I understand and accept that:

- This study will not be of direct benefit to me or my family.
- This is a research study and may not succeed in finding the BDA-1 gene. However, I will be provided with a summary of the progress and final results of the project.
- The data and any results from the study will be held in strict confidence and I/my family will not be identified in any presentation or publication arising from the project.
- My refusal to participate in the study would not in any way affect the care I/my family would receive at CHEO now or in the future.

Patient consent form page 2

- I may withdraw from the study at any time, even after I have agreed to participate, without prejudice to the care I/my family may receive at CHEO in the future. This includes asking to have my DNA sample destroyed.
- My DNA sample will not be used for any purpose, other than to look for the BDA-1 gene without my further specific written permission.
- If I wish information about the study I may contact Dr. Dennis Bulman in Ottawa
- If I have any further quesionts I may call Dr. Judith Allanson or Dr. Sarah Nikkel
- If I have questions about the ethical conduct of the study I may contact Dr. David Palframan, chair of the CHEO Research Ethics Committee . He is not in a position to discuss the scientific aspects of the study.

In signing this consent, I am indicating that I have had this study explained to my by _____ and that I have read this consent form. I agree that I understand the nature of the research project and the contents of the consent form, and I am willing to participate in the study, and/or have my child participate.

Name _____ Relationship to participant _____

Signature _____ Date _____

Witness _____ Signature _____ Date _____

Children who are old enough to have a basic understanding of their participation in the study should be asked to provide their written agreement/assent to participation. They should understand that they do not have to participate and will not be punished in any way if they do not. They should know that they will be measured by a doctor, they may have an x-ray of a hand and will have a blood sample taken; if they wish, using an anaesthetic cream.

Child providing assent _____ Signed _____ Date _____

Clinical evaluation form

Name _____ D.O.B. :_____Pedigree # _____

Address_____

Home # _____ Work # _____ Fax # _____

email _____

Height _____ Span _____ Lower segment_____ U/L ratio _____

Hand _____ Middle Finger _____ Foot _____

Hand description:

Foot description:

Major health concerns:

Blood Pressure: _____ Lymphedema _____

Arthritis : _____

Nystagmus/Eye : _____

Clinical opinion: ☐ affected ☐ unaffected ☐ unsure

☐ blood taken Xray : ☐ hands ☐ arm

☐ photo of hands ☐ feet ☐ pelvis

☐ consent ☐ shoulder ☐ other - specify: _____

☐ metacarpal -phalangeal profile
result : _____

Other / Notes:

Appendix B.

Appendix B Table 1. Primer sequences used for amplification and sequencing of genomic features within the *BDA1B* critical region during the early build of hg18.

Primer	Sequence
NPR3-32745045-F	GGCAGAATCATATCGCCATT
NPR3-32750497-R	GCCAGGTCACTGTTGGAAAT
NPR3-32745442-R	AGAGCCACTAACCAGGAGCA
NPR3-32745663-R	AAAGGCAAACTGGGGTTTCT
NPR3-32746017-R	GGAGAAGTCCGTGACCAGAG
NPR3-32746567-R	GTCAGGGAACAAGGACCAAG
NPR3-32746979-R	CTGTCCCTAACCACCACTCC
NPR3-32746921-F	GGCGATTTCAGCTTTAAGGA
NPR3-32747471-R	CGTCCTTCTCTGCAATGTCA
NPR3-32747336-F	TGTATAAACGGAGGGCGAAT
NPR3-32747852-R	CCGGGTGAGTGAAAACAAGT
NPR3-32747559-F	AGTGGGGAGGAAAGAGGAAG
NPR3-32748060-R	CTGCTGCATACTCGCACACT
NPR3-32748016-F	CCAAGCCAGACCTTATCCTG
NPR3-32748608-R	TGGGACCCTCTACGTACACC
NPR3-32748244-F	TGGTCTACAGCGACGACAAG
NPR3-32749049-R	TCGCCAGAATTCAGACACAC
NPR3-32748889-F	GCTCTTGGGGTTTCTCTGACT
NPR3-32749448-R	ATTGCACCACTCACATTCCA
NPR3-32749167-F	TTTTCTCCATGGGTCTTTGG
NPR3-32749713-R	TCAAACACCTCTCGCCTCTT
NPR3-32749613-F	AGTGGACAGAGAAGCCATCG
NPR3-32750179-R	TCCTCTGGTCTCACACATGC
SUB1-1f	TTTCCCTCAATCAGCAAAGG
SUB1-1r	GCAATGTTCATGACCACGTT
SUB1-2f	TGCAAAATGGAGCAGAAACA
SUB1-2r	CTTTTGCTCTCCCCATCTCA
SUB1-3f	GGCCCTTTAACGCATACAGA
SUB1-3r	GTGCAAGTTTGCAGAAAGCA
SUB1-4f	CAGCGTTTTATGACCTGGTG
SUB1-4r	TTGGCCGTATCACCAAAATA
SUB1-5f	TGGTGATACGGCCAAAAAGT
SUB1-5r	GGACAAGTTCCACGGTTCAT

Primer	Sequence
SUB1-6f	AGGAGTGTATGACATTTAGTTCATTG
SUB1-6r	CCGTACCTCCAGAAATACCC
SUB1-7f	GCTGCACCAAGTCATTTTGG
SUB1-7r	CCTTATGTGCAGAATAAACACCA
SUB1-8f	CCGTTATTTAGAAATTTACCAGATTTT
SUB1-1f	TTTCCCTCAATCAGCAAAGG
SUB1-1r	GCAATGTTCATGACCACGTT
SUB1-2f	TGCAAAATGGAGCAGAAACA
SUB1-2r	CTTTTGCTCTCCCCATCTCA
SUB1-3f	GGCCCTTTAACGCATACAGA
SUB1-3r	GTGCAAGTTTGCAGAAAGCA
SUB1-4f	CAGCGTTTTATGACCTGGTG
SUB1-4r	TTGGCCGTATCACCAAAATA
SUB1-5f	TGGTGATACGGCCAAAAAGT
SUB1-5r	GGACAAGTTCCACGGTTCAT
SUB1-6f	AGGAGTGTATGACATTTAGTTCATTG
SUB1-6r	CCGTACCTCCAGAAATACCC
SUB1-7f	GCTGCACCAAGTCATTTTGG
SUB1-7r	CCTTATGTGCAGAATAAACACCA
SUB1-8f	CCGTTATTTAGAAATTTACCAGATTTT
SUB1-8r	CACGACCAACTTATTCTATTTCTAGG
SUB1-9f	AGATGACAGCTGCACCGTA
SUB1-9r	GGGACAAACAAAAAGTTAGCTC
AK022112.1-Ex1-1F	TCCCAAGCCTCTTAGCATTG
AK022112.1-Ex1-1R	AAATATGGCATCGGCCACT
AK022112.1-Ex1-2F	ACCACTTGTTTGCTTCATGC
AK022112.1-Ex1-2R	TGTGAGATATGTCTTTCCAGTTTAAGA
AK022112.1-Ex1-3F	GCCAGTTCTTGTTTACTTCTCTGTTT
AK022112.1-Ex1-3R	TTCCAGCCTCACTTTCACTAA
AK022112.1-Ex1-4F	AGGTGATATGCTAAGTTCATTATTCA
AK022112.1-Ex1-4R	AGCTGGTTCCAATATTTGCC
AK022112.1-Ex1-5F	CCCGGGTATACTCTCTGAGG
AK022112.1-Ex1-5R	TCATATCCAGTCTTACTTTCCACA
AK022112.1-Ex1-6F	TTTAGCCTGATAGTTGACGGG
AK022112.1-Ex1-6R	ACCTGGGAGGTGGAAGTTAC
ENSG00000210286-F	CCTTGCCAGTCTGTCAGTGT
ENSG00000210286-R	CTTCACTCCATGAAATTTGTCC
ENSG00000210296-F	CCTGGAGACGGGTAGTGGT
ENSG00000210296-R	AGGTGATCTGCCTGCCTG
ENSG00000210290-F	CATCCTGGCTTTAGAATCAGC
ENSG00000210290-R	GCAATCGTTCCCTCTGAAGT
ENSG00000200065-F	TTAGGATCATGCCACTGCAC

Primer	Sequence
ENSG00000200065-R	TCCTATTGGATTATTCTTCTGTCA
ENSG00000199731-F	CCCAGCTTCAACACTTGCTT
ENSG00000199731-R	GAGTCCCTCTTAGGAACCTGTG
ENSG00000207052-F	TGCACTTCAACCAGGGTTCT
ENSG00000207052-R	GCCATTTTAACTGGGATGAGA
ENSG00000210335-F	ACCAAAGACAATGGGCAAAC
ENSG00000210335-R	CAGCTGATTCCTCAATAACAATTT
ENSG00000201623-F	CAAGGCATCTTTTTCCCTCA
ENSG00000201623-R	GAAAGGGATCTGAGAAATTCAA
28S-rRNA-related-F	TCAGAGGATTGGATGAGGTG
28S-rRNA-related-R	GCAGGGAAAGGTCAGAGAGA
BU171287-F	GTGCCCAGTATTTTCCTCCA
BU171287-R	CCCCAGGTCAGAGAACAAAA
AK127389-F	ACTGTGTTGCCATTGTGCAT
AK127389-R	TCGTTGTTCAACCACAAACA
AW268575-F	GGCAAAGATGCTTTTATTTCCTT
AW268575-R	TTTTCCAACTACCACATGGAGA
AF138859-1F	GCAATGGCTAAGCATTTCAG
AF138859-1R	AAGGCCTAACCCATCTGCTAC
AF138859-2F	CATCCGGCCTTATCTCACTG
AF138859-2R	GCACCCAGTTGTAGAGCAATATG
AF138859-3F	TGAACTAAGAAACTCATCCACATTC
AF138859-3R	CACAGCCCAGCTTCTCTCTC
AF138859-4F	CTCCTTGTTCATTCTGGAACAC
AF138859-4R	TCTGTAATGGCTTGACACTTAGC
AF138859-5F	TTGCATCATGGGTTGTGAAG
AF138859-5R	TGCAGTACCTGGTGTGTCATAAG
AF138859-6F	GGGTTACCCTTGCATAGAACATAG
AF138859-6R	TGGCGATAAGGTTTCAACAG
BU626326-F	AAGGTTCCTGTCTCCTACTCTCC
BU626326-R	CAACATAGAAGCCTATGTGACTTAAC
CF130386-F	TGAAGAATTGCATCGTGCTC
CF130386-R	AGGAGACTGCTGATTTTGGC
c5orf23-1F	TGGCAGAACAAATCATGAGG
c5orf23-1R	TGACCATAAGACAGACACTTATTTCC
c5orf23-2F	AAATCCAGGGTGTTCAGATTTC
c5orf23-2R	AGGGAGAAGTGAGGGCATTC
c5orf23-3F	AACCCATGTTTAATGGAGGG
c5orf23-3R	TCAGGATCTGAGTGCTTTGTG
c5orf23-4F	TTGGGAGATCAAATAGAGTATTATGC
c5orf23-4R	TAAAGACAGTGGCAATGGGC

Primer	Sequence
c5orf23-5F	AATCAATAATTTAGTGCCCCTTC
c5orf23-5R	ACAAACTCCAATCCAGCACC
c5orf23-6F	CCTGGCTTTGGTGTTCAGC
c5orf23-6R	CCGTGACAGCTTTGTTCTCC
c5orf23-7F	GCTTTGATTCATGTTTAAAGACC
c5orf23-7R	GACTCATGATAGATTTGTACTGTTTGG
c5orf23-8F	GACAGACCAATTCTGTGACCC
c5orf23-8R	GTCCCAGGAGAACAAAAGCC
C1QTNF 3'UTR-1F	AAGAGCTGGTTGTTCATGGC
C1QTNF 3'UTR-1R	TTTTAGGTGCCAAGGAAAGAG
C1QTNF 3'UTR-2F	TGTTGTTCACGCTACAGGTACAC
C1QTNF 3'UTR-2R	CAACCACATTACTGGTCAAGC
C1QTNF 3'UTR-3F	TTCAGCTTAGCCTTTGACCC
C1QTNF 3'UTR-3R	TGGCTGTTCACATCATCTGC
C1QTNF 3'UTR-4F	GAGCAATATATGGAAATAAACACACC
C1QTNF 3'UTR-4R	TGGGACACTTGTGAAATCAG
C1QTNF 3'UTR-5F	AACAAGTCCCAGGTGTGTGG
C1QTNF 3'UTR-5R	TTTGGAAGACCGAGGCAG
C1QTNF 3'UTR-6F	CCCACCACCAGGACCAG
C1QTNF 3'UTR-6R	TGCCTGGAATAGCACAGTATC
C1QTNF 3'UTR-7F	TTGTATCATGAATAAAAGCTGAAGTC
C1QTNF 3'UTR-7R	GCCATAAATACATGCAGGAAAAG
C1QTNF 3'UTR-8F	CAGAGACAATTTCTTGCTTTGG
C1QTNF 3'UTR-8R	TCCTTTTGAATAAAGTCCCTCC

Appendix C.

A catalogue of sequence variants identified within the *BDA1B* critical region (chr5p13.3) prior to HTS.

Background: Prior to my involvement with the *BDA1B* project, all of the protein coding genes annotated through UCSC reference builds hg16 and hg17 were sequenced in several members of Family-1 and unaffected individuals by previous graduate students. The sequencing also focused on exons derived from ESTs and hypothetical genes. Despite the identification of several "novel" sequence variants during the early years of the project, all of them were eventually discounted as causal since they were either not identified in related affected members or were observed in unaffected individuals.

Rationale: A catalogue of sequence variants dedicated to the *BDA1B* critical region was created out of necessity to: 1) Catalogue all sequenced areas, 2) Prevent resequencing of a variant and 3) Limit the number of novel sequence variants when the time came to perform HTS on the targeted locus.

Design: Migrate all sequence variants, which were identified over the course of 10 years prior to my characterization of the *BDA1B* critical region, into a central laboratory spreadsheet. MS Excel spreadsheet was used to perform this task as this was a familiar and easily accessible utility within our laboratory. Variants were annotated with current genomic coordinates via LiftOver (UCSC Genome Browser Tools) and binned into categories reflecting the type of change and any associated genome feature. Intersection of genomic coordinates was performed using the VLOOKUP syntax.

Results: A total of 55 sequence variants, which were not reported in the public databases as of June 2006, were identified in only one sequenced BDA1-affected individual. These

variants were also not found in our unaffected controls. As of February 12, 2015, 37 of the 55 variants were present in dbSNP142. After the targeted resequencing of the *BDA1B* locus in two related and affected individuals from Family-1 (P1-06 and P1-64), we did not observe any sharing of their novel sequence variants with the remaining 18 in our chr5p13.3 catalogue (see Table below). Since these variants were not shared between BDA1-affected family members and therefore not in linkage disequilibrium with the affected haplotype in Family-1, we concluded that they are not causal.

Appendix C Table 1. Catalogue of novel sequence variants identified before targeted resequencing of the *BDA1B* locus. UCSC LiftOver tool was used to convert genome coordinates. The last column indicates if the reported variant was observed in both aligned HTS reads of P1-06 and P1-64.

EST or mRNA	UCSC Gene	Feature	Genome change	hg18 coordinates	hg19 coordinates	cDNA	Protein	Prediction	Sharing with P1-06 and P1-64
BC057283	*PDZD2*	intron	T>A	chr5:31896332-31896332	chr5:31860575-31860575				not shared
BC057283	*PDZD2*	intron	T insertion	chr5:31895999-31896000	chr5:31860242-31860243				not shared
BX648242	*PDZD2*	intron	C>T	chr5:32088924-32088924	chr5:32053167-32053167				not shared
AK128686 AK309794	*PDZD2*	intron	A>T	chr5:32136755-32136755	chr5:32100998-32100998				not shared
BC032023	*PDZD2*	intron	C>A	chr5:32143238-32143238	chr5:32107481-32107481				not shared
	PDZD2	3'UTR	A>T	chr5:32144629-32144629	chr5:32108872-32108872				not shared
	MTMR12	intron	G>A	chr5:32284021-32284021	chr5:32248264-32248264				not shared
	SUB1	5'UTR	C>T	chr5:32621472-32621472	chr5:32585715-32585715				not shared
BC044935	*LOC340113*	exon	C>T	chr5:32997301-32997301	chr5:32961544-32961544				not shared
	TARS	intron	A>G	chr5:33489124-33489124	chr5:33453367-33453367				not shared
	ADAMTS12	exon	C>G	chr5:33581943-33581943	chr5:33546186-33546186	c.4424G>C	p.W1425S	damaging	not shared
	ADAMTS12	exon	C>A	chr5:33581967-33581967	chr5:33546210-33546210	c.4400G>T	p.C1467F	damaging	not shared
	ADAMTS12	intron	T>C	chr5:33624691-33624691	chr5:33588934-33588934				not shared
	RXFP3	5'UTR	T>C	chr5:33972477-33972477	chr5:33936720-33936720				not shared
	C1QTNF3	intron	G>C	chr5:34100192-34100192	chr5:34064435-34064435				not shared
	C1QTNF3	intron	G>T	chr5:34100182-34100182	chr5:34064425-34064425				not shared
BF892342 DB446659 BM475197 AA584640 AW081720 AA846941 AI673003 BF850793 BF738763			A>G	chr5:34225254-34225254	chr5:34189497-34189497				not shared
	RAI14	intron	T>G	chr5:34793243-34793243	chr5:34757486-34757486				not shared

Curriculum Vitae

Lemuel Jean Racacho

EDUCATION

University of Ottawa, Ottawa, ON, Canada
Doctor of Philosophy, in progress
Department of Biochemistry (Specialization in Human and Molecular Genetics)
Dissertation: The genetic heterogeneity of brachydactyly type A1: Identifying the molecular pathways.
Supervisor: Dr. Dennis E. Bulman

- Identified and characterized an intergenic microduplication as a cause for BDA1 by next-generation sequencing of the targeted *BDA1B* locus.
- Identified two novel mutations in *BMPR1B* which are associated with BDA1, thus supporting the role of the BMP-SMAD pathway in phalangeal development.
- Collaborated in the mutation screening of *IHH* and *GDF5* in our BDA1 cohort.

University of Ottawa, Ottawa, ON, Canada
Master of Science, 2007-2009 (transfer to PhD)
Department of Biochemistry (Specialization in Human and Molecular Genetics)
Supervisor: Dr. Dennis E. Bulman

University of Western Ontario, London, ON, Canada
Bachelor of Science, Biology, 1991

CÉGEP Marianopolis College, Montréal, QC, Canada
D.E.C. Health Sciences, 1988

TEACHING EXPERIENCE

Canadian Gene Cure Foundation "Gene Researcher for a Week"
Co-supervisor, 2002-2011

Ottawa high school co-op students (Hillcrest H.S., Lisgar Collegiate, Rideau H.S.)
Supervisor, 2011-2013
Co-supervisor, 1998-2011

University of Ottawa, Ottawa, ON, Canada
Department of Epidemiology and Community Medicine, 2005

- Taught one day introductory course on genetic databases to clinicians and graduate students.

WORK EXPERIENCE

Bioinformatics collaborator, 2012-present
Regenerative Medicine Program, Ottawa Hospital Research Insitute, Ottawa, ON
Drs. David J. Picketts, Michael Huh and Matias Saavreda-Alvarez

- RNA-seq and ChIP-seq set-up, analyses and interpretation for Atrx and Snf2h data using bioinformatics tools deposited at Galaxy, Cistrome, and Bioconductor.
- Performed Atrx ChIP on mouse myoblasts, Covaris sonication of ChIP samples, and Western detection of Atrx.
- Analyzed mouse Affymetrix gene expression data using MEV and gene ontology by gProfiler and DAVID.

Laboratory Manager and Senior Research Technician, 1997-2007
Regnerative Medicine Program, OHRI, Ottawa, ON
Supervisor: Dr. Dennis E. Bulman

- Performed daily laboratory operations including purchasing, managing personnel, creating SOPs and the training of students and technicians.
- Maintained and operated denaturing high performance liguid chromotography, Biomek FX automated workstation, AB 3130*xl* Genetic Analyzer and Li-Cor sequencers.

Manager, 1997-2008
GE Amersham biobar, OHRI, Ottawa, ON

- Provided onsite products and services on behalf of GE Amersham.
- Reported to regional sales manager, Mr. Marc Rispler.

Manager, 2002-2008
Sigma-Aldrich biobar, OHRI, Ottawa, ON

- Provided onsite products and services on behalf of Sigma-Aldrich.
- Reported to regional sales manager, Dr. Tanya Trepanier.

Junior Laboratory Technician, 1994-1997
Department of Clinical Neurological Sciences, University Hospital, London, ON
Supervisor: Dr George C. Ebers

- Genotyping of sib-pairs for multiple sclerosis linkage study by radiolabeled probe hybridization.

PROFESSIONAL DEVELOPMENT

Stemgent, LaJolla, CA, USA
iPSCs Training Course and Workshop, 2010

- Theory and laboratory training on reprogramming human dermal fibroblasts into induced pluripotent stem cells using lentiviral KOSM.

Human Genome Variation Society
LOVD Training Course - Bethesda, MD, USA, 2010

- Training on the annotation and curation of genes using the Leiden Open Variation Database platform.

Ottawa Hospital, Ottawa, ON
Clinical Research Training Course, 2005

- Introductory course on biostatistics, epidemiology, clinical equipoise, and clinical trial design.

Canadian Genetic Diseases Network (Canadian Bioinformatics Workshop)
Certificate in Bioinformatics (Genomics & Proteomics), 2002

- Accredited at the universities of British Columbia, New Brunswick and Toronto.

INVITED PRESENTATIONS

Targeted genomic enrichment and next-generation sequencing of an autosomal Dominant bone disorder. 2010 *Invited Speaker*. 2nd Annual Children's Hospital of Eastern Ontario Genetics Research Day, Ottawa, ON

Linkage analysis of Parkinsonian trait in a Canadian family - Evaluation of new data. 2005 *Invited Speaker*. UOttawa Parkinson Consortium, OHRI, Ottawa, ON

Genetic heterogeneity in febrile convulsions. 1997 *Platform Session*. Canadian Congress of Neurological Sciences, London, ON

PEER REVIEWED PUBLICATIONS

Racacho L, Nikkel SM, MacKenzie J, Armour CM, McCready ME, De Repentigny Y, Kothary R, Pennacchio LA, Bulman DE. An intergenic 9.5 kb duplication at chromosome 5p13.3 as a cause of BDA1. (*Submitted*).

Racacho L, Byrnes AM, MacDonald H, Dranse HJ, Nikkel SM, Allanson J, Rosser E, Underhill TM, Bulman DE Two novel disease causing variants in BMPR1B are associated with brachydactyly type A1. Eur J Hum Genet. 2015 (*in press*).

Lahiry P, **Racacho L**, Wang J, Robinson J, Gloor GB, Rupar CA, Siu VM, Bulman DE, Hegele RA. A mutation in the serine protease TMPRSS4 in a novel pediatric neurodegenerative disorder. Orphanet J Rare Dis. 2013 Aug 17;8(1):126.

Shi G, Lee J, Grimes D, **Racacho L**, Ye D, Yang H, Ross O, Farrer M, McQuibban A, Bulman D. Functional alteration of PARL contributes to mitochondrial dysregulation in Parkinson's disease. Hum Mol Genet. 2011 May 15;20(10):1966-74.

Byrnes AM, **Racacho L**, Nikkel SM, Xiao F, MacDonald H, Underhill TM, Bulman DE. Mutations in GDF5 presenting as semidominant brachydactyly A1. Hum Mutat. 2010 Oct;31(10):1155-62.

Byrnes AM, **Racacho L**, Grimsey A, Hudgins L, Kwan AC, Sangalli M, Kidd A, YaronY, Lau YL, Nikkel SM, Bulman DE. Brachydactyly A-1 mutations restricted to the central region of the N-terminal active fragment of Indian Hedgehog. Eur J Hum Genet. 2009 Sep;17(9):1112-20.

Han F, **Racacho L**, Yang H, Read T, Suchowersky O, Lang AE, Grimes DA, Bulman DE. Large deletions account for an increasing number of mutations in SGCE. Mov Disord. 2008 Feb 15;23(3):456-60.

Grimes DA, **Racacho L**, Han F, Panisset M, Bulman DE. LRRK2 screening in a Canadian Parkinson's disease cohort. Can J Neurol Sci. 2007 Aug;34(3):336-8.

Han F, **Racacho L**, Lang AE, Bulman DE, Grimes DA. Refinement of the DYT15 locus in myoclonus dystonia. Mov Disord. 2007 Apr 30;22(6):888-92.

Grimes DA, Han F, Panisset M, **Racacho L**, Xiao F, Zou R, Westaff K, Bulman DE. Translated mutation in the Nurr1 gene as a cause for Parkinson's disease. Mov Disord. 2006 Jul;21(7):906-9.

Huang XS, Yin JG, Wei JK, Gu RJ, Lu H, Wei H, Huang SJ, Jia FJ, Le C, Huo WH, **Racacho L**, Wang JQ, Guo XP, Bulman D. Linkage mapping of the generalized epilepsy with febrile seizures plus gene. Chin J Neurol. 2005 38;4:239-42.

Huang XS, Yin JG, Wei JK, Gu RJ, LU H, Wei H, Huang SJ, Jia FJ, Li C, Huo WH, **Racacho L**, Wang JQ, Guo XP, Bulman D. Mapping generalized epilepsies with febrile seizures plus gene and sequencing analysis GABRA6 gene. J App Clin Ped. 2004 8:676-9.

Han F, Lang AE, **Racacho L**, Bulman DE, Grimes DA. Mutations in the epsilon-sarcoglycan gene found to be uncommon in seven myoclonus-dystonia families. Neurology. 2003 Jul 22;61(2):244-6.

Grimes DA, Grimes JD, **Racacho L**, Scoggan KA, Han F, Schwarz BA, Woulfe J, Bulman D. Large French-Canadian family with Lewy body parkinsonism: exclusion of known loci. Mov Disord. 2002 Nov;17(6):1205-12.

Grimes DA, Han F, Lang AE, St George-Hyssop P, **Racacho L**, Bulman DE. A novel locus for inherited myoclonus-dystonia on 18p11. Neurology. 2002 Oct; 22;59(8):1183-6.

McCready ME, Sweeney E, Fryer AE, Donnai D, Baig A, **Racacho L**, Warman ML, Hunter AG, Bulman DE. A novel mutation in the IHH gene causes brachydactyly type A1: A 95-year-old mystery resolved. Hum Genet. 2002 Oct;111(4-5):368-75.

Racacho LJ, McLachlan RS, Ebers GC, Maher J, Bulman DE. Evidence favoring genetic heterogeneity for febrile convulsions. Epilepsia. 2000 Feb;41(2):132-9.

PUBLISHED ABSTRACTS

Racacho L, Nikkel SM, MacKenzie J, Armour CM, McCready ME, De Repentigny Y, Kothary R, Pennacchio LA, Bulman DE. An intergenic 9.4 kb microduplication at chromosome 5p13 as a cause of BDA1B. Program # 2987M. 64th Annual Meeting of American Society of Human Genetics, October 20, 2014, San Diego, CA.

Racacho L, Nikkel SM, MacKenzie J, Hunter A, Bulman DE. Targeted genomic enrichment of an autosomal dominant trait linked to chromosome 5p13. 60th Annual Meeting of American Society of Human Genetics, November 2-6 2010, Washington, D.C.

Huang L, **Racacho L**, McDonnell L, Douglas S, Bulman DE, Boycott KM. Application of exome resequencing with targeted analysis for autosomal dominant disorders with positional information. 60th Annual Meeting of American Society of Human Genetics, November 2-6, 2010, Washington, D.C.

Racacho L and Bulman D.E. Identifying a novel gene for brachydactyly type A1. 2010 3rd Annual Canadian Human Genetics Conference, St. Sauveur, Québec.

Bulman DE, **Racacho L**, Byrnes AM, Dranse H, Underhill TM, Allanson J,Nikkel SM. Mutations in GDF5 and in its receptor BMPR1B cause Brachydactyly Type A1. Platform Session 49. 58th Annual Meeting of American Society of Human Genetics, October 20-24, 2009, Honolulu, HI.

Grimes DA, Bulman DE, Kock N, **Racacho L**, Woulfe J. Clinical and pathologic findings in a parkinsonism family. 2009 Mov Disord 24:S402-S403 Suppl. 1.

Racacho L, Byrnes A, Nikkel SA, MacKenzie J, Bulman DE. A1620. Identifying novel genes for brachydactyly type A-1. 57th Annual Meeting of American Society of Human Genetics, November 11-15, 2008 Philadelphia, PA.

Racacho L, Grimes DA, Han F, Panniset M, Bulman DE. A1852. LRRK2 screening in a Canadian Parkinson's disease cohort. 56th Annual Meeting of American Society of Human Genetics, October 23-27, 2007, San Diego, CA.

Han F, Bulman DE, **Racacho L**, Grimes DA. Sequencing of the candidate gene LAMA1 in DYT15 Locus for myoclonus-dystonia. 2005 Can J Neurol Sci. 32 Suppl. 1.

Badhwar A, **Racacho L**, Dagostino D, Dubeau F, Andermann F, Bulman D, Andermann E. Absence of LGI1 mutations in familial mesial temporal lobe epilepsy with or without auditory features and in sporadic temporal lobe epilepsy with auditory features. 2004 Neurology 62:7 Suppl. 5 A252.

Badhwar A, **Racacho L**, Kobayashi E, D'Agositino D, Dubeau F, Andermann F, Bulman D, Andermann E. Familial mesial and lateral temporal lobe epilepsies: Is there a common genetic link? 2004 Epilepsia 45 Suppl. 7:219.

Badhwar, A, **Racacho L**, Kobayashi E, D'Agostino D, Dubeau F, Andermann F, Bulman D, Andermann E. Absence of LGI1 mutations in familial mesial temporal lobe epilepsy patients with or without auditory hallucinations. 2004 Ann Neurol. 56 Suppl. 8:S23.

Grimes DA, Han F, Panisset M, **Racacho L**, Xiao F, Bulman DE. A novel mutation in the Nurr1 gene in Parkinson's disease. 2004 Mov Disord. 19:9;1120.

Badhwar A, **Racacho L**, D'Agostino D, Dubeau F, Andermann F, Bulman D, Andermann E. Non-alliec genetic heterogeneity in autosomal dominant lateral temporal lobe epilepsy and absence of LGI1 mutation in familial mesial temporal lobe epilepsy. 2003 Am J Hum Genet. 73:5;510 A1995.

Badhwar A, **Racacho L**, D'Agostino D, Dubeau F, Andermann F, Bulman D, Andermann E. Absence of mutations in LGI1 in patients with familial mesial temporal lobe epilepsy. 2003 Epilepsia 44 Suppl. 8; 170.

Scoggan KA, Grimes DA, Grimes JD, **Racacho L**, Han F, Schwarz BA, Woulfe J, Bulman DE. Exclusion of genetic linkage to known loci in a large French Canadian family with Lewy body parkinsonism. 2001 Am J Hum Genet. 69 Suppl. 4; 513.

Grimes DA, Bulman, DE, **Racacho L**, Lang AE, St. George-Hyslop P. Inherited myoclonus-dystonia: Results from a 25 cM genome scan. 2000 Can J Neurol Sci. 27 Suppl. 2; S17.

McLachlan RS, **Racacho LJ**, Maher J, Ebers GC, Bulman DE. Exclusion of the familial febrile convulsions locus at 8q13-21 for linkage in two large kindreds segregating febrile seizures: Evidence for genetic heterogeneity. 1996 Epilepsia 37 Suppl. 5; 114.

Racacho LJ, Maher J, Ebers GC, McLachlan RS, Bulman DE. Linkage study of autosomal dominant febrile convulsions in two multigenerational pedigrees. 1996 Can J Neurol Sci. 23; S30.

McLachlan RS, Maher J, Bulman DE**, Racacho L**, Ebers G. Genetic studies of febrile convulsions in selected families. 1995 Epilepsia 36; 5S.

AWARDS

First place, UOttawa BMI department annual student seminar, 2009
Ontario Graduate Studentship, 2007-2008

COMMITTEES

2010-2011	OHRI RMP Trainee Committee, member
2002-2010	OHRI Lab Operations Committee, member
2009-2010	UOttawa BMI Graduate Student Council, President
2009-2010	UOttawa Faculty of Medicine Graduate Studies Council, member
1997-2009	OHRI Health and Safety Committee, member

MEMBERSHIP

American Society of Human Genetics
Human Genome Variation Society